UNIVERSITY OF OKLAHOMA

GRADUATE COLLEGE

COSMOLOGY OF THE PQMSSM

A DISSERTATION

SUBMITTED TO THE GRADUATE FACULTY

in partial fullfillment of the requirements for the

degree of

DOCTOR OF PHILOSOPHY

By

ANDRE LESSA
Norman, Oklahoma
2011

COSMOLOGY OF THE PQMSSM

A DISSERTATION APPROVED FOR THE
HOMER L. DODGE DEPARTMENT OF PHYSICS AND ASTRONOMY

By

Dr. Howard Baer, Chair

Dr. Phillip Gutierrez

Dr. Chung Kao

Dr. Keri Kornelson

Dr. Yun Wang

To my uncle, Ricardo, who has always loved science and knowledge.

Acknowledgements

This work would have never come to life without the help and support of several colleagues and friends. In case I miss one of you (and I will!), I thank everyone who helped me during these last four years and more. In special I thank my family, who showed me the pleasure of science and its importance. The satisfaction of learning something new is an invaluable gift.

My interest for symmetries and particle physics was born during my first undergrad years and were essential for leading me towards this work. I would probably be working on some boring condensed matter topic (joke!) if it was not for the wonderful discussions with Marcelo Guzzo, Guillermo Cabrera, Eduardo Miranda and, most of all, Orlando Peres, who first "infected" me with the "SUSY fever".

However none of the above would have mattered, if it was not for my advisor, Howie Baer, who was the main driving force behind this work. The amount of knowledge I have learned from him during these last years is immeasurable. It is always a gift to be able to discuss physics with someone with such a vast knowledge and passion for it.

I would also like to thank Xerxes Tata, who gave me the most enlightening phone calls ever. This work would not have been possible without the invaluable contributions of Sabine Kraml, Sezen Sekmen, Warintorn Sreethawong and specially Shibi Rajagopalan, who made the years in Norman much more fun.

Many thanks to all of you.

Table of Contents

Abstract vii

Introduction 1

I PQMSSM: An Introduction 3

1 The Strong CP Problem 5
1.1 The Peccei-Quinn Solution . . . 9

2 The Hierarchy Problem 16
2.1 The Supersymmetric Solution . . . 17

3 PQMSSM 21
3.1 The Axion . . . 22
3.2 The Axino . . . 23
3.3 The Saxion . . . 26

II The PQMSSM Cosmology 27

4 Brief Review of the MSSM Cosmology 29
4.1 Big-Bang Nucleosynthesis and New Physics . . . 34
4.2 The Gravitino Problem . . . 37
4.3 Neutralino Dark Matter . . . 45

5 General Implications of the PQMSSM 47
5.1 Thermal Production . . . 48
5.2 Coherent Oscillation . . . 49
5.3 Early Matter Dominated Universe . . . 54
5.4 Summary . . . 61

6 The Axino LSP 63
6.1 Thermal Leptogenesis and the Axino LSP . . . 72
6.2 The Saxion Effect . . . 85
6.3 Summary . . . 104

7 The Neutralino LSP 116
7.1 Summary . . . 137

8 The Large f_a Scenario 139
8.1 Summary . . . 168

Conclusions 170

References 173

III Appendix **178**

A PQ Models **179**
A.1 DFSZ 179
A.2 KSVZ 182
A.3 Supersymmetric KSVZ 183

B Axion and Neutralino Relic Densities **189**

Abstract

This work presents the main implications of simultaneously considering the Peccei-Quinn solution to the Strong CP Problem and the supersymmetric solution to the Hierarchy Problem. We focus our discussion on the cosmological consequences of the resulting low energy effective theory, the Minimal Supersymmetric Standard Model augmented with the axion supermultiplet or PQMSSM. Here we review the main ideas and concepts necessary for discussing the PQMSSM cosmology and apply these to particular PQMSSM scenarios, such as the axino LSP and the neutralino LSP cases. In particular we discuss how these scenarios can be made consistent with cosmological constraints, such as the observed Dark Matter relic density and Big Bang nucleosynthesis. The implications for collider and dark matter experiments are also presented.

Introduction

The Standard Model (SM) is frequently labeled as the most successful theory of the history of science. Despite its indisputable achievements in describing and predicting an amazing and ever-growing amount of experimental data, there are several theoretical and experimental motivations for considering Beyond the Standard Model (BSM) theories. Amongst these is the notorious fine-tuning problem in the Higgs and electroweak sector of the SM, also known as the Hierarchy Problem. Another less well known, but equally important fine-tuning problem is the Strong CP Problem, which is found in the quantum chromodynamics (QCD) sector of the Standard Model. Several solutions for both the electroweak and strong fine-tuning problems have been extensively discussed in the literature. The most compelling ones are the supersymmetry (SUSY) solution to the Hierarchy Problem and the Peccei-Quinn (PQ) solution to the Strong CP Problem. These can also explain the observed value for the Dark Matter relic density, which can not be accommodated within the Standard Model. When simultaneously considered, supersymmetry and the PQ mechanism have several important consequences for the cosmological history of the universe. Here we discuss such implications in the context of the PQMSSM, the low energy effective theory that implements both the PQ and the SUSY solutions for the fine-tuning problems mentioned above.

In the first part of this work we briefly review the motivations for considering the PQMSSM, which is defined in detail in Section 3. In this section we also present some general properties for this class of models. Particular realizations of PQ models and

their supersymmetric version are presented in Appendix A. In Part II we discuss the main subject of this work, the Cosmology of the PQMSSM. Section 4 reviews the basic cosmological framework necessary to discuss the standard MSSM cosmology, which is then extended to include the axion supermultiplet in Sec.5. Due to its very distinct phenomenology, we divide the PQMSSM models into two scenarios: models with an axino as the lightest supersymmetric particle (LSP) and models with a neutralino LSP. The first case is discussed in Sec.6, while the second is presented in Sec.7. Finally, in Section 8, we discuss a class of PQMSSM models related to grand unified and string theories. Some analytical expressions necessary for discussing the axion and neutralino relic densities in the PQMSSM framework are derived in Appendix B.

An exhaustive review of supersymmetry and PQ models is beyond the scope of this work and can be found in several text-books and published reviews. Instead, we aim here to collect several concepts and ideas pertaining to the cosmology of the PQMSSM models, which are scattered in the literature, many times with conflicting conclusions and/or notation. However, we also point out that the cosmology of the PQMSSM is not an exhausted topic and although some of the results presented here have not been discussed before, some scenarios still need to be investigated and are not contained in this work. Whenever possible we try to explicitly present our assumptions and possible extensions and/or exceptions to the scenarios presented here.

Part I

PQMSSM: An Introduction

The first Part of this work briefly reviews the theoretical motivations for the supersymmetric PQ model (PQMSSM). In Sec.1, we present the main motivation behind the introduction of the PQ symmetry, known as the Strong CP Problem, as well as the original solution proposed by Peccei and Quinn. The Strong CP Problem can be viewed as a fine-tuning (or naturalness) problem in the strong sector. A distinct fine-tuning problem in the electroweak sector, known as the Hierarchy Problem, constitutes the main theoretical argument for weak scale Supersymmetry (SUSY) and is discussed in Sec.2. Since both supersymmetry (as well as the minimal supersymmetric version of the Standard Model or MSSM) and the PQ solution have been discussed at length in the literature, we will just present the basic ideas necessary to motivate our subsequent discussion of the PQMSSM cosmology. In Sec.3 we summarize the main consequences of simultaneously considering the PQ solution to the Strong CP Problem and the supersymmetric solution to the Hierarchy problem. The basic characteristics of the resulting (PQMSSM) model are presented. A more detailed discussion of particular realizations of the PQMSSM scenario is discussed in Appendix A.

Chapter 1

The Strong CP Problem

In the early 70's, it was realized that non-abelian gauge theories admit a non-trivial vacuum structure[1, 2]. Before this realization, perturbative quantum field theory was constructed as perturbations on the vacuum state $\phi(x) = 0$, where ϕ represents all the fields in the theory. Thus, gauge invariant terms such as

$$\mathrm{Tr}(F_{\mu\nu}\tilde{F}^{\mu\nu}) = \epsilon^{\mu\nu\rho\sigma}\partial_\mu\left(A^a_\nu F^a_{\rho\sigma} - \frac{2}{3}if_{abc}A^a_\nu A^b_\rho A^c_\sigma\right) \equiv \partial_\mu K^\mu \tag{1.1}$$

could be neglected when computing the action, since it corresponds to a surface term, which vanishes since $A^a_\mu \xrightarrow{x\to\pm\infty} 0$. In Eq.(1.1) above A_μ are the gauge fields, $F_{\mu\nu}$ is the gauge strength tensor, $\tilde{F}^{\mu\nu} \equiv \epsilon^{\mu\nu\sigma\rho}F_{\sigma\rho}/2$ its dual and f_{abc} the gauge group structure constants. However, the condition $A_\mu = 0$ is not gauge invariant. Instead, the physical condition for defining the vacuum state of gauge theories is:

$$F_{\mu\nu} \xrightarrow{x\to\pm\infty} 0\ , \tag{1.2}$$

which implies

$$\mathbf{A}_\mu \xrightarrow{x\to\pm\infty} U^{-1}\partial_\mu\ , U \tag{1.3}$$

where U is a unitary gauge transformation and $\mathbf{A}_\mu = A^a_\mu T^a$. Here T^a are the generators of the gauge group. The existence of these non-trivial vacuum solutions implies that surface terms, such as the one in Eq.(1.1), can not be neglected, except in abelian theories, where $f_{abc} = 0$ results in $K_\mu \xrightarrow{x\to\pm\infty} 0$.

The non-triviality of vacuum solutions in non-abelian theories has important consequences for the Standard Model (SM), since it contains the unbroken $SU(3)_C$ sym-

metry. The QCD vacuum structure is closely related to the homotopy classes of $SU(3)$[3]. It has been shown[1, 2] that non-abelian theories can have an infinite number of nonequivalent vacuum states, which give rise to distinct physical theories. In QCD, all the possible gauge invariant vacua can be parametrized by their phase (θ) under gauge transformations. Assuming a specific gauge invariant vacuum for the theory and expanding the gauge fields in the gauge invariant vacuum ($|\theta\rangle$) gives:

$$\langle\theta|\mathcal{O}|\theta\rangle = \lim_{t\to\infty(1-i\epsilon)} \frac{\int D\phi\mathcal{O}\exp[i\int d^4x\mathcal{L}_{eff}]}{\int D\phi\exp[i\int d^4x\mathcal{L}_{eff}]} \tag{1.4}$$

where $\mathcal{O}$ represents a time ordered operator and

$$\mathcal{L}_{eff} = \mathcal{L}_{QCD} + \alpha_s\frac{\theta}{8\pi}Tr(G_{\mu\nu}\tilde{G}^{\mu\nu}) \tag{1.5}$$

where $G_{\mu\nu}$ is the gluon field tensor and $\alpha_s = g^2/4\pi$ is the strong coupling constant. Therefore, unless $\theta = 0$, the non-trivial QCD vacuum will contribute with the effective interaction term in Eq.(1.5).

The above picture can significantly change once quark fields are considered. Assuming massless quarks, the Standard Model is invariant under the global chiral symmetry:

$$q_f \to e^{i\alpha_f\gamma^5}q_f \tag{1.6}$$

where f labels quark flavor and α_f is the $U(1)$ transformation parameter. Although the above symmetry is clearly violated by quark masses, even in the massless case, it is not conserved at the quantum level, since it is not anomaly free. It is well known that applying the above transformation for the quark fields induces the following

terms in the SM Lagrangian:

$$\mathcal{L}_{SM} \to \mathcal{L}_{SM} + \sum_{f,f'} (M_q)_{ff'} \bar{q}_f e^{i(\alpha_f + \alpha_{f'})\gamma^5} q_{f'} - 2\left(\sum_f \alpha_f\right) \frac{g^2}{32\pi^2} G_{\mu\nu}\tilde{G}^{\mu\nu} \tag{1.7}$$

where M_q is the quark mass matrix. Therefore, in the limit that at least one of the quark flavors is massless, we can choose $\sum_f \alpha_f = \theta/2$ and eliminate the θ dependence in the SM. This is simply a reflection that, for a (classically) conserved chiral symmetry, all distinct QCD vacua are related by chiral transformations and consequently equivalent. In this case θ is an unphysical parameter. On the other hand, for massive quarks, the chiral transformation can be used to eliminate phases in the quark mass matrix and rotate the quark fields to the mass basis. In this basis, α_f is fixed by the phases in the quark mass matrix M_q, resulting in a redefinition of the θ parameter:

$$\theta \to \bar{\theta} = \theta + \sum_f \alpha_f = \theta + \text{Arg}[\text{Det}(M_q)] \ . \tag{1.8}$$

Since most of the SM computations are done in the mass basis, $\bar{\theta}$ is the physical parameter to be considered. Furthermore, from the electroweak interactions, we know that the quark mass matrix in the interaction basis is not real, hence we see that, even if $\theta = 0$ in the interaction basis, $\bar{\theta}$ is non zero, as seen from Eq.(1.8).

A non zero $\bar{\theta}$ has important physical implications. As an example, consider the transformation of the $\bar{\theta}$ term under time reversal (T):

$$\begin{array}{l} G_{0i} \xrightarrow{T} G_{0i} \text{ and } G_{ij} \xrightarrow{T} -G_{ij} \\ \tilde{G}_{0i} \xrightarrow{T} -\tilde{G}_{0i} \text{ and } \tilde{G}_{ij} \xrightarrow{T} \tilde{G}_{ij} \end{array} \Rightarrow G_{\mu\nu}\tilde{G}^{\mu\nu} \xrightarrow{T} -G_{\mu\nu}\tilde{G}^{\mu\nu} \ .$$

Hence $\mathcal{L}_{eff}$ violates T and consequently CP, for $\bar{\theta} \neq 0$. This clearly shows that theories with distinct vacua (parametrized by distinct $\bar{\theta}$ values) have distinct physics

(if all quarks are massive). An important example of the consequences of strong CP violation is the contribution of the $\bar{\theta}$ term to the neutron electric dipole moment (d_n), which is estimated as[4]

$$d_n = g_{NN\pi}\bar{g}_{NN\pi}\ln(\frac{M_N}{m_\pi})\frac{1}{4\pi^2 M_N} \tag{1.9}$$

where M_N and m_π are the neutron and pion masses and, for $m_{u,d} \ll m_s$,

$$\begin{aligned} g_{NN\pi} &\simeq 13.4 \\ \bar{g}_{NN\pi} &\simeq \frac{m_u m_d}{m_u + m_d}\bar{\theta}(M_\Xi - M_N)\frac{2m_s - m_u - m_d}{f_\pi} \sim 0.038\bar{\theta}\ . \end{aligned} \tag{1.10}$$

The above expression clearly shows that if one of the light quarks is massless, $\bar{\theta}$ has no physical consequences, as expected from the above discussion. However, for $m_u m_d \neq 0$, the above result gives[4]:

$$d_n \simeq 5.2 \times 10^{-16}\bar{\theta}\ e\text{cm}\ . \tag{1.11}$$

But experimental measurements constrain d_n to[5]:

$$d_n < 2.9 \times 10^{-26}\ e\text{cm}\ . \tag{1.12}$$

which requires $\bar{\theta} < 10^{-10}$. Such a tiny value would require an enormous fine-tuning between the θ and Arg[Det(M_q)] terms in Eq.(1.8). This is known as the *Strong CP Problem*. An obvious solution for eliminating the $\bar{\theta}$ contribution to d_n is to assume a massless quark. However this seems to be strongly disfavored by current experimental data. In the next section we discuss an alternative solution, initially proposed by Peccei and Quinn[6].

1.1 The Peccei-Quinn Solution

The Peccei-Quinn[6] solution for the Strong CP Problem relies on the fact that, if the Standard Model has an anomalous chiral symmetry ($U(1)_{PQ}$), the θ parameter can be rotated away, as discussed in the previous Section. However, such symmetry is clearly not present at low energies and must be broken. The importance of Peccei and Quinn's work was to show that $\bar{\theta}$ is naturally zero if $U(1)_{PQ}$ is spontaneously broken. As a consequence, a Goldstone boson must appear in the low energy theory, commonly named the *axion* (a)[7, 8], which transforms under $U(1)_{PQ}$ as:

$$a \rightarrow a + \xi \ . \tag{1.13}$$

As shown in Appendix A, the PQ symmetry induces the following effective axion-gluon-gluon interaction:

$$\mathcal{L}_{aGG} = \alpha_s \frac{a}{8\pi f_a} G_{\mu\nu}\tilde{G}^{\mu\nu} \ , \tag{1.14}$$

where f_a is related to the PQ breaking scale. Neglecting the electroweak sector for now we have:

$$\begin{aligned} \mathcal{L}_{eff} &= \frac{1}{2}(\partial^\mu a)^2 + \sum_f \bar{q}_f(i\gamma^\mu D_\mu - m_f)q_f - \frac{1}{4}G_{\mu\nu}G^{\mu\nu} \\ &+ \frac{\alpha_s\bar{\theta}}{8\pi}G_{\mu\nu}\tilde{G}^{\mu\nu} + \frac{\alpha_s a}{8\pi f_a}G_{\mu\nu}\tilde{G}^{\mu\nu} \ . \end{aligned} \tag{1.15}$$

Now consider the effective potential for the axion field in Euclidean space ($t \rightarrow it$):

$$\exp\left[-\int d^4x V_{eff}(\langle a\rangle)\right] = \int \mathcal{D}\phi \exp\left[-\int d^4x \bar{\mathcal{L}}(\langle a\rangle)\right] \ , \tag{1.16}$$

where $\bar{\mathcal{L}}$ is the Euclidean Lagrangian, with $t \rightarrow it$:

$$\bar{\mathcal{L}}(\langle a\rangle) = \frac{1}{4}G_{\mu\nu}G^{\mu\nu} + \sum_f \bar{q}_f(\gamma^\mu D_\mu + m_f q_f) - \frac{i\alpha_s(\langle a\rangle + f_a\bar{\theta})}{8\pi f_a}G_{\mu\nu}\tilde{G}^{\mu\nu} \ . \tag{1.17}$$

After integrating out the quark fields, it can be shown[9] that Eq.(1.16) can be written as:

$$\begin{aligned} \exp\left[-\int d^4x V_{eff}(\langle a\rangle)\right] &= \int \mathcal{D}A_\mu \prod_f \mathrm{Det}(\gamma^\mu D_\mu + m_f) \\ &\times \exp\left[-\int d^4x \left(\frac{1}{4}G_{\mu\nu}G^{\mu\nu} - \frac{i\alpha_s(\langle a\rangle + f_a\bar{\theta}))}{8\pi f_a}G_{\mu\nu}\tilde{G}^{\mu\nu}\right)\right] \end{aligned} \tag{1.18}$$

where $\mathrm{Det}(\gamma^\mu D_\mu + m_f) > 0$ in Euclidean space. Therefore, since the $G_{\mu\nu}G^{\mu\nu}$ term is real and $i(\langle a\rangle + f_a\bar{\theta})G_{\mu\nu}\tilde{G}^{\mu\nu}$ is pure imaginary:

$$\exp\left[-\int d^4x V_{eff}(\langle a\rangle)\right] \leq \int \mathcal{D}A_\mu \prod_f \mathrm{Det}(\gamma^\mu D_\mu + m_f)|e^{A+iB}| \tag{1.19}$$

where

$$\begin{aligned} A &= -\frac{1}{4}\int d^4x G_{\mu\nu}G^{\mu\nu} \text{ and} \\ B &= -\frac{\alpha_s}{8\pi f_a}(\langle a\rangle + f_a\bar{\theta})\int d^4x G_{\mu\nu}\tilde{G}^{\mu\nu}\ . \end{aligned} \tag{1.20}$$

Hence:

$$\begin{aligned} \exp\left[-\int d^4x V_{eff}(\langle a\rangle)\right] &\leq \int \mathcal{D}A_\mu \prod_f \mathrm{Det}(\gamma^\mu D_\mu + m_f)e^A \\ &= \exp\left[-\int d^4x V_{eff}(\langle a\rangle = -\bar{\theta}f_a)\right] \end{aligned} \tag{1.21}$$

$$\Rightarrow V_{eff}(\langle a\rangle) \geq V_{eff}(\langle a\rangle = -f_a\bar{\theta})\ . \tag{1.22}$$

This shows that the minimum of the potential always happens for $\langle a\rangle/f_a + \bar{\theta} = 0$. Therefore, the PQ axion acquires a vacuum expectation value that exactly cancels the original $\bar{\theta}$ term, guaranteeing that the CP violating term ($G\tilde{G}$) vanishes to all orders. Clearly, this can only be achieved if the theory contains the $U(1)_{PQ}$ Goldstone boson,

which allows the $\bar{\theta} + \langle a \rangle$ angle to become a dynamical variable. Although the above result only holds for the QCD Lagrangian, it has been shown that the electroweak sector only results in corrections to $\bar{\theta}$ of order 10^{-14}[10, 11], still well below the experimental constraints.

From the above results, we see that the PQ solution to the Strong CP Problem only requires the introduction of a spontaneously broken axial symmetry and a $aG\tilde{G}$ effective coupling. There are several different ways of introducing the $U(1)_{PQ}$ symmetry in the SM. The minimal model, proposed by Peccei and Quinn[12] in 1977, requires two Higgs doublets, which transform under $U(1)_{PQ}$ as

$$\phi_1 \to e^{iQ_1\alpha}\phi_1 \text{ and } \phi_2 \to e^{iQ_2\alpha}\phi_2 \tag{1.23}$$

with $Q_1 \neq Q_2$. This minimal scenario was studied in detail by Weinberg[7], who showed that the spontaneous breaking of $U(1)_{PQ}$ and the electroweak symmetry happen simultaneously, as the ϕ_i fields acquire non zero vacuum expectation values (v_i). As a result, the axion couplings with leptons and quarks are completely fixed and must be of order m_f/v, where $v \equiv \sqrt{v_1^2 + v_2^2} \sim 240$ GeV. Furthermore, the axion mass is generated due to the anomalous violation of the $U(1)_{PQ}$ symmetry and is given by:

$$m_a \simeq \frac{f_\pi m_{\pi^0}}{v} \sim 100\,\text{keV}\ . \tag{1.24}$$

The existence of such a light particle with order m_f/v interactions has been long ruled out by constraints on hadronic decays such as $K^+ \to \pi^+ + a$[11].

Since the original PQ-Weinberg-Wilczek model, several other SM extensions have

been proposed in order to accommodate the $U(1)_{PQ}$ and avoid the experimental constraints. The most studied scenarios are the KSVZ[13, 14] and DFSZ[15, 16] models. In these, extra scalars and/or heavy quark fields are introduced in such a way that the breaking of $U(1)_{PQ}$ is no longer related to the $SU(2)_L \times U(1)_Y$ breaking and it is assumed to happen at a much higher scale, $f_a \gg v$. As a result, the axion mass and interactions are now suppressed by $1/f_a$ and can evade the experimental constraints. These models are also known as *invisible axion* models.

Despite the very distinct UV completion of the KSVZ and DFSZ models, at low energies ($\ll f_a$), both scenarios share the same basic properties. Here we present the most relevant ones for our subsequent discussion. More details about the KSVZ and DFSZ models are discussed in Appendix A.

In both models, the effective axion Lagrangian assumes the form[17]:

$$\begin{aligned}
\mathcal{L}_{a,eff} &= \frac{1}{2}\partial_\mu a \partial^\mu a \\
&+ \frac{c_1^q}{f_a}\partial_\mu a \bar{q}\gamma^\mu\gamma^5 q - (\frac{1}{f_a} m_q \bar{q}_L q_R e^{ic_2^q a/f_a} + h.c.) \\
&+ \frac{c_1^l}{f_a}\partial_\mu a \bar{l}\gamma^\mu\gamma^5 l - (\frac{1}{f_a} m_l \bar{l}_L l_R e^{ic_2^l a/f_a} + h.c.) \\
&+ \frac{c_s \alpha_s}{8\pi f_a} a G_{\mu\nu}\tilde{G}^{\mu\nu} + \frac{c_W \alpha_W}{8\pi f_a} a W_{\mu\nu}\tilde{W}^{\mu\nu} + \frac{c_Y \alpha_Y}{8\pi f_a} a B_{\mu\nu}\tilde{B}^{\mu\nu}
\end{aligned} \tag{1.25}$$

where we have omitted generation indices, q (l) represents a quark (charged lepton) spinor and $G_{\mu\nu}$, $W_{\mu\nu}$ and $B_{\mu\nu}$ are the $SU(3)_C$, $SU(2)_L$ and $U(1)_Y$ tensor fields, respectively. The constants c_i depend on the particular axion model. For the KSVZ model, $c_1^{q,l} = c_2^{q,l} = 0$ and $c_s \neq 0$, while for DFSZ, $c_1^{q,l} = 0$, $c_2^d = c_2^l \neq 0$, $c_2^u \neq 0$ and c_s is only generated at the one loop level, as shown in Appendix A.

Requiring $\mathcal{L}_{a,eff}$ to be invariant (at the classical level) under the PQ transformation

$$q \to e^{i\gamma^5 \alpha Q_q} q, \quad l \to e^{i\gamma^5 \alpha Q_l} l \quad \text{and} \quad a \to a + f_a \alpha \tag{1.26}$$

implies

$$\begin{gathered} c_2^q + 2Q_q = 0, \quad c_2^l + 2Q_l = 0, \\ c_s - 2Q_q = 0, \quad c_W - 6Q_q - 2Q_l = 0, \\ \text{and} \quad c_Y - 6Y_q^2 Q_q - 2Y_l^2 Q_l = 0 \end{gathered} \tag{1.27}$$

where Y_q and Y_l are the hypercharge of the quark and charged lepton, respectively. The f_a constant is usually defined such that $c_s = 1$. Furthermore, in most models $c_2^q = c_2^l$, so the above constraints fix all the model dependent coupling constants c_i and the charges Q_q, Q_l. However, if the lepton masses can be neglected (which is always a good approximation in our case), the second constraint no longer applies and we can always rotate the lepton fields by a chiral transformation so that $c_W = 0$ or $c_Y = 0$. For our purposes it is convenient to work in the basis where $c_W = 0$, which will be assumed from now on. This arbitrariness in choosing the value of c_W (or c_Y) is analogous to the massless quark case discussed at the end of Sec.1, where $\bar{\theta}$ is no longer physical if one of the quarks is massless and therefore can be chosen as zero. We also point out that the effective axion Lagrangian given in Eq.(1.25) is only valid above the QCD chiral symmetry breaking scale (Λ_{QCD}) and must be modified below Λ_{QCD}[18]. However, Eq.(1.25) will be sufficient for our subsequent discussion.

As in the PQ-Weinberg-Wilczek model, the axion mass is suppressed by the PQ

breaking scale (f_a) and is generated by the $U(1)_{PQ}$ anomaly. However, in the KSVZ and DFSZ models, $f_a \gg v$, so[19, 7]:

$$m_a = \frac{m_\pi f_\pi}{f_a} \frac{\sqrt{Z}}{1+Z} \tag{1.28}$$

where $m_\pi \simeq 135$ MeV and $f_\pi \simeq 93$ MeV are the pion mass and structure constant and $Z = m_u/m_d \simeq 0.56$. Hence:

$$m_a \simeq 6 \text{ eV } \frac{10^6 \text{ GeV}}{f_a} \ll 100 \text{ keV } . \tag{1.29}$$

Furthermore, the anomalous axion coupling to the gluon field tensor generates the following axion effective potential[18, 20, 21]:

$$V_{eff}(a) \simeq m_a^2 f_a^2 [1 - \cos(a/f_a)] \, . \tag{1.30}$$

The above equation shows that the minimum of the potential is at $a = 0$, as expected from the discussion leading to Eq.(1.22). Astrophysical constraints on invisible axion models arising from stellar energy loss via axion radiation[11] usually require $f_a \gtrsim 10^9$ GeV. Therefore, despite its tiny mass, production of axions in laboratory experiments is extremely suppressed. Thus, for most purposes, the axion field completely decouples from the SM at low energies. An exception is the possible detection of axions through the $a - \gamma - \gamma$ coupling in microwave cavity experiments[22, 23, 24]. Nonetheless, the axion has important consequences in cosmology, as discussed in Sec.II. Furthermore, the introduction of the axion field implies an upper cut-off for the Standard Model of the order f_a, where the new degrees of freedom introduced in the DFSZ or KSVZ models must be included. This leads us to another well known

fine-tuning problem in the SM, known as the Hierarchy Problem, discussed in the next Section.

Chapter 2

The Hierarchy Problem

In Sec.1, we presented the Strong CP Problem, which is essentially a fine-tuning problem in the QCD Lagrangian, since $\bar{\theta}$ is required to be unnaturally small. The electroweak sector of the Standard Model also has another notorious fine-tuning problem, known as the Hierarchy Problem.

In the SM, it is assumed that the $SU(2)_L \times U(1)_Y$ symmetry is spontaneously broken by one Higgs doublet (ϕ), giving mass to the fermions and $W^{\pm}$ and Z gauge bosons. Therefore, all the mass scales in the SM are given by one single parameter $\langle\phi\rangle = v \simeq 240$ GeV. All the mass hierarchies are then due to distinct Yukawa or gauge couplings between the fermions or gauge bosons and the Higgs doublet. Although this is a tree level result, the higher order corrections to the fermions and gauge masses obey:

$$\delta m^2_{f,V} = (m^0_{f,V})^2(c \ln \Lambda + d) \tag{2.1}$$

where Λ is the UV cut-off of the theory, $m^0_{f,V}$ are the tree level fermion (f) and gauge (V) masses and c and d are constants. The logarithmic dependence on the cut-off is due to the broken chiral and gauge symmetries of the SM. The first is restored at $v \to 0$ and (except for small anomalous corrections) implies that $m_f = 0$ at all orders in perturbation theory. Thus, higher order corrections to m_f must be proportional to v. The same is true for the gauge bosons, which are massless at all orders if $v = 0$, due to the gauge symmetry. In this sense, the fermion and gauge masses are *protected*

by the approximate chiral and gauge symmetries. On the other hand, in the SM, the Higgs mass is not protected by any symmetry and higher order corrections to its mass are not restricted to a logarithmic dependence on the cut-off:

$$\delta m_h^2 = a\Lambda^2 + b\Lambda + c\ln\Lambda + d \tag{2.2}$$

As discussed in Sec.1.1, if we want to solve the Strong CP problem through the PQ solution, the SM is an effective theory at energies smaller than the PQ breaking scale (f_a). Therefore, the SM will necessarily have a cut-off at $\Lambda \sim f_a \gg v$. Although this only introduces corrections of order $m_{f,V}^0$ to the fermion and gauge boson masses, the Higgs mass receives corrections of order $\Lambda \gg m_h^0$, where m_h^0 is the Higgs tree level mass. However, experimental data and unitarity arguments require $m_h < 1$ TeV. In order to obtain this relatively light Higgs mass in the SM model, it is necessary to fine-tune the bare Higgs mass (m_h^0), so it almost exactly cancels the large radiative corrections, resulting in a physical mass of order v. This electroweak fine-tuning problem in the Standard Model is commonly known as the *Hierarchy Problem*.

2.1 The Supersymmetric Solution

As discussed in Sec.2, the Hierarchy Problem is only present in the SM because there are no symmetries protecting the Higgs mass from quadratic radiative corrections. Therefore, a natural solution to the problem is to enlarge the SM symmetry in order to protect the Higgs mass. This can be achieved (at least at 1 loop) with an extended gauge symmetry, such as in Little Higgs models[25]. Another compelling solution is

Supersymmetry (SUSY).

Unlike an internal (gauge) symmetry, SUSY is an extension of the space-time symmetry of the SM. It introduces new quantum (anti-commuting) dimensions (θ_a), extending the four dimensional Minkowski space-time (x^μ) to a 8-dimensional space, known as superspace (x^μ, θ_a). The usual 4-dimensional fields are then extended to superfields, which are functions of (x^μ, θ_a) and now include both fermionic and bosonic degrees of freedom. In the same way that three dimensional rotations relates the spin components of a field, rotations in superspace relates the spin-half and spin-0 (for chiral superfields) or spin-1 (for vectorial superfields) of a superfield.

Since under supersymmetry the Higgs field is related to a fermionic field, the chiral symmetry that protects the fermion masses is extended to the Higgs field, forbidding quadratic corrections[1]. This clearly solves the Hierarchy Problem if supersymmetry is exact.

However, SUSY cannot be an exact symmetry at low energies, since this would imply low energy sparticles, such as a 0.5 MeV scalar electron (or selectron), clearly not seen in low energy data. Nonetheless, the Hierarchy Problem can still be solved in the broken SUSY regime, since in this case the radiative corrections for the Higgs mass are given by[27]:

$$\delta m_h^2 = a(m_f^2 - m_{\tilde{f}}^2) \ln \frac{m_f^2}{m_{\tilde{f}}^2} + b(m_V^2 - m_{\tilde{V}}^2) \ln \frac{m_f^2}{m_{\tilde{f}}^2} + c \tag{2.3}$$

where $m_{\tilde{f},\tilde{V}}$ are the matter fermion and gauge boson superpartners, also known as sfermions and gauginos, respectively. From the above expression, we see that the

[1] It can be shown that, for unbroken SUSY, all corrections to the Higgs mass cancel at all orders in perturbation theory. This is a particular consequence of the *Non-Renormalization Theorem*[26].

corrections to m_h^0 are still suppressed as long as $m_{\tilde{f},\tilde{V}}$ is not much larger than $m_{f,V}$. In this, case a small fine-tuning usually requires $m_{\tilde{f},\tilde{V}} \lesssim 1$ TeV[28].

Several realistic SUSY breaking models have been constructed in order to satisfy all experimental bounds on sparticle masses and at the same time solve the Hierarchy Problem[27]. The minimal supersymmetric version of the Standard Model (MSSM) and its phenomenological implications have been discussed at length in the literature and is beyond the scope of this work. However, we mention that, in most of the viable MSSM scenarios, the lightest supersymmetric particle is a stable neutral bino (superpartner of the $U(1)_Y$ gauge boson), wino (superpartner of the $SU(2)_L$ neutral gauge boson) or higgsino (superpartner of the Higgs scalar) and can be a viable candidate for Dark Matter. This important feature of the MSSM will be essential for our further discussion of the PQMSSM cosmology and will be discussed in more detail in Sec.4. To conclude, we list in Table 2.1 the MSSM superfields (particles and sparticles), in the interaction $(SU(3)_C \times SU(2)_L \times U(1)_Y)$ basis and their respective sparticle mass eigenstates.

Superfields	$SU(3)_C$	$SU(2)_L$	$U(1)_Y$	Sparticle Mass Eigenstates
$L = L(\tilde{l}, l)$	**1**	**2**	-1	Sleptons $(\tilde{e}_1, \tilde{e}_2)$ and Sneutrinos $(\tilde{\nu})$
$E^C = E^C(\tilde{e}^C, e_L^C)$	**1**	**1**	2	
$Q = Q(\tilde{q}, q)$	**3**	**2**	1/3	Squarks $(\tilde{u}_1, \tilde{u}_2, \tilde{d}_1, \tilde{d}_2)$
$U^C = U^C(\tilde{u}^C, u_L^C)$	**3***	**1**	- 4/3	
$D^C = D^C(\tilde{d}^C, d_L^C)$	**3***	**1**	2/3	
$H_u = H_u(\tilde{h}_u, h_u)$	**1**	**2**	1	Charginos $(\widetilde{W}_1, \widetilde{W}_2)$ and Neutralinos $(\widetilde{Z}_1, \widetilde{Z}_2, \widetilde{Z}_3, \widetilde{Z}_4)$
$H_d = H_d(\tilde{h}_d, h_d)$	**1**	**2***	-1	
$V^a = V^a(\tilde{W}^a, W^a)$	**1**	**3**	0	
$V' = V'(\tilde{B}, B)$	**1**	**1**	0	
$G = G(\tilde{g}, g)$	**8**	**1**	0	Gluinos $(\tilde{g})$

Table 2.1: MSSM fields and their representations. The last column shows the respective sparticle mass eigenstates.

Chapter 3

PQMSSM

In the last two Sections, we discussed how the Standard Model requires a large amount of fine-tuning in the QCD Lagrangian in order to satisfy the experimental constraints on strong CP violation and in the Higgs sector in order to stabilize the electroweak potential at the weak scale. We also presented two possible solutions for these issues, both involving an extension of the symmetries of the Standard Model: the inclusion of the global $U(1)_{PQ}$ symmetry and supersymmetry. Here we discuss what are the implications of simultaneously requiring these two symmetries, so both the strong CP and Hierarchy Problems are solved. We label the minimal class of models which accommodates both SUSY and the PQ symmetry, the *PQMSSM*.

In order to implement the PQ mechanism in supersymmetric theories, PQ charges have to be assigned to the MSSM fields and new PQ superfields must be introduced. The axion superfield is a singlet under the MSSM gauge group and in most scenarios is mainly composed of linear combinations of other elementary (non-MSSM) fields. Even though the full field content of the PQMSSM is highly model dependent, it must contain an axion superfield composed of a complex scalar field (ϕ) and a Majorana fermion ($\tilde{a}$). The complex scalar field is usually divided into its axion (a) and saxion (s) components:

$$\phi = \frac{s + ia}{\sqrt{2}}$$

and the fermionic component is named *axino*.

In order to solve the strong CP problem, the axion field must have effective couplings to the $SU(3)$ gauge fields of the form

$$\mathcal{L}_{aG\tilde{G}} = \frac{\alpha_s}{8\pi f_a} a G_{\mu\nu} \tilde{G}^{\mu\nu} \ . \tag{3.1}$$

Furthermore, as shown in Appendix A, an anomalous interaction with the $B_{\mu\nu}$ is also present in most models[1]:

$$\mathcal{L}_{aB\tilde{B}} = \frac{\alpha_Y c_Y}{8\pi f_a} a B_{\mu\nu} \tilde{B}^{\mu\nu} \ . \tag{3.2}$$

Also, as seen in Eq.(1.25), other non-minimal interactions are possible, but since they are strongly model dependent, they will be neglected here.

The supersymmetric version of Eqs.(3.1) and (3.2) implies the following couplings for the saxion and axino fields:

$$\begin{aligned} \mathcal{L}_{eff} &= \frac{\alpha_s}{8\pi}\frac{s}{f_a}(G_{\mu\nu}G^{\mu\nu} + 2i\bar{\tilde{g}}\gamma^\mu D_\mu \tilde{g}) + i\frac{\alpha_s}{16\pi}\frac{\bar{\tilde{a}}}{f_a}\gamma_5[\gamma^\mu,\gamma^\nu]\tilde{g}G_{\mu\nu} \\ &+ \frac{\alpha_Y c_Y}{8\pi}\frac{s}{f_a}(B_{\mu\nu}B^{\mu\nu} + 2i\bar{\widetilde{B}}\gamma^\mu D_\mu \widetilde{B}) + i\frac{\alpha_Y c_Y}{16\pi}\frac{\bar{\tilde{a}}}{f_a}\gamma_5[\gamma^\mu,\gamma^\nu]\widetilde{B}B_{\mu\nu} \end{aligned} \tag{3.3}$$

where terms of order $\mathcal{O}(\alpha_s^{3/2})$ and $\mathcal{O}(\alpha_Y^{3/2})$ were neglected.

3.1 The Axion

Since the axion field is the $U(1)_{PQ}$ pseudo-Goldstone boson, it is massless, except for anomalous corrections coming from the QCD chiral anomaly. For temperatures well above Λ_{QCD} (the QCD chiral breaking scale), the axion is essentially massless, while for $T \ll \Lambda_{QCD}$ the QCD chiral anomaly induces a non-zero mass for the axion field.

[1] As discussed in Sec.1.1, interactions with the $SU(2)_L$ tensor field can always be rotated away in the approximation that the lepton Yukawa couplings are zero.

The temperature dependent axion mass is approximately given by[21]:

$$m_a(T) = \begin{cases} m_a^0 & \text{, if } \Lambda_{QCD} > T \\ m_a^0 \times b \left(\frac{\Lambda_{QCD}}{T}\right)^4 & \text{, if } \Lambda_{QCD} < T \end{cases}, \tag{3.4}$$

where $b \simeq 0.018$, $m_a^0 = 6.2 \times 10^{-3}$ GeV$/f_a$, $\Lambda_{QCD} = 200$ MeV and T always refers to the thermal bath temperature. Therefore the effective thermal potential for the axion field becomes:

$$V_{eff}(a) = m_a(T)^2 f_a^2 [1 - \cos(a/f_a)] \tag{3.5}$$

Due to its small mass and suppressed interactions, the axion lifetime (axions can decay to $\gamma\gamma$) is much larger than the age of the universe, hence the axion can be considered stable for all purposes.

3.2 The Axino

From Eq.(3.3), we have the following (minimal) couplings for the axino field :

$$\mathcal{L}_{\tilde{a}} = i\frac{\alpha_s}{16\pi}\frac{\bar{\tilde{a}}}{f_a}\gamma_5[\gamma^\mu, \gamma^\nu]\tilde{g}G_{\mu\nu} + i\frac{\alpha_Y c_Y}{16\pi}\frac{\bar{\tilde{a}}}{f_a}\gamma_5[\gamma^\mu, \gamma^\nu]\widetilde{B}B_{\mu\nu} \tag{3.6}$$

where $c_Y = 8/3$ in the DFSZ model and $c_Y = 0$, $2/3$ or $8/3$ in the KSVZ model, as shown in Appendix A.

If supersymmetry is unbroken, the axino is degenerate with the axion field, hence massless, except for the tiny QCD anomaly contribution. Furthermore, since the axino is the Majorana component of a chiral superfield, it cannot receive tree level soft masses. Hence, any mass operator for the axino field has to be non-renormalizable, which makes the axino mass highly dependent on the supersymmetric PQ model and

on the SUSY breaking mechanism. In particular, the supersymmetric DFSZ model gives[29]:

$$m_{\tilde{a}} \simeq \frac{kv^2 + bm_{3/2}^2}{f_a} \tag{3.7}$$

where $k \lesssim 10^{-7}$, $m_{3/2}$ is the gravitino mass and b is a model dependent constant. Thus, in this case, the axino mass is at most 10 MeV and the axino will likely be the lightest supersymmetric particle (LSP). However, depending on the axion supermultiplet couplings with the SUSY breaking (hidden) sector, the axino mass can receive large corrections at 1-loop. For the supersymmetric KSVZ model discussed in Appendix A.3, the axino is massless at tree level, but loop corrections give[30]:

$$m_{\tilde{a}} \simeq m_{3/2} \ . \tag{3.8}$$

As seen from the above arguments, in the most common models, the axino is expected to be extremely light or of order the other SUSY particle masses. Nonetheless, for most of the subsequent analysis, we will consider $m_{\tilde{a}}$ as a free parameter.

Since the axino has $1/f_a$ suppressed interactions with gauge bosons and gauginos, as seen from Eq.(3.6), it will be a long lived particle if it is not the LSP or it will make the lightest MSSM particle (usually the lightest neutralino) unstable, if the axino is the LSP. For the latter case, using Eq.(3.6), we obtain the following decay rates:

$$\begin{aligned}
\Gamma(\widetilde{Z}_1 \to \tilde{a} + \gamma) &= \frac{\alpha_Y^2 C_{aYY}^2 \cos^2\theta_w Z_{1B}^2}{128\pi^3 f_a^2} m_{\widetilde{Z}_1}^3 (1 - \frac{m_{\tilde{a}}^2}{m_{\widetilde{Z}_1}^2})^3 \\
\Gamma(\widetilde{Z}_1 \to \tilde{a} + Z) &= \frac{\alpha_Y^2 C_{aYY}^2 \sin^2\theta_w Z_{1B}^2}{128\pi^3 f_a^2} m_{\widetilde{Z}_1}^3 \lambda^{1/2}(1, \frac{m_{\tilde{a}}^2}{m_{\widetilde{Z}_1}^2}, \frac{m_Z^2}{m_{\widetilde{Z}_1}^2}) \\
&\quad \cdot \left\{ \left(1 - \frac{m_{\tilde{a}}^2}{m_{\widetilde{Z}_1}^2}\right)^2 + 3\frac{m_{\widetilde{Z}} m_Z^2}{m_{\widetilde{Z}_1}^3} - \frac{m_Z^2}{2m_{\widetilde{Z}_1}^2}\left(1 + \frac{m_{\widetilde{Z}}^2}{m_{\widetilde{Z}_1}^2} + \frac{m_Z^2}{m_{\widetilde{Z}_1}^2}\right) \right\}
\end{aligned} \tag{3.9}$$

where $Z_{1B} = \langle \widetilde{Z}_1 | \widetilde{B} \rangle$ is the bino component of the neutralino field. Three-body decays of neutralinos into quarks have been computed in Ref.[31], including the γ/Z interference terms and is given by:

$$\begin{aligned}\frac{d\Gamma}{d\mu_k}(\widetilde{Z}_1 \;\;\rightarrow\;\; \tilde{a} + q\bar{q}) = \frac{\alpha\alpha_Y^2 C_{aYY}^2 Z_{1B}^2}{768\pi^4 f_a^2} m_{\widetilde{Z}_1}^3 \Bigg[Q^2 \cos^2\theta_w \frac{(1-\mu_k)^2(2+\mu_k)}{\mu_k} \\ + \;\; \frac{(g_V^2+g_A^2)}{\cos^2\theta_w} \frac{(1-\mu_k)^2(2+\mu_k)\mu_k}{\frac{m_Z^2\Gamma_Z^2}{m_{\widetilde{Z}_1}^4} + (\frac{m_Z^2}{m_{\widetilde{Z}_1}^2} - \mu_k)^2} + 2 g_V Q Re \left[\frac{(1-\mu_k)^2(2+\mu_k)}{\mu_k - \frac{m_Z^2}{m_{\widetilde{Z}_1}^2} + i\frac{\Gamma_Z m_Z}{m_{\widetilde{Z}_1}^2}} \right] \Bigg],\end{aligned} \tag{3.10}$$

where the axino and quark masses have been neglected. In the above, $g_V = \frac{T_3}{2} - Q\sin^2\theta_w$ and $g_A = -T_3/2$, where T_3 is the weak isospin of the quark q and Q its electric charge. The above differential width is integrated over the range $\mu_k : 4m_q^2/m_{\widetilde{Z}_1}^2 \rightarrow 1$. The quark mass acts as a regulator for the otherwise divergent photon-mediated contribution.

On the other hand, if the axino is not the LSP, we have:

$$\begin{aligned}\Gamma(\tilde{a} \rightarrow \tilde{g}g) &= \frac{8\alpha_s^2}{128\pi^3 f_a^2} m_{\tilde{a}}^3 \left(1 - \frac{m_{\tilde{g}}^2}{m_{\tilde{a}}^2}\right)^3 \\ \Gamma(\tilde{a} \rightarrow \widetilde{Z}_i + \gamma) &= \frac{\alpha_Y^2 C_{aYY}^2 \cos^2\theta_w Z_{iB}^2}{128\pi^3 f_a^2} m_{\tilde{a}}^3 \left(1 - \frac{m_{\widetilde{Z}_i}^2}{m_{\tilde{a}}^2}\right)^3 \\ \Gamma(\tilde{a} \rightarrow \widetilde{Z}_i + Z) &= \frac{\alpha_Y^2 C_{aYY}^2 \sin^2\theta_w Z_{iB}^2}{128\pi^3 f_a^2} m_{\tilde{a}}^3 \lambda^{1/2}\left(1, \frac{m_{\widetilde{Z}_i}^2}{m_{\tilde{a}}^2}, \frac{m_Z^2}{m_{\tilde{a}}^2}\right) \\ &\quad \cdot \left\{ \left(1 - \frac{m_{\widetilde{Z}_i}^2}{m_{\tilde{a}}^2}\right)^2 + 3\frac{m_{\widetilde{Z}_i} m_Z^2}{m_{\tilde{a}}^3} - \frac{m_Z^2}{2m_{\tilde{a}}^2}\left(1 + \frac{m_{\widetilde{Z}_i}^2}{m_{\tilde{a}}^2} + \frac{m_Z^2}{m_{\tilde{a}}^2}\right) \right\}\end{aligned} \tag{3.11}$$

where Z_{iB} is the bino component of the $\widetilde{Z}_i$ field and $\lambda(1,a,b) = 1+a^2+b^2-2a-2b-2ab$.

3.3 The Saxion

The saxion is the R-even partner of the axion field. As shown in Appendix A.2, the saxion receives a soft mass of order $m_{3/2}$ and couples to gauge bosons and gauginos through the effective interactions in Eq.(3.3):

$$\mathcal{L}_{eff} = \frac{\alpha_s}{8\pi}\frac{s}{f_a}(G_{\mu\nu}G^{\mu\nu} + 2i\bar{\tilde{g}}\gamma^\mu D_\mu \tilde{g}) + \frac{\alpha_Y c_Y}{8\pi}\frac{s}{f_a}(B_{\mu\nu}B^{\mu\nu} + 2i\bar{\widetilde{B}}\gamma^\mu D_\mu \widetilde{B}) \ . \tag{3.12}$$

The saxion can also have an effective coupling with axions of the form[32, 33, 34]:

$$\mathcal{L}_{saa} = \frac{C_{saa}}{f_a} s\partial_\mu a \partial^\mu a \tag{3.13}$$

where C_{saa} is a model dependent constant, which can be zero or of $\mathcal{O}(1)$.

Using the above interactions we obtain the following decay rates for the saxion field:

$$\begin{aligned} \Gamma(s \to aa) &= \frac{C_{saa}^2}{32\pi f_a^2} m_s^3 \\ \Gamma(s \to gg) &= \frac{\alpha_s^2 m_s^3}{32\pi^3 f_a^2} \\ \Gamma(s \to \tilde{g}\tilde{g}) &= \frac{\alpha_s^2 m_s m_{\tilde{g}}^2}{8\pi^3 f_a^2}\left(1 - \frac{4m_{\tilde{g}}^2}{m_s^2}\right)^{3/2} \ . \end{aligned} \tag{3.14}$$

Therefore, the saxion, like the heavy axino, is long lived and can have important cosmological consequences, as discussed later.

Part II

The PQMSSM Cosmology

Before discussing the consequences of the axion supermultiplet for the cosmological evolution of the universe we first briefly review the thermal evolution of the ΛCDM scenario. A detailed discussion of the thermal history of the universe is out of the scope of this work and can be found in several standard text books[35, 36, 37]. Here we will simply present the main ingredients necessary to investigate the PQMSSM cosmology. Since astrophysical observations undoubtedly point to the existence of a cold Dark Matter (DM) component in the total energy density of the universe with relic density $\Omega_{DM}h^2 \simeq 0.11$, in Sec.4 we assume the MSSM with a neutralino LSP as our prototype model; to be extended later, in Sec.5, with the axion supermultiplet[2]. Sec.4 outlines the main phases of the early thermal history of the MSSM and introduces the basic formalism used later to discuss the PQMSSM cosmology. We also present some of the main challenges faced by the standard MSSM cosmology, such as the Gravitino Problem and the overproduction of dark matter. Then, in Sec.5, we introduce the general features of the axion supermultiplet cosmology. Finally, in Secs.6-8, we discuss particular PQMSSM models and their cosmological implications.

[2]Once the axino LSP scenario is considered, the neutralino no longer has to be the next-to-lightest SUSY particle (NLSP) and interesting new possibilities open up, such as a stau NLSP[38]. However, these cases require a distinct treatment and will not be included in our discussion.

Chapter 4

Brief Review of the MSSM Cosmology

The ΛCDM picture assumes that at very early times the universe was mainly composed of a extremely hot gas of relativistic particles, coupled through electroweak and strong interactions. This initial phase was supposedly preceded by a fast expansion phase (inflation) where the energy density was dominated by the potential energy of a scalar field (the inflaton). During the inflaton decay, the universe was re-heated to a temperature T_R, given by[35]:

$$T_R \simeq \frac{g_*^{-1/4}(T_R)}{2}\sqrt{M_{Pl}\Gamma_\phi} \tag{4.1}$$

where $M_{Pl} = 1.22 \times 10^{19}$ GeV is the Planck mass, Γ_ϕ is the inflaton decay width and $g_*(T)$ is the number of relativistic degrees of freedom at temperature T, given by:

$$g_* \equiv \sum_{Bosons}\left(\frac{T_B}{T}\right)^4 + \frac{7}{8}\sum_{Fermions}\left(\frac{T_F}{T}\right)^4 \tag{4.2}$$

where T_B (T_F) is the temperature of the bosonic (fermionic) relativistic degrees of freedom.

After the inflaton decay, the energy density of the universe becomes dominated by the radiation gas, with an expansion rate given by

$$H \equiv \frac{\dot{R}}{R} = \sqrt{\frac{8\pi}{3M_{Pl}^2}\rho_R} \tag{4.3}$$

and the thermal bath energy density, ρ_R, evolves according to

$$\dot{\rho}_R + 4H\rho_R = 0 \tag{4.4}$$

Using $\rho_R = \pi^2 g_*(T) T^4/30$, we obtain $T \propto R^{-1}$, so the thermal bath cools down as the universe expands.

The dynamics of the distinct particle species interacting with the radiation gas is governed by the Boltzmann equation, which in its simplified form reads[35]:

$$\dot{n_i} + 3Hn_i = -\langle \sigma_{ii\to jj} v \rangle (n_i^2 - \bar{n}_i^2) - \Gamma_{i\to X} n_i + \Gamma_{j\to i+X} n_j \tag{4.5}$$

where i and j label different particle species (j is assumed to be in thermal equilibrium), $\bar{n}_i$ is the equilibrium number density of particle i, $\langle \sigma_{ii\to jj} v \rangle$ is the velocity averaged annihilation cross-section for the process $i + i \to j + j$ and $\Gamma_{i\to X}$, $\Gamma_{j\to i+X}$ are the decay rates for $i \to X$ and $j \to i + X$, respectively. For the cases of interest here, the right-hand side of Eq.(4.5) is dominated either by the annihilation or by the decay term. In the first case, we have:

$$\frac{1}{n_i H}\dot{n_i} = -3 - \frac{\langle \sigma_{ii\to jj} v \rangle}{H} n_i (1 - \frac{\bar{n}_i^2}{n_i^2}) \tag{4.6}$$

Therefore, for $\langle \sigma_{ii\to jj} v \rangle n_i/H \gg 1$, the second term dominates and $n_i = \bar{n}_i$. As the temperature decreases and becomes smaller than the particle's mass, $\bar{n}_i(T) \propto e^{-m_i/T}$, the second term quickly becomes sub-dominant and the number density freezes-out. The freeze-out temperature (T_{fr}) can be approximately computed using the freeze-out condition:

$$\langle \sigma_{ii\to jj} v \rangle \bar{n}_i(T_{fr}) = H(T_{fr}) \; . \tag{4.7}$$

Once a particle species decouples, its number density is simply diluted due to the expansion of the universe, so $n_i \propto R^{-3}$. In the MSSM with a neutralino LSP, all heavier sparticle states will eventually decay to the neutralino LSP, which then

freezes-out at temperatures of order $T_{fr} \sim m_{\widetilde{Z}_1}/20$. Since in the MSSM the neutralino is stable, its energy density today is given by:

$$m_{\widetilde{Z}_1} n^0_{\widetilde{Z}_1} = m_{\widetilde{Z}_1} \bar{n}_{\widetilde{Z}_1}(T_{fr}) \left(\frac{R^3_{fr}}{R^3_0}\right) \tag{4.8}$$

where $n^0_{\widetilde{Z}_1}$ is the number density of neutralinos today and R_{fr} (R_0) is the scale factor at freeze-out (today). Assuming conservation of entropy, $g_*(T)T^3R^3 = const$ [1], we have

$$\rho_{\widetilde{Z}_1} = m_{\widetilde{Z}_1} \bar{n}_{\widetilde{Z}_1}(T_{fr}) \left(\frac{g_*(T_0)T^3_0}{g_*(T_{fr})T^3_{fr}}\right) . \tag{4.10}$$

Combining Eqs.(4.7) and (4.10) we estimate the neutralino relic density as:

$$\Omega_{\widetilde{Z}_1} h^2 \equiv \frac{\rho^0_{\widetilde{Z}_1}}{\rho_c/h^2} = \frac{H(T_{fr})}{\rho_c/h^2} \frac{m_{\widetilde{Z}_1}}{\langle\sigma v\rangle} \frac{g_*(T_0)}{g_*(T_{fr})} \frac{T^3_0}{T^3_{fr}} \tag{4.11}$$

where $\rho_c = 8.1h^2 \times 10^{-47}$ GeV^4 is the critical density and $h = 0.73$. Assuming freeze-out during a radiation dominated universe and $T_{fr} \simeq m_{\widetilde{Z}_1}/20$, we obtain:

$$\Omega_{\widetilde{Z}_1} h^2 \simeq \left(\frac{1.7 \times 10^{-10}\ \text{GeV}^{-2}}{\langle\sigma v\rangle}\right) . \tag{4.12}$$

After neutralino freeze-out the universe is mainly composed of a non-relativistic neutralino component and the radiation gas, composed only of SM particles in thermal equilibrium. The neutralino energy density simply scales as R^{-3}, while $\rho_R \propto R^{-4}$.

[1] This relation is only valid under the assumption that entropy is conserved and $g_{*S} = g_*$, so $S = g_{*S}T^3R^3 = g_*T^3R^3 = const$, where g_{*S} counts the number of relativistic degrees of freedom contributing to the entropy and is given by

$$g_{*S} \equiv \sum_{Bosons} \left(\frac{T_B}{T}\right)^3 + \frac{7}{8} \sum_{Fermions} \left(\frac{T_F}{T}\right)^3 \tag{4.9}$$

Although the conservation of entropy assumption can be violated in the PQMSSM, as discussed in Sec.5.3, the approximation $g_{*S} = g_*$ is always valid for temperatures above 1 MeV, where the electroweak and strong interaction rates are sufficiently high to keep all light (relativistic) particles in thermal equilibrium, so $T_F = T_B = T$ and $g_* = g_{*S}$ (see Eq.(4.2)). Since all of our results only concern temperatures above 1 MeV, we will always assume $g_{*S} = g_*$.

Therefore, for low enough temperatures (or large enough R), $\rho_{\widetilde{Z}_1} > \rho_R$ and the universe becomes matter dominated. Imposing $\Omega_{\widetilde{Z}_1} h^2 = \Omega_{DM} h^2 = 0.1123$ we have:

$$T_{\widetilde{Z}_1 = R} \simeq 5.5 \text{ eV} \quad (\text{matter} - \text{radiation equality}) \, . \tag{4.13}$$

However, for T much above the matter-radiation equality temperature, the neutralino component can be neglected and the universe is radiation dominated. After neutralino freeze-out the next particle species to decouple from the thermal bath are neutrons and neutrinos, since these only interact through weak interactions. Neutrinos are kept in thermal equilibrium through $e^+ + e^- \leftrightarrow \bar{\nu} + \nu$, while neutrons stay in equilibrium through $e^+ + \nu \leftrightarrow \bar{n} + p$ and its associated processes. Assuming $T \gtrsim m_e$, the cross-sections for the above processes are of order $G_F^2 T^2$. Since $\bar{n}_{e,\nu} \sim T^3$, Eq.(4.7) gives:

$$G_F^2 T_{fr}^2 \times T_{fr}^3 = H(T_{fr}) \Rightarrow T_{fr} \sim \left(M_{Pl} G_F^2\right)^{-1/3} \sim 1 \text{ MeV} \, . \tag{4.14}$$

Therefore neutrinos and neutrons decouple at temperatures of order 1 MeV.

For $T < 1$ MeV, neutrinos will simply evolve as a decoupled relativistic fluid, since they are stable. On the other hand, neutrons have a lifetime of $\sim$ 15min and after decoupling will decay to protons. Thus, from Eq.(4.5), we have that after decoupling the neutron number will approximately follow:

$$N_n(T) = (n_n R^3) = (\bar{n}_n(T_{fr}) R^3) e^{-t/\tau_n} \quad (\text{for T} \ll 1 \text{ MeV}) \, . \tag{4.15}$$

The neutron to proton conversion stops once neutrons and protons start to form ${}^4H_e$. This happens around $T = T_{NC} \sim 0.1$ MeV ($t \sim$ 3min). The abundance of ${}^4H_e$ is largely controlled by the neutron-to-proton ratio at these temperatures. Since the

total number of nucleons (protons plus neutrons) is conserved, we have:

$$\bar{N}_n(T_{fr}) + \bar{N}_p(T_{fr}) = N_n(T_{NC}) + N_p(T_{NC}) \ . \tag{4.16}$$

Combining the above expression with Eq.(4.15) and the neutron and proton equilibrium densities ($\bar{n}_{p,n} = 2(m_{p,n}T/2\pi)^{3/2}\exp[-m_{p,n}/T]$), we have:

$$\frac{N_p(T_{NC})}{N_n(T_{NC})} = e^{t_{NC}/\tau_n}\left(1 + \exp[(m_n - M_{Pl})/T_{fr}]\right) - 1 \sim 7 \tag{4.17}$$

where we used $T_{fr} = 0.8$ MeV. The above result is extremely important for constraining new physics and will be discussed in more detail in Sec.4.1.

Although ^4He is abundantly produced in the early universe, smaller quantities of ^2H, ^3He and ^7Li are also produced at relevant quantities. The abundance of all of these are essentially a function of only two parameters, the neutron and proton number densities at temperatures near 0.1 MeV. If we assume the standard thermal history described above, the neutron-to-proton ratio is fixed at $\sim 1/7$ and all the light element abundances become a function of a single parameter, the total number of nucleons, or as more commonly used, the nucleon-to-photon ratio:

$$\eta \equiv \frac{n_N}{n_\gamma} = 2.68 \times 10^{-8}(\Omega_B h^2) \tag{4.18}$$

where Ω_B is the baryon relic density. The synthesis of light elements (also known as Big Bang Nucleosynthesis) stops at temperatures of order $T \sim 0.01$ MeV ($t \sim 1$hr). Although light elements are still synthesized in stars at much later times, most of their current abundance is still determined by the primordial nucleosynthesis and can be obtained from astrophysical data. The fact that all the measured values for

the light element abundances consistently give the same value for η (within their experimental and theoretical uncertainties) represents a great achievement of the standard cosmological picture outlined above. The combined result gives[5]:

$$\eta = (6.2 \pm 0.2) \times 10^{-10} \, . \tag{4.19}$$

The fact that the above number is so small, but not zero, is known as the *Matter-Antimatter Asymmetry Problem*, discussed in Sec.4.2.

Although the evolution of the universe after the end of Big Bang nucleosynthesis (BBN) is an extremely rich subject and still a very active area of research, it is not relevant for most of our subsequent discussion. This is in part due to the successful predictions of BBN which strongly constrain the physics at $T \lesssim 1$ MeV to be "Standard Model-like" (plus a dark matter component). Therefore, instead of proceeding with our discussion of the thermal history of the universe, in the next Section we re-examine BBN in more detail, focusing on how it constrains physics beyond the Standard Model (or MSSM).

4.1 Big-Bang Nucleosynthesis and New Physics

As discussed in the last section, the abundance of ^4He is an important prediction of BBN. The $^4He/H$ ratio is given by the neutron-to-proton ratio, estimated in Eq.(4.17) under the assumption that only Standard Model particles (namely γ's, e's, p's, n's and ν's) and a (harmless) cold dark matter component were present at $T \lesssim 1$ MeV. Here we review the implications of relaxing this assumption and how it affects the

neutron-to-proton ratio prediction.

New particles present at $T \sim 1$ MeV can affect n_n/n_p even if they have already decoupled at the time of neutron freeze-out. This can happen through their contribution to the total energy density of the universe. The success of BBN predictions require a radiation dominated universe at $T \lesssim 1$ MeV, since the neutron freeze-out temperature depends on $H(T_{fr})$, as shown in Eq.(4.7). If we parametrize any new source of energy as:

$$\rho_x = \rho_R \frac{\Delta g_*(T)}{g_*(T)} \tag{4.20}$$

we have

$$H(T) = \sqrt{\frac{8\pi^2}{90}} \frac{T^2}{M_{Pl}} \left(g_*(T) + \Delta g_*(T)\right)^{1/2} \ . \tag{4.21}$$

Then the measured ^4He abundance requires[39]:

$$g_*(T_{fr}) + \Delta g_*(T_{fr}) < 12.25 \Rightarrow \Delta g_*(\sim 1 \text{ MeV}) < 1.5 \tag{4.22}$$

where we have assumed three neutrino flavors. If the new particle is a relativistic boson (fermion), the above constraint implies $T_x/T \lesssim 1.10(1.14) g_x^{-1/4}$, where g_x is the number of new degrees of freedom and T_x is the temperature of the (decoupled) new particle gas.

Although extra relativistic degrees of freedom can also be constrained from the Cosmic Microwave Background (CMB) data since they affect the temperature of matter-radiation equality, these constraints are usually milder than the BBN one just discussed. Therefore we will not consider them.

Big Bang nucleosynthesis also provides important constraints on unstable particles

with lifetimes greater than 10^{-2}s. Late decaying particles can inject high energy photons, electrons or hadrons into the thermal bath and destroy already formed light elements or affect their formation. The effects of extra electromagnetic and hadronic energy injected in the primordial plasma requires a complex calculation, which has been carried out in detail by several groups[40, 41, 42]. These groups have shown that the injection of hadronic energy tends to convert protons into neutrons and results in an overproduction of ^4He, ^2H, ^6Li and ^3He. For unstable relics with lifetimes $\tau_x \lesssim 10^2$s, the strongest constraints come from overproduction of ^4He, while for $10^2\text{s} \lesssim \tau_x \lesssim 10^3$s, the most stringent constraint comes from overproduction of ^2H[40]. For even larger lifetimes, overproduction of ^6Li and ^3He requires extremely small unstable relic densities in order to satisfy the BBN constraints. However, if the unstable relic has a small branching ratio to hadrons, the constraints are much milder, since the neutron-to-proton ratio is not significantly altered. Nonetheless, highly energetic electrons and photons can still destroy light elements and suppress their formation. In this case, the constraints are only relevant for lifetimes greater than 10^4s.

For all our subsequent analysis we will use the BBN bounds obtained in Ref.[40], where it is assumed that the unstable particle decays into $\bar{q}q$ pairs with branching ratio B_h and into electrons and photons with branching ratio $1 - B_h$. In both cases the total energy of the final particles is assumed to be M_x, the late decaying particle mass. For the convenience of the reader, we reproduce in Fig.4.1 the bounds from Ref.[40], used in Secs.6-8.

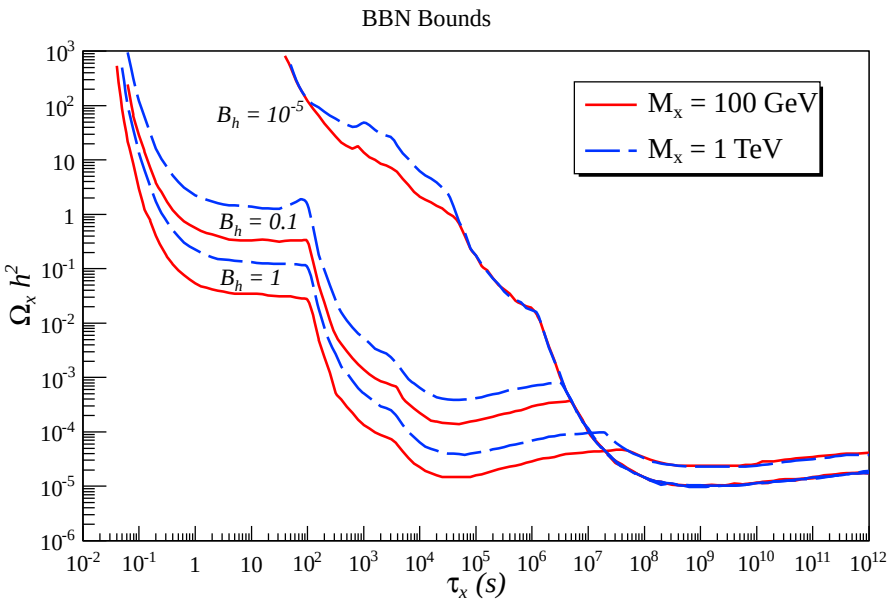

Figure 4.1: BBN constraints on the relic density of late decaying particles as a function of their lifetime. The area to the right of the curve is excluded. The red-solid lines corresponds to $M_x = 100$ GeV, while the dashed-blue lines to $M_x = 1$ TeV. For each mass, the distinct curves correspond to hadronic branching ratio (B_h) values equal to 1, 0.1 and 10^{-5} (bottom to top). Plot reproduced from Jedamzik, Ref.[40].

4.2 The Gravitino Problem

During the discussion of the thermal history of the MSSM cosmology at the beginning of Sec.4, we assumed that, by the time of neutralino freeze-out ($T_{fr} \sim m_{\widetilde{Z}_1}/20$), all other sparticles had already decayed or co-annihilated. Hence, for $T < T_{fr}$, the only consequence of supersymmetrizing the SM was the presence of a cold and decoupled neutralino DM component. However, this picture ignores an important implication of the MSSM, the presence of the Gravitino ($\widetilde{G}$). This R-parity-odd, spin 3/2 particle is

the superpartner of the spin 2 graviton and acquires a mass $m_{\widetilde{G}} \equiv m_{3/2} \sim M_S^2/M_{Pl}$, where M_S is the SUSY breaking scale and M_{Pl} is the Planck mass. Since all the gravitino interactions to the visible sector are suppressed by $1/M_{Pl}$, it was never in thermal equilibrium with the primordial plasma. Nonetheless, gravitinos can still be produced out-of-equilibrium as shown by Eq.(4.5):

$$\dot{n}_{\widetilde{G}} + 3Hn_{\widetilde{G}} = -\langle\sigma v\rangle(n_{\widetilde{G}}^2 - \bar{n}_{\widetilde{G}}^2) + \Gamma_{j\to\widetilde{G}+X}\bar{n}_j \tag{4.23}$$

where we have assumed high temperatures (early times), so the gravitino decay term can be safely neglected. The equilibrium value for the gravitino number density ($\bar{n}_{\widetilde{G}}$) is always much smaller than its actual number density ($n_{\widetilde{G}}$), since $\langle\sigma v\rangle \ll 1$. Hence:

$$\dot{n}_{\widetilde{G}} + 3Hn_{\widetilde{G}} \simeq \langle\sigma v\rangle\bar{n}_{\widetilde{G}}^2 + \Gamma_{j\to\widetilde{G}+X}\bar{n}_j \ . \tag{4.24}$$

Therefore, although extremely suppressed when compared with the number densities of other particles in thermal equilibrium, the gravitino will still have a non-zero number density, given by the integral of Eq.(4.24) from T_R to T[43]:

$$\frac{n_{\widetilde{G}}}{s} = Y_{\widetilde{G}} \simeq \frac{\gamma}{Hs}|_{T=T_R} \quad (\text{for } T \ll T_R) \tag{4.25}$$

where $\gamma = \langle\sigma v\rangle\bar{n}_{\widetilde{G}}^2 + \Gamma_{j\to\widetilde{G}+X}\bar{n}_j$ and $s = 2\pi^2 g_*(T)T^3/45$ is the entropy density. The production rate γ and the solution to Eq.(4.24) have been computed in Refs.[44, 45, 43]. Here, we use the expression obtained in Ref.[45], which is appropriate for the case of non-universal gaugino masses:

$$\Omega_{\widetilde{G}}^{\rm TP}h^2 = \sum_{i=1}^{3}\omega_i g_i^2(T_R)\left(1 + \frac{M_i^2(T_R)}{3m_{\widetilde{G}}^2}\right)\ln\left(\frac{k_i}{g_i(T_R)}\right)\left(\frac{m_{\widetilde{G}}}{100\ \text{GeV}}\right)\left(\frac{T_R}{10^{10}\ \text{GeV}}\right) \tag{4.26}$$

where $\omega_i = (0.018, 0.044, 0.117)$, $k_i = (1.266, 1.312, 1.271)$, g_i are the gauge couplings evaluated at $Q = T_R$ and M_i are the gaugino masses also evaluated at $Q = T_R$.

If the gravitino is the LSP, it is stable and composes part (or all) of the DM relic density. On the other hand, if the gravitino is not the LSP, it cascade decays to the LSP particle. In this case, from Eq.(4.5) (with $T \ll T_{fr}^{LSP}$) we have:

$$\dot{n}_{LSP} + 3Hn_{LSP} = \Gamma_{\widetilde{G}\to LSP+X} n_{\widetilde{G}} \tag{4.27}$$

Since for $T < m$, number and energy density are related by[35] $\rho = m \times n$, the above equation gives:

$$\dot{\rho}_{LSP} + 3H\rho_{LSP} = \frac{m_{LSP}}{m_{\widetilde{G}}} \Gamma_{\widetilde{G}\to LSP+X} \rho_{\widetilde{G}} \, . \tag{4.28}$$

Therefore, the gravitino contribution to the LSP relic density is given by

$$\Omega_{LSP}^{\widetilde{G}} h^2 = \frac{m_{LSP}}{m_{\widetilde{G}}} \Omega_{\widetilde{G}} h^2 \tag{4.29}$$

where the above equation also applies to the gravitino LSP scenario, since in this case the mass ratio on the left-hand side of Eq.(4.29) is one. Fig.4.2a shows contours of $\Omega_{\widetilde{G}} h^2$, given by Eq.(4.26), in the $m_{\widetilde{G}}$ *vs.* T_R plane, with $(m_{\tilde{g}}, m_{\widetilde{W}}, m_{\widetilde{B}}) = (1060, 350, 180)$ GeV. The gravitino relic density decreases with the gravitino mass until $m_{\widetilde{G}} \sim m_{\tilde{g}}$, when it starts to increase, since the $M_i^2/3m_{\widetilde{G}}^2$ term in Eq.(4.26) becomes suppressed. As we can see, a large portion of the $m_{\widetilde{G}}$ *vs.* T_R plane gives too much dark matter ($\Omega_{\widetilde{G}} h^2 > 0.1123$) for a gravitino LSP. This is still true if the gravitino is not the LSP, but $m_{LSP} \sim m_{\widetilde{G}}$, as seen from Eq.(4.29). The fact that, for a large portion of parameter space, $\Omega_{DM}^{\widetilde{G}}$ exceeds the dark matter relic density consists the first part of the Gravitino Problem. As we can see from Fig.4.2 and Eq.(4.29)

it can be solved within the MSSM for low values of the re-heat temperature and/or heavy gravitino masses and a light LSP.

The second part of the Gravitino Problem concerns the BBN bounds. Since the gravitino interactions are suppressed by $1/M_{Pl}$, the gravitino will be long-lived if it is not the LSP. On the other hand, for models with a $\widetilde{G}$ LSP, the NLSP will be long lived instead. Therefore, in both scenarios we have an unstable relic which might decay during or after BBN. The gravitino lifetime has been computed for a generic MSSM model in Ref.[46]. In Fig.4.2b we show the gravitino lifetime versus its mass, assuming two mSUGRA points, one with a light and one with a heavy SUSY spectrum. As we can see, unless the gravitino is extremely heavy ($m_{\widetilde{G}} \gtrsim 50$ TeV), its lifetime can easily exceed 10^{-2}s, where the BBN bounds start to apply. Since in SUGRA models the gravitino mass is expected to be of order the other sparticles, we expect in this case $m_{\widetilde{G}} \sim 1$ TeV, which gives $\tau_{\widetilde{G}} \sim 10^5$s. For such long lifetimes, the BBN constraints require $\Omega_{\widetilde{G}} h^2 \lesssim 10^{-5}$ (see Fig.4.1). Therefore, from Fig.4.2a, we see that BBN bounds require $m_{\widetilde{G}} \gtrsim 50$ TeV or $T_R \lesssim 10^5$ GeV (for $m_{\widetilde{G}} \lesssim 1$ TeV). Since in supergravity (SUGRA) models we expect $m_{\widetilde{G}} \sim m_{sparticles}$, the first condition is in tension with the naturalness arguments from Sec.2.1, which require $m_{sparticles} \lesssim 1$ TeV. The second requirement, a low re-heat temperature, can conflict with baryogenesis mechanisms, such as thermal leptogenesis, as discussed next.

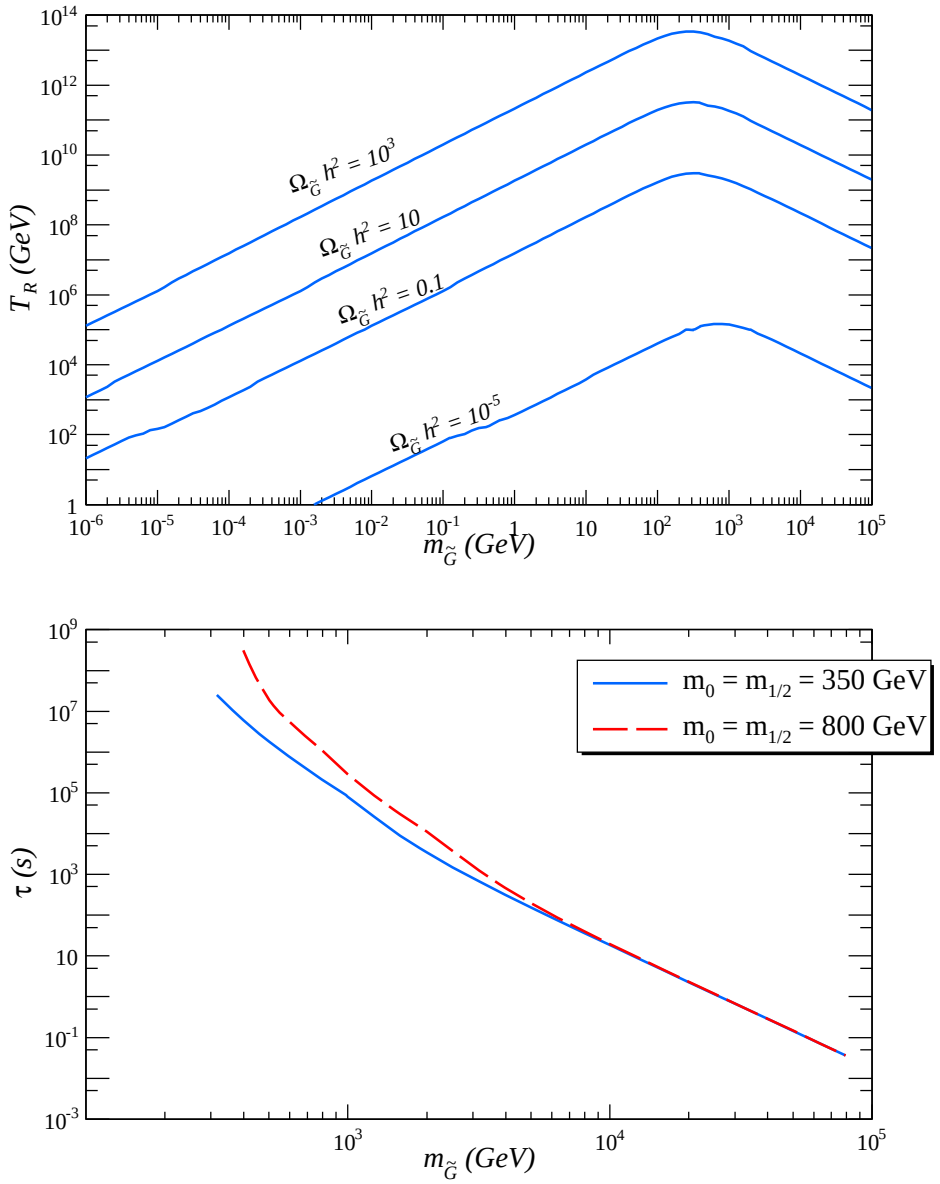

Figure 4.2: *Upper Frame*: Contours of $\Omega_{\widetilde{G}}h^2$ in the T_R *vs.* $m_{\widetilde{G}}$ plane obtained using Eq.(4.26). The assumed SUSY spectrum has $(m_{\tilde{g}}, m_{\widetilde{W}}, m_{\widetilde{B}}) = (1060, 350, 180)$ GeV. *Lower Frame*: Gravitino lifetime as function of the gravitino mass. The solid blue line corresponds to the mSUGRA point $(m_0, m_{1/2}, A_0, \tan\beta, \mu) = (350\ \text{GeV}, 350\ \text{GeV}, 0, 10, > 0)$, while the red dashed line has $(m_0, m_{1/2}, A_0, \tan\beta, \mu) = (800\ \text{GeV}, 800\ \text{GeV}, 0, 10, > 0)$.

From the arguments in Sec.4, we see that T_R has to be at least bigger than the neutralino freeze-out temperature, so neutralinos were in thermal equilibrium in the primordial plasma (after inflation). However, a much stronger lower limit on T_R comes from baryogenesis arguments. As mentioned in Secs.4 and 4.1, in order to explain the observed $^4He/H$ ratio, the number density of baryons has to be extremely small[5]:

$$\eta = \frac{n_b}{n_\gamma} = (6.2 \pm 0.2) \times 10^{-10} \Rightarrow n_b = (2.56 \pm 0.07) \times 10^{-7} \text{ cm}^{-3} . \tag{4.30}$$

Several mechanisms have been proposed to dynamically explain the above value[47] and all of them require at least $T_R \gtrsim 100$ GeV. One of the most attractive ones is thermal leptogenesis[48].

Thermal leptogenesis is a natural mechanism for dynamically generating a non-zero baryon density, once the see-saw mechanism is assumed to generate light neutrino masses. In this scenario, lepton number and CP are violated by the neutrino interactions, since the see-saw mechanism assumes the following Lagrangian:

$$\mathcal{L} = h_{ij} \bar{L}_i N_j \phi + \frac{1}{2} M_i \bar{N}_i^c N_i + h.c. + ... \tag{4.31}$$

where L and ϕ are the lepton and Higgs doublets and N_i are heavy Majorana neutrinos. From the above interactions we see that, if the heavy neutrino states were present in the primordial plasma, after decoupling their decays into leptons and Higgs scalars would violate lepton number and CP, resulting in $\langle L \rangle \neq 0$, as shown by the diagrams in Fig.4.3. Then sphaleron effects can partially convert the non-zero lepton number into baryon number, dynamically generating a non-zero η. As we can see from Eq.(4.31), the interesting feature of thermal leptogenesis scenarios is that the same parameters

that control the amount of lepton number violation are related to the light neutrino masses ($m_\nu \sim h\langle\phi\rangle^2/M$).

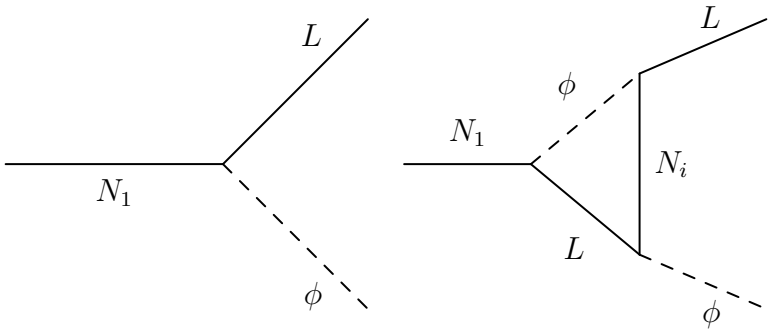

Figure 4.3: Diagrams for heavy neutrino decays leading to CP and Lepton Number violation in the early universe.

Assuming that at least the lightest N_i state (N_1) was in thermal equilibrium at $T = T_R$, the baryon number density is given by[48]:

$$\eta \simeq 0.96 \times 10^{-2} \epsilon_1 \kappa_f \tag{4.32}$$

where ϵ_1 parametrizes the amount of CP violation in the neutrino Yukawa couplings (h_{ij}) and κ_f is an efficiency factor given by:

$$k_f = (2 \pm 1) \times 10^{-2} \left(\frac{0.01 \text{ eV}}{\tilde{m}_1} \right)^{1.1 \pm 0.1} \tag{4.33}$$

where $\tilde{m}_1$ is the effective light neutrino mass, expected to be of order of m_ν. The parameter ϵ_1 is strongly model dependent, since it is given by the phases of h_{ij}. However, the maximum value of ϵ_1 can be estimated as[48]:

$$\epsilon_1 \lesssim 10^{-6} \left(\frac{M_1}{10^{10} \text{ GeV}} \right) \tag{4.34}$$

where M_1 is the mass of the lightest heavy neutrino state. Combining Eqs.(4.32), (4.33) and (4.34), we have:

$$\eta \lesssim 3 \times 10^{-31} \frac{M_1}{\tilde{m}_1} \ . \tag{4.35}$$

Imposing $\eta > 6.2 \times 10^{-10}$ and $\tilde{m}_1 > 8 \times 10^{-3}$ (the solar neutrino mass scale), we obtain the following lower limit on M_1:

$$M_1 \gtrsim 10^{10} \text{ GeV} \ . \tag{4.36}$$

Since we assumed that N_1 was in thermal equilibrium after inflation, the above lower limit on M_1 implies a lower limit on T_R. Although it is always sufficient to impose $T_R > M_1$, it can be shown that this limit can be relaxed, depending on the parameters of the model. In the general case, the minimum T_R value consistent with thermal leptogenesis is[48]:

$$T_R > 2 \times 10^9 \text{ GeV} \ . \tag{4.37}$$

From Fig.4.2, we see that the above constraint on the re-heat temperature gives $\Omega_{\widetilde{G}} h^2 \gtrsim 1$ for any value of $m_{\widetilde{G}}$. Therefore, in the thermal leptogenesis framework, both the first (too much dark matter) and second (violation of BBN bounds) parts of the Gravitino Problem can only be solved for a very heavy gravitino (to suppress its lifetime) and a much lighter LSP particle (to suppress $\Omega_{DM}^{\widetilde{G}}$). As already mentioned before, in most MSSM scenarios this is a rather unnatural condition, since the sparticle masses (including the LSP's) are expected to be of order the gravitino mass. Possible solutions for this problem in the PQMSSM framework will be discussed in Sec.6.

4.3 Neutralino Dark Matter

As shown by Eqs.(4.12) and (4.29), for the case of a neutralino LSP we have:

$$\Omega_{\widetilde{Z}_1} h^2 \simeq \left(\frac{1.7 \times 10^{-10} \text{ GeV}^{-2}}{\langle \sigma v \rangle} \right) + \frac{m_{LSP}}{m_{\widetilde{G}}} \Omega_{\widetilde{G}} h^2 \, , \tag{4.38}$$

where we have included the contribution from gravitino decays. Therefore, in order to satisfy the measured value of $\Omega_{DM} h^2 (= 0.1123)$, we need:

$$\langle \sigma v \rangle \gtrsim 1.7 \times 10^{-9} \text{ GeV}^{-2} \, . \tag{4.39}$$

However, for a bino $\widetilde{Z}_1$, which is the most natural scenario in most of the MSSM parameter space, we have:

$$\langle \sigma(\widetilde{Z}_1 + \widetilde{Z}_1 \to X) v \rangle \sim \left(\frac{\alpha^2}{m^2_{\widetilde{Z}_1}} \right) \sim 6 \times 10^{-9} \left(\frac{100 \text{ GeV}}{m_{\widetilde{Z}_1}} \right)^2 \tag{4.40}$$

where we have assumed $T \ll m_{\widetilde{Z}_1}$, which is a reasonable approximation for temperatures near freeze-out, since $T_{fr} \sim m_{\widetilde{Z}_1}/20$. Although the above result satisfies Eq.(4.39) for $m_{\widetilde{Z}_1} \lesssim 100$ GeV, more detailed calculations usually give $\langle \sigma v \rangle \lesssim 10^{-10}$ GeV^{-2} for a bino $\widetilde{Z}_1$. Therefore, in order to satisfy the dark matter relic density constraint, the neutralino cross-section has to be enhanced by new processes. This is a longstanding issue with the bino LSP scenario, but several models have been found where $\langle \sigma v \rangle$ is enhanced due to resonances, co-annihilations or through a wino/higgsino neutralino. Nonetheless, these requirements strongly constraint the MSSM parameter space, as shown in Ref.[49]. To illustrate this problem, we reproduce results from Ref.[50], where a scan over all the pMSSM (phenomenological MSSM[51]) parameter space was performed. The result can be seen in Fig.4.4, where

the number of models is plotted against their respective $\Omega_{\widetilde{Z}_1}h^2$ values. As we can see, most models indeed give too much dark matter, since they usually have a bino LSP, unless there is a significant fine-tuning of parameters. On the other hand, a considerable fraction of models have a wino or higgsino LSP and give too little dark matter, as seen in Fig.4.4. We also see that the measured dark matter relic density value lies in the "least probable" region. This shows that in general, MSSM models satisfying the dark matter constraint can be considered unnatural.

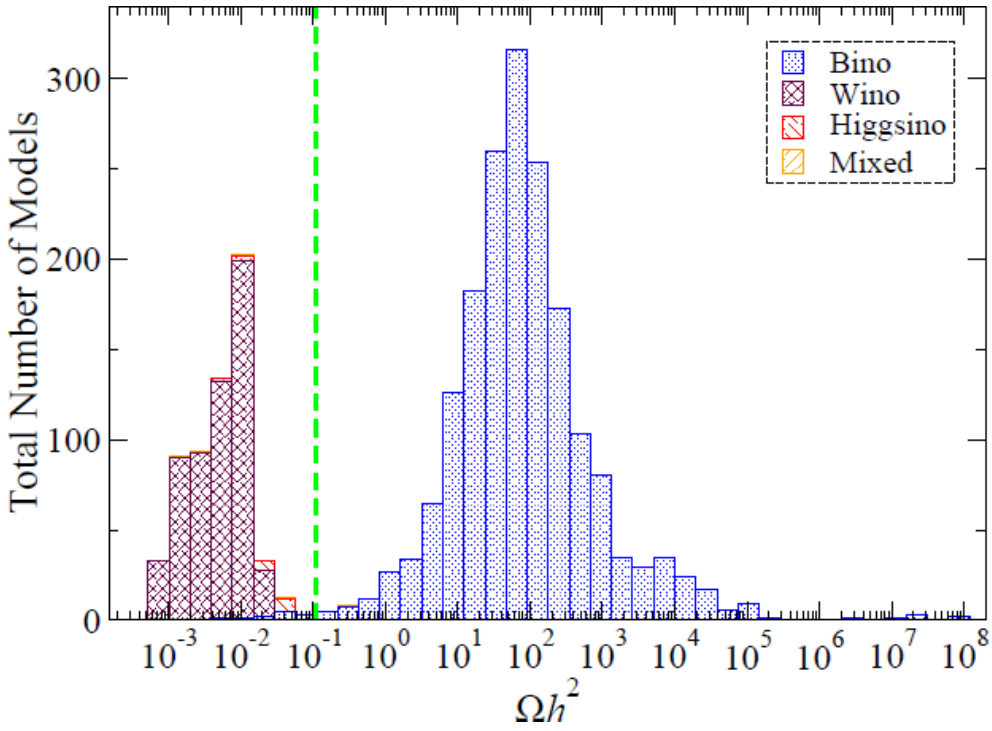

Figure 4.4: Projection of the number of models generated by a linear scan over the pMSSM parameters, versus neutralino relic density. Models with mainly bino, wino, higgsino or a mixture are indicated by the various color and symbol choices. All models are required to have $m_{\widetilde{Z}_1} < 500$ GeV to avoid too large fine-tuning in the SUSY parameters. Plot reproduced from Ref.[50]

Chapter 5

General Implications of the PQMSSM

The cosmology of PQMSSM models is very rich and has to be carefully examined. In Sec.4, we briefly reviewed the relevant aspects of the MSSM cosmology. Here we extend the previous discussion to include the axion supermultiplet, which contains the axion, saxion and axino. As we will see below, the simple inclusion of these three weakly interacting particles opens up a number of different cosmological scenarios, depending on the PQMSSM parameters.

In Secs.5.1 and 5.2, we present two mechanisms for production of axions, saxions and axinos: Thermal Production and Coherent Oscillations. A third possibility is non-thermal production of axinos from sparticle decays (if the axino is the LSP) or non-thermal production of axions from saxion decays (if the decay width of Eq.(3.14) is not suppressed). However, these are model dependent and will be discussed within the specific models presented in Secs.6-8.

Sec.5.3 discusses a possible deviation from the standard cosmological scenario described in Sec.4, where axinos or saxions may come to temporarily dominate the energy density of the universe at early times. Since in this scenario the expansion of the universe is no longer governed by the radiation component, we will briefly review the necessary ingredients required to describe the evolution of the neutralino and axion superfield in this case. Finally, in Sec.5.4 we summarize the results presented in the previous sections, which will then be applied to the particular models of Secs.6-

8.

5.1 Thermal Production

In a way very similar to the gravitino case discussed in Sec.4.2, axions, saxions and axinos can be produced in the early thermal plasma from scattering of particles in equilibrium. Their relic density can then be computed using Eqs.(4.24) and (4.25) with $n_{\widetilde{G}} \to n_i$ and the appropriate cross-sections (γ terms). However, unlike the gravitino, the axion superfield may also be in thermal equilibrium at early times, if the re-heat temperature (T_R) is higher than its decoupling temperature[29]:

$$T_{dec} = 10^{11}\ \text{GeV} \left(\frac{f_a}{10^{12}\text{GeV}}\right)^2 \left(\frac{0.1}{\alpha_s}\right)^3 . \tag{5.1}$$

In this case, their thermal abundances are simply given by the equilibrium value[35]:

$$\bar{n}_a = \bar{n}_s = \frac{\xi(3)}{\pi^2} T^3 \ \text{ and } \ \bar{n}_{\tilde{a}} = \frac{3\xi(3)}{2\pi^2} T^3 . \tag{5.2}$$

Combining these two results, the axion, saxion and axino thermal yields are estimated as[52, 53, 54]:

$$\begin{aligned}
Y_a = \frac{n_a}{s} &\approx \begin{cases} 1.2 \times 10^{-3} & , \text{if } T_R > T_{dec} \\ 18.6 g_s^6 \ln(\frac{1.501}{g_s})(\frac{T_R}{10^{14}\ \text{GeV}})(\frac{10^{12}\ \text{GeV}}{f_a})^2 & , \text{if } T_R < T_{dec} \end{cases} \\
Y_s = \frac{n_s}{s} &\approx \begin{cases} 1.2 \times 10^{-3} & , \text{if } T_R > T_{dec} \\ (\frac{T_R}{10^{14}\ \text{GeV}})(\frac{10^{12}\ \text{GeV}}{f_a})^2 & , \text{if } T_R < T_{dec} \end{cases} \\
Y_{\tilde{a}} = \frac{n_{\tilde{a}}}{s} &\approx \begin{cases} 1.8 \times 10^{-3} & , \text{if } T_R > T_{dec} \\ 9.2 g_s^6 \ln(\frac{3}{g_s})(\frac{T_R}{10^{14}\ \text{GeV}})(\frac{10^{12}\ \text{GeV}}{f_a})^2 & , \text{if } T_R < T_{dec} \end{cases}
\end{aligned} \tag{5.3}$$

where g_s is the strong coupling constant at $T = T_R$. If entropy is always conserved from T_R to T_0, the above expressions are still valid at $T = T_0$ and can be used to compute the thermal relic density today:

$$\Omega_i^{TP} h^2 = \frac{s(T_0)}{\rho_c/h^2} m_i \frac{n_i}{s} \simeq 2.741 \times 10^8 \frac{m_i}{\text{GeV}} Y_i \tag{5.4}$$

where $i = a, s$ or $\tilde{a}$.

5.2 Coherent Oscillation

Besides being produced from scattering of particles in the thermal bath, the saxion and axion fields can also contribute to the energy density through coherent oscillations. The theory of cosmological coherent oscillations has been discussed in detail in Ref.[55]. Here, we present a simplified discussion, but sufficient for the axion and saxion cases.

The equation of motion for (homogeneous) axion or saxion fields in an expanding universe is given by:

$$\ddot{\phi} + 3H\dot{\phi} + \frac{dV}{d\phi} = 0 \tag{5.5}$$

where $\phi = a$ or s, $V(\phi)$ is the scalar potential for ϕ and H is the expansion rate, as usual. Eq.(5.5) can also be conveniently written as:

$$\dot{\rho} = -3H\dot{\phi}^2 + \frac{\partial V}{\partial t} \tag{5.6}$$

where $\rho = \dot{\phi}^2/2 + V$ is the energy density of ϕ. For small values of ϕ, the scalar potential is dominated by the mass term: $V \simeq m^2\phi^2/2$. Thus, in the limit $m^2\phi/\dot{\phi} \ll$

H, Eq.(5.5) gives $\phi \simeq const.$ On the other hand, for $m^2\phi/\dot{\phi} \gg H$, we have

$$\ddot{\phi} \simeq -m^2\phi \Rightarrow \phi \sim e^{i\omega t} \tag{5.7}$$

where $\omega = m \sim \dot{\phi}/\phi$. Therefore, for $\omega \ll H$ we have a constant field, while for $\omega \gg H$ we have a highly oscillatory field.

Since we are interested in the cosmological evolution of ϕ, which happens at time scales $1/H$, in the highly oscillatory regime we can take the average over oscillations, so

$$\langle\dot{\phi}^2\rangle = m^2\langle\phi^2\rangle = 2\langle V\rangle \Rightarrow \langle\rho\rangle = 2\langle V\rangle = \langle\dot{\phi}^2\rangle \, . \tag{5.8}$$

Hence, from Eq.(5.6):

$$\dot{\rho} = -3H\rho + \frac{\partial V}{\partial t} \tag{5.9}$$

where we have dropped the time average brackets for simplicity. Assuming $V = m^2\langle\phi^2\rangle/2 = m^2\rho/2$ (where m may be time dependent), the above equation gives:

$$\dot{\rho} + 3\frac{\rho}{R}\dot{R} - \frac{\rho}{m}\dot{m} = 0 \Rightarrow \frac{d}{dt}\left(\frac{\rho R^3}{m}\right) = 0 \, . \tag{5.10}$$

If m is time independent, $\rho \propto R^{-3}$, so ρ behaves as the energy density of a matter fluid.

From the above discussion we see that coherent oscillations will approximately start when

$$3H = \omega \Rightarrow 3H(T_{osc}) = m(T_{osc}) \tag{5.11}$$

where we have allowed for the possibility of a temperature (or time) dependent mass. For a radiation dominated universe $H(T) \sim T^2/M_{Pl}$, so the oscillations start at

$T \sim \sqrt{M_{Pl} m} \gg m$. Therefore, ρ behaves as matter density, despite the universe temperature being much above the field's mass. We also point out that for coherent oscillations to take place the field needs to have $\partial_\mu \phi / \phi \ll 1$ and $\phi \neq 0$ at early times ($H \gg \omega$). This is definitely not valid for particles produced thermally. The solution of Eq.(5.10) gives:

$$\rho = \rho_{osc} \left(\frac{R_{osc}}{R} \right)^3 \frac{m(T)}{m(T_{osc})} \tag{5.12}$$

where R_{osc} is the universe scale factor at $T = T_{osc}$ and ρ_{osc} is the initial energy density:

$$\rho_{osc} = \frac{1}{2}\dot{\phi}^2 + V \simeq \frac{1}{2} m^2(T_{osc}) \phi_0^2 \tag{5.13}$$

since $\dot{\phi}$ is supposed to be small before the field starts to oscillate.

Since the saxion mass is approximately fixed as $m_{3/2}$ after SUSY breaking, applying Eq.(5.12) for the saxion field gives:

$$\rho_s^{CO} = \frac{1}{2} m_s^2 s_i^2 \left(\frac{R_{osc}}{R} \right)^3 \tag{5.14}$$

where s_i is the initial saxion field amplitude.

On the other hand, the axion field only acquires a mass after the QCD phase transition (where the chiral anomaly becomes relevant), so its potential is given by (see Sec.3.1):

$$V_{eff}(a) = m_a(T)^2 f_a^2 [1 - \cos(a/f_a)] \simeq \frac{1}{2} m_a(T)^2 a^2 \tag{5.15}$$

where we assumed small axion field values and $m_a(T)$ is given by Eq.(3.4). Hence, for $T < \Lambda_{QCD}$,

$$\rho_a^{CO} = \frac{1}{2} m_a(T_a) m_a^0 \theta_i^2 f_a^2 \left(\frac{R_{osc}}{R} \right)^3 \tag{5.16}$$

where $\theta_i f_a$ is the initial axion field amplitude. A more detailed calculation, also valid for large θ_i, gives[56, 21]

$$\rho_a^{CO} = \frac{1}{2}\chi f(\theta_i) m_a(T_a) m_a^0 \theta_i^2 f_a^2 \left(\frac{R_{osc}}{R}\right)^3 \tag{5.17}$$

where $\chi = 1.44$ corrects for the continuous transition from the static to the oscillatory regime and $f(\theta_i) = \ln[e/(1-\theta_i^2/\pi^2)]^{7/6}$ is a correction factor for large θ_i values.

A comment is in order about the initial field amplitudes for the axion and saxion fields (θ_i and s_i). In principle these are fixed at very high energies by the specific form of the PQMSSM scalar potential, which must include supergravity corrections and the full PQMSSM model, including its heavy PQ modes, such as the heavy quark superfields in the KSVZ model or the singlet superfields in the DFSZ model. Nonetheless, in the absence of fine-tuning, the natural value for s_i and θ_i is the PQ scale, f_a, since the field amplitudes are fixed at this scale.

Applying Eq.(5.11) for the saxion and axion fields we have:

$$3H(T_s) = m_s \;\text{ and }\; 3H(T_a) = m_a(T_a)\ . \tag{5.18}$$

To compute T_s and T_a, as well as the R/R_{osc} factor in Eqs.(5.14) and (5.17), we need to know $H(T)$. Assuming a radiation dominated universe and conservation of entropy,

$$H(T) = \sqrt{\frac{8\pi^3}{90} g_*(T)}\frac{T^2}{M_{Pl}} \;\text{ and }\; g_*(T)T^3R^3 = g_*(T_{osc})T_{osc}^3 R_{osc}^3, \tag{5.19}$$

gives

$$
\begin{aligned}
T_s &= \sqrt{M_{Pl} m_s} \left(\frac{5}{4\pi^3} \frac{1}{g_*(T_s)} \right)^{1/4} \\
T_a &= \begin{cases} \sqrt{M_{Pl} m_a^0} \left(\frac{5}{4\pi^3} \frac{1}{g_*(T_a)} \right)^{1/4}, & \text{if } T_a < \Lambda_{QCD} \\ \left(M_{Pl} m_a^0 b \Lambda_{QCD}^4 \right)^{1/6} \left(\frac{5}{4\pi^3} \frac{1}{g_*(T_a)} \right)^{1/12}, & \text{if } T_a > \Lambda_{QCD} \end{cases} .
\end{aligned} \tag{5.20}
$$

Using the above results and Eq.(5.14) for the saxion energy density we obtain:

$$
\frac{\rho_s}{s} = 2.97 \times 10^{-4} g_*(T_s)^{-1/4} \left(\frac{m_s}{\text{GeV}} \right)^{1/2} \left(\frac{s_i}{f_a} \right)^2 \left(\frac{f_a}{10^{12}\ \text{GeV}} \right)^2 \tag{5.21}
$$

while for the axion:

$$
\frac{\rho_a}{s} = \begin{cases} 3.37 \times 10^{-11} f(\theta_i) \theta_i^2 g_*(T_a)^{-1/4} \left(\frac{f_a}{10^{12}\ \text{GeV}} \right)^{3/2} & , \text{ if } T_a < \Lambda_{QCD} \\ 4.77 \times 10^{-9} f(\theta_i) \theta_i^2 g_*(T_a)^{-5/12} \left(\frac{f_a}{10^{12}\ \text{GeV}} \right)^{7/6} & , \text{ if } T_a > \Lambda_{QCD} \end{cases} \tag{5.22}
$$

where we used Eq.(3.4) for the temperature dependent axion mass.

There are two possible exceptions for the results obtained above, both coming from a deviation from a radiation dominated universe at the beginning of oscillations. The first one concerns saxion oscillations. As discussed just after Eq.(5.11), the saxion starts to oscillate at $T_s \sim \sqrt{M_{Pl} m_s}$ for a radiation dominated universe. However, due to the (possibly) large saxion mass, we may have $T_s > T_R$. At temperatures above the re-heat temperature the universe is no longer dominated by the thermal plasma, but by the inflaton field and Eq.(5.19) no longer applies. Instead, during the re-heating period, the inflaton-dominated universe satisfies[35]:

$$
H(T) = H(T_R) \frac{g_*(T) T^4}{g_*(T_R) T_R^4} \quad \text{and} \quad \frac{g_*(T) T^4}{g_*(T_R) T_R^4} = \left(\frac{R_{T_R}}{R} \right)^{3/2} . \tag{5.23}
$$

Using the above expressions in Eqs.(5.18) and (5.14) and combining with our previous

result for $T_s < T_R$ (Eq.(5.21)), we obtain[1]:

$$\frac{\rho_s}{s} = \begin{cases} 2.97 \times 10^{-4} g_*(T_s)^{-1/4} \left(\frac{m_s}{\text{GeV}}\right)^{1/2} \left(\frac{s_i}{f_a}\right)^2 \left(\frac{f_a}{10^{12}\ \text{GeV}}\right)^2 & , \text{ if } T_s < T_R \\ 1.9 \times 10^{-8} \frac{T_R}{10^5\ \text{GeV}} \left(\frac{s_i}{f_a}\right)^2 \left(\frac{f_a}{10^{12}\ \text{GeV}}\right)^2 & , \text{ if } T_s > T_R \end{cases} . \quad (5.24)$$

The second scenario, which invalidates Eq.(5.22), is the one where the universe becomes matter dominated at some temperature 5 MeV $\lesssim T < T_R$ (the lower bound comes from the BBN constraints) and the axion starts to oscillate during this era[2]. This early matter dominated scenario is discussed below.

5.3 Early Matter Dominated Universe

An interesting possibility in PQMSSM models is the scenario where one of the components of the axion supermultiplet is produced at large rates in the early universe (before BBN) and, as the universe cools down, becomes the dominant form of energy at some temperature T_e. This is possible because, for non-relativistic or coherent oscillating particles, the energy density decreases as R^{-3}, while $\rho_R \propto R^{-4}$. Therefore, at some temperature the former will surpass the latter and dominate the energy density. It is clear, however, that in order to preserve the successful BBN predictions, this particle has to decay before light elements start to form at $T \sim 5$ MeV. This clearly excludes an early axion domination, since the axion is stable. Thus we only need to consider the possibility of an early saxion or axino dominated scenario. Since most

[1] Eq.(5.24) for the energy density of coherent oscillating saxions differ from the ones computed in Refs.[57] and [53] by a numerical factor, because these authors assume the oscillation condition $H(T_s) = m_s$ instead of Eq.(5.11).

[2] In principle, there can also be scenarios where the saxion starts to oscillate in an axino dominated era. However we will not consider such cases in our subsequent discussion.

of the discussion is identical to both saxions and axinos, we will generically denote both fields by X.

To discuss this scenario we define the following relevant temperatures:

- T_e: the temperature at which X starts to dominate the energy density. T_e can be calculated imposing $\rho_X(T_e) = \rho_R(T_e)$:

$$T_e = \frac{4}{3}\frac{\rho_X}{s} \ . \tag{5.25}$$

- T_S: the temperature at which X starts to decay and inject entropy in the cosmic soup. An approximate expression for T_S is derived in Appendix B, which gives:

$$T_S \simeq \left(T_e T_D^4\right)^{1/5} \ . \tag{5.26}$$

- T_D: the temperature at which the matter dominated era ends and the radiation domination resumes. During the X dominated era, we have, from Eq.(4.5),

$$\dot{\rho}_X + 3H\rho_X + \Gamma_X \rho_X = 0 \tag{5.27}$$

where Γ_X is the axino/saxion decay width. From the above equation we see that, for $H \ll \Gamma_X$, ρ_X becomes exponentially suppressed and the matter dominated era ends. Therefore we can estimate T_D by:

$$H(T_D) = \Gamma_X \Rightarrow T_D = \sqrt{M_{Pl}\Gamma_X}\left(\frac{45}{4\pi^3}\frac{1}{g_*(T_D)}\right)^{1/4} \ . \tag{5.28}$$

From the above discussion, it is clear that in order for the X dominated era to take place we must have:

$$T_D < T_e \Rightarrow \frac{\rho_X}{s} > \frac{3}{4}\sqrt{M_{Pl}\Gamma_X}\left(\frac{45}{4\pi^3}\frac{1}{g_*(T_D)}\right)^{1/4} \ . \tag{5.29}$$

Therefore, the condition for an early matter dominated universe requires a large initial energy density and a small decay width, since otherwise X would decay before dominating the energy density. Because saxions and axinos have $\Gamma \propto 1/f_a^2$, as shown in Eqs.(3.11) and (3.14), they are naturally long-lived and Eq.(5.29) can be satisfied if ρ_X is large enough. This usually requires large re-heat temperatures for saxions/axinos produced thermally and large s_i for coherent oscillating saxions. Assuming that the above condition is satisfied we now proceed to investigate what are the consequences of an early saxion/axino dominated era[3].

For $T_S < T < T_e$ the universe is matter dominated (MD) and there is no significant entropy injection from X decays (entropy is conserved). In this case we have:

$$H(T) = \sqrt{\frac{8\pi}{3}\frac{\rho_X}{M_{Pl}^2}} \text{ and } S \equiv g_*(T)T^3R^3 = const\ . \tag{5.30}$$

Using Eq.(5.25) we can express ρ_X in terms of T_e:

$$\frac{\rho_X}{s}(T) = \frac{\rho_X}{s}(T_e) \Rightarrow \rho_X(T) = \frac{3}{4}T_e s = \frac{\pi^2}{30}g_*(T)T_e T^3 \tag{5.31}$$

so

$$H(T) = \sqrt{\frac{4\pi^3}{45}g_*(T)}\frac{\sqrt{T_e T^3}}{M_{Pl}}\ . \tag{5.32}$$

For $T_D < T < T_S$, the universe is dominated by the decaying X particle (DD), so entropy is no longer conserved[35]. This regime is analogous to the re-heating period after inflation, discussed at the end of Sec.5.2. Assuming that most of ρ_X goes into radiation, ρ_R obeys:

$$\rho_R + 4H\rho_R = \Gamma_X \rho_X \tag{5.33}$$

[3]We always assume that either the saxion or axino comes to dominate the energy density. Although this is true for most of the PQMSSM parameter space, in principle there are some scenarios where *both* fields dominate the energy density at different times.

and we have[4]

$$H(T) = \sqrt{\frac{8\pi}{3}\frac{\rho_X}{M_{Pl}^2}} \propto R^{-3/2} \text{ and } g_*(T)T^4R^{3/2} = const\ , \tag{5.34}$$

so that

$$H(T) = H(T_D)\frac{g_*(T)T^4}{g_*(T_D)T_D^4} = \sqrt{\frac{4\pi^3}{45}}\frac{g_*(T)}{\sqrt{g_*(T_D)}}\frac{T^4}{M_{Pl}T_D^2}\ . \tag{5.35}$$

The ratio of entropy before and after X decays can be computed using Eq.(5.34):

$$r \equiv \frac{S_f}{S_i} = \frac{g_*(T_D)T_D^3R_D^3}{g_*(T_S)T_S^3R_S^3} = \frac{g_*(T_S)T_S^5}{g_*(T_D)T_D^5} = \frac{g_*(T_S)T_e}{g_*(T_D)T_D} \simeq \frac{T_e}{T_D} \tag{5.36}$$

where we have used Eq.(5.26). Clearly the above expression for r is only valid for $T_e > T_D$ (X dominated universe) or $r > 1$. However, if the X never dominates the universe, the entropy injection is negligible[58], so we assume $r = 1$ if $T_e < T_D$.

Finally, for $T < T_D$, the universe is once again radiation dominated (RD) and entropy is conserved:

$$H(T) = \sqrt{\frac{4\pi^3}{45}g_*(T)}\frac{T^2}{M_{Pl}} \text{ and } S \equiv g_*(T)T^3R^3 = const\ . \tag{5.37}$$

As already mentioned in Sec.5.2, the energy density for coherent oscillating saxions and axions depends on $H(T)$ and will be different if the oscillation starts in a matter-dominated (MD), decaying-particle-dominated (DD) or radiation-dominated (RD) universe. Furthermore, the expression for the neutralino relic density also depends on $H(T)$ through the freeze-out condition (see Eq.(4.7)), hence Eq.(4.12) is not valid if the neutralino decouples in a MD or DD universe. The procedure for computing the axion and neutralino relic densities in a MD and DD is identical to the one already

[4]We always assume the sudden decay approximation, so $\rho_X \propto R^{-3/2}$ for $T > T_D$ and $\rho_X = 0$, for $T < T_D$.

outlined in the radiation dominated case, so we will not repeat it here. Explicit analytical expressions for the RD, MD and DD regimes are listed in Appendix B.

To illustrate the cosmological evolution of the early matter dominated scenario, we show in Fig.5.1a the evolution of the radiation, neutralino, gravitino, axion, saxion and axino energy densities as well as the entropy ratio as a function of the scale factor R computed using the system of coupled Boltzmann equations. The gravitino and axino densities are only shown for $T < m_{\tilde{a},\widetilde{G}}$, since their contribution is negligible at higher temperatures. For simplicity, we also neglected the sub-dominant thermal axion component. As we can see, at very early times ($R \sim R_{T_R}$ or $T \sim T_R$), the energy density is dominated by radiation with a small contribution of coherent oscillating saxions (for our choice of parameters saxions start to oscillate with $T_s > T_R$ and the thermal saxion component is always sub-dominant). At $R/R_{TR} \sim 10^7$ ($T = T_e$), the saxions start to dominate the energy density and the MD era begins. At later times ($R/R_{TR} \sim 10^9$ or $T = T_{fr}$), the neutralino freezes-out and decouples from the thermal bath. This is an example where the neutralino relic density can no longer be computed using Eq.(4.12) and the equation for $\Omega^{MD}_{\widetilde{Z}_1}h^2$ from Appendix B has to be used instead. At $R/R_{TR} \sim 10^{12}$ ($T = T_a$), coherent oscillations of axions start. Since this happens during the MD era, the axion relic density will be given by the expression for $\Omega^{MD}_a h^2$ from Appendix B. At $R/R_{TR} \sim 10^{13}$ ($T = T_S$) the saxion starts to decay and inject entropy in the thermal bath, as shown by the entropy curve. This is the beginning of the decaying particle regime (DD), which ends with the complete decay of saxions at $R/R_{TR} \sim 10^{16}$ ($T = T_D$). This is where the radiation dominated (RD) era

resumes. Finally, neutralinos and gravitinos decay to axinos around $R/R_{TR} \sim 10^{18}$ ($T = T_D^{\widetilde{Z}_1}$) and $R/R_{TR} \sim 10^{19}$ ($T = T_D^{\widetilde{G}}$), respectively. In Fig.5.1b, we show the same results but as a function of the thermal bath temperature T. As we can see, the saxion entropy injection between T_S and T_D relatively re-heats[5] the thermal bath with respect to the other decoupled particles. The resulting effect is a dilution of the axion, neutralino, gravitino and axino densities as seen in Fig.5.1b. The wiggle lines around $T \sim 0.5$ GeV are due to the QCD phase transition, where the relativistic degrees of freedom become hadrons and mesons instead of quarks and gluons. We also note that for the specific choice of parameters used in Fig.5.1, the saxion dominated era ends at $T \sim 0.3$ MeV and would violate the BBN bounds discussed in Sec.4.1.

[5]Fig.5.1a shows that during the saxion decay period the energy density of radiation never increases, it only decreases with a smaller slope. Since $T \sim \rho_R^{1/4}$, the thermal bath temperature does not increase either, it only decreases more slowly. That is why the radiation re-heat is only relative in this case.

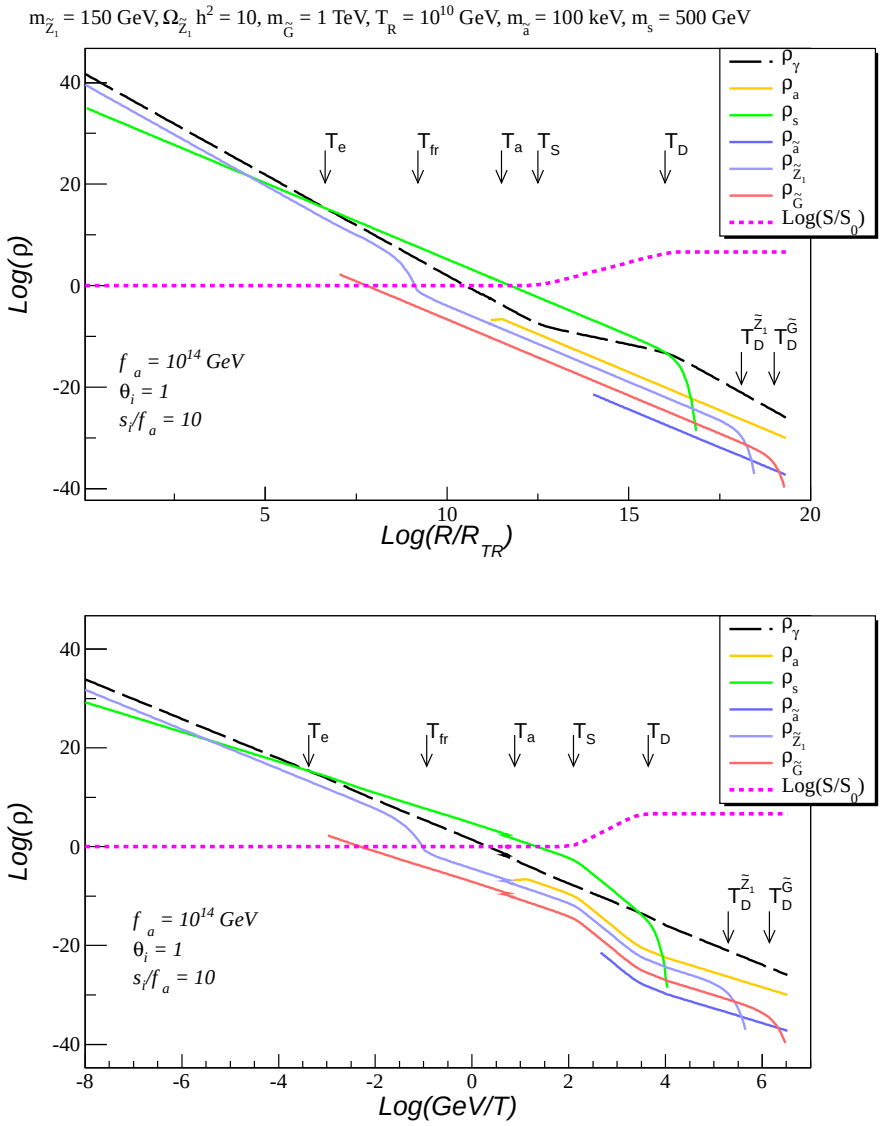

Figure 5.1: Evolution of the radiation, neutralino, gravitino, axion, saxion and axino energy densities and the entropy ratio as a function of the scale factor R (Upper Frame) and temperature (Lower Frame). We also show the temperature of saxion-radiation equality (T_e), the neutralino freeze-out temperature (T_{fr}), the temperature at which the DD era begins (T_S) and the MD era ends (T_D), the axion oscillation temperature (T_a) and the neutralino ($T_D^{\widetilde{Z}_1}$) and gravitino ($T_D^{\widetilde{G}}$) decay temperatures. The PQMSSM parameters are: $f_a = 10^{14}$ GeV, $m_s = 500$ GeV, $m_{\tilde{a}} = 100$ keV, $\theta_i = 1$, $s_i = 10 f_a$, $T_R = 10^{10}$ GeV, $m_{\widetilde{G}} = 1$ TeV, $m_{\widetilde{Z}_1} = 150$ GeV and $\Omega_{\widetilde{Z}_1}^{MSSM} h^2 = 10$.

5.4 Summary

PQMSSM models are an extension of the MSSM, where the axion superfield is included, resulting in the introduction of three new weakly interacting particles: the scalar saxion, pseudoscalar axion and the Majorana fermion axino. All of these are produced thermally in the early universe with yield proportional to $1/f_a^2$ (for $T_R < T_{dec}$), where f_a is the PQ scale, as shown in Eq.(5.3). In addition, saxions and axions can also contribute to the energy density through coherent oscillations if, at the PQ or SUSY breaking scales, they are displaced from the minimum of their (low energy) potential, resulting in a non-zero initial field amplitude θ_i and s_i.

Axions are extremely light and stable; thus cosmological axions contribute to the Dark Matter density today. While coherent axions behave as cold DM, thermal axions are likely warm or hot DM, depending on the axion mass, fixed by the PQ scale (see Eq.(3.4)). On the other hand, saxions are expected to have a mass of order $m_{3/2}$ and decay with lifetime proportional to f_a^2/m_s^3 (see Eq.(3.14)). Their decay can inject energy into the primordial plasma or add to the hot axion component, if their (model dependent) decay into axions is significant. The axino mass is highly model dependent and can take very small values of order $m_{3/2}^2/f_a$ or be at the soft SUSY scale, as the saxion mass. Light axinos are likely the LSP, hence stable. As the axion, they may constitute hot, warm or cold DM depending on the value of $m_{\tilde{a}}$. In the axino LSP scenario, the thermally produced NLSP decays to $\tilde{a}$ with the decay rates shown in Eq.(3.9), adding to the total axino abundance. Thus, the DM today would consist of a mixture of axinos and axions. On the other hand, if axinos are heavy,

they cascade decay to the LSP (here assumed to be the lightest neutralino), with the decay widths listed in Eq.(3.11). In this scenario, DM would consist of a mixture of axions and neutralinos.

If saxions are produced at large rates in the early universe (due to a large T_R, small f_a or large s_i), they can temporarily dominate the energy density of the universe, as discussed in Sec.5.3. In this scenario, all other particles decoupled from the thermal plasma during the saxion decay (such as axions, axinos, gravitinos and in some cases neutralinos), will have their energy densities diluted, as seen in Fig.5.1b. The same scenario can also happen for heavy axinos, if they are thermally produced at large rates in the early universe.

From our previous discussion we see that for most cosmological purposes, the PQMSSM parameter space can be restricted to:

$$\left\{ f_a,\ m_{\tilde{a}},\ m_s,\ s_i,\ \theta_i,\ T_R,\ \Omega^{MSSM}_{\widetilde{Z}_1} h^2 \right\} \ + \text{SUSY spectrum} \tag{5.38}$$

where the dependence on the SUSY spectrum enters indirectly through the axino or neutralino decay widths, Eqs.(3.11) and (3.9), and the gravitino relic density, Eq.(4.26). In the next Sections, we present explicit results for the different cosmological PQMSSM scenarios mentioned above and discuss what regions of the PQMSSM parameter space are consistent with the dark matter and BBN constraints.

Chapter 6

The Axino LSP

PQMSSM models with light axinos can be realized in DFSZ-type models, where the couplings between the MSSM sector and the axion superfield are very small[29], suppressing possible large corrections to the axino mass, which is zero at tree level. Here, we discuss the cosmological implications of this scenario, assuming an axino LSP and a neutralino or gravitino NLSP. As a first approximation, we will neglect the saxion component and consider only the axion and axino contributions to the thermal evolution of the universe. In Sec.6.2, we comment on the implications of including the saxion field. The discussion presented here follows closely Refs.[31, 59].

The immediate consequence of an axino LSP is that all other SUSY particles eventually cascade decay to the axino state. Since the decay rates to axinos are suppressed by $1/f_a$, we assume that all MSSM sparticles first decay to the lightest neutralino, which then decays to the axino LSP. As a result, the total dark matter relic density in this scenario is given by

$$\Omega_{DM}h^2 = \Omega_{a\tilde{a}}h^2 = \Omega_a h^2 + \Omega_{\tilde{a}}^{TP}h^2 + \Omega_{\tilde{a}}^{\widetilde{Z}}h^2 + \Omega_{\tilde{a}}^{\widetilde{G}}h^2 \tag{6.1}$$

where the last two terms represent the contributions from neutralino and gravitino decays (see Eq.(4.29))[1],

$$\Omega_{\tilde{a}}^{\widetilde{Z}} = \frac{m_{\tilde{a}}}{m_{\widetilde{Z}_1}}\Omega_{\widetilde{Z}}^{TP} \text{ and } \Omega_{\tilde{a}}^{\widetilde{G}} = \frac{m_{\tilde{a}}}{m_{\widetilde{G}}}\Omega_{\widetilde{G}}^{TP} \tag{6.2}$$

[1]Here we assume that gravitinos decay after neutralino freeze-out and axino decoupling, which is always valid for $m_{\widetilde{G}} < 10^3$ TeV

and we neglected the thermal axion component, which consists of hot dark matter. The axion, axino, neutralino and gravitino relic abundances are given by Eqs. (5.22), (5.3), (4.11) and (4.26), which give[2]

$$\begin{aligned}\Omega_{a\tilde{a}}h^2 &\simeq 0.23\theta_i^2 f(\theta_i)\left(\frac{f_a}{10^{12}\text{ GeV}}\right)^{7/6} \\ &+ 3\left(\frac{m_{\tilde{a}}}{1\text{ GeV}}\right)\left(\frac{T_R}{10^{14}\text{ GeV}}\right)\left[1+6\times 10^8\left(\frac{10^{12}\text{ GeV}}{f_a}\right)^2\right]+\frac{m_{\tilde{a}}}{m_{\widetilde{Z}_1}}\Omega_{\widetilde{Z}_1}h^2\end{aligned} \tag{6.3}$$

The first term above is the coherent axion contribution, while the term proportional to the re-heat temperature corresponds to the thermal gravitino and axino contributions. The last term comes from thermally produced neutralinos.

From Eq.(6.3), we see that the gravitino and neutralino contributions to the dark matter relic abundance are suppressed by $m_{\tilde{a}}/m_{\widetilde{G},\widetilde{Z}_1}$. This naturally ameliorates the first part of the gravitino problem (overproduction of dark matter) and loosens the dark matter constraints on the MSSM parameters, since now $\Omega_{\widetilde{Z}_1}h^2 \gg 1$ is allowed if $m_{\tilde{a}}/m_{\widetilde{Z}_1} \ll 1$. We also see that the gravitino contribution can be neglected except for $f_a \sim M_{Pl}$, where the axino interactions become suppressed by the Planck scale. Therefore, suitable choices of f_a, θ_i, T_R and $m_{\tilde{a}}$ can easily satisfy the DM constraint for almost any values of $\Omega_{\widetilde{Z}_1}$, $m_{\widetilde{Z}_1}$ and $m_{\widetilde{G}}$. In particular, the neutralino contribution can always be suppressed for sufficiently light axinos, while the gravitino and axino contributions can be suppressed by small T_R and/or small $m_{\tilde{a}}$. Finally, the axion contribution can be suppressed by small f_a or θ_i. The latter option is less desirable, since an unnaturally small θ_i value represents a fine-tuned solution.

In Fig.6.1a, we show the contributions from each component in Eq.(6.1) as a

[2]Here we assume, for simplicity, $m_{\widetilde{G}} \gtrsim M_i$ in Eq.(4.26) and $\alpha_s(T_R) \sim 1/15$.

function of f_a for $m_{\tilde{a}} = 100$ keV and $\theta_i = 0.05$. For each f_a value, the value of the re-heat temperature (T_R) is adjusted so $\Omega_{a\tilde{a}}h^2 = 0.1123$. We can see that for low f_a values, the TP axino contribution is dominant. But as f_a increases, the axion component grows until, at $f_a \sim 4 \times 10^{13}$ GeV, it becomes dominant. For even higher f_a it saturates the DM relic density and the dark matter constraint can no longer be satisfied unless we choose a smaller θ_i value. The value of T_R which is needed to satisfy $\Omega_{DM}h^2 = 0.1123$ is shown in Fig. 6.1b. We see that T_R grows quickly with increasing f_a. This is because the thermal axino production decreases as the inverse square of f_a, so larger values of T_R are needed to keep $\Omega_{a\tilde{a}}h^2 = 0.1123$. We see that T_R can reach $\sim 10^{11}$ GeV in the case of mainly axion CDM. In our case here, allowing a smaller value of θ_i allows higher values of f_a to be found, which in turn requires much higher values of T_R, into the range needed for thermal leptogenesis.

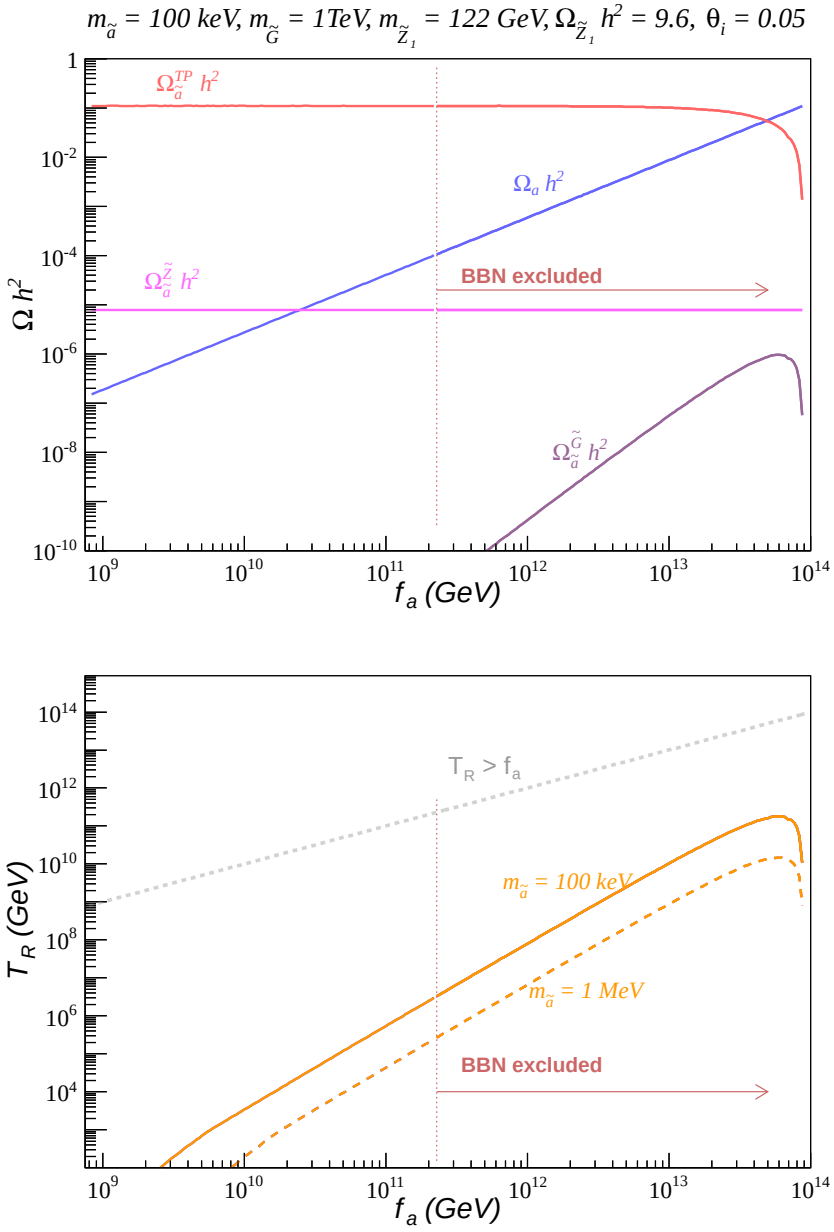

Figure 6.1: *Upper frame*: Contribution of axions and TP and NTP axinos to the DM density as a function of the PQ breaking scale f_a, for an mSUGRA point with $m_0 = 1000$ GeV, $m_{1/2} = 300$ GeV, $A_0 = 0$, $\tan\beta = 10$ and $\mu > 0$, and fixing $m_{\tilde{a}} = 100$ keV and $\theta_i = 0.05$; T_R is adjusted such that $\Omega_{a\tilde{a}} h^2 = 0.1123$. *Lower frame*: the T_R that is needed to achieve $\Omega_{a\tilde{a}} h^2 = 0.1123$ for $m_{\tilde{a}} = 0.1$ and 1 MeV, for the same mSUGRA point and θ_i.

From the above discussion and Eq.(6.3), we see that a very light axino is desirable in some cases, in order to accommodate models with large $\Omega_{\widetilde{Z}_1}h^2$ and/or large $\Omega_{\widetilde{G}}h^2$. However, very light axinos might constitute warm (WDM) or hot (HDM) dark matter, depending on their mass. Such cases are severely constrained by the matter power spectrum and reionization [60, 61]. Since the bounds on the amount of HDM/WDM are model dependent [62], we do not impose such constraints on our results. However, as a guidance, we will distinguish cases with

- $m_{\tilde{a}} < 100$ keV and $\Omega_{\tilde{a}}/\Omega_{DM} > 0.2$ (WDM) or
- $m_{\tilde{a}} < 1$ keV and $\Omega_{\tilde{a}}/\Omega_{DM} > 0.01$ (HDM),

where $\Omega_{\tilde{a}} = \Omega_{\tilde{a}}^{TP} + \Omega_{\tilde{a}}^{\widetilde{G}} + \Omega_{\tilde{a}}^{\widetilde{Z}}$[3].

So far we have neglected the BBN bounds for the axino LSP case. Since the axino-NLSP coupling is suppressed by $1/f_a$ (for a neutralino NLSP) or $1/M_{Pl}$ (for a gravitino NLSP), the next-to-lightest SUSY particle will be long-lived and possibly conflict with BBN bounds. As shown in Fig.4.1, this can be avoided if the NLSP is sufficiently heavy, so its lifetime is small, or if $\Omega_{NLSP} \ll 1$, so the energy injection during BBN is suppressed. In the axino LSP scenario, both gravitinos and neutralinos may be long-lived so the BBN constraints will apply to their decays. First we discuss the constraints on neutralino decays.

In Fig.6.2, we show the neutralino lifetime (τ) as function of $m_{\widetilde{Z}_1}$ for different values of f_a as well as its hadronic branching ratio. As we can see, τ can span a wide

[3] A rough estimate based on the neutrino mass limit [63] from cosmological data, $\sum m_\nu < 0.41$ to 0.44 eV, gives that up to 4–5% HDM contribution could be acceptable.

range of values depending on the neutralino mass, its bino composition and the value of the PQ scale. In Fig.6.3, we show the BBN bounds from Ref.[40] (or Fig.4.1) in the $m_{\widetilde{Z}_1}$ *vs.* $\Omega_{\widetilde{Z}_1}h^2$ plane for different f_a/Z_{1B} values. As we can see from Figs.6.2 and 6.3, for a bino $\widetilde{Z}_1$ ($Z_{1B} = 1$), $f_a < 10^{10}$ GeV gives $\tau < 10^{-2}$s and the BBN constraints can be easily avoided for any value of $\Omega_{\widetilde{Z}_1}h^2$, except for extremely light neutralinos. On the other hand, for $f_a > 10^{12}$ GeV, the BBN bounds require a heavy neutralino and/or $\Omega_{\widetilde{Z}_1}h^2 < 1$. In particular, for the choice of parameters in Fig.6.1, BBN constraints require $f_a \lesssim 2 \times 10^{11}$ GeV, as indicated in the plot. Therefore, models with large neutralino relic abundance can still satisfy both the DM and BBN constraints if $f_a \lesssim 10^{10} - 10^{11}$ GeV.

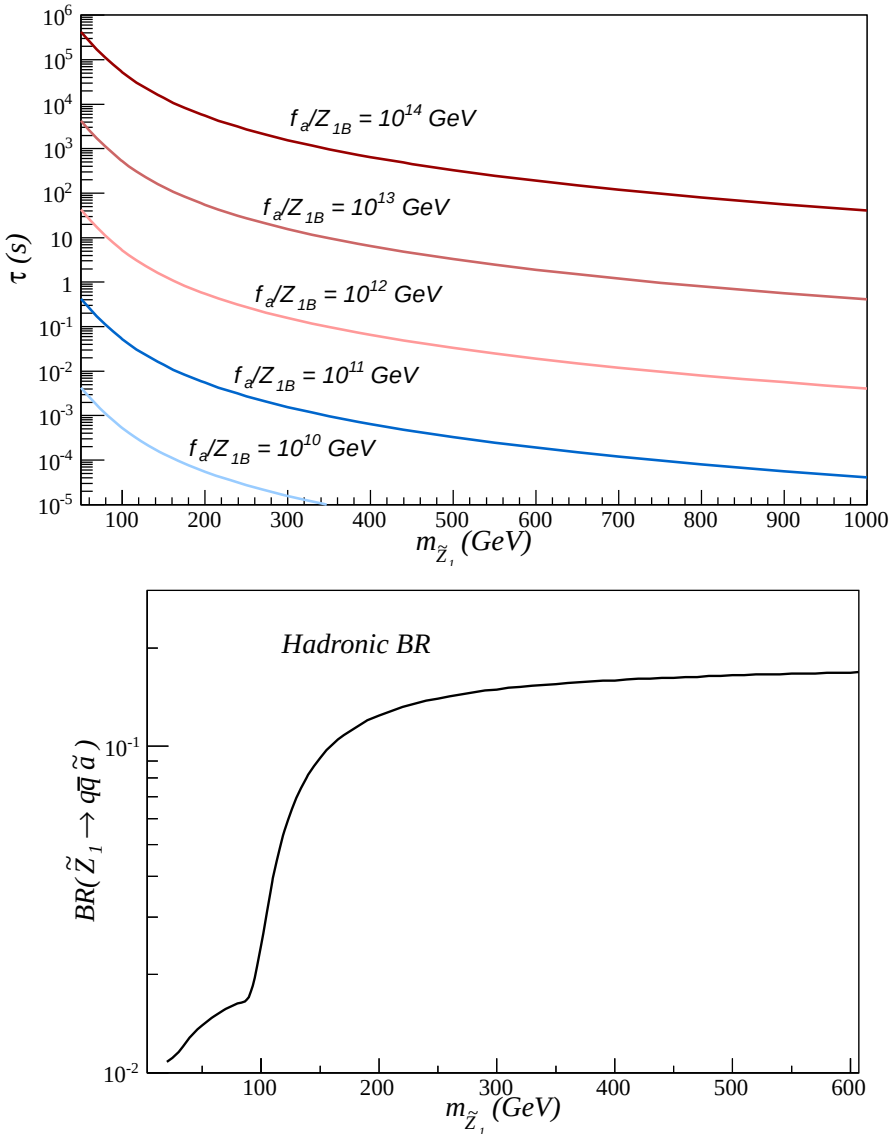

Figure 6.2: *Upper Frame*: Lifetime (in seconds) of a $\widetilde{Z}_1$ NLSP with a $\tilde{a}$ as LSP versus $m_{\widetilde{Z}_1}$, for various choices of f_a/Z_{1B}, computed using Eq.(3.9). We take $C_{aYY} = 8/3$. *Lower Frame*: Branching fraction of $\widetilde{Z}_1 \to \tilde{a} + hadrons$ versus $m_{\widetilde{Z}_1}$, computed using Eq.(3.10).

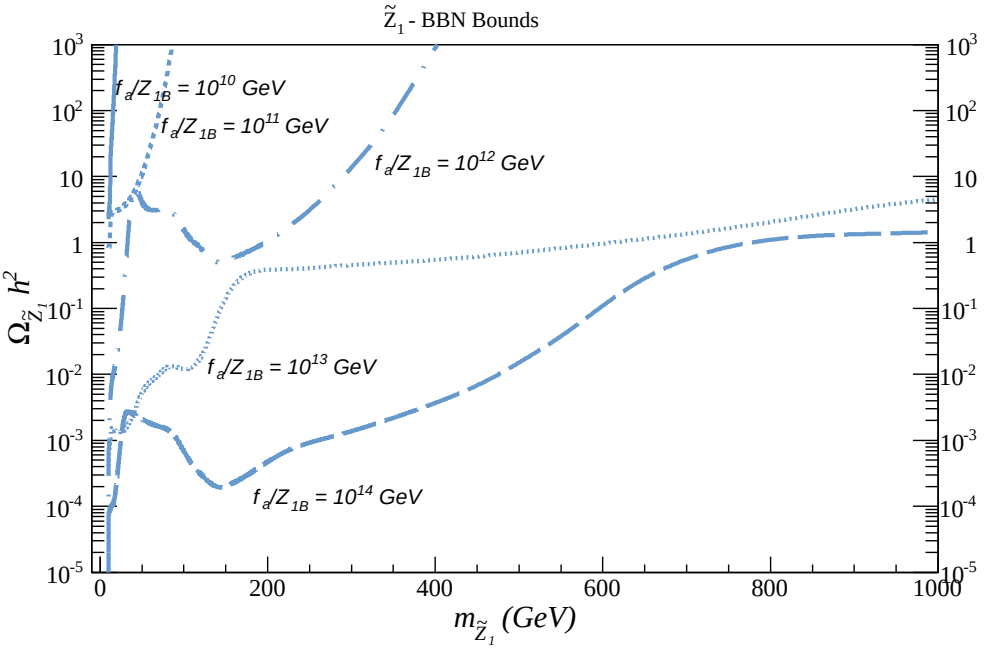

Figure 6.3: BBN bounds on late decaying neutralinos ($\widetilde{Z}_1 \to Z/\gamma + \tilde{a}$) from Ref. [40] as a function of $m_{\widetilde{Z}_1}$ for different values of f_a/N, assuming a bino $\widetilde{Z}_1$ and $m_{\widetilde{Z}_1} \gg m_{\tilde{a}}$. The values of $\Omega_{\widetilde{Z}_1} h^2$ above the curves are excluded by BBN constraints.

The discussion of the BBN bounds for the gravitino depends on the $m_{\widetilde{G}} - m_{\widetilde{Z}_1}$ hierarchy. For $m_{\widetilde{G}} > m_{\widetilde{Z}_1}$ (as expected from most SUGRA models), gravitinos cascade decay to neutralinos[4] which eventually decay to axinos. Therefore, in the $\widetilde{Z}_1$ NLSP case, the BBN bounds for late decaying gravitinos are identical to the MSSM case with a neutralino LSP, which has been discussed in Sec.4.2 and constitutes the second part of the Gravitino Problem. Hence, although the introduction of a light axino can easily solve the first part of the Gravitino Problem (overproduction of DM),

[4]The gravitino couplings to all SUSY particles are model independent and of order $1/M_{Pl}$. Therefore, direct decays to axino plus axion are suppressed with respect to $\widetilde{G} \to Y \to \widetilde{Z}_1 + X$ simply due to the multiplicity of final states (here Y represent all the MSSM fields). This is only violated if the SUSY spectrum is highly compressed or if $m_{\widetilde{G}} < m_{\widetilde{Z}_1}$.

as discussed above, the second part of the Gravitino Problem (violation of BBN constraints) remains the same as in the MSSM. A possible way to avoid the BBN constraints in this case is to assume low re-heat temperatures, so $\Omega_{\widetilde{G}} \ll 1$, or heavy gravitinos, so $\tau_{\widetilde{G}} \lesssim 1$s.

A third alternative for solving the second part of the Gravitino Problem in the axino LSP scenario is to assume $m_{\tilde{a}} < m_{\widetilde{G}} < m_{\widetilde{Z}_1}$ [64], since in this case the $\widetilde{G} \to \widetilde{Z}_1 + X$ decay is kinematically forbidden and direct decays to axino plus axion are the only open channel. Since axions and axinos from gravitino decays have no sizeable interactions with the thermal plasma during BBN, they do not affect the formation of light elements and there are no BBN constraints on late decaying gravitinos. Although this is an elegant solution to the Gravitino Problem in PQMSSM models, it requires a very specific mass spectrum, with a gravitino NLSP, which may not easily be obtained in realistic models.

From the above discussion, we see that – although the BBN bounds imposes severe constraints on late decaying neutralinos and gravitinos – these can be easily avoided in the axino LSP scenario, if $f_a \lesssim 10^{10}$ GeV (so neutralinos are short-lived) and $m_{\widetilde{G}}$ is in the multi-TeV range (short-lived gravitinos) or $m_{\widetilde{G}} < m_{\widetilde{Z}_1}$ (invisible decays) or small T_R (small $\Omega_{\widetilde{G}}^{TP} h^2$). Furthermore, the PQMSSM model has enough parameter freedom to satisfy the DM constraints, as shown by the example in Fig.6.1. However, as seen in this Figure, the BBN consistent region requires low f_a/low T_R, which conflicts with the implementation of thermal leptogenesis, discussed in Sec.4.2. In the next section, we discuss the necessary conditions for thermal leptogenesis to be

realized in PQMSSM models with an axino LSP and show that the parameter space becomes highly constrained once we require $T_R > 2 \times 10^9$ GeV.

6.1 Thermal Leptogenesis and the Axino LSP

In order to conciliate high re-heat temperatures ($> 2 \times 10^9$ GeV, as required by thermal leptogenesis) with the BBN constrains on late decaying gravitinos, we need either a multi-TeV gravitino or $m_{\widetilde{G}} < m_{\widetilde{Z}_1}$, as discussed in the last section. Since the latter scenario is harder to obtain in most MSSM models, we will first focus on the heavy gravitino solution. In the following, we assume $m_{\widetilde{G}} \gtrsim 30$ TeV, so $\tau_{\widetilde{G}} \lesssim 1$s and the BBN bounds on $\Omega_{\widetilde{G}}^{TP}$ are satisfied even at large T_R[46].

To discuss the conditions necessary for achieving high T_R in the axino LSP scenario, we impose $\Omega_{a\tilde{a}}h^2 = 0.11$ in Eq.(6.3) and solve for T_R:

$$T_R \simeq \left[0.11 - 2.3 \times 10^{-15} \left(\frac{f_a}{\text{GeV}}\right)^{7/6} \theta_i^2\right] \frac{f_a^2}{(18 \times 10^{18}) m_{\tilde{a}}} \tag{6.4}$$

where we have neglected the (sub-dominant) neutralino and gravitino contributions and assumed $\theta_i \lesssim 1$, so $f(\theta_i) \simeq 1$. If we take f_a as a free parameter, the maximum achievable re-heat temperature is approximately given by:

$$T_R^{max} \simeq 3 \times 10^5 \text{ GeV} \left(\frac{\text{MeV}}{m_{\tilde{a}}}\right) \theta_i^{-24/7} \tag{6.5}$$

which is achieved at $f_a^{max} \simeq 3.6 \times 10^{11} \theta_i^{-12/7}$ GeV, so

$$T_R^{max} \simeq 2 \times 10^6 \text{ GeV} \left(\frac{\text{MeV}}{m_{\tilde{a}}}\right) \left(\frac{f_a^{max}}{10^{12} \text{ GeV}}\right)^2 . \tag{6.6}$$

From Eqs.(6.5) and (6.6), it is clear that large T_R values are only possible at low $m_{\tilde{a}}$ and θ_i, with large f_a. For $m_{\tilde{a}} = 100$ keV and $\theta_i = 0.05$, we obtain from Eq. (6.5):

$T_R^{max} \simeq 9 \times 10^{10}$ GeV. As seen in Fig. 6.1b, this result is slightly underestimated, due to the running of g_s, which has been neglected when deriving Eq.(6.5). Nonetheless, it illustrates the general conditions on f_a, θ_i and $m_{\tilde{a}}$ necessary for obtaining large T_R values.

The above result is clearly in tension with the BBN bounds on late decaying neutralinos, since the large f_a values ($\gtrsim 10^{12}$ GeV) necessary to obtain $T_R > 2 \times 10^9$ GeV result in neutralinos with $\tau \gtrsim 0.1$s, unless $m_{\widetilde{Z}_1} \gtrsim 300$ GeV, as shown in Fig.6.2. Hence the BBN bounds require small $\Omega_{\widetilde{Z}_1} h^2$ (< 1), unless $m_{\widetilde{Z}_1} \lesssim 300$ GeV, as seen in Fig.6.3. But, as shown by Fig.4.4, most MSSM models have $\Omega_{\widetilde{Z}_1} h^2 > 1$. Therefore, imposing high re-heat temperatures strongly constrains the MSSM sector. In order to illustrate these constraints, we perform a scan over the PQMSSM parameters over the following range:

$$\begin{aligned} m_{\tilde{a}} &\in [10^{-7},\ 10]\ \text{GeV}\,, \\ f_a &\in [10^{8},\ 10^{15}]\ \text{GeV}\,, \\ \theta_i &\in [0,\ \pi] \\ \Omega_{\widetilde{Z}_1} h^2 &\in [10^{-5}, 10^{3}]. \end{aligned} \tag{6.7}$$

assuming a bino neutralino with $m_{\widetilde{Z}_1} = 50$ and 500 GeV. The result is seen in Fig.6.4, which shows, in the $\Omega_{\widetilde{Z}_1} h^2$ *vs.* f_a plane, the solutions satisfying $\Omega_{DM} h^2 = 0.1123$ and $T_R > 2 \times 10^9$ GeV. The red dot solutions violate the BBN bounds on late decaying neutralinos, while the blue ones are allowed. Points in light blue or light red have too much warm or hot dark matter ($m_{\tilde{a}} < 100$ keV and $\Omega_{\tilde{a}}/\Omega_{a\tilde{a}} > 0.2$ or $m_{\tilde{a}} < 1$

keV and $\Omega_{\tilde{a}}/\Omega_{a\tilde{a}} > 0.01$). As we can see from Fig.6.4, high re-heat temperatures with $f_a \lesssim 10^{12}$ GeV usually have too much HDM/WDM, since they require very light axinos, as shown by the approximate formula in Eq.(6.6)[5]. We also see that models with light neutralinos require $\Omega_{\widetilde{Z}_1} h^2 \lesssim 10^{-3}$, while models with heavy neutralinos admit $\Omega_{\widetilde{Z}_1} h^2 \lesssim 1$. We point out that these results assume a bino-like neutralino ($Z_{1B} \simeq 1$) and would be more constraining for the case of a higgsino or wino $\widetilde{Z}_1$. Below, we present a specific example of a non-mSUGRA model which satisfy all the conditions discussed so far, allowing for high T_R values and the implementation of thermal leptogenesis.

[5] An alternative are models with very small mis-alignment angles, as shown by Eq.(6.5). However our random scan strongly disfavors such highly fine-tuned solutions, which do not appear in Fig.6.4.

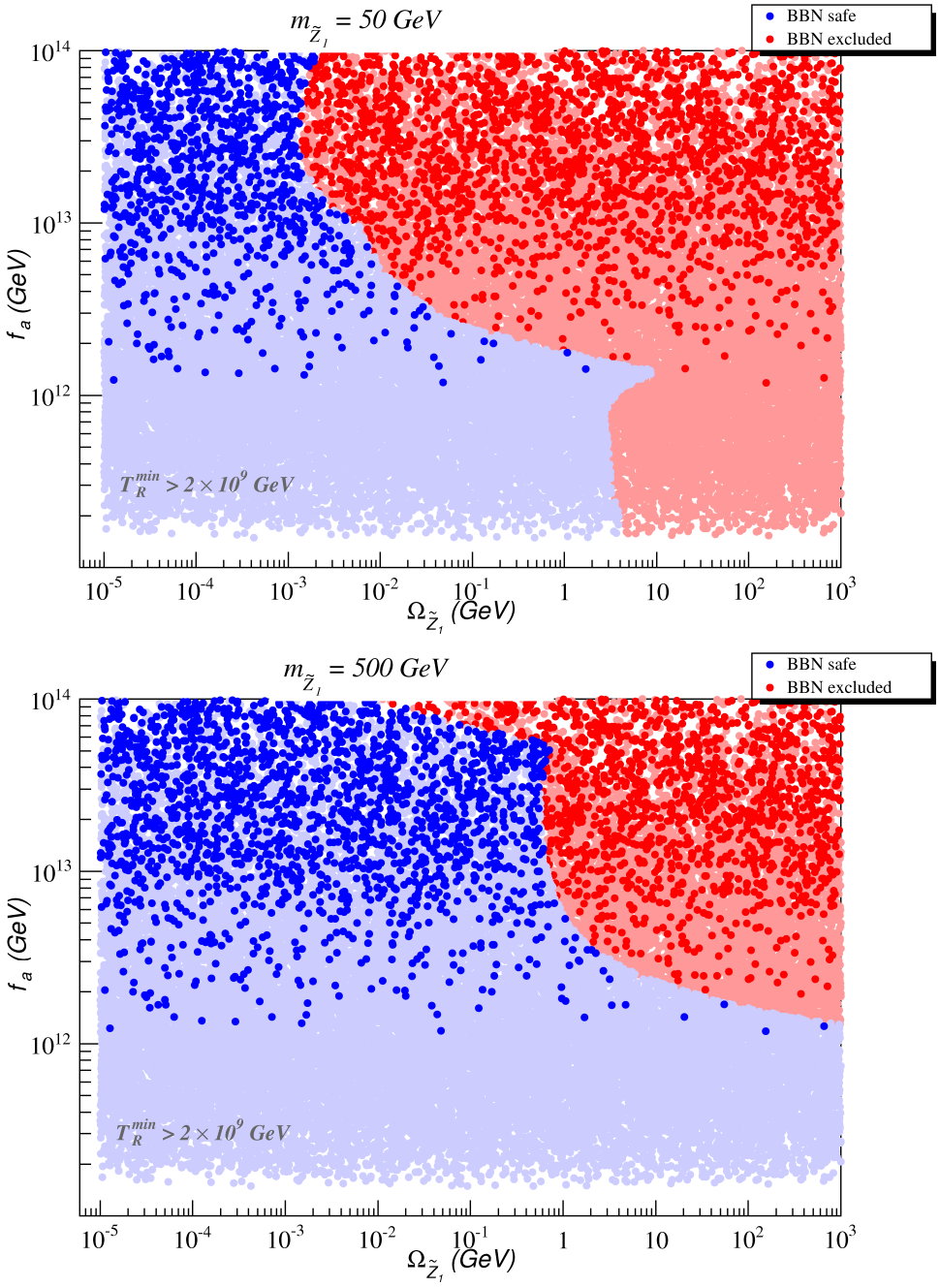

Figure 6.4: Model-independent scatter plot of points with $T_R \gtrsim 2 \times 10^9$ GeV in the $\Omega_{\tilde{Z}_1} h^2$ *vs.* f_a plane for $m_{\tilde{Z}_1} = 50$ GeV (upper frame) $m_{\tilde{Z}_1} = 500$ GeV (lower frame). The blue points respect the $\widetilde{Z}_1 \to \tilde{a} + hadrons$ BBN bound, while the red points violate the BBN constraint. Points shown in light blue or light red have $> 20\%$ WDM or $> 1\%$ HDM, as discussed in the text.

A type of gravity mediation model which would be consistent with $\sim$ 30 TeV gravitinos is effective SUSY, or ESUSY[65, 66]. In Ref.[66], these models were explored with GUT scale soft SUSY breaking boundary conditions. For ESUSY models, first/second generation scalars have mass $m_0(1,2)$ in the multi-TeV range at the GUT scale, while third generation scalar masses $m_0(3)$ are in the few TeV to multi-TeV range. Upon evolution through the renormalization group equations (RGE), first/second generation scalars remain in the multi-TeV range, while third generation scalar masses are suppressed by both the contributions from Yukawa couplings and two-loop RGE terms, and are sub-TeV at the weak scale. Since only third generation scalars and gauginos significantly contribute to the fine-tuning in the Higgs sector, this class of models conciliate a multi-TeV first/second generation and gravitino with a low value of electroweak fine-tuning. In Table 6.1, we present a benchmark point for the ESUSY scenario, which has a mixed bino-higgsino NLSP with mass $m_{\widetilde{Z}_1} = 414$ GeV. The $\widetilde{Z}_2$ and $\widetilde{W}_1$ are quite close in mass to the $\widetilde{Z}_1$, followed by $\tilde{t}_1$ and $\tilde{b}_1$ which are just 60% heavier. This leads to $\Omega_{\widetilde{Z}_1}h^2 \sim 0.04$ due to simultaneous mixed bino-higgsino-wino enhanced annihilation, and also a contribution from stop and sbottom co-annihilation. The low $\Omega_{\widetilde{Z}_1}h^2$ value allows $\widetilde{Z}_1$ lifetimes up to $\sim$ 200 sec, corresponding to f_a values as high as 10^{13} GeV.

As shown by Fig.6.1, such high f_a values suppress the thermal production of axino dark matter, while low values of θ_i suppress the axion relic abundance. Repeating the same scan over PQMSSM parameters performed for Fig.6.4, but now with $m_{\widetilde{Z}_1} = 414$ GeV and $\Omega_{\widetilde{Z}_1}h^2$ fixed at 0.04, reveals that re-heat temperatures

above 10^{12} GeV can be generated while avoiding overproduction of dark matter and maintaining consistency with BBN bounds, as seen in Figs.6.5-6.6. The light points correspond to very light axinos ($m_{\tilde{a}} < 100$ keV) and can give the maximum T_R values, as shown by Eq.(6.6). The maximum value of T_R (for a fixed f_a value) obtained in this region comes from the minimum $m_{\tilde{a}}$ value considered in our scan ($m_{\tilde{a}} = 0.1$ keV). However, these light axino solutions likely violate the bounds on WDM/HDM, as discussed in Sec.6. If we only consider solutions with cold axinos ($m_{\tilde{a}} > 100$ keV), Eq.(6.6) gives:

$$T_R \lesssim 2 \times 10^7 \left(\frac{f_a}{10^{12}\ \text{GeV}} \right)^2 . \tag{6.8}$$

The above expression describes well the CDM-WDM transition line seen in Fig.6.5. The few dark blue points above this line simultaneously have large values of θ_i and very small $m_{\tilde{a}}$, so the axino contribution to $\Omega_{DM}h^2$ is highly suppressed and the fraction of WDM (HDM) is below 20% (1%).

Once we impose $T_R > 2 \times 10^9$ GeV, shown by the dotted gray line in Figs.6.5-6.6, we see that most solutions require $m_{\tilde{a}} \lesssim 200$ keV to suppress the axino contribution and $\theta_i \lesssim 0.5$ to suppress the axion contribution. These conditions can also be seen from the approximate expression for T_R^{max} obtained in Eqs.(6.5) and (6.6). Furthermore, we see from Fig.6.6 that solutions consistent with thermal leptogenesis have the DM relic abundance dominated either by axions or by axinos. Thus, ESUSY models with a low abundance of neutralinos, mixed axion/axino dark matter with a high PQ scale and low θ_i can apparently reconcile thermal leptogenesis with the gravitino problem, although most of the solutions for the benchmark point chosen

have a potentially dangerous fraction of HDM/WDM (light blue points). We point out, however, that the BBN bounds will be less severe for similar scenarios with a bino $\widetilde{Z}_1$ or smaller $\Omega_{\widetilde{Z}_1}h^2$; examples are discussed in Ref.[66].

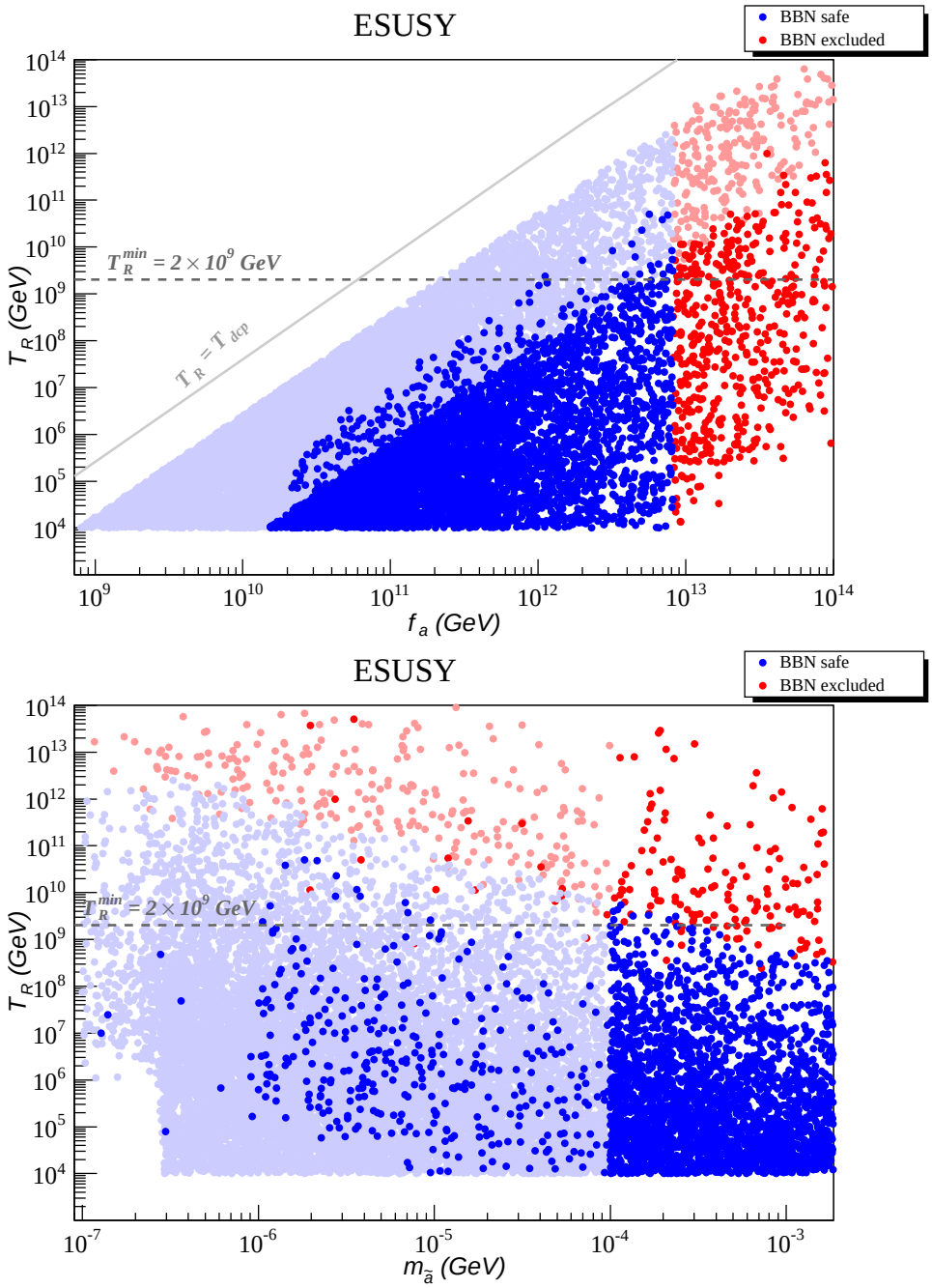

Figure 6.5: Scan over PQ parameters for the ESUSY benchmark point discussed in the text, plotted in the T_R *vs.* f_a (upper frame) and T_R *vs.* $m_{\tilde{a}}$ (lower frame) planes. Same color code as in Fig.6.4.

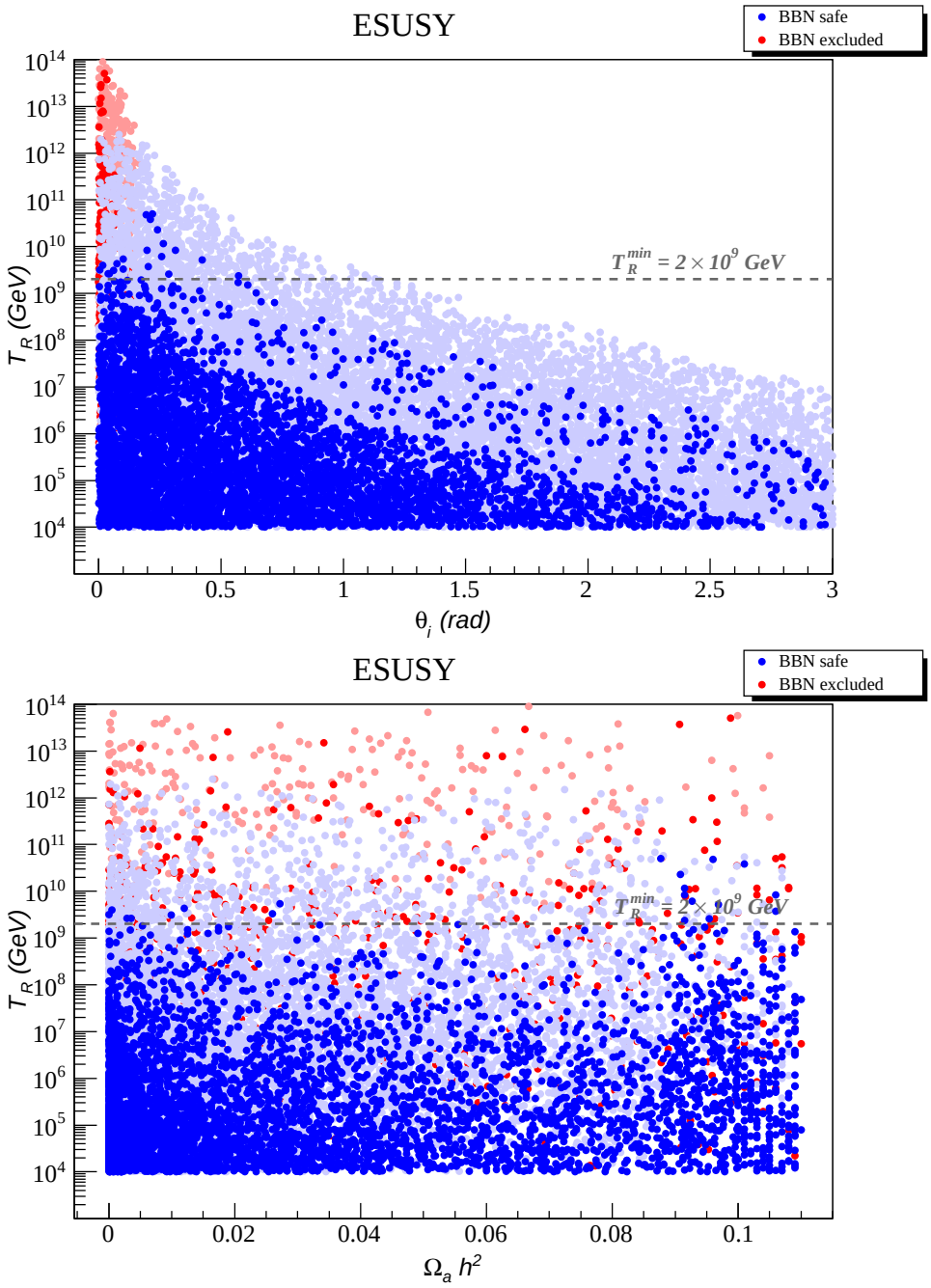

Figure 6.6: Scan over PQ parameters for the ESUSY benchmark point discussed in the text, plotted in the T_R *vs.* θ_i (upper frame) and T_R *vs.* $\Omega_a h^2$ (lower frame) planes. Same color code as in Fig.6.4.

Effective SUSY					
Input Parameters (GeV)		Masses (GeV)		Other Observables	
$m_{\widetilde{G}}$ [TeV]	30	μ	418.6		
$m_0(1,2)$	20575.6	$m_{\tilde{g}}$	3507.1	Δa_μ	2.4×10^{-13}
$m_0(3)$	2922.94	$m_{\tilde{u}_L}$	20739.8	$BF(b \to s\gamma)$	2.9×10^{-4}
$m_{1/2}$	1457.17	$m_{\tilde{t}_1}$	652.8	$BF(B_s \to \mu\mu)$	3.8×10^{-9}
A_0	2177.84	$m_{\tilde{b}_1}$	671.7	Z_{1B}	0.14
m_{H_d}	3099.42	$m_{\widetilde{W}_1}$	428.0	$\Omega h^2_{\widetilde{Z}_1}$	0.04
m_{H_u}	2783.53	$m_{\widetilde{Z}_1}$	414.2	$\sigma(\widetilde{Z}_1 p)$ [pb]	6.6×10^{-9}
$\tan\beta$	6.87475	m_h	117.5		

Table 6.1: Masses and parameters in GeV units for the Effective SUSY benchmark point, computed with Isajet 7.81 using $m_t = 173.1$ GeV.

Gravitino NLSP

We now discuss the gravitino NLSP scenario, first proposed in Ref.[64]. As discussed in the last section, a gravitino NLSP decays invisibly into axions and axinos, thus avoiding all BBN constraints. Therefore, as in the $m_{\widetilde{G}} = 30$ TeV case presented above, we can once again ignore the BBN bounds on late decaying gravitinos. Nonetheless, neutralinos (assumed to be the next-to-next-to-lightest SUSY particle or NNLSP) still directly decay to axinos, since decays to gravitinos are suppressed by $1/M_{Pl}$[6]. Furthermore, the relic DM density in the gravitino NLSP scenario still is (approximately) given by Eq.(6.3). Therefore, all the results presented for the neutralino NLSP case are still valid if $m_{\widetilde{Z}_1} > m_{\widetilde{G}} > m_{\tilde{a}}$. To illustrate this, we once again perform a scan over the PQMSSM parameter space over the range in Eq.(6.7), but now assuming $m_{\widetilde{G}} = m_{\widetilde{Z}_1}/2$, $\Omega_{\widetilde{Z}_1}h^2 = 0.04$ and $m_{\widetilde{Z}_1} = 430$ GeV. Also, to illustrate how the results obtained for the ESUSY point would change for a bino-like neutralino, we now assume $Z_{1B} = 1$ (pure bino). The results are presented in Fig.6.7 and are identical to the ESUSY case shown in Fig.6.5, once the BBN constraint on f_a for the ESUSY point is re-scaled for a bino-like neutralino ($f_a \rightarrow f_a/Z_{1B} \lesssim 6 \times 10^{13}$ GeV). The same results obtained for the θ_i and $m_{\tilde{a}}$ parameters in Figs.6.5 and 6.6 are also valid in the gravitino NLSP scenario, so we do not repeat them here.

[6] If $m_{\widetilde{Z}_1} \gg m_{\widetilde{G}}$, the neutralino lifetime can be considerably reduced and the decay to gravitino can become the dominant mode. However, here we only consider cases where $m_{\widetilde{G}} \lesssim m_{\widetilde{Z}_1}$.

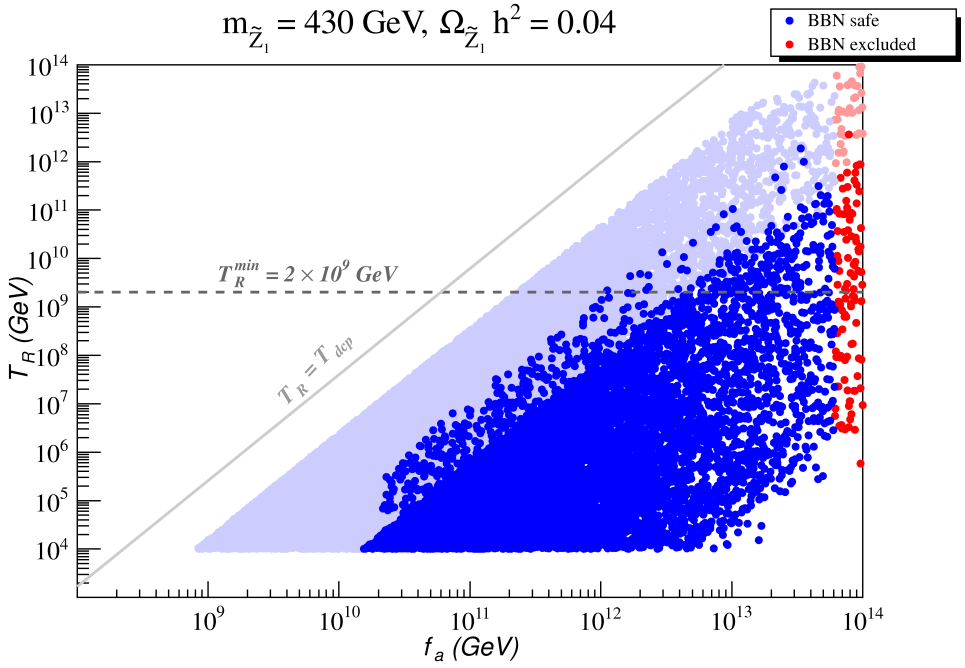

Figure 6.7: Allowed and disallowed points in the f_a *vs.* T_R plane for the gravitino NLSP case, with $m_{\widetilde{Z}_1} = 2m_{\widetilde{G}} = 430$ GeV and $\Omega_{\widetilde{Z}_1} h^2 = 0.04$, including BBN constraints on late $\widetilde{Z}_1$ decay. Same color code as in Fig. 6.4.

In order to illustrate how imposing $T_R > 2 \times 10^9$ GeV along with the BBN and WDM/CDM bounds constrains the MSSM sector of PQMSSM models (here parametrized by $\Omega_{\widetilde{Z}_1} h^2$, $m_{\widetilde{Z}_1}$ and Z_{1B}), we include $\Omega_{\widetilde{Z}_1} h^2$ and $m_{\widetilde{Z}_1}$ in our scan over the PQMSSM parameter space and select all solutions satisfying $T_R > 2 \times 10^9$ GeV. The result is shown in Fig.6.8. The blue points are BBN-allowed, while red points violate BBN bounds. Once $m_{\widetilde{Z}_1}$ and $\Omega_{\widetilde{Z}_1} h^2$ are fixed, then the BBN bounds just forbid f_a from rising above some ($m_{\widetilde{Z}_1}$ and $\Omega_{\widetilde{Z}_1} h^2$ dependent) maximum value.

The dashed line indicates the boundary below which 99% of the CDM/BBN consistent solutions lie and can be interpreted as a natural upper bound for $\Omega_{\widetilde{Z}_1} h^2$ as

a function of $m_{\widetilde{Z}_1}$. From this, we see that models with $m_{\widetilde{Z}_1} \lesssim 10$ GeV require $\Omega_{\widetilde{Z}_1} h^2 \lesssim 10^{-3}$, while values of $\Omega_{\widetilde{Z}_1} h^2$ as high as 10^3 can be consistent with thermal leptogenesis if the neutralino is in the TeV range. Although these limits assume the gravitino NLSP scenario, the results are also valid for the heavy gravitino case ($m_{\widetilde{G}} \gtrsim 30$ TeV) discussed at the beginning of this Section.

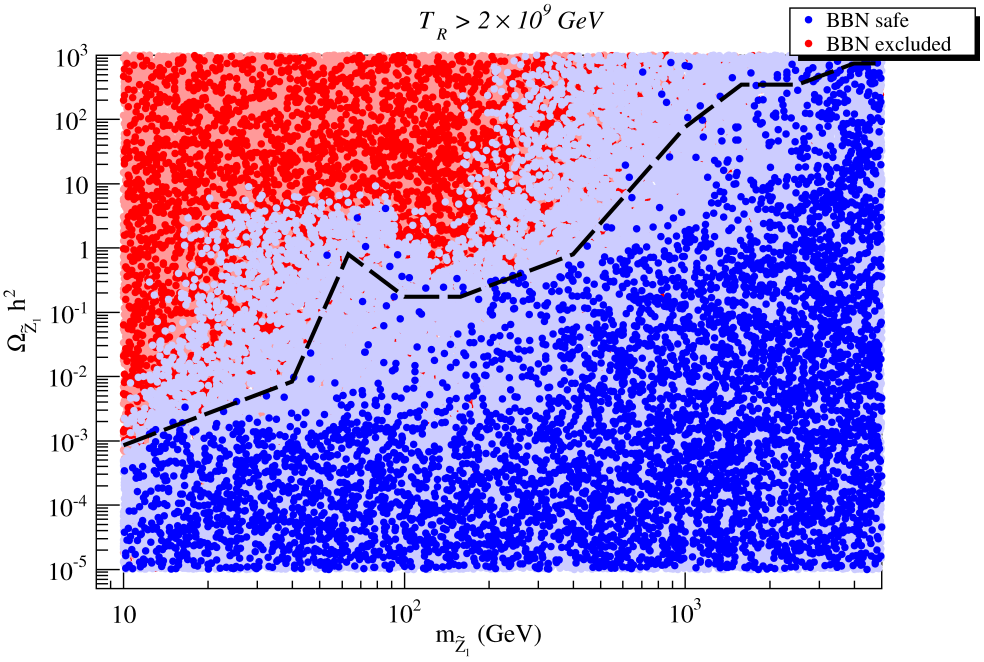

Figure 6.8: Allowed and disallowed points in the $\Omega_{\widetilde{Z}_1} h^2$ *vs.* $m_{\widetilde{Z}_1}$ plane for a general scan over SUSY models with a bino $\widetilde{Z}_1$. For all points, we require $T_R > 2 \times 10^9$ GeV and assume $m_{\widetilde{G}} = m_{\widetilde{Z}_1}/2$. Dark blue points are consistent with BBN and have mainly CDM with at most 20% WDM and/or 1% HDM admixture. The region below the dashed line represents the MSSM parameter space where 99% of the CDM/BBN consistent solutions lie.

6.2 The Saxion Effect

Up to this point, we have neglected an important element of the axion supermultiplet, namely the spin-0 saxion field $s(x)$. As discussed in Sec.5, saxions can be produced in thermal equilibrium (if $T_R > T_{dec}$) or out of equilibrium from scatterings of particles in the plasma (if $T_R < T_{dec}$) and can also contribute to the energy density in the form of coherent oscillations. Unlike axinos or axions, saxions are always expected to be heavy ($m_s \sim m_{3/2}$) and unstable, with decay widths given by Eq.(3.14). Since the decay into axions is strongly model dependent, we will neglect it here. In Fig.6.9 we show the saxion decay width into gluons and gluinos as a function of the gluino mass, for $m_s = 1$ TeV and $f_a = 10^{12}$ GeV. As we can see, the decay into gluinos is always sub-dominant. Hence, for simplicity, from now on we assume $BR(s \to gg) = 1$. Thus, saxions will not enhance the LSP relic abundance. Nonetheless, saxion decays inject energetic gluons into the thermal plasma and the BBN bounds shown in Fig.4.1 (with $B_h = 1$) will apply, if $\tau_s \gtrsim 10^{-2}$s.

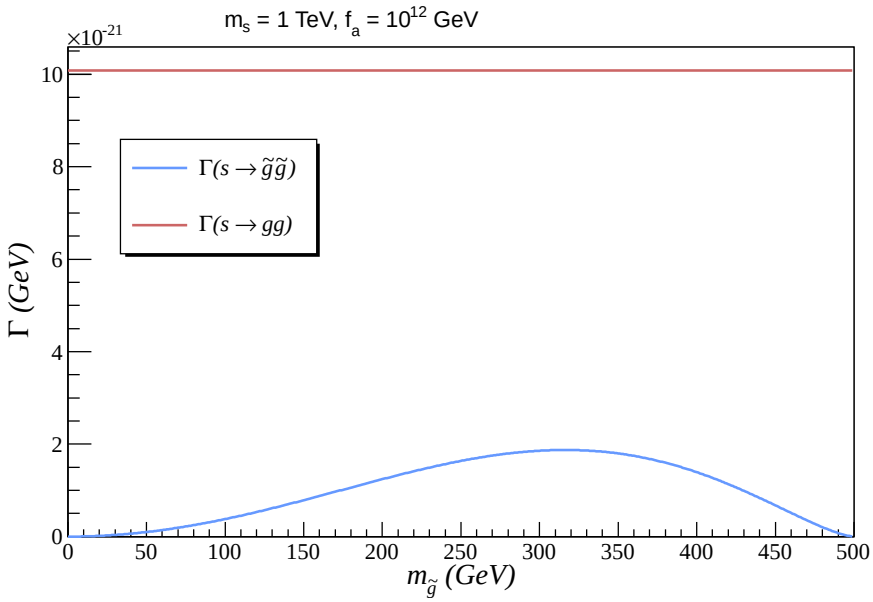

Figure 6.9: Decay widths for $s \to gg$ and $s \to \tilde{g}\tilde{g}$ as a function of $m_{\tilde{g}}$ for $f_a = 10^{12}$ GeV and $m_s = 1$ TeV.

The saxion lifetime can be computed from Eq.(3.14), which gives (assuming $BR(s \to gg) = 1$):

$$\tau_s \simeq 6.5 \times 10^{-5} \left(\frac{10^3 \text{ GeV}}{m_s}\right)^3 \left(\frac{f_a}{10^{12} \text{ GeV}}\right)^2 \tag{6.9}$$

while the saxion thermal abundance is given by Eq.(5.3):

$$\Omega_s^{TP} h^2 \simeq \begin{cases} 2.7 \times 10^{11} \left(\frac{T_R}{10^{14} \text{ GeV}}\right) \left(\frac{m_s}{10^3 \text{ GeV}}\right) \left(\frac{10^{12} \text{ GeV}}{f_a}\right)^2 & , \text{ if } T_R < T_{dec} \\ 3.3 \times 10^8 \left(\frac{m_s}{10^3 \text{ GeV}}\right) & , \text{ if } T_R > T_{dec} \end{cases} . \tag{6.10}$$

Armed with the above expressions for $\Omega_s h^2$ and τ_s, we can translate the BBN bounds in Fig.4.1 into limits for T_R, f_a and m_s, once the BBN constraints are applied to late decaying saxions. In Fig.6.10, we show the BBN bounds for thermally produced saxions in the f_a *vs.* T_R plane (red curves) for different values of the saxion mass. As

we can see, the bounds can be easily satisfied if $f_a \lesssim 10^{11}$ GeV and $m_s \gtrsim 50$ GeV. Therefore, the inclusion of thermal saxions does not introduce extra constraints on PQMSSM models, if $f_a \lesssim 10^{11}$ GeV. However, as discussed in the last section, thermal leptogenesis requires $T_R > 2 \times 10^9$ GeV which can only be obtained for $f_a \gtrsim 10^{12}$ GeV. In this case, the BBN bounds on saxion decays can only be satisfied for $m_s \gtrsim 500$ GeV. This condition is easily satisfied in the ESUSY (or heavy gravitino) scenario, since $m_s \sim m_{3/2} \sim 30$ TeV. On the other hand, in the gravitino NLSP scenario, besides giving a light gravitino, the SUSY breaking mechanism would have to generate a saxion mass $m_s \gg m_{\widetilde{G}}$. We also point out that for $m_s > 10$ TeV, thermal saxions always decays before BBN or have too small relic density, hence there is no upper limit on f_a from BBN, as seen in Fig.6.10.

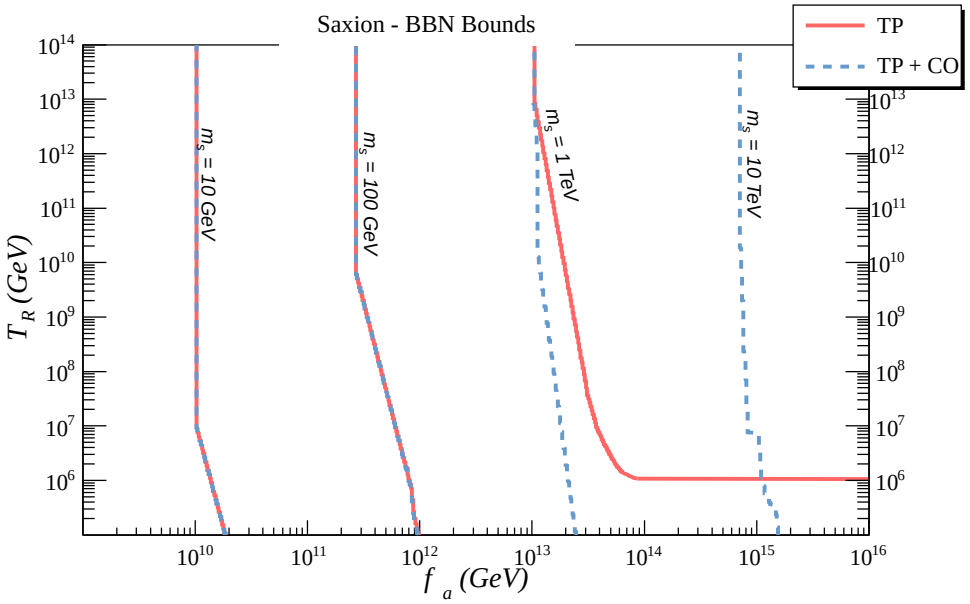

Figure 6.10: BBN bounds for thermally produced saxions (red curves) in the f_a *vs.* T_R plane for $m_s = 10, 10^2, 10^3$ and 10^4 GeV. We also show the same bounds after the inclusion of the coherent oscillation component assuming $s_i = f_a$ (blue curves). The region to the right of the curves is excluded by BBN constraints on $s \to gg$ decays.

So far we have neglected the contribution from coherent oscillating saxions. While thermal saxions are always present in PQMSSM models, coherent oscillations depend on the saxion initial field amplitude (s_i) and can be neglected if $s_i \ll f_a$, as discussed in Sec.5.2. The expression for the energy density of coherent oscillating saxions is given by Eq.(5.24). In Fig.6.11, we show the contributions from thermal and coherent oscillating saxions to the total saxion yield as a function of f_a, for $T_R = 10^9$ GeV and $m_s = 0.1$ and 1 TeV. As we can see, for $f_a \lesssim 10^{12}$ GeV, the saxion yield is dominated by its thermal component and decreases with f_a. For larger f_a values, the coherent

oscillation component becomes dominant and increases with f_a, since we assume $s_i = f_a$. Therefore, for the large f_a values relevant for thermal leptogenesis, we cannot neglect the coherent oscillation contribution, unless $s_i \ll f_a$. In Fig.6.10, we show in dashed blue lines the BBN bounds including the coherent oscillating saxion component for distinct m_s values. As we can see, the coherent oscillation component only affects the bounds on f_a and T_R for $m_s > 1$ TeV. The main consequence of assuming $s_i = f_a$ is that the BBN bounds on very heavy saxions become much stronger, as shown by the $m_s = 1$ and 10 TeV curves in Fig.6.10. This is simply due to the fact that for such large f_a values ($\gtrsim 10^{13}$ GeV), the thermal production of saxions is negligible, while the coherent oscillation component is greatly enhanced. Nonetheless, the upper limit on f_a still is high enough to allow thermal leptogenesis in the ESUSY point discussed in the last Section, where $m_s \sim 30$ TeV. For this point, the BBN bounds on late decaying neutralinos are more constraining, as shown by Fig.6.5.

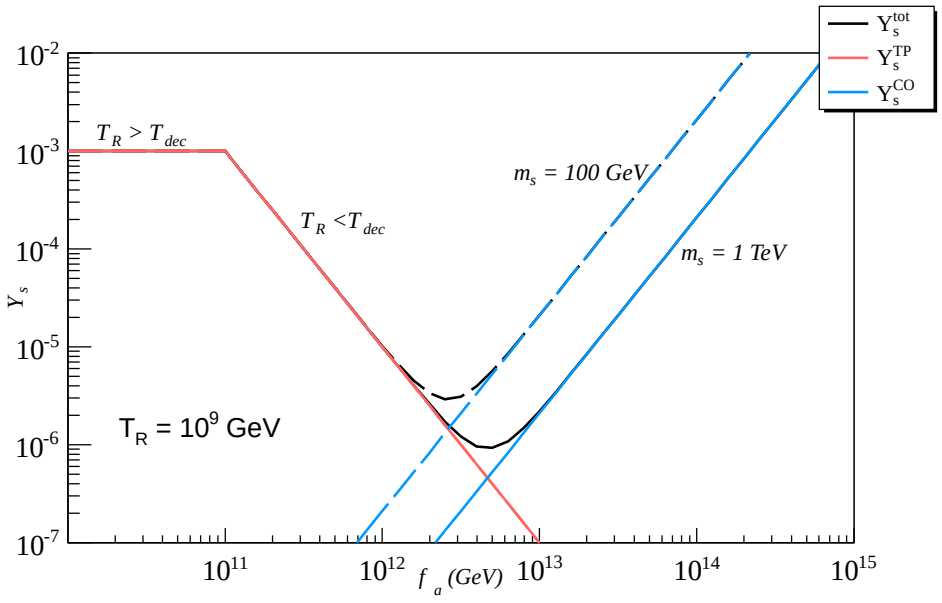

Figure 6.11: Saxion yield Y_s versus f_a for $T_R = 10^9$ GeV and $m_s = 0.1$ and 1 TeV. We assume $s_i/f_a = 1$.

As mentioned at the beginning of this section, saxions do not contribute to the DM relic abundance, since they decay predominantly to gluon pairs. However, the inclusion of the saxion field may still indirectly affect the axion and axino relic abundances. As discussed in Sec.5.3, if the production of saxions in the early universe is large enough, these might come to temporarily dominate the energy density of the universe, which then becomes matter dominated until the saxions decay. If this happens, during the saxion decay, significant entropy is injected and the energy densities of gravitinos, axinos, axions, neutralinos and baryons may be diluted with respect to ρ_R, as illustrated by the example in Fig.5.1b. The condition for a saxion-dominated

universe is given by Eq.(5.29):

$$T_D < T_e \ \text{ or } \ \frac{\rho_s}{s} > \frac{3}{4}\sqrt{M_{Pl}\Gamma_s}\left(\frac{45}{4\pi^3}\frac{1}{g_*(T_D)}\right)^{1/4} \tag{6.11}$$

where T_e is the temperature at which $\rho_s = \rho_R$ and T_D is the saxion decay temperature.

In Fig.6.12, we show the value of T_D (blue horizontal lines) and the value of T_e (red lines) for $f_a = 10^{12}$ and 10^{14} GeV. For T_R greater than the $r = 1$ intersection points, the universe has a saxion dominated era and significant entropy injection can occur.

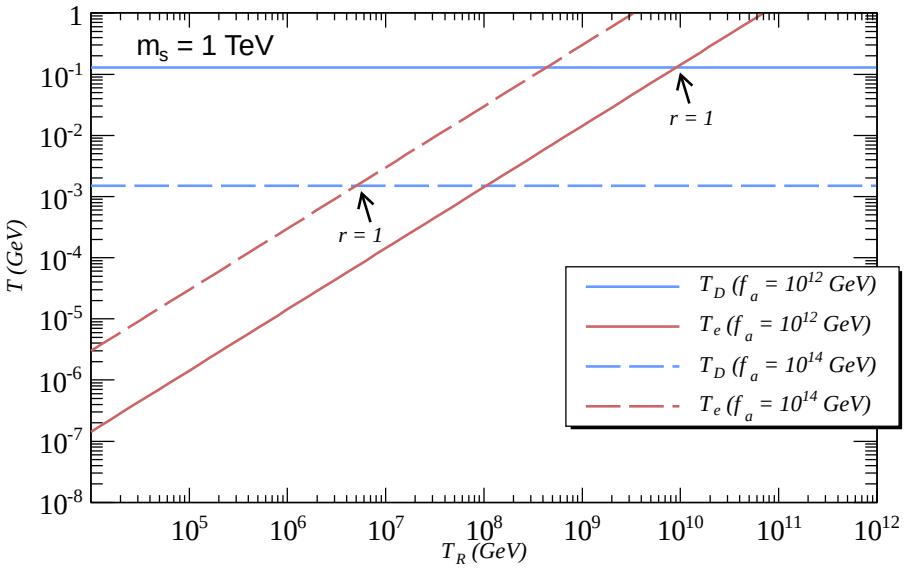

Figure 6.12: Temperatures T_D and T_e versus T_R for $f_a = 10^{12}$ and 10^{14} GeV and for $m_s = 1$ TeV.

If $r > 1$, T_D must satisfy $T_D \gtrsim 5$ MeV, so the universe becomes radiation dominated before BBN starts (see the discussion in Sec.4.1). As discussed in Sec.5.3, the

ratio of entropy injection before and after the saxion decay can be approximated by

$$r = \frac{S_f}{S_i} \simeq \frac{T_e}{T_D} \,. \tag{6.12}$$

Since, if the saxion never dominates the energy density of the universe ($T_e < T_D$), the injection of entropy is negligible, we assume $r = 1$ (no entropy injection) for $T_e < T_D$.

We plot in Fig. 6.13a the value of r in the f_a *vs.* T_R plane for $m_s = 0.1,\ 1$ and 10 TeV, assuming $s_i/f_a = 1$ (for production from coherent oscillations). The solid lines all maintain $T_D > 5$ MeV, while dashed lines violate this constraint. The various contours of constant r initially increase with T_R. In this case, the saxion production is dominantly thermal. When the curves turn over, saxion production is dominated by coherent oscillations. In this case, as f_a increases, the saxion field strength also increases (since s_i/f_a is fixed to 1), and much lower T_R values are allowed for substantial entropy production. The region above the solid gray line, where $T_R > f_a$, has the PQ symmetry broken only after inflation. In this case, the universe breaks into domains of different θ_i and s_i values at $T \lesssim f_a$ and a modified treatment of dark matter is needed. Since this scenario seems disfavoured by the uniformity of the CMB, we only consider regions with $T_R < f_a$. We also see that significant entropy production only occurs for $T_R \gtrsim 10^8$ GeV or $f_a \gtrsim 10^{13}$ GeV. Therefore, all the DM and BBN allowed scenarios at low f_a/low T_R discussed in Sec.6 are not modified by the inclusion of the saxion field. However, the same is not valid for the large T_R/large f_a region necessary by thermal leptogenesis.

Finally, when we compare Figs.6.5 and 6.7 to Fig. 6.13, we see that the range of $T_R \sim 10^9 - 10^{11}$ GeV for $f_a \sim 10^{12} - 10^{14}$ implies that entropy dilution from saxion

decay needs to be included in our calculations, if $s_i/f_a \gtrsim 1$.

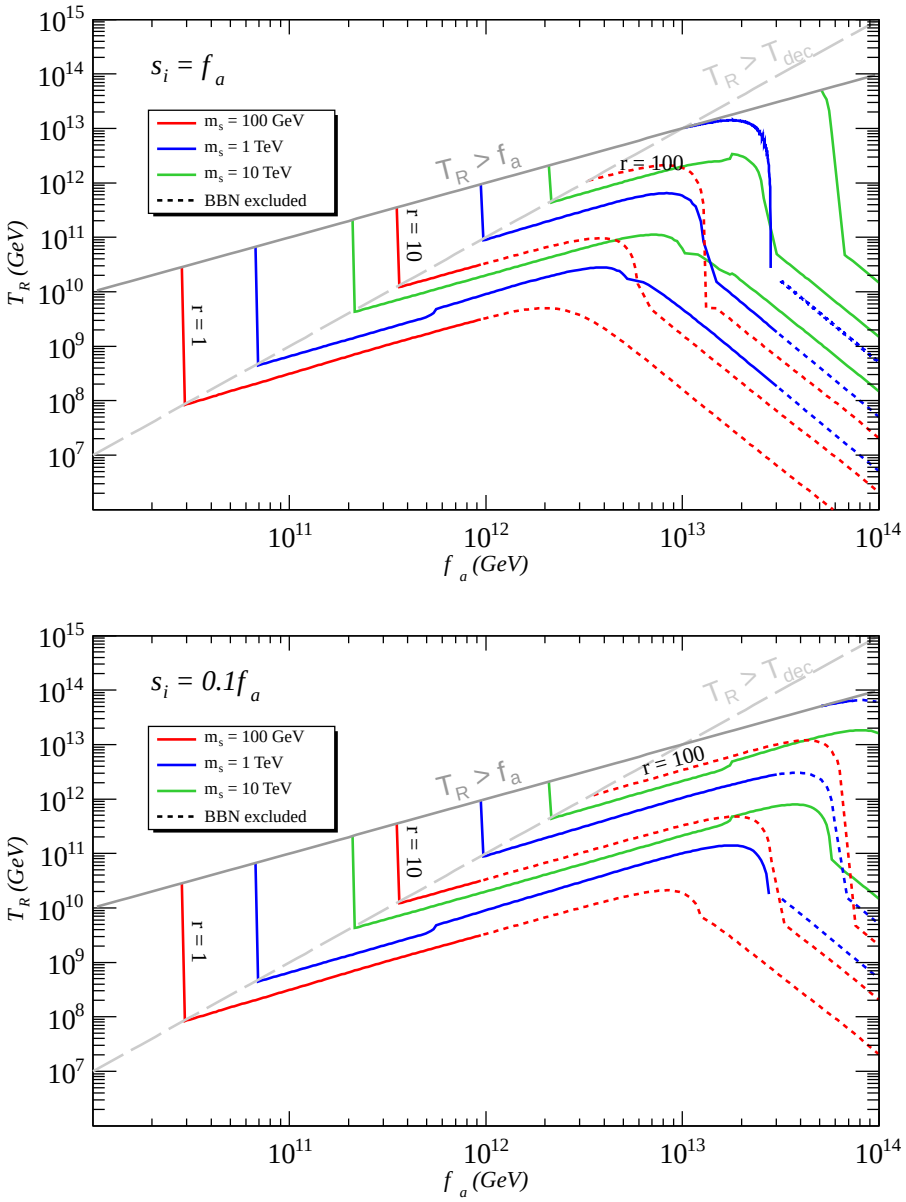

Figure 6.13: Ratio of entropy r before and after saxion decay in the f_a *vs.* T_R plane for $m_s = 0.1,\ 1,\ 10$ TeV and for $s_i/f_a = 1$ (upper frame) and $s_i/f_a = 0.1$ (lower frame). The dashed lines correspond to $T_D < 5$ MeV, when the entropy from saxion decay is injected after the beginning of BBN; these regions are likely excluded.

In Fig. 6.13b, we plot again the entropy ratio contours, but this time taking $s_i/f_a = 0.1$. In this case, saxion production from coherent oscillations is suppressed by the smaller initial saxion field strength value. This expands the range of large T_R at high f_a where entropy injection is negligible. In cases such as these, the results of the previous section remain viable and entropy injection from saxion decay would be a negligible effect. For the remaining of this Section, we will assume $s_i/f_a = 1$.

If $r > 1$, the energy densities of neutralinos (before their decay) and axions are modified according to the discussion in Sec.5.3 and are given by Eqs.(B.6) and (B.13). As shown in Fig.6.12, T_e is usually in the GeV range or below, so axinos and gravitinos are already decoupled by the time the universe becomes saxion dominated. In this case, their energy densities are simply diluted by $1/r$. Furthermore, since most baryogenesis mechanisms generate the matter-antimatter asymmetry at temperatures $T \gg T_e$, the baryon number density (η) will also be diluted by $1/r$. In this case, for the thermal leptogenesis mechanism discussed in Sec.4.2, Eq.(4.35) becomes:

$$\eta(T_0) \lesssim 3 \times 10^{-31} \frac{M_1}{\tilde{m}_1} \times \frac{1}{r} \tag{6.13}$$

so, for $r > 1$, we need (see Eq.(4.36))

$$M_1/r \gtrsim 10^{10} \text{ GeV} \Rightarrow T_R/r > 2 \times 10^9 \text{ GeV} . \tag{6.14}$$

Hence larger re-heat temperatures are required if $r > 1$. We also point out that, although $\Omega_{\tilde{G}} h^2$ gets diluted by $1/r$, the Gravitino Problem is not ameliorated by the saxion entropy injection, since the re-heat temperature required by thermal leptogenesis is also increased by exactly the same factor.

To illustrate the entropy dilution effect, in Fig.6.14 we show the relic abundance of thermally produced axinos (red), axions (blue), gravitino produced axinos (lavender) and neutralino produced axinos (magenta) for the same parameters used in Fig.6.1, but now including the saxion field with $m_s = 1$ TeV and $s_i = f_a$. Once again, the value of T_R is always adjusted to maintain $\Omega_{a\tilde{a}} = 0.1123$. As we can see, for low values of f_a, the relic abundance curves track the values shown in Fig. 6.1. In this case the saxion is short-lived and decays before dominating the energy density, so no significant entropy production occurs. As f_a increases, the thermal axino production drops, and the value of T_R must compensate by increasing the thermal yield of axinos so that $\Omega_{a\tilde{a}}h^2 = 0.1123$ is maintained. At around $f_a \sim 5 \times 10^{12}$ GeV, the value of T_D drops below T_e ($r > 1$) and significant entropy production from saxion decay occurs. The entropy injection dilutes the thermal axino and also axion production, so that a sharp increase in T_R is needed to offset the dilution effect: the dark matter abundance remains dominated by thermal axino production. However, the axion abundance is independent of T_R, so its dilution due to saxion decay is plain to see in Fig.6.14a. We also see that the neutralino relic density is diluted, once $r > 1$. On the other hand, the gravitino density is practically unaffected by the saxion entropy injection, since the dilution is compensated by the increase in T_R. For $f_a \gtrsim 3 \times 10^{13}$ GeV, the required T_R value to satisfy the DM constraint is above f_a, as seen in Fig.6.14b. For such high values of T_R, the PQ symmetry is restored during re-heat, and re-broken during subsequent cooling. The universe should break into domains of different θ_i and s_i values and a modified treatment of dark matter is needed. Therefore we

restrict our results to the $T_R < f_a$ region. We also note that, for the $\Omega_{\widetilde{Z}_1} h^2$ and $m_{\widetilde{Z}_1}$ values chosen in Fig.6.14, the BBN bounds on late decaying neutralinos are always more constraining than the bounds on saxion decays, as shown by the dotted line in Fig.6.14.

The upshot of Fig.6.14b is that, for f_a slightly above 10^{13} GeV, the value of T_R has increased to over 10^{11} GeV while maintaining $\Omega_{a\tilde{a}} h^2 = 0.1123$. Although the saxion entropy injection leads to higher values of T_R (when compared to Fig.6.1b), the allowed range for the relevant temperature for leptogenesis (T_R/r) is practically unaltered. Comparing Figs.6.1 and 6.14 we can see that, at least for this case, the range of f_a values which accommodates thermal leptogenesis is actually *reduced* when the saxion entropy injection effect is included, due to the $T_R < f_a$ condition.

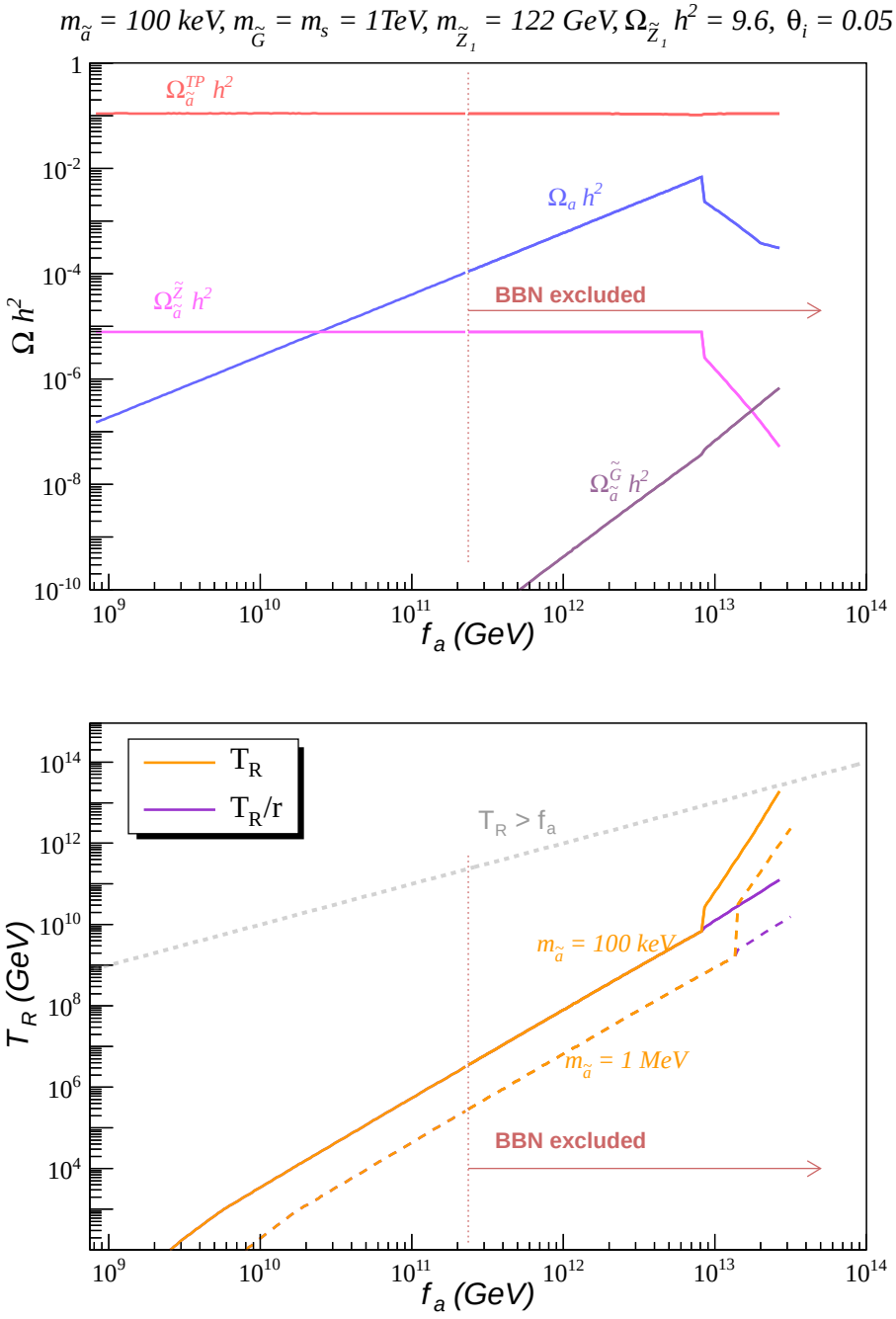

Figure 6.14: Same as Fig.6.1, but including the saxion contribution with $m_s = 1$ TeV and $s_i = f_a$.

In order to discuss the effects of including the saxion field for other choices of

PQMSSM parameters, we re-do the same scan performed over the PQMSSM parameters for the heavy gravitino (ESUSY point) scenario, but now including the saxion with $s_i = f_a$ and $m_s = m_{\widetilde{G}} = 30$ TeV. Furthermore, we differentiate solutions excluded by the BBN bounds on late decaying saxions (green points). Since in this case the relevant temperature for thermal leptogenesis is T_R/r, we show in Fig.6.15 the results in the f_a *vs.* T_R/r plane. As we can see, the region with $r > 1$, where the effect of saxion entropy injection is relevant, only affects points with $f_a \gtrsim 10^{13}$ GeV, which are excluded by the BBN constraints on late decaying neutralinos. Also, due to its heavy mass, BBN constraints on late decaying saxions are only relevant for $f_a \gtrsim 10^{15}$ GeV, as seen in Fig.6.10, and do not appear in Fig.6.15. Furthermore, we see that, even in models where $f_a \gtrsim 10^{13}$ GeV is allowed by the BBN bounds, the saxion entropy injection does not have a significant effect. Therefore we conclude that, for the heavy gravitino scenario (here illustrated by the ESUSY point from Table 6.1), the inclusion of the saxion field does not significantly change the results obtained in the last Section.

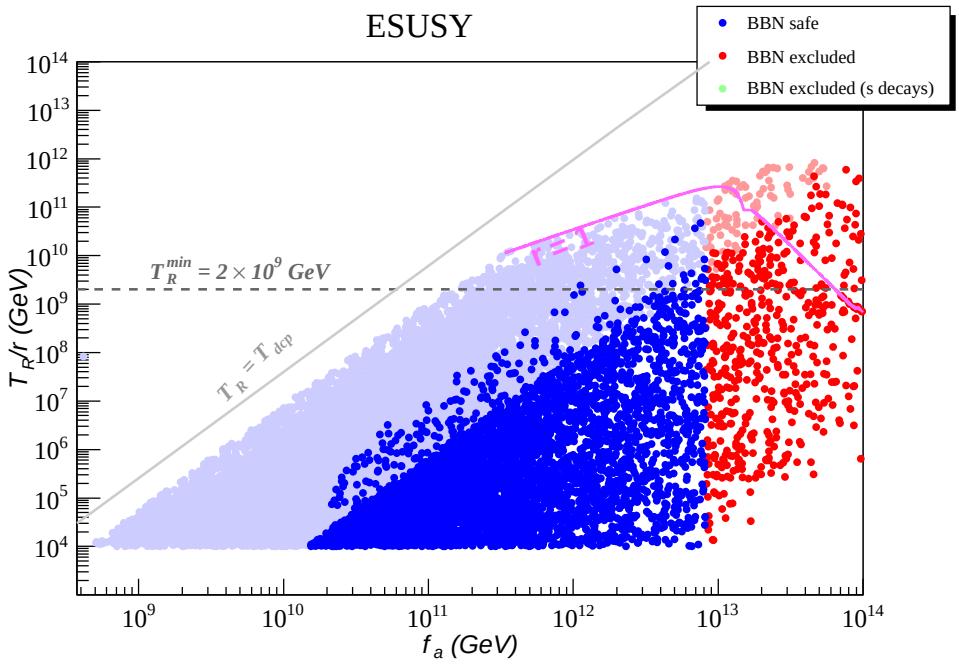

Figure 6.15: Scan over PQ parameters for the ESUSY benchmark point discussed in the text, plotted in the T_R/r *vs.* f_a plane, including the saxion field with $m_s = 30$ TeV and $s_i = f_a$. Same color code as in Fig.6.4.

However, as shown by Figs.6.13 and 6.14, if $m_s \lesssim 1$ TeV, significant entropy may be produced and, if $f_a > 10^{13}$ GeV, there will be extra constraints from the BBN bounds on saxion decays, as shown by Fig.6.10. Since a lighter saxion is compatible with models with a NLSP gravitino, we now consider the effects of including a 1 TeV saxion in the PQMSSM models of Fig.6.7, where $m_{\widetilde{G}} = m_{\widetilde{Z}_1}/2$. The results are shown in Figs.6.16-6.18.

By including dilution of DM from saxion production and decay, the allowed points can now reach to T_R as high as $\sim 10^{13}$ GeV for $f_a \sim 1.5 \times 10^{13}$ GeV, although the value of T_R/r reaches only as high as $\sim 10^{11}$ GeV. These points with $T_R/r \gtrsim 2 \times 10^9$

GeV evidently reconcile thermal leptogenesis with the gravitino problem even in the presence of entropy injection from saxion decay.

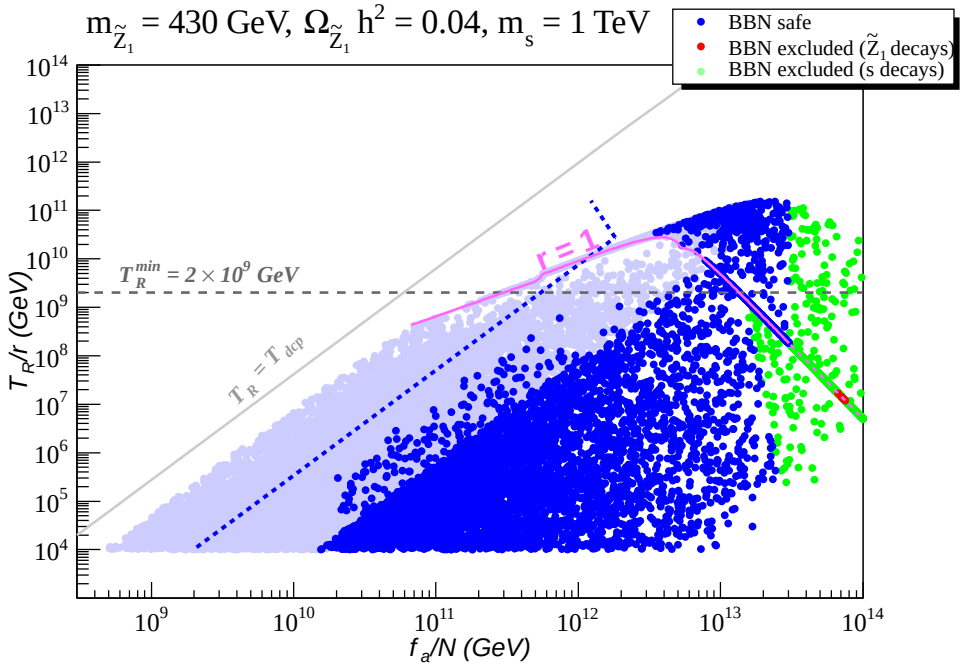

Figure 6.16: Same as Fig.6.7, but now including the saxion field with $m_s = 1$ TeV and $s_i = f_a$. Points in green are excluded due to BBN constraints on late decaying saxions.

In Fig.6.17, we plot the axion mis-alignment angle θ_i. Unlike the previous results in Fig.6.6 with no entropy injection, the allowed values of θ_i with $T_R/r > 2 \times 10^9$ GeV span a range from 0 to ~ 1 radians: for higher values of T_R, larger values of θ_i can be tolerated since the relic abundance of axions is now diluted by saxion decay. Therefore, in this case, the axion mis-alignment angle is not required to take unnaturally small values, as opposed to the case without the saxion dilution, shown in Fig.6.6.

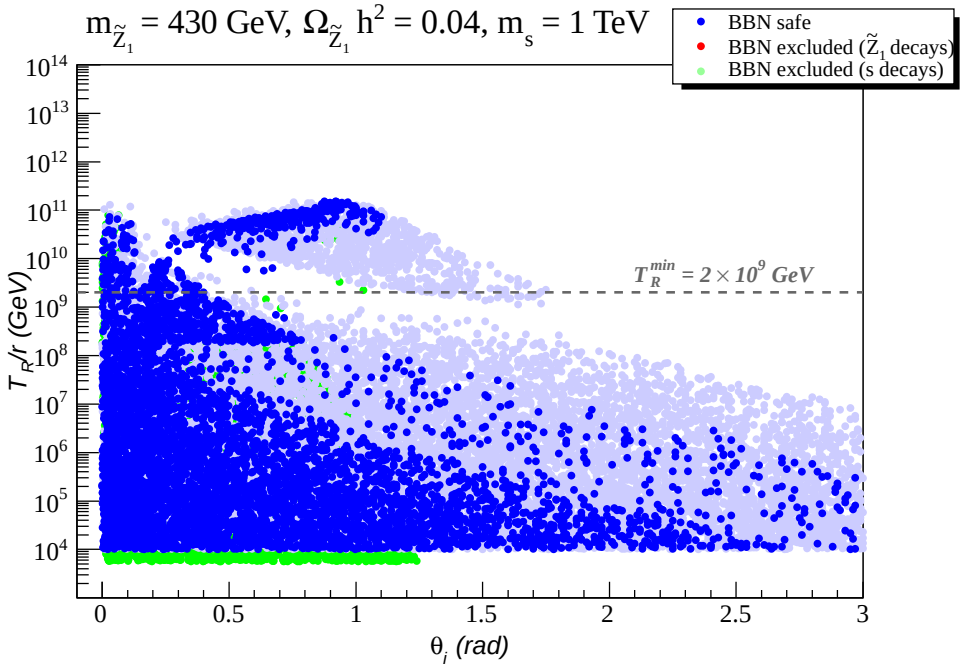

Figure 6.17: Allowed and disallowed points in the θ_i *vs.* T_R/r plane for $\Omega_{\widetilde{Z}_1}h^2 = 0.04$ and $m_{\widetilde{Z}_1} = 430$ GeV, with $m_s = 1$ TeV.

To see whether axinos or axions dominate the DM density including entropy from saxions, in Fig.6.18 we plot the same points, but this time versus axion relic density $\Omega_a h^2$. We see that the bulk of points with $T_R/r > 2 \times 10^9$ GeV that are BBN-allowed indeed have *mainly axion* CDM. Note that the point shown in Fig.6.14, which has $\theta_i = 0.05$ and mainly axino DM (at $T_R > 2 \times 10^9$ GeV), corresponds to the few points of Fig.6.18 at low $\Omega_a h^2$ and is not the most common scenario, since it requires quite small values of the mis-alignment angle.

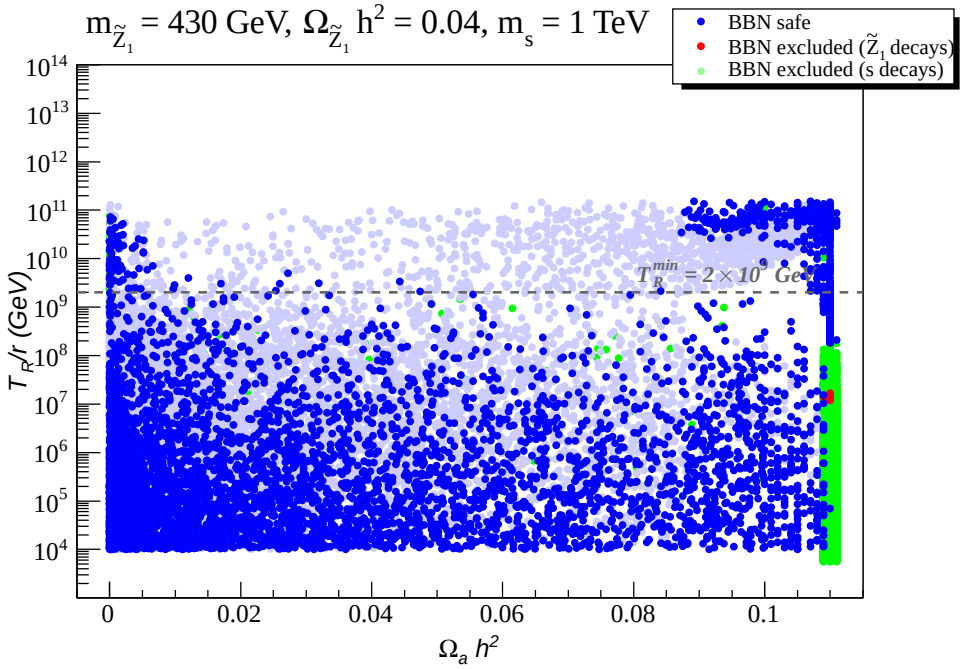

Figure 6.18: Allowed and disallowed points in the $\Omega_a h^2$ *vs.* T_R/r plane for $\Omega_{\widetilde{Z}_1} h^2 = 0.04$ and $m_{\widetilde{Z}_1} = 430$ GeV, with $m_s = 1$ TeV.

To conclude this section we present model independent constraints on MSSM models imposed by the $T_R/r > 2 \times 10^9$ GeV requirement. We re-do the same scan performed in Fig.6.8, but now including a 1 TeV saxion with $s_i = f_a$. The results are shown in Fig.6.19, where the red points are excluded due to the BBN constraints on $\widetilde{Z}_1$ decays; no green points due to constraints from BBN on saxion decay are visible. By comparing Figs. 6.8 and 6.19, we see that due to the saxion dilution of the neutralino relic density, the BBN bounds on $\Omega_{\widetilde{Z}_1}$ are less severe and a larger portion of the MSSM parameter space can be consistent with thermal leptogenesis.

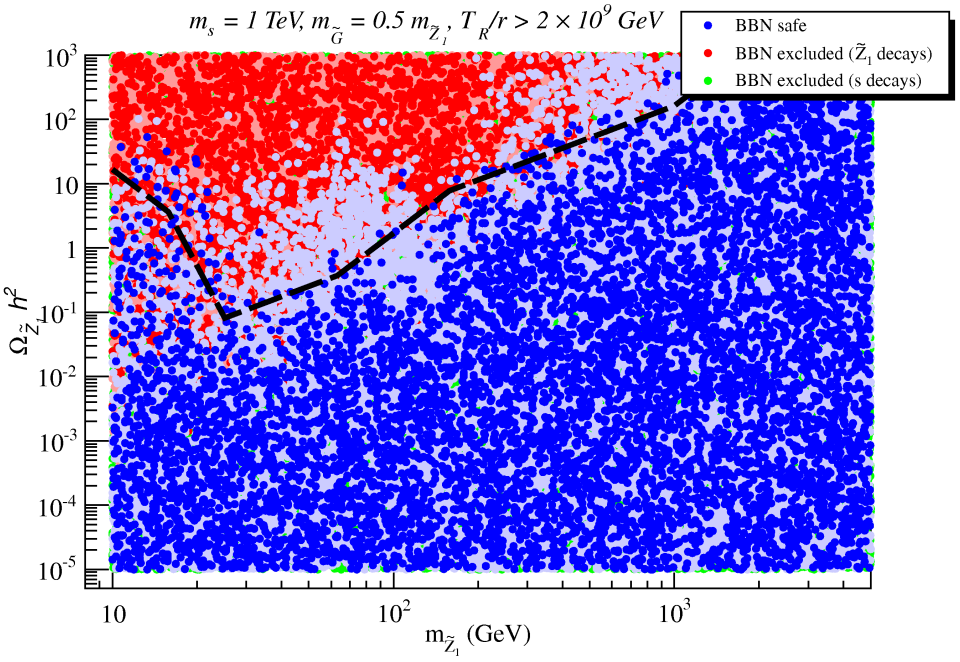

Figure 6.19: Allowed and disallowed points in the $\Omega_{\widetilde{Z}_1} h^2$ *vs.*$m_{\widetilde{Z}_1}$ plane for a general scan over SUSY models with a bino $\widetilde{Z}_1$. For all points, we require $T_R > 2\times 10^9$ GeV and assume $m_{\widetilde{G}} = m_{\widetilde{Z}_1}/2$. Dark blue points are consistent with BBN and have mainly CDM with at most 20% WDM and/or 1% HDM admixture. The region below the dashed line represents the MSSM parameter space where 99% of the CDM/BBN consistent solutions lie.

Although we have assumed a gravitino NLSP for the results in Figs.6.16-6.19, we stress that the same results are valid in the heavy gravitino ($m_{\widetilde{G}} \gtrsim 30$ TeV) case, as long as we keep $m_s = 1$ TeV. This is simply due to the fact that gravitinos do not significantly contribute to $\Omega_{a\tilde{a}}h^2$ in the axino LSP scenario, as shown by Eq.(6.3). Furthermore, the BBN bounds on gravitino decays can always be neglected if $m_{\widetilde{G}} \gtrsim 30$ TeV or $m_{\widetilde{G}} < m_{\widetilde{Z}_1}$.

6.3 Summary

The axino LSP scenario discussed here has the important property of providing a solution for the first part of the Gravitino Problem (overproduction of DM) as well as loosening the dark matter constraints on the MSSM sector of the theory. We have shown that almost any values of $\Omega_{\tilde{Z}_1}h^2$ and $m_{\tilde{Z}_1}$ are allowed if:

- $f_a \lesssim 10^{11}$ GeV, so neutralinos decay before BBN,
- $T_R \lesssim 10^6$ GeV, so thermal axinos are not overproduced and
- $m_s \gtrsim 100$ GeV, so saxions decay before BBN.

As discussed in Sec.6.2, the above conditions also assure that the saxion field does not have a significant impact on the thermal evolution of the universe, since, for the above range of f_a and T_R values, saxions are never produced in enough abundance to dominate the energy density of the universe (see Fig.6.12).

The second part of the Gravitino Problem (violation of BBN constraints) can be solved if:

- $m_{\tilde{G}} \gtrsim 30$ TeV or $T_R \lesssim 10^6$ GeV (this solution is independent of the PQ sector and also works within the MSSM) or
- $m_{\tilde{a}} < m_{\tilde{G}} < m_{\tilde{Z}_1}$, so gravitino decays are invisible and do not affect BBN; this solution is clearly only possible within the PQMSSM.

The conditions listed above are quite general and, for a suitable choice of the other PQ parameters $(m_{\tilde{a}}, \theta_i, m_s, s_i)$, can make almost any MSSM model with a neutralino

LSP (or NLSP for the case of $m_{\widetilde{G}} < m_{\widetilde{Z}_1}$) consistent with DM and BBN constraints once the axion supermultiplet is introduced.

In Fig.6.20, we show the evolution of the relic densities as a function of temperature for a choice of PQMSSM parameters that satisfies all the above conditions and has $\Omega_{DM}h^2 = 0.115$. The thermal saxion, axino and gravitino components are only shown after they have become non-relativistic. For the parameters chosen, the saxion starts to oscillate during the decay of the inflaton field, at $T > T_R$, as discussed in Sec.5.2. For $T > m_s$ (1 TeV), we just show the coherent oscillation component and at $T = 1$ TeV we add the non-relativistic saxion contribution, which causes the jump seen in Fig.6.20. As we can see, for such low f_a and T_R, the saxion energy density is dominated by its thermal component and it is always much smaller than ρ_R, so the universe is always radiation dominated. Although neutralinos and saxions decay before BBN, the gravitino decays at $T \sim 3$ keV, after the formation of light elements. However, due to the low re-heat temperature, the gravitino relic density (before decay) is $\Omega_{\widetilde{G}}h^2 \simeq 10^{-5}$, so its decay does not violate the BBN bounds, shown in Fig.4.1. For the parameters chosen, $\Omega_{\tilde{a}}h^2 = 0.11$ and $\Omega_a h^2 = 0.004$, so dark matter is predominantly composed of axinos.

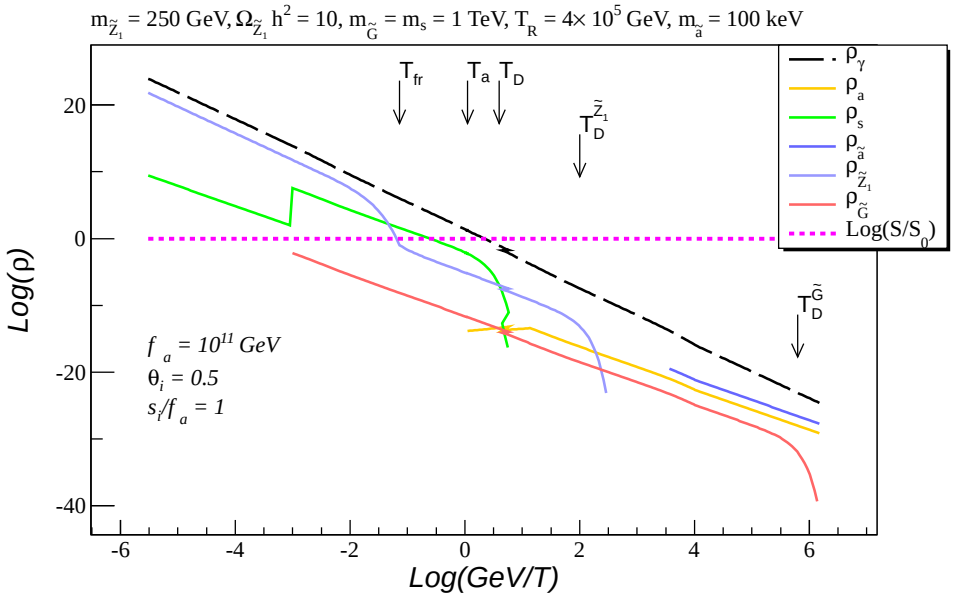

Figure 6.20: Evolution of the radiation, neutralino, gravitino, axion, saxion and axino energy densities and the entropy ratio as a function of the temperature. We also show the neutralino freeze-out temperature (T_{fr}), the axion oscillation temperature (T_a), the saxion decay temperature (T_D) and the neutralino ($T_D^{\widetilde{Z}_1}$) and gravitino ($T_D^{\widetilde{G}}$) decay temperatures. The PQMSSM parameters are: $f_a = 10^{11}$ GeV, $m_s = 1$ TeV, $m_{\tilde{a}} = 100$ keV, $\theta_i = 0.5$, $s_i = f_a$, $T_R = 4 \times 10^5$ GeV, $m_{\widetilde{G}} = 1$ TeV, $m_{\widetilde{Z}_1} = 250$ GeV and $\Omega_{\widetilde{Z}_1} h^2 = 10$.

The low T_R necessary to suppress axino overproduction required by the above conditions does not allow for the implementation of the thermal leptogenesis mechanism, which requires $T_R/r > 2 \times 10^9$ GeV. As discussed in Sec.6.1, requiring large re-heat temperatures significantly constrains the PQMSSM parameters space. From Figs.6.5, 6.7 and 6.16 we see that $T_R/r > 2 \times 10^9$ GeV requires $f_a \gtrsim 10^{12}$ GeV and neutralinos and saxions will be long-lived ($\tau \gtrsim 10^{-2}$s), unless $m_{\widetilde{Z}_1,s} \gtrsim 0.5$ TeV. As shown in

Sec.6.2, the range of PQMSSM parameters required to implement thermal leptogenesis strongly depends on the saxion sector, since for such large T_R and f_a values, the universe may become temporarily saxion dominated. In this case, significant entropy injection and dilution of the neutralino, gravitino, axion and axino relic densities can occur. However, we have shown that, if $m_s \gtrsim 10$ TeV, the inclusion of the saxion field has no relevant consequences (see Fig.6.15). Thus in the multi-TeV saxion case, the conditions for achieving $T_R/r > 2 \times 10^9$ GeV are the same as the ones for when the saxion is neglected, shown in Figs.6.5-6.6:

- $m_{\tilde{a}} \lesssim 200$ keV to suppress the contribution of thermal axinos to $\Omega_{DM}h^2$,
- $\theta_i \lesssim 0.5$ to suppress the axion contribution to $\Omega_{DM}h^2$,
- $\Omega_{\widetilde{Z}_1} \lesssim 0.1(1)$, for $m_{\widetilde{Z}_1} \lesssim 100(500)$ GeV in order to avoid the BBN bounds on late decaying neutralinos and
- $m_{\widetilde{G}} \gtrsim 30$ TeV or $m_{\widetilde{G}} < m_{\widetilde{Z}_1}$ to avoid the BBN bounds on late decaying gravitinos.

In Fig.6.21, we once again show the evolution of the energy densities, but now for a point consistent with thermal leptogenesis and satisfying the above conditions with a multi-TeV saxion. Also, to give an example of the gravitino NLSP scenario, we choose $m_{\widetilde{G}} = 100$ GeV. As we can see, due to their large mass, saxions decay just before ρ_s becomes larger than the radiation energy density, so the universe is always radiation dominated. While saxions decay before BBN ($T_D \simeq 5$ MeV), due to the large f_a value, neutralinos decay during the formation of light elements ($T_D^{\widetilde{Z}_1} \simeq 0.1$ MeV), but

the BBN bounds are not violated due to its small relic abundance. Gravitinos decay after BBN, but since they decay exclusively into axions and axinos, the abundance of light elements is not affected[7]. Finally, we note that for the parameters chosen, dark matter is almost exclusively composed of axions.

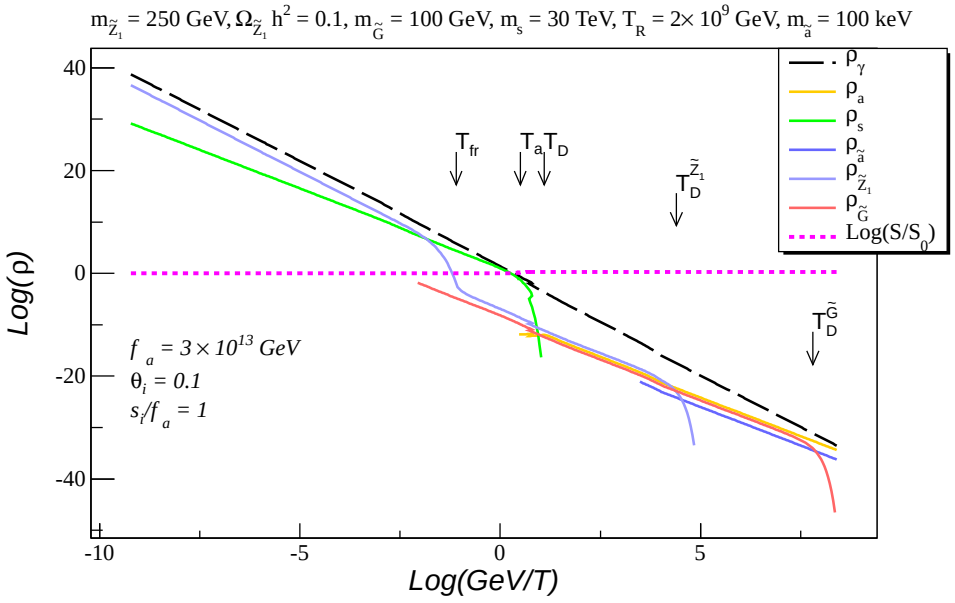

Figure 6.21: Evolution of the radiation, neutralino, gravitino, axion, saxion and axino energy densities and the entropy ratio as a function of the temperature. We also show the neutralino freeze-out temperature (T_{fr}), the axion oscillation temperature (T_a), the saxion decay temperature (T_D) and the neutralino ($T_D^{\widetilde{Z}_1}$) and gravitino ($T_D^{\widetilde{G}}$) decay temperatures. The PQMSSM parameters are: $f_a = 3 \times 10^{13}$ GeV, $m_s = 30$ TeV, $m_{\tilde{a}} = 100$ keV, $\theta_i = 0.1$, $s_i = f_a$, $T_R = 2 \times 10^9$ GeV, $m_{\widetilde{G}} = 100$ GeV, $m_{\widetilde{Z}_1} = 250$ GeV and $\Omega_{\widetilde{Z}_1} h^2 = 0.1$.

[7]Here we neglect possible bounds on $\rho_{\widetilde{G}}$ from the CMB spectrum.

From Fig.6.21, we see that a multi-TeV saxion decays before it can dominate the energy density of the universe, even for large values of f_a and T_R. On the other hand, if $m_s \lesssim 1$ TeV, saxions will have larger lifetimes and the entropy injection from saxion decays may significantly dilute the axion, axino, neutralino and gravitino energy densities. Furthermore, saxions may decay during BBN, so the BBN constraints on late decaying saxions impose an upper bound on the PQ scale, which depends only on m_s and T_R, as shown by Fig.6.10. In particular, for a 1 TeV saxion and $s_i = f_a$, we have shown that thermal leptogenesis can be made viable if

- $f_a \lesssim 2 \times 10^{13}$ GeV to avoid the BBN bounds on saxion decays,
- $m_{\tilde{a}} \lesssim 2$ MeV to suppress the contribution of thermal axinos to $\Omega_{DM}h^2$,
- $\theta_i \lesssim 1$ to suppress the axion contribution to $\Omega_{DM}h^2$,
- $\Omega_{\widetilde{Z}_1} \lesssim 1(10)$, for $m_{\widetilde{Z}_1} \lesssim 100(500)$ GeV in order to avoid the BBN bounds on late decaying neutralinos.

Furthermore, as discussed in Sec.6.2, the inclusion of the saxion has no effect on the Gravitino Problem, hence the conditions on the gravitino mass are the same as before:

- $m_{\widetilde{G}} \gtrsim 30$ TeV or $m_{\widetilde{G}} < m_{\widetilde{Z}_1}$ to avoid the BBN bounds on late decaying gravitinos.

From the above conditions on the PQMSSM parameters, we see that – once a TeV scale saxion is included – the entropy dilution effect allows for a wider range of $m_{\tilde{a}}$, θ_i and $\Omega_{\widetilde{Z}_1}h^2$ values. On the other hand, due to the BBN constraints on late

decaying saxions, there is now an upper limit on the PQ scale: $f_a \lesssim 2 \times 10^{13}$ GeV, for $m_s = 1$ TeV. We point out that this upper limit is distinct from the one imposed by the BBN constraints on neutralinos (red points in the scatter plots), since the latter can be relaxed without affecting any of the previous results if MSSM models with smaller neutralino relic densities are considered.

In Fig.6.22, we show the same evolution of energy densities shown in Fig.6.21, but now assuming a light saxion ($m_s = 500$ GeV). In this case, the universe becomes saxion dominated for $T_D < T < T_e$, as seen in Fig.6.22. We choose $f_a = 10^{13}$ GeV, so $T_D \simeq 5$ MeV and the saxion-dominated era ends before neutron decoupling, thus avoiding the BBN constraints discussed in Sec.4.1. For the parameters chosen, the entropy production factor is $r \simeq 11$ and since the axion starts to oscillate before the saxion dominated era begins ($T_a > T_e$), its relic abundance is diluted by $1/r$ (see Eq.(B.6)). As a consequence, a larger θ_i value (when compared to Fig.6.21) is required to satisfy $\Omega_{DM}h^2 = 0.11$, which again is dominated by the axion component. The neutralino, gravitino and axino abundances are also diluted by $1/r$.

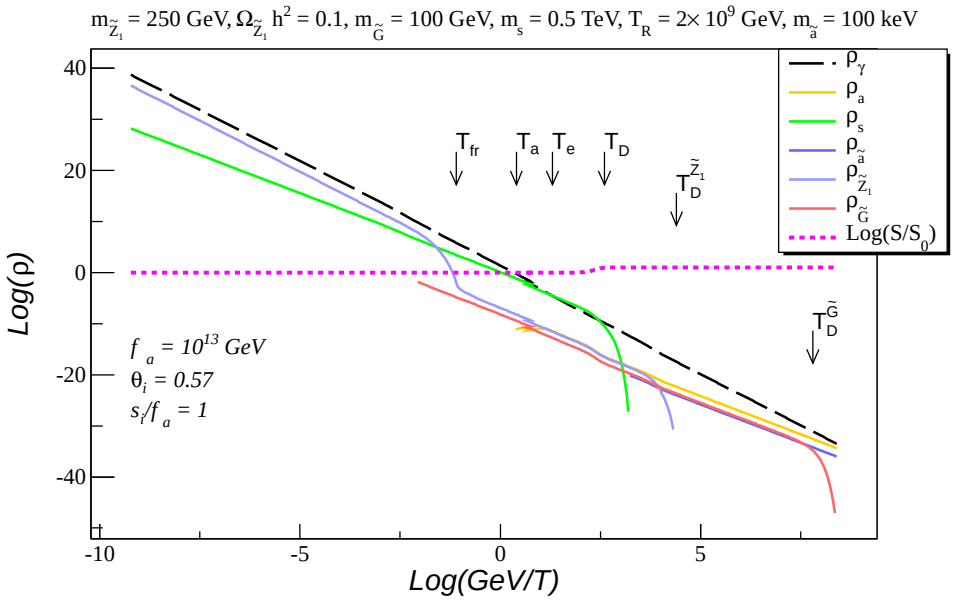

Figure 6.22: Evolution of the radiation, neutralino, gravitino, axion, saxion and axino energy densities and the entropy ratio as a function of the temperature. We also show the neutralino freeze-out temperature (T_{fr}), the axion oscillation temperature (T_a), the temperature when the universe becomes saxion dominated (T_e), and the saxion (T_D), neutralino ($T_D^{\widetilde{Z}_1}$) and gravitino ($T_D^{\widetilde{G}}$) decay temperatures. The PQMSSM parameters are: $f_a = 10^{13}$ GeV, $m_s = 0.5$ TeV, $m_{\tilde{a}} = 100$ keV, $\theta_i = 0.57$, $s_i = f_a$, $T_R = 2 \times 10^9$ GeV, $m_{\widetilde{G}} = 100$ GeV, $m_{\widetilde{Z}_1} = 250$ GeV and $\Omega_{\widetilde{Z}_1} h^2 = 0.1$.

To conclude this Section, we illustrate the bounds on MSSM models in the axino LSP scenario, assuming $T_R/r > 2 \times 10^9$ GeV and $m_{\widetilde{G}} > 30$ TeV or $m_{\widetilde{G}} < m_{\widetilde{Z}_1}$, so the BBN bounds on gravitinos can be neglected. In Figs.6.8 and 6.19, the dashed lines approximately show the region in the $m_{\widetilde{Z}_1}$ *vs.* $\Omega_{\widetilde{Z}_1} h^2$ plane consistent with thermal leptogenesis, once the other PQMSSM parameters are free to variate in the range of Eq.(6.7). Fig.6.8 shows results for a very heavy saxion or $s_i \ll f_a$ (so the saxion

component can be neglected), while 6.19 shows the result for a 1 TeV saxion with $s_i = f_a$. We may then translate this into a contour in the m_0 *vs.* $m_{1/2}$ plane of mSUGRA for $A_0 = 0$, $\mu > 0$ and constant $\tan\beta$, as shown for the cases of $\tan\beta = 10$, 50 and 55 in Fig. 6.23. The gray regions are excluded because they violate the LEP2 limits on Higgs or sparticle masses[8]; the green-shaded regions contain a $\tilde{\tau}_1$ as NNLSP, for which a different treatment is needed[38].

First, we consider the heavy saxion scenario, where the saxion decays at very early times and can be neglected. In Fig.6.23a, we show the mSUGRA m_0 *vs.* $m_{1/2}$ plane for $\tan\beta = 10$. The strips of dark blue and purple points show the regions that allow for $T_R > 2 \times 10^9$ GeV, while maintaining $\Omega_{a\tilde{a}}h^2 = 0.1123$ and respecting bounds from BBN. The subset of purple points at low $m_{1/2}$ satisfies in addition the following constraints on low energy (LE) observables:

1. $\Delta a_\mu^{SUSY} = (7.90 - 37.39) \times 10^{-10}$,
2. $BR(b \to s\gamma) = (2.79 - 4.3) \times 10^{-4}$,
3. $BR(B_s \to \mu^+\mu^-) < 4.7 \times 10^{-8}$,
4. $0.55 < BR(B_u \to \tau^+\nu_\tau)^{\rm MSSM}/BR(B_u \to \tau^+\nu_\tau)^{\rm SM} < 2.71$

where $1. - 3.$ were calculated using Isajet/Isatools[68, 69] and 4. was calculated using SuperIso.

[8]The LEP2 limit on a SM-like Higgs scalar h is $m_h > 114.4$ GeV. Here, we use $m_h > 111$ GeV allowing for an approximate 3 GeV error on the theory calculation of m_h. For the SUSY mass limits we use those implemented in SuperIso[67].

We see that the consistent regions, although broader, are very similar to the classic mSUGRA regions with neutralino dark matter: the stau co-annihilation region at low m_0 and the light Higgs resonance region where $\widetilde{Z}_1\widetilde{Z}_1 \to h$ at $m_{1/2} \sim 150$ GeV. The reason is that a rather low abundance of thermal neutralinos is required in this scenario to satisfy BBN constraints on late decaying $\widetilde{Z}_1$s. For comparison, the classic mSUGRA strips where the neutralino relic density $\Omega_{\widetilde{Z}_1}h^2 = 0.1123 \pm 0.0105$ are shown as yellow/orange points.

Invoking next the $\Omega_{\widetilde{Z}_1}$ *vs.* $m_{\widetilde{Z}_1}$ contour of Fig.6.19, which includes the effect of entropy generation from a 1 TeV saxion, the consistent regions broaden out considerably. The region with $T_R/r > 2 \times 10^9$ GeV is denoted here by light blue points, and expands to fill the lower m_0 portion of the m_0 *vs.* $m_{1/2}$ plane along with a band around $m_{1/2} \sim 400$ where turn-on of the $\widetilde{Z}_1\widetilde{Z}_1 \to t\bar{t}$ annihilation channel reduces the neutralino abundance. The portion of the leptogenesis-consistent region including saxion decays and LE constraints is colored in pink and requires $m_{1/2} \lesssim 550$ GeV and $m_0 \lesssim 500$ GeV, so as to allow for a significant contribution to $(g-2)_\mu$ by light charginos and sneutrinos. The remaining unshaded (white) region of the mSUGRA plane does not allow for thermal leptogenesis because the relic density of neutralinos is so large that the BBN constraints on late decaying $\widetilde{Z}_1$ are violated.

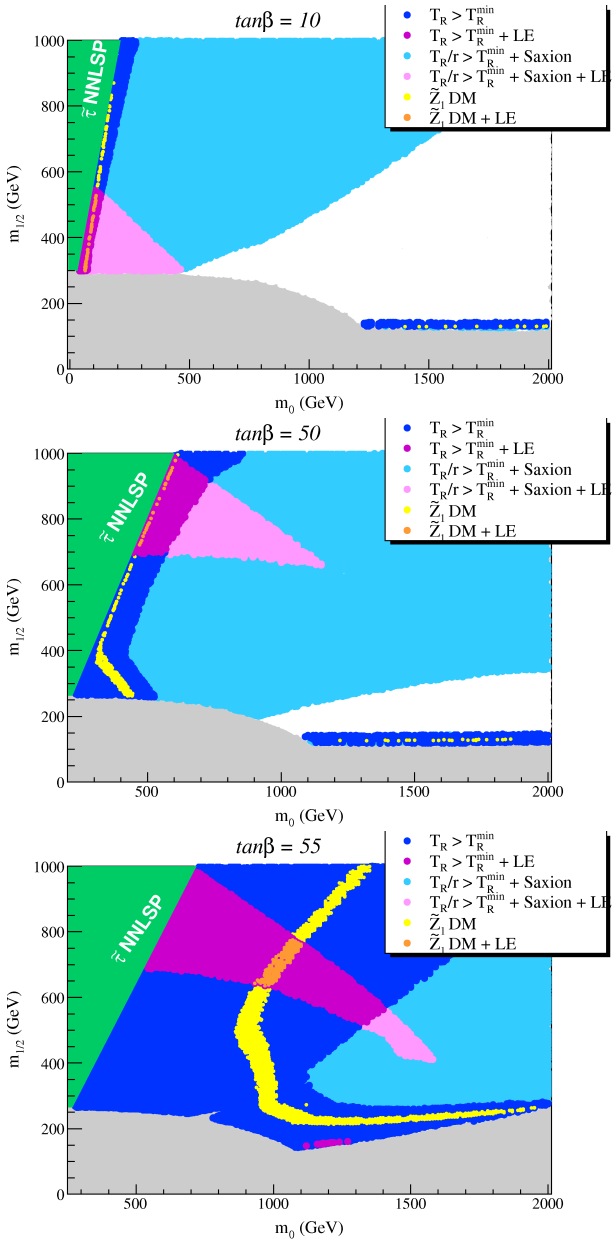

Figure 6.23: Regions in the m_0 *vs.* $m_{1/2}$ plane of the mSUGRA model with $A_0 = 0$ and $\mu > 0$ which satisfy 1. $T_R > T_R^{min} = 2 \times 10^9$ GeV (dark blue), 2. $T_R > T_R^{min}$ and LE constraints (purple), 3. $T_R/r > T_R^{min}$ with saxion entropy injection (light blue) and 4. $T_R/r > T_R^{min}$ with saxion entropy injection and LE constraints (pink). For comparison, the yellow/orange points indicate the classic mSUGRA regions with $\Omega_{\widetilde{Z}_1} h^2 = 0.1123 \pm 0.0105$. We show frames for *a*) $\tan\beta = 10$, *b*) $\tan\beta = 50$ and *c*) $\tan\beta = 55$.

Frame b of Fig.6.23, shows the analogous plot for $\tan\beta = 50$. In this case, b- and τ-Yukawa couplings increase greatly, while the value of m_A drops, enabling efficient annihilation of neutralinos via stau co-annihilation or s-channel A exchange. The neutralino abundance $\Omega_{\widetilde{Z}_1}h^2$ is severely reduced, and less constrained by BBN. The area of leptogenesis-consistent regions increases. Furthermore, the SUSY contributions to $b \to s\gamma$ and $(g-2)_\mu$ increase with increasing $\tan\beta$, and so the region which is consistent with LE constraints moves to higher $m_{1/2}$ values. If saxion entropy production is added, almost the whole plane is allowed.

Finally, frame c shows the case of $\tan\beta = 55$, where the A-resonance dominates the $\widetilde{Z}_1\widetilde{Z}_1$ annihilation amplitudes. Here, we see that a huge swath of parameter space is consistent with thermal leptogenesis, even without the effect of saxion decays. By including entropy from saxion decay, the entire m_0 $vs.$ $m_{1/2}$ plane is allowed. The part which is consistent with LE constraints follows suit, leading to a large region of parameter space that is consistent with all constraints.

Chapter 7

The Neutralino LSP

In the last Section, we discussed the axino LSP scenario, which can greatly expand the MSSM parameter space consistent with the BBN and DM constraints as well as thermal leptogenesis, as illustrated by Fig.6.23. Here, we discuss the possibility of the heavy axino scenario, which can happen in KSVZ-type models, as discussed in Sec.3.2. The main consequence of a heavy axino is that it will cascade decay to the LSP (here assumed to be the neutralino) and consequently enhance the neutralino relic abundance. Therefore, we expect that MSSM models with $\Omega_{\widetilde{Z}_1} h^2 \gtrsim 0.11$ will not be consistent with the DM constraints, once the axion superfield with a heavy axino is included. Another possible consequence of the heavy axino scenario is that the universe may become temporarily dominated by the axino field, in a way analogous to the light saxion case, discussed in last Section. The discussion here follows closely Ref.[70].

In the heavy axino scenario, the universe may have both an early saxion and/or axino dominated phases, so the early thermal history of the universe may become quite involved. The appropriate treatment in this case requires the use of the full set of coupled Boltzmann equations describing the axion supermultiplet, the neutralino, the gravitino and the radiation components. For simplicity, we will not pursue this approach here. Instead, we neglect the saxion field throughout this Section. This is justified in the heavy saxion limit ($m_s \gtrsim 10$ TeV), where saxions decay before the

neutralino freeze-out and the start of axion coherent oscillations. In this case, the only possible effect of the saxion field is to dilute the thermal gravitino and axino densities by $1/r_s$, where r_s is the entropy production from saxion decays. Since $\rho_{\widetilde{G},\tilde{a}} \propto T_R$, the entropy dilution by (heavy) saxion decays is equivalent to re-scaling T_R by $1/r_s$. In the following we simply assume $r_s = 1$, with the understanding that if a heavy saxion dominates the early universe, T_R should be rescaled. Obviously this is not valid for the light saxion scenario, where saxion decays may directly affect the neutralino and axion relic abundances. However, we will not consider such cases here.

Before discussing the heavy axino cosmology, we make one last simplifying assumption. In the neutralino LSP scenario, gravitinos cascade decay to neutralinos, hence the Gravitino Problem in this case is identical to the MSSM scenario, discussed in Sec.4.2. The only distinction is the possible dilution of gravitinos from axino (or saxion) decays. However, as discussed in Sec.6.2, this does not affect the Gravitino Problem (see discussion following Eq.(6.14)). Therefore, the conditions necessary for solving the Gravitino Problem in the PQMSSM with a neutralino LSP are identical to the solution within the MSSM: $m_{\widetilde{G}} \gtrsim 30$ TeV or $T_R \lesssim 10^6$ GeV. For the remainder of this Section, we assume $m_{\widetilde{G}} \gtrsim 30$ TeV, so gravitinos can be neglected[1].

Under the assumptions described above, we only need to consider the neutralino, axion and axino components when discussing the BBN and DM constraints on the neutralino LSP scenario. The BBN constraints apply to late decaying axinos and depend on the axino decay temperature (T_D). The axino lifetime is given by Eq.(3.11)

[1]The gravitino contribution to $\Omega_{\widetilde{Z}_1}$ is neglegible for most of the T_R and $m_{\widetilde{Z}_1}$ values assumed in this Section.

and is strongly dependent on the SUSY spectrum, since the $\widetilde{Z}_{2,3,4}$ and $\tilde{g}$ decay modes are kinematically allowed only if the axino is sufficiently heavy. Therefore it is necessary to choose a specific MSSM model when discussing the decay properties of axinos. Here we will present results for a mSUGRA point (SUGRA1) with $(m_0, m_{1/2}, A_0, \tan\beta, \mu) = (4525\ \text{GeV}, 275\ \text{GeV}, 0, 10, > 0)$, which has a LSP neutralino with mass 87.9 GeV, while the calculated freeze-out abundance of neutralinos in the MSSM, obtained from IsaReD[71], is $\Omega^{MSSM}_{\widetilde{Z}_1} h^2 = 0.05$. Many sparticle masses and low energy observables are listed in Table 7.1. Since the weak-scale value of the superpotential μ term is only 137.2 GeV, the $\widetilde{Z}_1$ is of mixed higgsino-bino-wino type. The axino decay widths for this model are shown as a function of the axino mass in Fig.7.1 for $f_a = 10^{12}$ GeV. We see that for very low axino masses ($m_{\tilde{a}} \sim m_{\widetilde{Z}_1}$), only the decay $\tilde{a} \to \widetilde{Z}_1 \gamma$ is open, and $\Gamma_{\tilde{a}}$ is very small. As $m_{\tilde{a}}$ increases, additional decay modes become allowed and contribute to $\Gamma_{\tilde{a}}$. Once the decay to $\tilde{g}g$ opens up, this mode is dominant. In this case the axino lifetime can be approximated by:

$$\tau_{\tilde{a}} \simeq 3 \times 10^{-5} s \left(\frac{f_a}{10^{12}\ \text{GeV}}\right)^2 \left(\frac{10^3\ \text{GeV}}{m_{\tilde{a}}}\right)^3 \left(1 - \frac{m_{\tilde{g}}^2}{m_{\tilde{a}}^2}\right)^{-3} \quad (\text{for } m_{\tilde{a}} > m_{\tilde{g}})\ . \quad (7.1)$$

Thus, if $m_{\tilde{a}} > m_{\tilde{g}}$ and $m_{\tilde{a}} \gtrsim 1$ TeV, the axino is short-lived and will decay before BBN ($\tau_{\tilde{a}} \lesssim 10^{-2}$), unless $f_a \gtrsim 10^{14}$ GeV. The BBN bounds on late decaying axinos are shown in Fig.7.2 in the $m_{\tilde{a}}$ *vs* T_R plane for $f_a = 10^{10} - 10^{14}$ GeV. Comparing with Fig.6.3, we see that the BBN bounds in the neutralino LSP scenario are more naturally avoided than in the axino LSP case, since, for the latter, neutralino decays to axinos are suppressed by the weak coupling constant and the smaller neutralino mass. The axino decay temperature can be obtained from the axino width using

Eq.(5.28):

$$T_D = \sqrt{M_{Pl}\Gamma_{\tilde{a}}}\left(\frac{45}{4\pi^3}\frac{1}{g_*(T_D)}\right)^{1/4} . \tag{7.2}$$

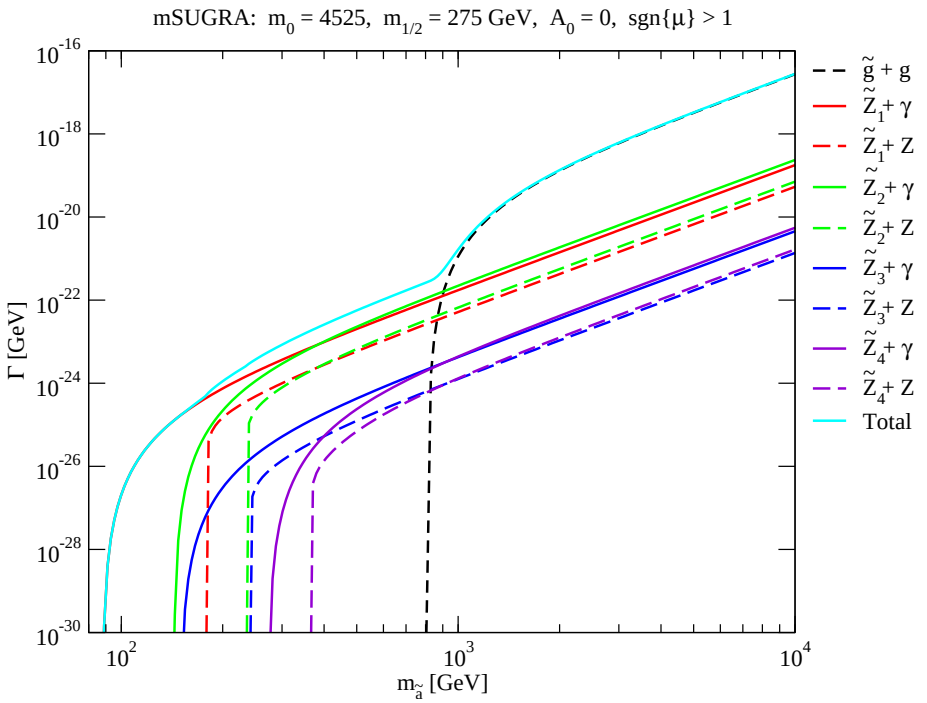

Figure 7.1: Partial and total decay width of axinos versus $m_{\tilde{a}}$ for the SUGRA1 point with $(m_0, m_{1/2}, A_0, \tan\beta, sign(mu)) = (4525, 275, 0, 10, +)$. We take $f_a = 10^{12}$ GeV.

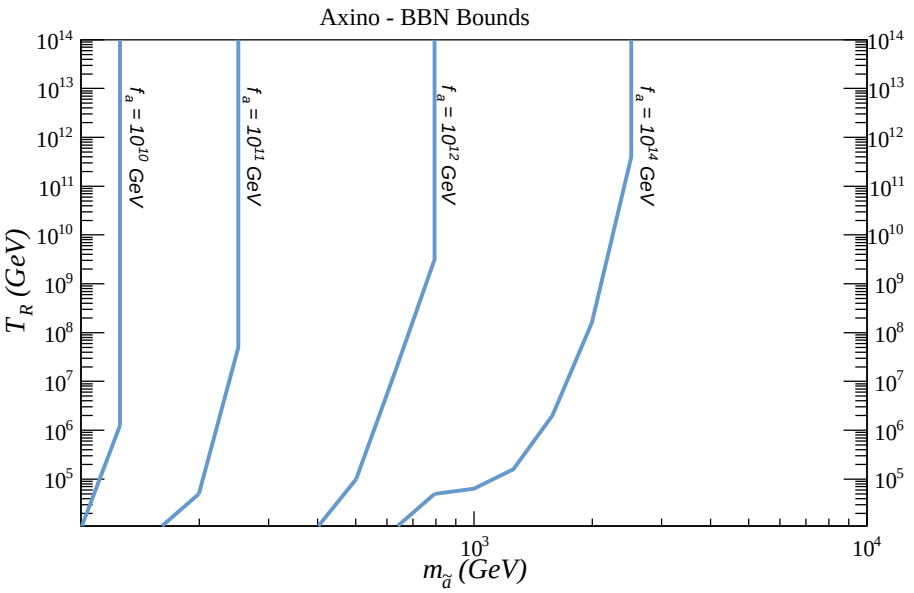

Figure 7.2: BBN bounds for thermally produced axinos in the $m_{\tilde{a}}$ *vs* T_R plane for $f_a = 10^{10}, 10^{11}, 10^{12}$ and 10^{14} GeV and the SUGRA1 point. The region to the left of the curves is excluded by BBN constraints on axino decays.

As mentioned above, if the axino is produced at large rates in the early universe, it may dominate the energy density before it decays. Once again, the condition for an early axino dominated universe is given by Eq.(5.29):

$$T_D < T_e \quad \text{or} \quad \frac{\rho_{\tilde{a}}}{s} > \frac{3}{4}\sqrt{M_{Pl}\Gamma_{\tilde{a}}}\left(\frac{45}{4\pi^3}\frac{1}{g_*(T_D)}\right)^{1/4} \tag{7.3}$$

where T_e is the temperature at which $\rho_{\tilde{a}} = \rho_R$, given by Eq.(5.25):

$$T_e = \frac{4}{3} m_{\tilde{a}} Y_{\tilde{a}} \ , \tag{7.4}$$

and $Y_{\tilde{a}}$ is the axino thermal production yield, given by Eq.(5.3). While T_D depends on the axino mass, the SUSY spectrum and f_a, T_e depends on the axino mass, the re-heat

SUGRA1 (HB/FP)					
Input Parameters (GeV)		Masses (GeV)		Other Observables	
		μ	137.2		
m_0	4525	$m_{\tilde{g}}$	810.4	Δa_μ	12.5×10^{-8}
$m_{1/2}$	275	$m_{\tilde{u}_L}$	4517.0	$BF(b \to s\gamma)$	3.1×10^{-4}
A_0	0	$m_{\widetilde{W}_1}$	121.1	$BF(B_s \to \mu\mu)$	3.8×10^{-9}
$\tan\beta$	10	$m_{\widetilde{Z}_4}$	273.4	Z_{1B}	0.65
		$m_{\widetilde{Z}_3}$	149.8	$\Omega_{\widetilde{Z}_1}h^2$	0.05
		$m_{\widetilde{Z}_2}$	143.1	T_{fr}	$m_{\widetilde{Z}_1}/23.2$
		$m_{\widetilde{Z}_1}$	87.9	$\langle\sigma v\rangle$ [GeV^{-2}]	2.3×10^{-9}
		m_A	4458.1	$\sigma(\widetilde{Z}_1 p)$ [pb]	3.3×10^{-8}
		m_h	119.6		

Table 7.1: Masses and parameters in GeV units for the HB/FP (SUGRA1) benchmark point computed with Isajet 7.81 using $m_t = 173.3$ GeV. The value of $\langle\sigma v\rangle$ shown corresponds to small relative velocities ($v \simeq 0$).

temperature and f_a. In Fig.7.3, we show the neutralino freeze-out temperature, as well as T_D and T_e as a function of the axino mass for $f_a = 10^{12}$ GeV and $T_R = 10^6$ GeV and 10^{10} GeV. As we can see, for values of $T_D \lesssim 5$ MeV (dashed curves), the parameters are likely excluded because axinos would inject entropy during the neutron freeze-out and affect the BBN results, as discussed in Sec.4.1. For $T_D > T_{fr}$– the high $m_{\tilde{a}}$ region– axinos decay to neutralinos before freeze-out. In this case, the neutralinos from axino decays thermalize and the neutralino relic abundance is given as usual by the standard calculation of WIMP thermal abundance in the MSSM. The region where $T_e > T_D$ is where axinos can dominate the universe. This occurs for $m_{\tilde{a}} \sim 10$ TeV in the $T_R = 10^{10}$ GeV case. Furthermore, the ratio between the T_e and T_D curves gives an approximate measure of the entropy injection from axino decay. We also see that, for $T_R = 10^6$ GeV, axinos never dominate the universe, since their thermal production is suppressed by the low re-heat temperature and they decay prior to the point where the axino energy density exceeds that of radiation.

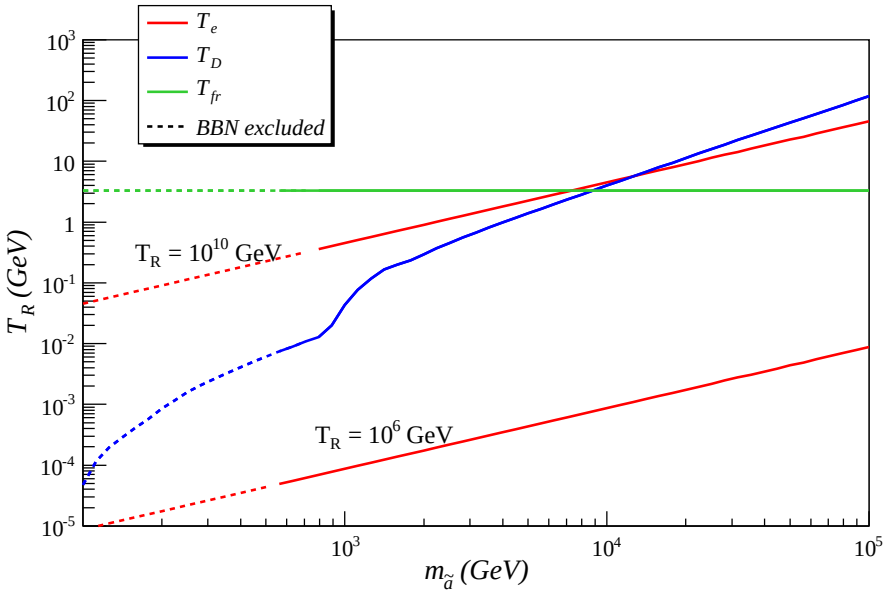

Figure 7.3: Plot of T_D, T_e and the neutralino freeze-out temperature (T_{fr}) versus $m_{\tilde{a}}$ in the SUGRA1 benchmark model with $f_a = 10^{12}$ GeV.

In order to see how large the increase in entropy due to axino decay can be, we plot in Fig.7.4 curves of constant $r = T_e/T_D$ ranging in value from 1 to 100 in the f_a *vs.* T_R plane for $m_{\tilde{a}} = 1$ TeV in the SUGRA1 scenario. The region with $f_a \gtrsim 8 \times 10^{13}$ GeV is likely BBN excluded since the axino decay temperature T_D drops below ~ 5 MeV. From Fig.7.4, we see that when $T_R < T_{dec}$ (below dashed gray line), axinos are produced out-of-equilibrium and r decreases with increasing f_a, since in this region $T_D \propto 1/f_a$ and $T_e \propto 1/f_a^2$, so $r \propto 1/f_a$. Also, r increases with increasing T_R due to enhanced thermal production of axinos. In contrast, when $T_R > T_{dec}$, the axinos are produced in thermal equilibrium and the production rate is independent of f_a or T_R. In this case, T_e is independent of T_R and f_a, while $T_D \propto 1/f_a$, so the r

contours increase with increasing f_a and are independent of T_R. We also see that the entropy production from axino decays is limited from above by the upper bound on the re-heat temperature, $T_R < f_a$. As discussed previously, for re-heat temperatures above f_a, the PQ symmetry would be broken after inflation and a distinct treatment would be required.

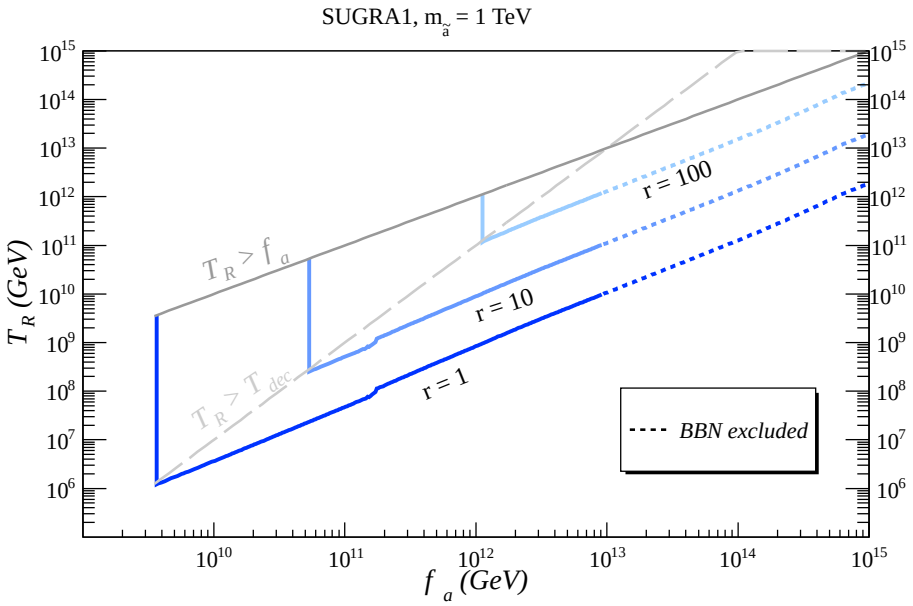

Figure 7.4: Plot of r values in the f_a *vs.* T_R plane for the HB/FP model SUGRA1 with $m_{\tilde{a}} = 1$ TeV.

We can now discuss the axino contribution to the DM relic density, composed of axions and neutralinos. In the axino LSP case, the neutralino contribution to the DM relic density was simply given by $(m_{\tilde{a}}/m_{\widetilde{Z}_1})\Omega_{\widetilde{Z}_1}$, if there was no significant entropy dilution from saxion decays. Thus, naively, we expect that, in the neutralino LSP scenario, the contribution from axino decays is given by $(m_{\widetilde{Z}_1}/m_{\tilde{a}})\Omega_{\tilde{a}}$. However, if axinos decay at temperatures above the neutralino freeze-out (T_{fr}), the $\widetilde{Z}_1$'s injected

from axino decays thermalize to their equilibrium value and axinos do not affect the neutralino relic abundance. On the other hand, if the axino decay temperature (T_D) is below T_{fr}, the number density of neutralinos suddenly increases after the axino decays and new re-annihilations may occur, reducing the final neutralino relic abundance[2].

To compute the final neutralino relic abundance including the effects described above, we must consider the Boltzmann equation for the neutralino number density, Eq.(4.5):

$$\dot{n}_{\widetilde{Z}_1} + 3Hn_{\widetilde{Z}_1} = -\langle\sigma v\rangle \left(n^2_{\widetilde{Z}_1} - \bar{n}^2_{\widetilde{Z}_1}\right) + \Gamma_{\tilde{a}} n_{\tilde{a}} \ . \tag{7.5}$$

If axinos decay before freeze-out ($T_D > T_{fr}$), then, for $T_{fr} < T < T_D$, Eq.(7.5) reduces to the MSSM case, discussed in Sec.4:

$$\dot{n}_{\widetilde{Z}_1} + 3Hn_{\widetilde{Z}_1} = -\langle\sigma v\rangle \left(n^2_{\widetilde{Z}_1} - \bar{n}^2_{\widetilde{Z}_1}\right) \tag{7.6}$$

and the neutralino freeze-out proceeds as in the MSSM (without the axino field), thus giving the MSSM value for $\Omega_{\widetilde{Z}_1}h^2$ ($= 0.05$ for the SUGRA1 point). Note that this result is valid even if there is an early axino dominated era ($r > 1$), as long as $T_D > T_{fr}$. In Fig.7.5, we show as dotted-dashed lines the evolution of the neutralino and axino energy densities as a function of temperature for $m_{\tilde{a}} = 50$ TeV, $f_a = 10^{12}$ GeV and $T_R = 10^6$ GeV. Once again we assume the SUGRA1 point for the MSSM sector. As we can see, for such large $m_{\tilde{a}}$, the axino decays before the neutralino freeze-out and the neutralinos from axino decays thermalize to their equilibrium value. Therefore $\rho_{\widetilde{Z}_1}$ tracks the MSSM evolution (gray dotted curve).

[2]The same effect was not present in the axino LSP scenario since axinos interact very weakly and their annihilation rates are always extremely small.

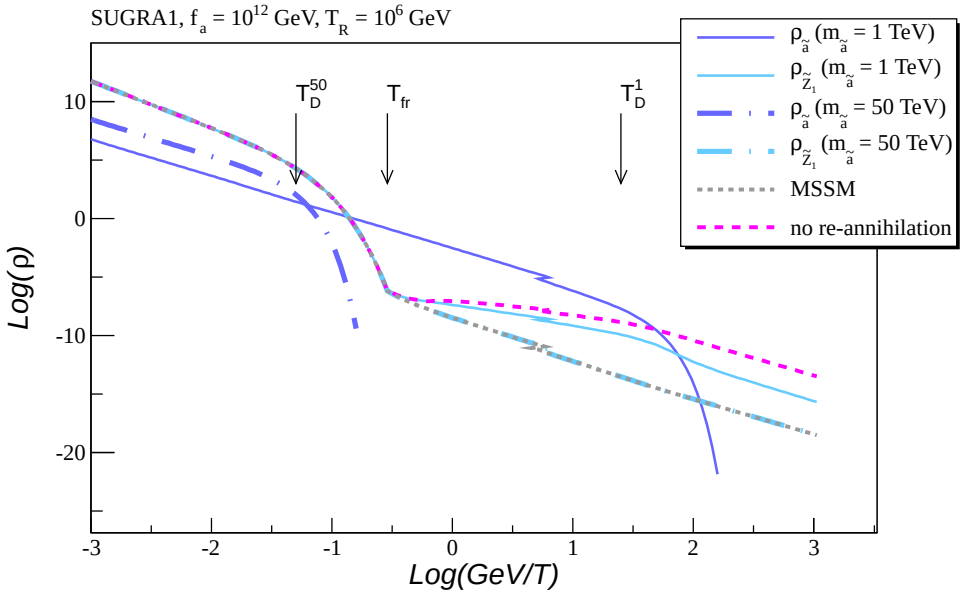

Figure 7.5: Evolution of the neutralino and axino energy densities as a function of the temperature. We also show the neutralino freeze-out temperature (T_{fr}), and the axino decay temperature for $m_{\tilde{a}} = 1(50)$ TeV, $T_D^{1(50)}$. For comparison, we include the evolution of neutralino energy density in the MSSM (dashed gray curve) and without the re-annihilation effect (dotted magenta) discussed in the text. The PQMSSM parameters are: $f_a = 10^{12}$ GeV, $T_R = 10^6$ GeV, $m_{\widetilde{Z}_1} = 87.9$ GeV and $\Omega_{\widetilde{Z}_1} h^2 = 0.05$. Solid lines have $m_{\tilde{a}} = 1$ TeV, while dotted-dashed curves have $m_{\tilde{a}} = 50$ TeV.

However, if $T_D < T_{fr}$, Eq.(7.5) gives (for $T < T_D$):

$$\dot{n}_{\widetilde{Z}_1} + 3Hn_{\widetilde{Z}_1} = -\langle\sigma v\rangle n^2_{\widetilde{Z}_1} \tag{7.7}$$

with the initial condition:

$$Y_{\widetilde{Z}_1}(T_D) = Y^{fr}_{\widetilde{Z}_1} + Y^{\tilde{a}}_{\widetilde{Z}_1} \tag{7.8}$$

where $Y^{fr}_{\widetilde{Z}_1}$ is the thermal freeze-out contribution given by Eq.(B.13)[3] and $Y^{\tilde{a}}_{\widetilde{Z}_1} = Y_{\tilde{a}}/r$ is the non-thermal contribution from axino decays. The entropy dilution factor $(1/r)$ must be included if the universe becomes temporarily axino dominated ($r > 1$). Eq.(7.7) can be rewritten in terms of the neutralino yield as

$$\frac{dY_{\widetilde{Z}_1}}{dt} = -\langle\sigma v\rangle Y^2_{\widetilde{Z}_1} s \ . \tag{7.9}$$

Since after the axino decay the universe is radiation dominated, we have $T \propto R^{-1}$ and $s = 2\pi^2 g_*(T)T^3/45$, so the above equation becomes:

$$\frac{dY_{\widetilde{Z}_1}}{dT} = Y^2_{\widetilde{Z}_1}\sqrt{\frac{g_*(T)\pi}{45}} M_{Pl}\langle\sigma v\rangle \ . \tag{7.10}$$

Therefore, for $T \ll T_D$, the solution for the above equation gives:

$$Y^{-1}_{\widetilde{Z}_1}(T) \simeq Y^{-1}_{\widetilde{Z}_1}(T_D) + \sqrt{\frac{g_*(T_D)\pi}{45}}\langle\sigma v\rangle M_{Pl} T_D \ . \tag{7.11}$$

From this result, we see that the neutralino yield is suppressed at low temperatures ($Y_{\widetilde{Z}_1}(T) \ll Y_{\widetilde{Z}_1}(T_D)$), if:

$$Y^{-1}_{\widetilde{Z}_1}(T_D) \ll \sqrt{\frac{g_*(T_D)\pi}{45}}\langle\sigma v\rangle M_{Pl} T_D \ ; \tag{7.12}$$

otherwise, the neutralino yield is approximately given by the sum of the thermal freeze-out and axino contributions ($Y_{\widetilde{Z}_1}(T) \simeq Y_{\widetilde{Z}_1}(T_D)$). The suppression of $Y_{\widetilde{Z}_1}(T)$ (if Eq.(7.12) is satisfied) happens when neutralinos from axino decays, injected at $T \sim T_D$, re-annihilate. This is more clearly seen if we rewrite Eq.(7.12) as

$$\langle\sigma v\rangle n_{\widetilde{Z}_1}(T_D) \gg H(T_D) \ . \tag{7.13}$$

[3] After the axino decay entropy is conserved, so $Y^{fr}_{\widetilde{Z}_1}$ (for $T \leq T_D$) can easily be obtained from Eq.(B.13), using $Y^{fr}_{\widetilde{Z}_1} = (\Omega_{\widetilde{Z}_1}\rho_c)/(m_{\widetilde{Z}_1} s(T_0)) \simeq (\Omega_{\widetilde{Z}_1} h^2)/(2.741 \times 10^8 \text{ GeV}^{-1} m_{\widetilde{Z}_1})$.

The above condition simply means that re-annihilations will occur at $T \sim T_D$ if the number of injected neutralinos from axino decays is sufficiently large to make the annihilation rate exceed the expansion rate at $T = T_D$. This effect is illustrated by the solid curves in Fig.7.5, which show the evolution of the neutralino and axino energy densities for $m_{\tilde{a}} = 1$ TeV, $f_a = 10^{12}$ GeV and $T_R = 10^6$ GeV. As seen from Fig.7.3, for these parameters we have $T_D \sim 0.07$ GeV $< T_{fr}$, so axinos decay after neutralino freeze-out and add to its final relic abundance, which, for $T < T_D$ becomes much larger than the MSSM value (dotted gray curve). For comparison purposes, we also show the neutralino relic abundance given by $Y^{fr}_{\tilde{Z}_1} + Y_{\tilde{a}}$, where the re-annihilation effect has been turned off (dotted magenta curve). As we can see, re-annihilations significantly reduce the final neutralino relic abundance by a factor of ~ 200 and can not be neglected in this case.

We also point out that, if $Y^{\tilde{a}}_{\tilde{Z}_1}$ is sufficiently large, the second term on the righ-hand side of Eq.(7.11) dominates and the final neutralino relic abundance becomes independent of the axino and thermal freeze-out yields:

$$\begin{aligned} Y_{\tilde{Z}_1}(T \ll T_D) &\simeq \sqrt{\frac{45}{g_*(T_D)\pi}}\frac{1}{\langle\sigma v\rangle M_{Pl} T_D} = \frac{H(T_D)}{s(T_D)\langle\sigma v\rangle} \\ \Rightarrow \Omega_{\tilde{Z}_1}h^2(T \ll T_D) &\simeq \frac{H(T_D)}{\rho_c/h^2}\frac{m_{\tilde{Z}_1}}{\langle\sigma v\rangle}\frac{g_*(T_0)}{g_*(T_D)}\frac{T_0^3}{T_D^3}\,. \end{aligned} \tag{7.14}$$

Comparing the above result with Eq.(4.11) we see that, in this case, the final neutralino relic abundance is given by the thermal freeze-out abundance, but with the freeze-out temperature replaced by T_D.

We can summarize all the previous results with the following expression for the

neutralino yield in the heavy axino scenario:

$$Y_{\widetilde{Z}_1} = \begin{cases} Y^{fr}_{\widetilde{Z}_1} & , \text{if } T_D > T_{fr} \\ \frac{Y^{fr}_{\widetilde{Z}_1} + Y_{\tilde{a}}/r}{1+\sqrt{\frac{g_*(T_D)\pi}{45}}\langle\sigma v\rangle M_{Pl} T_D (Y^{fr}_{\widetilde{Z}_1} + Y_{\tilde{a}}/r)} & , \text{if } T_D < T_{fr} \end{cases} \tag{7.15}$$

where $Y^{fr}_{\widetilde{Z}_1}$ is given by Eq.(B.13) and $Y_{\tilde{a}}$ by Eq.(5.3). As usual we take $r = 1$ if there is no early axino dominated era ($T_e < T_D$). In Fig.7.6 we show, in the T_R *vs.* $m_{\tilde{a}}$ plane, several regions relevant for the discussion of the neutralino relic abundance. We take $f_a = 10^{12}$ GeV and consider the SUGRA1 point shown in Table 7.1. The solid blue lines show contours of $r = 1, 10$ and 100, where axinos temporarily dominate the energy density of the universe. For $m_{\tilde{a}} > 9$ TeV (to the right of dashed blue line), axinos decay before neutralinos freeze-out and do not affect the neutralino relic abundance. The region to the right of the yellow contour and to the left of the dashed blue line has $T_D < T_{fr} < T_e$, so neutralinos decouple during the axino dominated era and their freeze-out relic abundance is given by Eq.(7.15)b. The BBN excluded region is shown by the dotted blue lines at $m_{\tilde{a}} \lesssim 400$ GeV ($T_D < 5$ MeV). Finally, the brown area at low $m_{\tilde{a}}$ and low T_R shows the region where Eq.(7.13) is *not* satisfied and the re-annihilation effect is negligible ($Y_{\widetilde{Z}_1}(T) > Y_{\widetilde{Z}_1}(T_D)/2$). At small T_R, the thermal production of axinos is suppressed and the number of neutralinos injected from axino decays are not sufficient for re-annihilations to take place. At small axino masses, the decay temperature (T_D) is small and suppresses the right-hand side of Eq.(7.12), once again suppressing re-annihilations. Nonetheless we see that, for most of the parameter space, neutralino re-annihilations at $T \sim T_D$ occur at large rates.

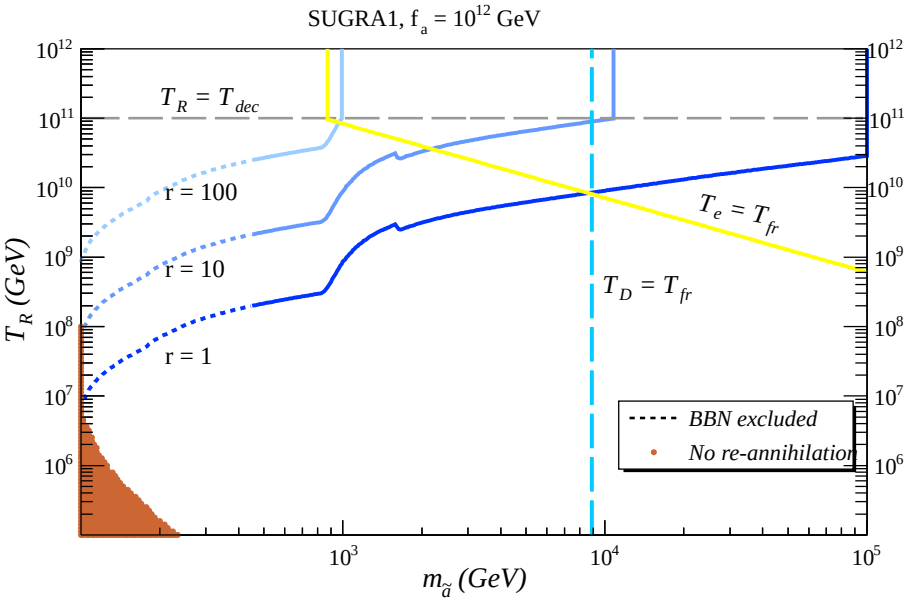

Figure 7.6: Plot of regions of $m_{\tilde{a}}$ *vs.* T_R plane where $T_{fr} < T_e$ (right of yellow contour) and where *no* additional neutralino annihilation occurs (brown), in the SUGRA1 (HB/FP) benchmark model. We also show regions of entropy generation r.

In the neutralino LSP scenario, the total DM relic density is given by

$$\Omega_{DM}h^2 = \Omega_{\widetilde{Z}_1}h^2 + \Omega_a h^2 \tag{7.16}$$

with $\Omega_{\widetilde{Z}_1}h^2$ computed using Eq.(7.15) and $\Omega_a h^2$ given by Eq.(B.6). In Fig.7.7, we plot the neutralino abundance, $\Omega_{\widetilde{Z}_1}h^2$, the axion abundance, $\Omega_a h^2$, and their sum, $\Omega_{a\widetilde{Z}_1}h^2$, versus $m_{\tilde{a}}$ for $f_a = 10^{12}$ GeV, with $T_R = 10^{10}$ GeV. For these parameters, the universe has an axino-dominated era for $m_{\tilde{a}} \lesssim 16$ TeV and the re-annihilation condition, Eq.(7.13), is always satisfied (for $T_D < T_{fr}$). We take the initial axion field value $\theta_i = 0.498$, which tunes the total dark matter abundance to the WMAP value for the case where there is no axino contribution ($T_D > T_{fr}$). The region to the left of

the dashed gray line ($m_{\tilde{a}} \lesssim 400$ GeV) is excluded by BBN constraints on late decaying axinos, since $T_D < 5$ MeV. For $m_{\tilde{a}}$ values just beyond the BBN constraint, the large thermal axino production rate is followed by decays to neutralinos at $T = T_D$. As relic neutralinos fill the universe, they proceed to re-annihilate so their final abundance is determined by Eq.(7.15)b. Since in this region $\Omega_{\widetilde{Z}_1}h^2 \sim 1/T_D$ (see Eq.(7.14)), and since $T_D \sim m_{\tilde{a}}^{3/2}$, we find the neutralino abundance decreasing with increasing $m_{\tilde{a}}$. The kink at $m_{\tilde{a}} \sim 900$ GeV occurs due to turn-on of the $\tilde{a} \to \tilde{g}g$ decay mode, which increases $\Gamma_{\tilde{a}}$, thus decreasing $\Omega_{\widetilde{Z}_1}h^2$ even further. While $\Omega_{\widetilde{Z}_1}h^2$ is decreasing with increasing $m_{\tilde{a}}$, it reaches 0.11 at $m_{\tilde{a}} \sim 6$ TeV and continues dropping until T_D exceeds T_{fr}. At this point, the thermal $\widetilde{Z}_1$ abundance assumes its MSSM value of $\Omega_{\widetilde{Z}_1}h^2 = 0.05$ since now axinos decay before freeze-out. For $m_{\tilde{a}} \gtrsim 8.5$ TeV, the CDM is a nearly equal mix of axions and neutralinos, due to our choice of θ_i. While $T_D \gtrsim 1$ GeV ($m_{\tilde{a}} \gtrsim 3$ TeV), axinos decay before the beginning of axion oscillations and the axion abundance assumes the form given in Eq.(5.22). However, for lower values of $m_{\tilde{a}}$, $T_D < 1$ GeV and the axion abundance is diluted by entropy production from axino decay and is given by Eq.(B.6).

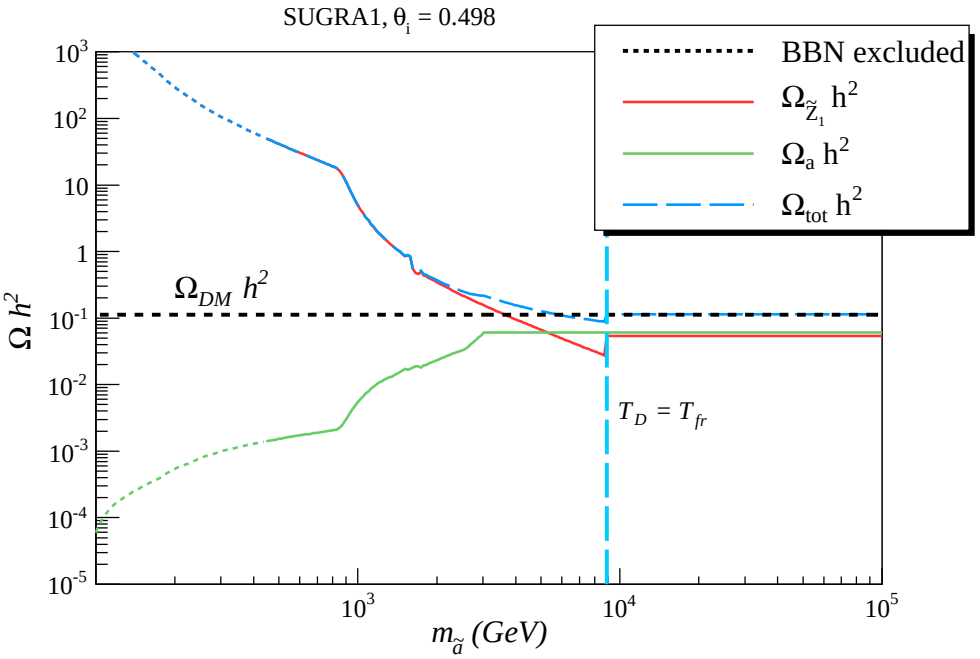

Figure 7.7: Plot of neutralino and axion relic densities Ωh^2 versus $m_{\tilde{a}}$ for $f_a = 10^{12}$ GeV and $T_R = 10^{10}$ GeV for the SUGRA1 model.

In Fig. 7.8, we show the mixed $a\widetilde{Z}_1$ abundance versus f_a for $m_{\tilde{a}} = 1$ TeV, $T_R = 10^{10}$ GeV and $\theta_i = 0.498$, once again assuming the SUGRA1 model. We see that for low f_a, the axino width $\Gamma_{\tilde{a}}$ is large, and T_D exceeds T_{fr}, so that axinos decay before freeze-out and the neutralino relic density assumes its MSSM value ($\Omega_{\widetilde{Z}_1} h^2 = 0.05$). Meanwhile, the axion density is extremely small due to the low value of f_a. Since $T_D \sim 1/f_a$, as f_a increases, T_D decreases. For $f_a \lesssim 10^{10}$ GeV, $T_D > T_{fr}$ and $T_D > 1$ GeV, so the neutralino abundance remains constant (Eq.(7.15)a), while the axion abundance, given by Eq.(5.22), increases with f_a. Around $f_a \sim 8 \times 10^{10}$ GeV, T_D falls below T_{fr} and the neutralino abundance is then given by Eq.(7.15)b. For higher f_a values, T_D continues to fall and since $\Omega_{\widetilde{Z}_1} h^2 \sim T_D^{-1}$ in this region, the neutralino

abundance steadily increases. For 2.5×10^{10} GeV $< f_a < 8 \times 10^{11}$ GeV, $T_D < T_a < T_e$ and axions starts to oscillate in the matter dominated (MD) regime (see Sec.5.3). In this case, due to entropy injection from axino decays, the axion relic density slowly increases with f_a, as shown by Eq.(B.7). For $f_a \gtrsim 10^{12}$ GeV, axinos only dominate the energy density after the axion oscillation has started ($T_e < T_a \sim 1$ GeV), so $\Omega_a h^2$ is once again given by Eq.(5.22), but now diluted by $1/r$ (see Eq.(B.6)). Since $1/r = T_D/T_e \propto f_a$, the entropy dilution makes $\Omega_a h^2$ increase with f_a at a faster rate. Finally, at $f_a \sim 10^{13}$ GeV, $T_e < T_D$ and there is no longer an axino-dominated era. In this case, $r = 1$, so the axion relic abundance is no longer diluted by entropy injection and its slope decreases, as seen in Fig.7.8. The BBN excluded region is shown by the dotted lines ($f_a \gtrsim 10^{13}$ GeV).

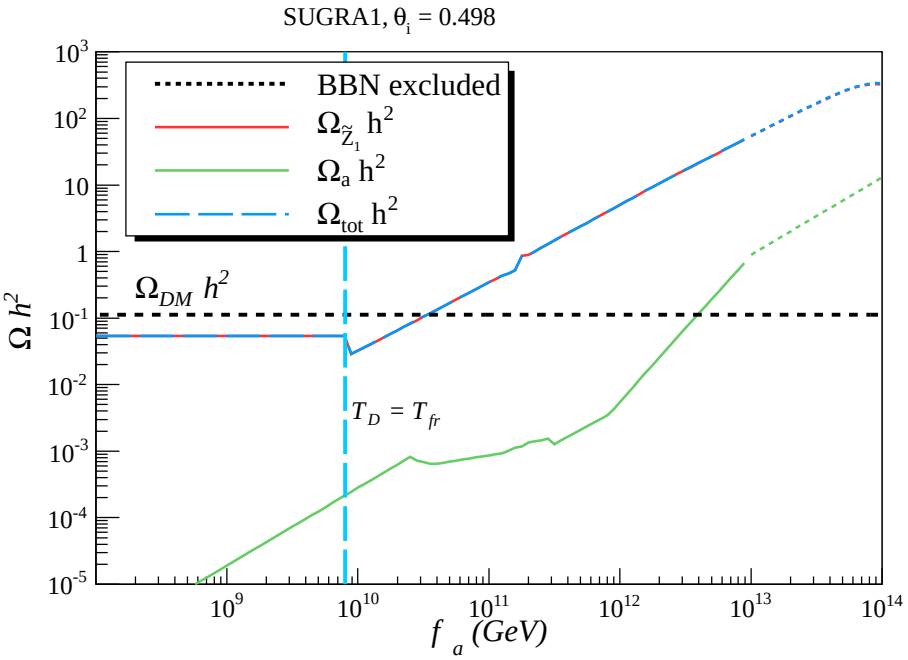

Figure 7.8: Plot of neutralino and axion relic densities Ωh^2 versus f_a for $m_{\tilde{a}} = 1$ TeV and $T_R = 10^{10}$ GeV for the SUGRA1 model.

In Fig.7.9, we show the mixed dark matter relic abundance versus T_R for $f_a = 10^{12}$ GeV and $m_{\tilde{a}} = 1$ TeV. In this case, T_D is fixed throughout the plots and, as seen from Fig.7.6, the neutralino relic density is given in the re-annihilation regime, Eq.(7.15)b. Since in this case $\Omega_{\tilde{Z}_1} h^2 \propto 1/T_D$, the neutralino relic abundance is nearly constant everywhere except at low $T_R \sim 10^4$ GeV, where thermal axino production is somewhat suppressed, and fewer neutralinos are produced at T_D to enter the re-annihilation process. Since f_a is fixed, the axion abundance is also constant throughout much of the plot. At $T_R \sim 10^9$ GeV, we enter the region where axinos can dominate the universe ($r > 1$), and entropy production from axino decay diminishes the axion abundance. For 10^9 GeV $\lesssim T_R \lesssim 10^{10}$ GeV, $T_a > T_e$, so the axion relic density is

simply diluted by $1/r$. For larger T_R values, $T_a < T_e$ and axions start to oscillate in the MD regime. At $T_R \sim 7 \times 10^{10}$ GeV, $T_R > T_{dec}$ and the axino production rate becomes independent of T_R (see Eq.(5.3)), hence T_e and r become constant with T_R. While the neutralino abundance always dominates the axion abundance in Fig.7.9, this is just a reflection of the value of $m_{\tilde{a}}$ chosen; for higher $m_{\tilde{a}}$, T_D will increase, leading to a diminution of $\Omega_{\widetilde{Z}_1} h^2$.

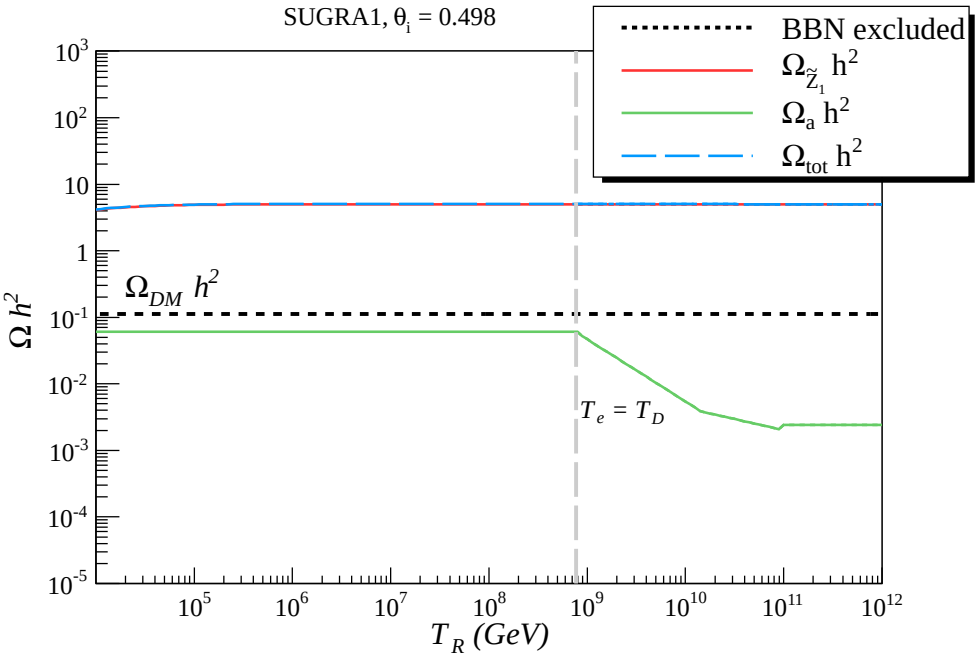

Figure 7.9: Plot of neutralino and axion relic densities Ωh^2 versus T_R for $m_{\tilde{a}} = 1$ TeV and $f_a = 10^{12}$ GeV for the SUGRA1 model.

We have seen that over most of the parameter space with $T_D < T_{fr}$, $\Omega_{\widetilde{Z}_1} h^2 \sim 1/T_D \sim \Gamma_{\tilde{a}}^{-1/2} \sim f_a/m_{\tilde{a}}^{3/2}$, with little dependence on T_R. Hence, a good way to display the relic density of dark matter in the mixed $a\widetilde{Z}_1$ CDM scenario is to display it in the $m_{\tilde{a}}$ *vs.* f_a plane. This is shown in Fig.7.10 for the SUGRA1 point, where we

take $\theta_i = 0.498$ so as to normalize the relic density $\Omega_{a\tilde{Z}_1}h^2$ to the measured value 0.1123 when $T_D > T_{fr}$ and $f_a = 10^{12}$ GeV. The black contour denotes the line where $T_D = T_{fr}$: below and right of this contour, the neutralino relic density is given by its MSSM thermal abundance ($\Omega_{\tilde{Z}_1}h^2 = 0.05$). In this region, the axion abundance increases with increasing f_a, so $\Omega_{a\tilde{Z}_1}h^2 = 0.1123$ at $f_a = 10^{12}$ GeV by design, with a roughly even admixture of mixed higgsino and axion dark matter in the narrow azure-shaded region. In the region to the left of the $T_D = T_{fr}$ contour, the neutralino abundance rapidly increases, and we have regions of dominantly WIMP CDM.

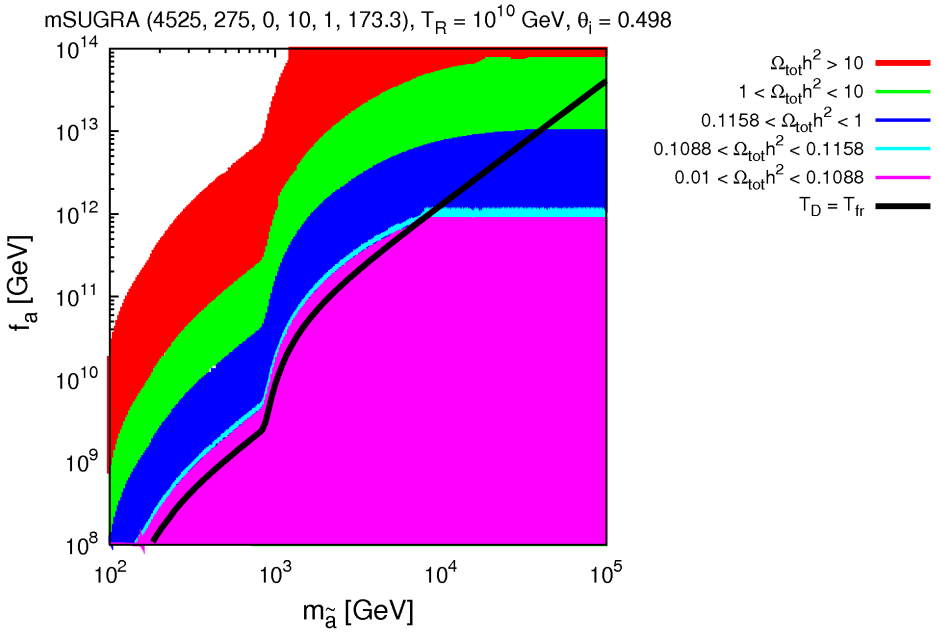

Figure 7.10: Regions of neutralino plus axion relic density $\Omega_{a\tilde{Z}_1}h^2$ in the $m_{\tilde{a}}$ *vs.* f_a plane for $T_R = 10^{10}$ GeV for the SUGRA1 model. The unshaded (white) regions are excluded by BBN bounds since $T_R < 2$ MeV.

7.1 Summary

From the above results, we see that the $a\widetilde{Z}_1$ scenario can be classified into two main cases:

- *A)*: decoupled axino ($T_D > T_{fr}$)
- *B)*: axino enhanced DM ($T_D < T_{fr}$) .

Case *A)* happens for high T_D values, which are obtained at low f_a and/or high $m_{\tilde{a}}$, as seen in Figs.7.7, 7.8 and 7.10. In this scenario, the axino has no effect on the DM relic density, which can be a mixture of axions and neutralinos. Since the axion mis-alignment angle (θ_i) can always be adjusted so that $\Omega_a h^2 = 0.1123$, there is no lower bound on $\Omega_{\widetilde{Z}_1} h^2$. Nonetheless the neutralino relic density must still satisfy:

$$\Omega_{\widetilde{Z}_1} h^2 = \Omega_{\widetilde{Z}_1}^{MSSM} h^2 \leq 0.1123 \;\; (T_D > T_{fr}) \tag{7.17}$$

where $\Omega_{\widetilde{Z}_1}^{MSSM} h^2$ is the standard neutralino freeze-out relic density in the MSSM, since there is no axino dilution or contribution in this case. Therefore, in Case A, any MSSM model satisfying Eq.(7.17) is allowed. For models where $\Omega_{\widetilde{Z}_1}^{MSSM} h^2 < 0.1123$, the remainder of the DM is composed of axions.

For Case *B)*, $T_D < T_{fr}$, which is obtained at high f_a and/or low $m_{\tilde{a}}$. In this case, for most of the parameter space, the neutralino relic density is dominated by the second (annihilation) term in Eq.(7.11) and the relic density can be approximated by (see Eq.(7.14)):

$$\Omega_{\widetilde{Z}_1} h^2 \simeq \Omega_{\widetilde{Z}_1}^{MSSM} h^2 \times \frac{T_{fr}}{T_D} \; . \tag{7.18}$$

Assuming[4] $T_{fr} \sim m_{\widetilde{Z}_1}/20$ and using Eqs.(7.2) and (7.1), we obtain:

$$\Omega_{\widetilde{Z}_1} h^2 \simeq 25 \times \Omega_{\widetilde{Z}_1}^{MSSM} h^2 \left(\frac{m_{\widetilde{Z}_1}}{100\ \text{GeV}}\right)\left(\frac{f_a}{10^{12}\ \text{GeV}}\right)\left(\frac{1\ \text{TeV}}{m_{\tilde{a}}}\right)^{3/2}\left(1-\frac{m_{\tilde{g}}^2}{m_{\tilde{a}}^2}\right)^{-3/2} \tag{7.19}$$

where we assumed $m_{\tilde{a}} \gtrsim m_{\tilde{g}}$. Now imposing the DM relic density constraint, we obtain:

$$\Omega_{\widetilde{Z}_1}^{MSSM} h^2 \lesssim 4{\times}10^{-3}\left(\frac{100\ \text{GeV}}{m_{\widetilde{Z}_1}}\right)\left(\frac{10^{12}\ \text{GeV}}{f_a}\right)\left(\frac{m_{\tilde{a}}}{1\ \text{TeV}}\right)^{3/2}\left(1-\frac{m_{\tilde{g}}^2}{m_{\tilde{a}}^2}\right)^{3/2} \quad (T_D < T_{fr}). \tag{7.20}$$

Therefore, in this case, the MSSM relic density has to be considerably suppressed in order to satisfy the above bound. Although the bound decreases with f_a and increases with $m_{\tilde{a}}$, for sufficiently low f_a and/or high $m_{\tilde{a}}$, we have $T_D > T_{fr}$ and the bound in Eq.(7.17) must be used instead. Both cases can be easily combined in one expression:

$$\Omega_{\widetilde{Z}_1}^{MSSM} h^2 \lesssim \min\left[0.1123, 4\times10^{-3}\left(\frac{100\ \text{GeV}}{m_{\widetilde{Z}_1}}\right)\left(\frac{10^{12}\ \text{GeV}}{f_a}\right)\left(\frac{m_{\tilde{a}}}{1\ \text{TeV}}\right)^{3/2}\left(1-\frac{m_{\tilde{g}}^2}{m_{\tilde{a}}^2}\right)^{3/2}\right]. \tag{7.21}$$

In the case where $T_D < T_{fr}$, the DM will likely be composed mainly of relic neutralinos, unless $\Omega_{\widetilde{Z}_1}^{MSSM} h^2$ is much smaller than Eq.(7.20). We also point out that the approximate bound in Eq.(7.20) is a conservative one, since, if $m_{\tilde{a}} < m_{\tilde{g}}$, the bound would be more strict. As discussed at the beginning of Sec.7, the above constraint can in principle be relaxed if the saxion field is included and decays after the neutralino freeze-out and axino decay, diluting $\Omega_{\widetilde{Z}_1} h^2$. Such an example is presented in Sec.8.

[4] As shown in Appendix B, the freeze-out temperature is weakly dependent on the values of T_e and T_D.

Chapter 8

The Large f_a Scenario

In the last Sections, we discussed the axino and neutralino LSP scenarios. In both cases, the dark matter relic density has an axion component, which, ignoring possible entropy dilution from saxions or axino decays, is given by Eq.(5.22):

$$\Omega_a h^2 = \begin{cases} 9.23 \times 10^{-3} f(\theta_i)\theta_i^2 g_*(T_a)^{-1/4} \left(\frac{f_a}{10^{12}\ \mathrm{GeV}}\right)^{3/2} & , \text{ if } T_a < \Lambda_{QCD} \\ 1.32\ f(\theta_i)\theta_i^2 g_*(T_a)^{-5/12} \left(\frac{f_a}{10^{12}\ \mathrm{GeV}}\right)^{7/6} & , \text{ if } T_a > \Lambda_{QCD} \end{cases} . \tag{8.1}$$

If we assume $\theta_i \sim 1$, the DM constraint, $\Omega_a h^2 < 0.1123$, implies $f_a \lesssim 10^{12}$ GeV. Furthermore, as discussed in Sec.1.1, low energy and astrophysical constraints on f_a require $f_a \gtrsim 10^9$ GeV. Therefore it is commonly assumed that the PQ scale lies in the interval:

$$10^9\ \mathrm{GeV} < f_a < 10^{12}\ \mathrm{GeV}\ . \tag{8.2}$$

It has been noticed early on[72] that the above interval falls within the desired range for the SUSY breaking scale (m_{SUSY}) in gravity-mediated SUSY breaking models:

$$m_{3/2} \sim m_{SUSY}^2/M_{Pl} \sim 1\ \mathrm{TeV} \Rightarrow m_{SUSY} \sim 10^{11}\ \ \mathrm{GeV}\ \sim f_a \tag{8.3}$$

As shown in Appendix A.3, it is possible to connect the SUSY and PQ breaking scales if the axion supermultiplet has tree level interactions with the hidden sector responsible for breaking SUSY (see Eq.(A.18)).

However, once a grand unified theory is assumed, the $U(1)_{PQ}$ symmetry can appear as an accidental global symmetry of the theory, as naturally occurs in several SUSY GUTS[73]. In this case, f_a will naturally be of order M_{GUT} and will strongly

violate its 10^{12} GeV upper limit. It is possible to protect f_a from obtaining M_{GUT} contributions, either by breaking the PQ symmetry at a lower scale or artificially suppressing the vacuum expectation value of the axion supermultiplet. Nonetheless, such mechanisms always requires the introduction of new superfields or fine-tuned parameters only for this purpose.

Furthermore, a survey of a variety of string models[74] indicates that while the PQ mechanism is easy to generate in string theory, the associated PQ scale tends to occur at or near the GUT scale rather than at some much lower intermediate scale. This is in apparent conflict with the simple limits on f_a from overproduction of dark matter as discussed above.

One solution to the apparent conflict which allows for $f_a \sim M_{GUT}$ is to invoke a tiny initial axion mis-alignment angle $\theta_i \sim 0.003$. In this case, one must accept a highly fine-tuned initial parameter which might emerge anthropically.

An alternative solution has already appeared in Sec.6.2, where the entropy injection from saxion decays significantly dilutes the axion density, allowing for larger values of f_a, as shown by Fig.6.14. This idea was initially proposed in one of the original papers calculating the cosmic abundance of relic axions[75], where it was suggested that additional massive fields may be present in the theory, whose late decays can inject substantial entropy into the universe at times after axion oscillations begin. In Ref.[75], it was proposed that the gravitino might play such a role. Several subsequent works have also explored the issue of dilution of (quasi)-stable relics via entropy injection[76, 77, 78, 79, 80]. Here we discuss the case of an early saxion dominated

universe, which occurs naturally in the large f_a scenario, as discussed below.

Assuming f_a to be of order the GUT scale ($\sim 10^{16}$ GeV) has several important consequences for the PQMSSM cosmology:

- The thermal production of all the components of the axion supermultiplet will be strongly suppressed by the large value of f_a (see Eq.(5.3)).[1] Therefore, the axino and thermal axion contributions to the DM density are negligible and the saxion and axion densities are dominated by the coherent oscillation component.

- Assuming $s_i \sim f_a$, large f_a will result in a large energy density for the coherent oscillating saxion field as shown by Eq.(5.24).

- Since $T_e \propto f_a^2$ (for coherent oscillating saxions) and $T_D \propto 1/f_a$, large f_a will usually result in a large entropy injection $r = \frac{T_e}{T_D}$ from saxion decays.

- The axion field will be extremely light ($\sim 10^{-10}$ eV).

- Since $\Gamma_s \propto 1/f_a^2$, saxions will be long-lived, potentially spoiling the BBN predictions.

- For an axino (neutralino) LSP, $\Gamma_{\widetilde{Z}_1(\tilde{a})} \propto 1/f_a^2$ and the neutralino (axino) will be long-lived and a threat to successful BBN.

From the above points, we see that $f_a \sim M_{GUT}$ naturally leads to a long-lived saxion with large energy density from coherent oscillations. As shown in Sec.5.3, this results in an early saxion dominated universe with a large dilution of other relics, due to the

[1] The thermal production could still be relevant for $T_R > f_a$, but as discussed previously, this scenario requires a different dark matter treatment, so we assume $T_R < f_a$.

entropy injection during saxion decays. Below, we will first discuss the axino LSP scenario and then present results for the neutralino LSP case.

As shown in Secs.5.3 and 6.2, the early saxion dominated era depends on the temperatures T_e and T_D, given by Eqs.(5.25) and (5.28). In Fig.8.1, we show T_e as a function of the reheat temperature for $m_s = 20$ TeV, $s_i = f_a$ and $f_a = 10^{15}$, 10^{16} and 10^{17} GeV. As we can see, T_e increases with T_R until $T_s < T_R$, when the saxion starts to oscillate after inflation (see Eq.(5.24)). In this regime, the saxion Yield and hence T_e becomes independent of T_R. From Fig.8.1, we see that for $f_a \sim 10^{16}$ GeV and $m_s = 20$ TeV, T_e can be as large as 10^6 GeV.

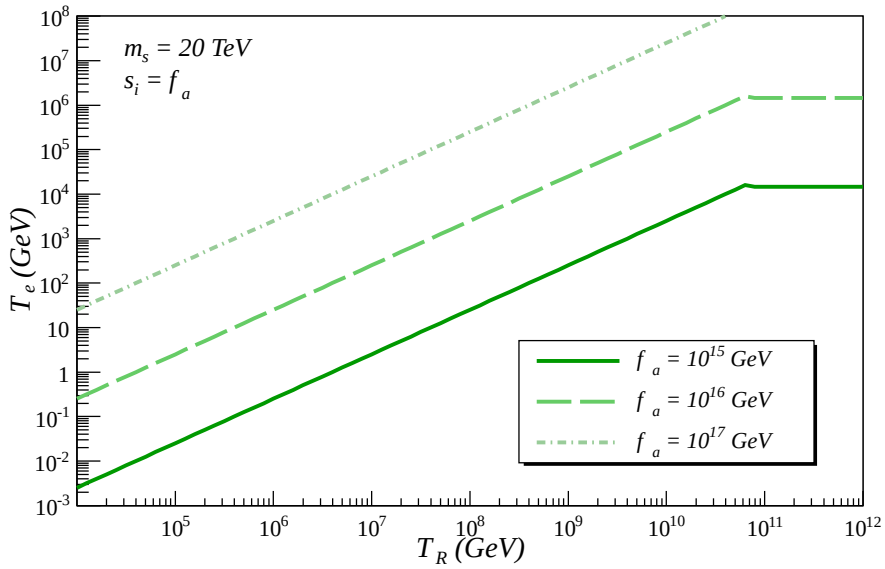

Figure 8.1: Saxion-radiation equality temperature (T_e) versus the reheat temperature after inflation (T_R) for $f_a = 10^{15}$, 10^{16} and 10^{17} GeV (bottom to top), $m_s = 20$ TeV and $s_i = f_a$.

In Fig.8.2, we plot T_D as a function of m_s for $f_a = 10^{15}$, 10^{16} and 10^{17} GeV. We

see that T_D can span a wide range of values, with $T_D \lesssim 0.1$ MeV for a sub-TeV saxion and $f_a \gtrsim 10^{15}$ GeV. However, if $T_D < 5$ MeV, entropy will be injected during the neutron freeze-out and the neutron-proton ratio will be significantly diluted, spoiling the successful BBN predictions, discussed in Sec.4.1. As shown in Fig.8.2, $T_D > 5$ MeV requires $m_s \gtrsim 50$ TeV for $f_a \sim 10^{16}$ GeV.

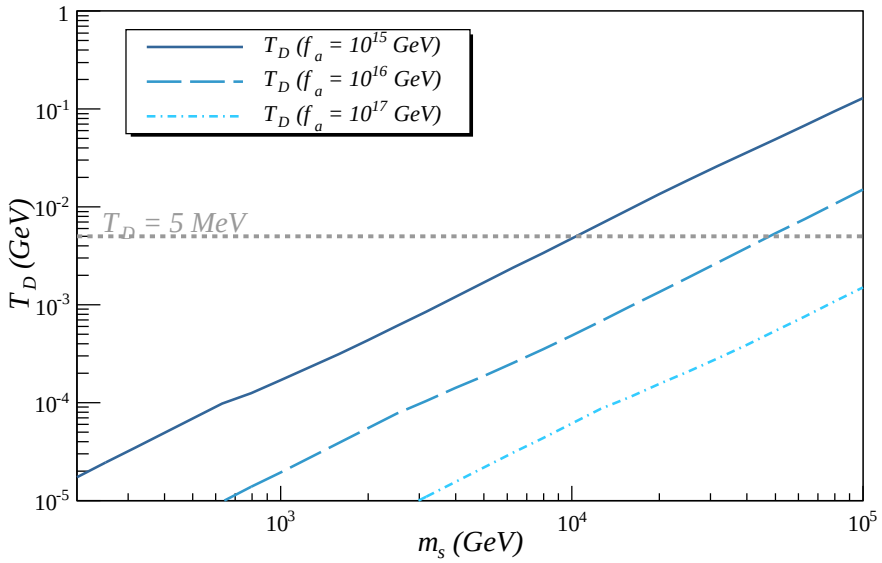

Figure 8.2: Saxion decay temperature (T_D) versus the saxion mass (m_s) for $f_a = 10^{15}$, 10^{16} and 10^{17} GeV (top to bottom). We also show in grey the BBN constraint on T_D ($T_D > 5$ MeV).

Once the saxion field starts to decay, entropy will be injected and effectively dilute all other relic densities already decoupled from the thermal bath, such as axinos, axions, gravitinos and possibly neutralinos. The entropy production during saxion decays is approximately given by Eq.(5.36), $r \simeq T_e/T_D$. Fig.8.3 shows contours of r values in the T_R *vs* f_a plane. We see that, for $s_i = f_a$ and $f_a \sim 10^{16}$ GeV, values of r

larger than 10^4 are easily obtained.

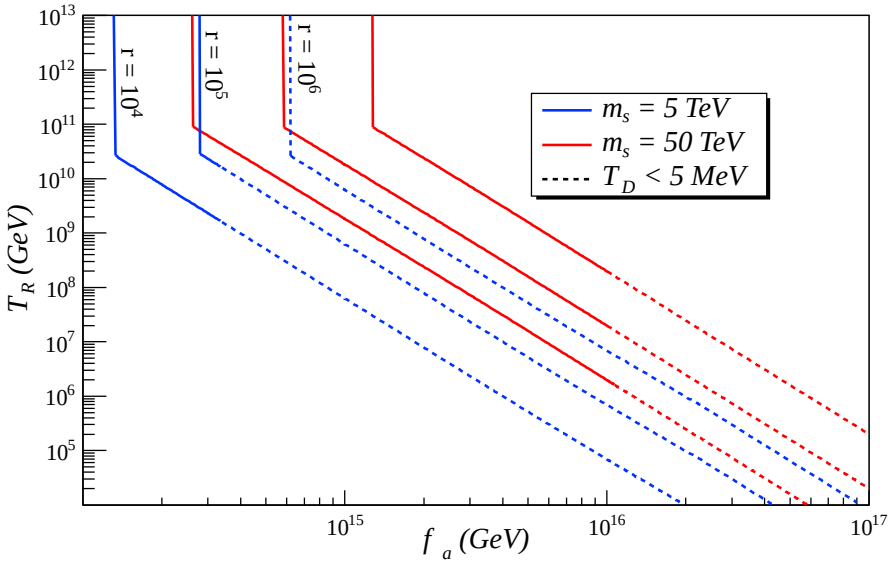

Figure 8.3: Entropy dilution factor (r) contours in the f_a-T_R plane for $m_s = 5$ and 50 TeV. The curves have r values 10^4, 10^5 and 10^6 from bottom to top. The dashed region is excluded by the BBN constraints on T_D.

As discussed in Sec.6.2 and Appendix B, the neutralino and axion relic densities are strongly dependent on the neutralino freeze-out (T_{fr}) and axion oscillation temperatures (T_a). If $T_{fr}(T_a) < T_D$, saxion decays have no effect on the neutralino (axion) relic density. On the other hand, if $T_{fr}(T_a) > T_D$ neutralinos (axions) may freeze-out (oscillate) in a radiation (RD), matter (MD), or decaying particle (DD) dominated universe. The explicit expressions for each of these cases are given in Appendix B

and can be summarized as:

$$\Omega_x = \begin{cases} \Omega_x^{RD}/r \text{ , if } T_e < T_x \\ \Omega_x^{MD} \text{ , if } T_S < T_x < T_e \\ \Omega_x^{DD} \text{ , if } T_D < T_x < T_S \\ \Omega_x^{RD} \text{ , if } T_x < T_D \end{cases} \tag{8.4}$$

where Ω_x represents the axion or neutralino relic densities, Ω_x^{RD} is the corresponding relic density in a radiation dominated (RD) universe (such as when there is no saxion dominated era, $T_D > T_e$), T_x is the freeze-out or axion oscillation temperature and T_S marks the transition between the matter-dominated phase (MD) and the decaying-particle-dominated phase (DD) (see Appendix B):

$$T_S = \left(\frac{g_*(T_D)}{g_*(T_x)} T_e T_D^4 \right)^{1/5} . \tag{8.5}$$

Since axinos and gravitinos always decouple before the saxion dominated phase, we have

$$\Omega_{\tilde{a},\tilde{G}} = \frac{1}{r} \Omega_{\tilde{a},\tilde{G}}^{RD} \tag{8.6}$$

where $\Omega_{\tilde{a},\tilde{G}}^{RD}$ is the axino/gravitino thermal density given by Eqs.(5.3) and (4.26).

To illustrate the behavior of $\Omega_{\widetilde{Z}_1}$ and Ω_a in the distinct regions of Eq.(8.4), we show in Fig.8.4 the relic densities versus T_e, with $T_D = 5$ MeV, $\theta_i = 0.4$ and $m_{\widetilde{Z}_1} = 150$ GeV, for $f_a = 10^{15}$, 10^{16} and 10^{17} GeV. As we can see, for small values of T_e ($< T_{a,fr}$), the axion and neutralino relic densities are simply diluted by $1/r$. Once $T_e \sim 0.1$ (10) GeV, the axion (neutralino) starts to oscillate (decouple) during the matter-dominated (MD) era. As a result, the relic density is no longer diluted by $1/r$, but

by a smaller factor. Once $T_e \gg T_a$, the axion starts to oscillate during the decaying-particle-dominated phase (DD) and becomes independent of T_e, despite the increase of entropy injection. Due to its large freeze-out temperature ($T_{fr} \sim 7$ GeV), the neutralino never decouples during the DD phase for the range of T_e values shown.

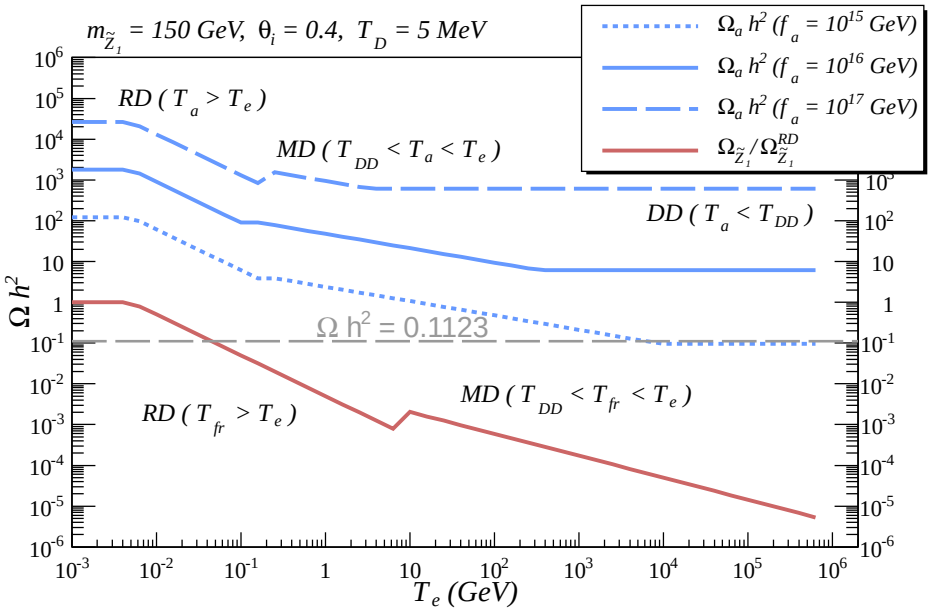

Figure 8.4: The axion and neutralino relic density versus T_e, the temperature at which the universe becomes saxion dominated. The saxion decay temperature is fixed at its minimum value allowed by BBN (5 MeV), $m_{\tilde{Z}_1} = 150$ GeV and $\theta_i = 0.4$. The dotted, solid and dashed blue lines corresponds to the axion relic density for $f_a = 10^{15}$, 10^{16} and 10^{17} GeV, respectively. We also show the regions where the axion (neutralino) starts to oscillate (decouple) during the radiation (RD), matter (MD) or decaying particle (DD) dominated era. The neutralino relic density is normalized by its MSSM value.

From Fig.8.4, we see that the dilution of the axion relic density saturates once

$T_e \gg T_D, T_a$. To understand this behavior and to estimated the maximum entropy dilution of $\Omega_a h^2$, we consider Eq.(B.6) with $T_a \gtrsim \Lambda_{QCD}$:

$$\Omega_a h^2 \propto \begin{cases} f_a^{7/6} \times T_D/T_e \text{ , if } T_e < T_a \\ f_a^{14/11} \times T_D/T_e^{4/11} \text{ , if } T_S < T_a < T_e \\ f_a^{3/2} \times T_D^2 \text{ , if } T_D < T_a < T_S. \end{cases} \tag{8.7}$$

Since $T_D \propto 1/f_a$ and $T_e \propto f_a^2$ (for coherent oscillating saxions), from Eq.(8.7) we see that the axion relic density actually *decreases* with f_a. In this case, the $f_a \lesssim 10^{12}$ GeV bound can be potentially avoided. On the other hand, if $T_a \lesssim \Lambda_{QCD}$, $\Omega_a h^2$ *increases* with f_a, unless $T_a > T_e$ (see Eq.(B.6)). In both cases, we see that $\Omega_a h^2$ is maximally suppressed for $T_D = T_D^{min} = 5$ MeV. From Fig.8.4, we see that the maximum dilution occurs in the DD regime with $T_a \gtrsim \Lambda_{QCD}$, which does not depend on T_e. The expression for $\Omega_a^{DD} h^2$ is given by Eq.(B.8):

$$\Omega_a^{DD} h^2 = 1.72\ \theta_i^2 f(\theta_i) \frac{g_*(T_D)^{1/4}}{\sqrt{g_*(T_a)}} \left(\frac{T_D}{\text{GeV}}\right)^2 \left(\frac{f_a}{10^{12}\ \text{GeV}}\right)^{3/2} \quad (T_a > \Lambda_{QCD}) \tag{8.8}$$

which gives the following expression for the dilution of the axion relic density:

$$r_{eff} \equiv \frac{\Omega_a^{RD} h^2}{\Omega_a^{DD} h^2} \simeq 0.8 \frac{g_*(T_a)^{1/12}}{g_*(T_D)^{1/4}} \left(\frac{\text{GeV}}{T_D}\right)^2 \left(\frac{10^{12}\ \text{GeV}}{f_a}\right)^{1/3} . \tag{8.9}$$

Therefore, the axion dilution decreases with f_a and increases with T_D. Assuming the minimum BBN allowed value for T_D ($\gtrsim 5$ MeV) gives:

$$r_{eff} \gtrsim 2.5 \times 10^4 \left(\frac{10^{12}\ \text{GeV}}{f_a}\right)^{1/3} . \tag{8.10}$$

Thus, for $f_a = 10^{16}(10^{15})$ GeV, saxion decays can dilute the axion relic density at most by $\sim 1(2.5) \times 10^3$. From Eq.(8.8) we can also estimate the maximum θ_i value

allowed by the DM constraint:

$$\Omega_a^{DD} h^2 < 0.11 \Rightarrow \theta_i < \theta_i^{max} \simeq (69 - 106) \left(\frac{5 \text{ MeV}}{T_D}\right) \left(\frac{10^{12} \text{ GeV}}{f_a}\right)^{3/4} \tag{8.11}$$

The uncertainty on θ_i^{max} comes from the uncertainty on the axion mass at $T_a \sim \Lambda_{QCD}$ (see Eq. (3.4)).

In the large f_a regime, the dark matter abundance is dominated by the axion field, since the other relic densities are strongly suppressed by the entropy dilution. Therefore, the nature of the LSP (if an axino or a neutralino) is mostly irrelevant for the discussion of DM constraints. However, as already pointed out in Sec.7, the BBN bounds are significantly different between the axino and neutralino LSP scenarios. We first discuss the neutralino NLSP with an axino LSP. In this case, the neutralino will decay into axinos and SM particles and can be long-lived for $f_a \sim M_{GUT}$. Furthermore, the PQMSSM will also contain long-lived gravitinos and saxions. All or any of these three fields can decay during or after BBN, potentially spoiling its successful predictions, unless their relic densities are extremely small at the time of their decay.

The $\widetilde{Z}_1$ decay width and hadronic branching fraction are given by Eqs.(3.9) and (3.10). Fig.8.5 shows the neutralino lifetime for a bino-like $\widetilde{Z}_1$ ($Z_{1B} = 1$), as a function of $m_{\widetilde{Z}_1}$, for $f_a = 10^{15}$, 10^{16} and 10^{17} GeV and $m_{\tilde{a}} \ll m_{\widetilde{Z}_1}$. From Fig.4.1, we see that the BBN bounds require:

$$\tau \lesssim 0.01s \text{ if } \Omega h^2 \gg 1 \text{ or } \Omega h^2 \lesssim 10^{-4} \text{ if } \tau \gtrsim 10^4 s. \tag{8.12}$$

From Fig.8.5, we see that unless $m_{\widetilde{Z}_1}$ is in the multi-TeV range, the neutralino life-time

($\tau_{\widetilde{Z}_1}$) will be well above 10^4s. Thus, to maintain sub-TeV values of $m_{\widetilde{Z}_1}$, extremely small values of $\Omega_{\widetilde{Z}_1}h^2$ are required in order to satisfy the BBN constraints. Since in almost all of the MSSM parameter space $10^{-3} < \Omega^{MSSM}_{\widetilde{Z}_1}h^2 < 10^3$ (see Fig.4.4), the BBN constraints would require an enormous fine-tuning of the MSSM parameters. However, if neutralinos decouple from the thermal bath before saxions have decayed, their relic density will also be diluted by the saxion decay, according to Eq.(8.4). As seen in Fig.8.4, the neutralino dilution can exceed 10^5 for large enough T_e. Hence, the BBN bounds on late $\widetilde{Z}_1$ decays can be potentially avoided due to the large suppression of $\Omega_{\widetilde{Z}_1}h^2$, without the need for fine-tuned MSSM parameters.

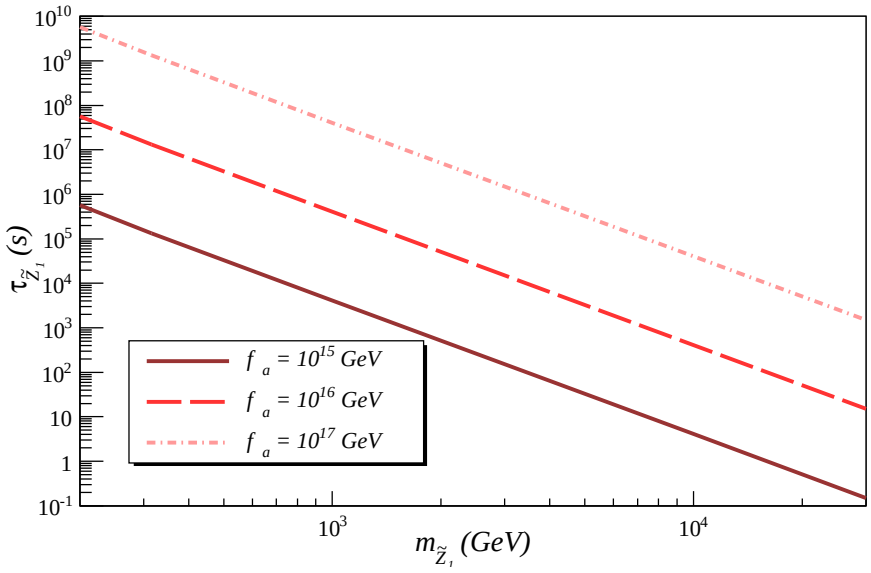

Figure 8.5: The neutralino lifetime as a function of the neutralino mass for $f_a = 10^{15}$, 10^{16} and 10^{17} GeV (bottom to top) and $m_{\tilde{a}} \ll m_{\widetilde{Z}_1}$.

Thermal gravitinos are produced out of equilibrium via radiation off of particles in

the thermal bath (see Eq. (4.26)) and have decay rates suppressed by $1/M_{Pl}^2$, decaying during or after BBN, for $m_{\widetilde{G}} \lesssim 30$ TeV (see Fig.4.2). Therefore, as discussed in Sec.4.2, if T_R is large enough to significantly produce gravitinos in the early universe, their late decay will spoil the BBN predictions and may overproduce dark matter. However, since gravitinos always have decoupling temperatures larger than the reheat temperature, the gravitino relic density is diluted by $1/r$, as shown in Eq.(8.6). Since r can easily exceed 10^4 for $f_a \sim M_{GUT}$, as seen in Fig.8.3, the gravitino relic density will be strongly suppressed. However, as already pointed out in Sec.6.2, this does not ameliorate the Gravitino Problem, since, to compensate the dilution of the baryon density, larger re-heat temperatures are required (see Eq.(6.14)). Thus, although the early saxion dominated scenario allows for larger T_R, the relevant temperature for baryogenesis (T_R/r) still is limited by the same exact constraints as in the MSSM.

In the scenario where $m_{\tilde{a}} \sim m_{3/2}$ and the neutralino is the LSP, axinos will cascade decay to neutralinos. In this case, the BBN bounds on late decaying axinos are easily avoided since $Y_{\tilde{a}}^{TP}$ is suppressed for large f_a and the axino relic density is diluted by $1/r$. Furthermore, if $m_{\tilde{a}} \gtrsim m_{\tilde{g}}$, the decay mode $\tilde{a} \to \tilde{g}g$ considerably reduces the axino lifetime.

Finally, as already discussed in Sec.6.2, the BBN bounds on late decaying saxions in an early saxion dominated universe require $T_D > 5$ MeV. Using Eqs.(3.14)[2] and (5.28), we have:

$$T_D > 5 \text{ MeV} \Rightarrow m_s \gtrsim 0.1 \text{ TeV} \left(\frac{f_a}{10^{12} \text{ GeV}}\right)^{2/3}. \tag{8.13}$$

[2]Once again we neglect decays into axions and gluinos.

Thus, as already shown by Fig.8.2, BBN bounds on saxion decays require $m_s \gtrsim$ 50 TeV, for $f_a \sim 10^{16}$ GeV.

In the axino LSP scenario, for large f_a, the total dark matter relic density is given by:

$$\Omega_{DM}h^2 = \Omega_a h^2 + \Omega_{\tilde{a}}^{TP}h^2 + \frac{m_{\tilde{a}}}{m_{\widetilde{Z}_1}}\Omega_{\widetilde{Z}_1}h^2 + \frac{m_{\tilde{a}}}{m_{\widetilde{G}}}\Omega_{\widetilde{G}}h^2 \tag{8.14}$$

where we have neglected the sub-dominant contributions from thermal axions. To compute the above relic densities, we use Eqs.(8.6), (5.3), (4.26), (B.6) and (B.13). Fig.8.6 shows the axion, axino, neutralino and gravitino relic densities as a function of f_a. For the PQMSSM parameters, we take $m_s = 50$ TeV, $s_i = 10 f_a$, $m_{\widetilde{G}} = 1$ TeV, $T_R = 10^{11}$ GeV and $m_{\tilde{a}} = 0.1$ MeV. We assume $m_{\widetilde{Z}_1} = 150$ GeV and the neutralino relic density *before* dilution to be $\Omega_{\widetilde{Z}_1}^{MSSM}h^2 = 10$. For each f_a value, a different value for θ_i is chosen so that $\Omega_{DM}h^2 = 0.1123$ is satisfied. As we can see from Fig.8.6, the dilution of the axino, neutralino and gravitino relic densities rapidly increases with f_a due to the increasing rate of saxion production via oscillations. For $f_a \lesssim 7\times 10^{14}$ GeV, we have $\Omega_{\widetilde{Z}_1}h^2 \gtrsim 10^{-4}$ and BBN constraints on late decaying neutralinos exclude this region. However, if a smaller value of $\Omega_{\widetilde{Z}_1}^{MSSM}$ had been chosen, smaller f_a values would be allowed. Once $f_a \sim 10^{15}$ GeV, the entropy injection from saxion decays dilutes the neutralino relic density to values below 10^{-4}, making these high f_a values consistent with BBN. Finally, when $f_a \sim 10^{16}$ GeV, the saxion starts to decay at $T = T_D < 5$ MeV and these solutions become once again excluded by the BBN constraints. We can also see that the gravitino relic density is strongly suppressed despite the large T_R value, easily avoiding the BBN constraints on late decaying

gravitinos. Also, despite being the LSP, the axino does not significantly contribute to $\Omega_{DM}h^2$, and the cosmologically allowed region around $f_a \sim 10^{16}$ GeV has little dependence on $m_{\tilde{a}}$.

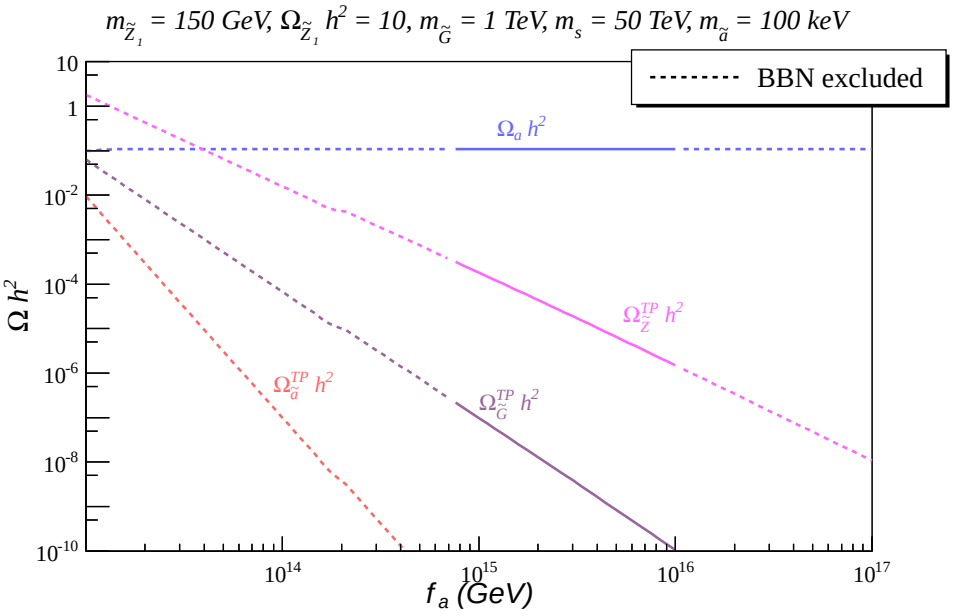

Figure 8.6: The axion, axino, neutralino and gravitino relic densities as a function of f_a for $m_{\widetilde{Z}_1} = 150$ GeV, $\Omega_{\widetilde{Z}_1}h^2 = 10$, $m_{\tilde{a}} = 100$ keV, $m_{\widetilde{G}} = 1$ TeV, $m_s = 50$ TeV, $T_R = 10^{11}$ GeV and $s_i = 10 f_a$. The misalignment angle (θ_i) is chosen such as $\Omega_{DM}h^2 \simeq \Omega_a h^2 = 0.1123$. The dashed region is excluded by BBN bounds on neutralino and gravitino late decays (for $f_a \lesssim 7 \times 10^{14}$ GeV) or $T_D < 5$ MeV (for $f_a \gtrsim 10^{16}$ GeV).

In Fig.8.7, we show the values of θ_i necessary to satisfy the dark matter constraint for the same PQMSSM parameter values used in Fig.8.6. For $f_a \lesssim 10^{14}$ GeV, the axion oscillates after the saxion has decayed ($T_a < T_D$) and $\Omega_a h^2$ is not diluted by the early entropy injection. In this regime, the values of θ_i required to satisfy $\Omega_a h^2 = 0.1123$ rapidly decrease with f_a, since the axion relic density increases with

f_a for $T_a < T_D$. For 10^{14} GeV $\lesssim f_a \lesssim 6\times10^{15}$ GeV, the axion starts to oscillate in the decaying particle dominated (DD) regime ($T_D < T_a < T_{DD}$) and $\Omega_a h^2$ *decreases* with f_a, as discussed above. As a result, θ_i increases with f_a, although it is still required to be small ($\lesssim 0.07$). Once $f_a \gtrsim 6\times10^{15}$ GeV, the axion oscillation still starts in the DD era, but now with $T_a < \Lambda_{QCD}$. As shown by Eq.(B.8), in this case $\Omega_a h^2 \propto f_a$ and the mis-alignment angle once again decreases as f_a increases, although with a smaller slope than in the RD era.

From Figs.8.6 and 8.7, we see that $f_a \sim M_{GUT}$ can indeed be consistent with the dark matter and BBN bounds. However, for the above choice of PQMSSM parameters, the region of parameter space consistent with all bounds is considerably restricted. Furthermore, θ_i still has to take small values, as would be the case in the standard PQ cosmology, where the saxion field is neglected and $f_a \sim M_{GUT}$ can be obtained if we take $\theta_i \lesssim 3\times10^{-3}$[81]. Since the main purpose of the PQ mechanism is to avoid a huge fine-tuning in θ_{QCD}, it is desirable to avoid unnaturally small values for the mis-alignment angle as well. With this in mind, we point out that θ_i can take considerably larger values (~ 0.07) once the saxion and axino fields are included. Furthermore, the dilution of the neutralino and gravitino relic densities allows for an elegant way of avoiding the BBN constraints without having to assume extremely small $\Omega_{\widetilde{Z}_1}h^2$, low reheat temperatures or a multi-TeV gravitino.

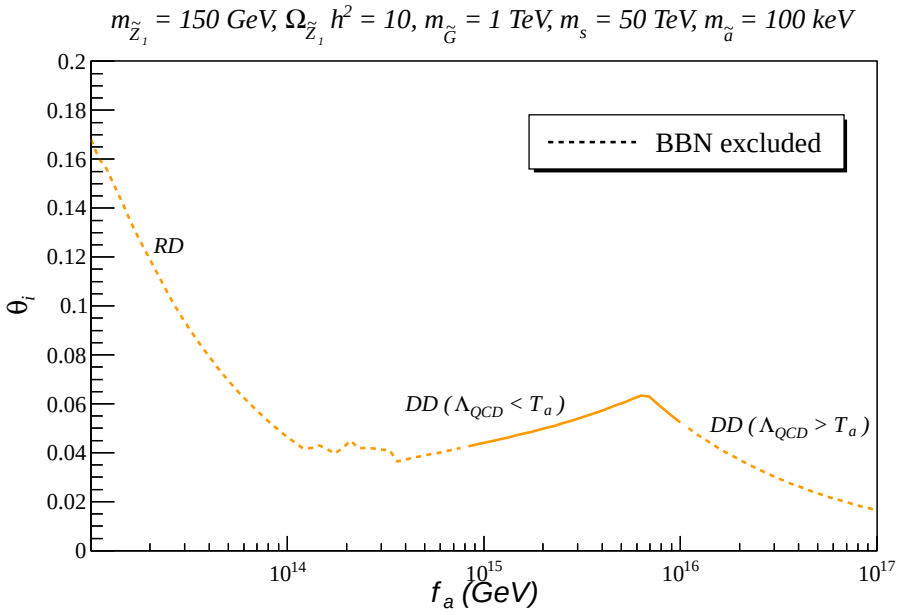

Figure 8.7: The misalignment angle required for $\Omega_{DM}h^2 = 0.1123$ as a function of f_a for $m_{\widetilde{Z}_1} = 150$ GeV, $\Omega_{\widetilde{Z}_1}h^2 = 10$, $m_{\tilde{a}} = 100$ keV, $m_{\widetilde{G}} = 1$ TeV, $m_s = 50$ TeV, $T_R = 10^{11}$ GeV and $s_i = 10 f_a$. The dashed region is excluded by BBN bounds on neutralino and gravitino late decays (for $f_a \lesssim 7 \times 10^{14}$ GeV) or $T_D < 5$ MeV (for $f_a \gtrsim 10^{16}$ GeV).

The above arguments are, however, limited by our choice of the PQMSSM parameters used in Figs.8.6 and 8.7. In order to generalize these results, we perform a random scan over the following parameters:

$$\begin{aligned} f_a &\in [10^{15},\ 10^{17}]\ \text{GeV}\,, \\ m_s &\in [10^{3},\ 10^{5}]\ \text{GeV}\,, \\ s_i/f_a &\in [10^{-2},\ 10^{2}]\,, \\ T_R &\in [10^{4},\ f_a]\ \text{GeV} \end{aligned} \tag{8.15}$$

and take $m_{\widetilde{G}} = 1$ TeV, $m_{\tilde{a}} = 100$ keV, $m_{\widetilde{Z}_1} = 150$ GeV and $\Omega_{\widetilde{Z}_1}^{MSSM}h^2 = 10$, as before. Our results will hardly depend on reasonable variation of these latter parameters, due to the enormous suppression of long-lived relics due to saxion production and decay. For each set of PQMSSM values, the mis-alignment angle is chosen to enforce $\Omega_{DM}h^2 = 0.1123$. The BBN bounds on late decaying saxions, neutralinos and gravitinos are once again applied and solutions which satisfy all constraints are represented by blue dots. In order to differentiate the solutions excluded due to late decaying neutralinos or gravitinos from solutions excluded due to late decaying saxions ($T_D < 5$ MeV), we represent the former by red dots and the latter by green dots.

Fig.8.8 shows the scan results for the misalignment angle θ_i versus f_a. As we can see, $f_a \sim 10^{16}$ requires $\theta_i \lesssim 0.07$. Although small θ_i values are still required in order to obtain $f_a \sim M_{GUT}$, the mis-alignment angle can now be twenty times larger than in the non-SUSY PQ scenario where the saxion/axino fields are neglected. Furthermore, if we require $f_a \sim 10^{15}$ GeV instead, θ_i can be as large as 0.4. We also point out that these conclusions are independent of our choice of $m_{\widetilde{Z}_1}$ and $\Omega_{\widetilde{Z}_1}^{MSSM}$, since the upper limit on θ_i comes entirely from the $T_D > 5$ MeV constraint. These results also verify our estimate for θ_i^{max} in Eq. (8.11), which gives $\theta_i \lesssim 0.07 - 0.1(0.4 - 0.6)$ for $f_a = 10^{16}(10^{15})$ GeV.

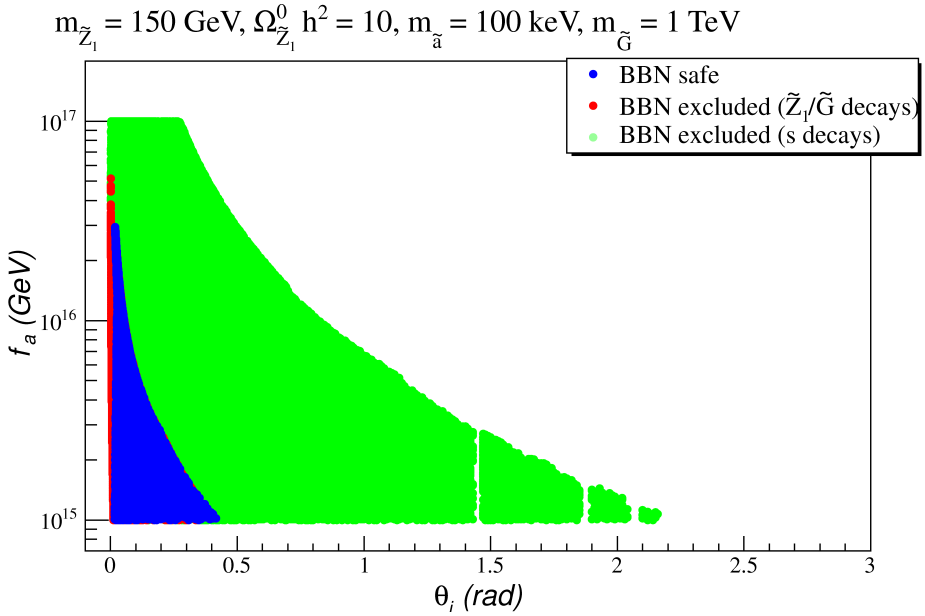

Figure 8.8: The mis-alignment angle versus f_a for a scan over the PQMSSM parameters as discussed in the text. All points satisfy $\Omega_{DM}h^2 = 0.1123$, while the green points are excluded by BBN constraints on late entropy injection from saxion decays ($T_D < 5$ MeV). The red points are excluded by BBN bounds on late decaying neutralinos or gravitinos and the blue points satisfy both the BBN and dark matter constraints.

In Fig.8.9, we show the saxion mass versus f_a for the same points exhibited in Fig.8.8. As already shown by Eq.(8.13), the BBN constraint on late decaying saxions ($T_D > 5$ MeV) requires m_s to be in the multi-TeV range. Since we expect $m_s \sim m_{3/2}$, models with large $m_{3/2} \sim 10 - 50$ TeV such as Yukawa-unified SUSY[82, 83], mirage unification[84, 85, 86, 87, 88], effective SUSY[65, 66], AMSB[89, 90] or string-motivated models such as G2-MSSM[91] would naturally yield such heavy saxions.

We also see that the BBN bounds on late decaying neutralinos do not significantly

constrain the saxion mass, since allowed (blue) solutions can be found for any m_s value as long as the bound in Eq.(8.13) is satisfied. We also point out that the red points with saxion masses below the limit in Eq.(8.13) correspond to the case $T_e < T_D$, where saxions decay before dominating the energy density of the universe. All these solutions have extremely small θ_i values, which lie in the narrow band at $\theta_i \sim 0.001$ seen in Fig.8.8.

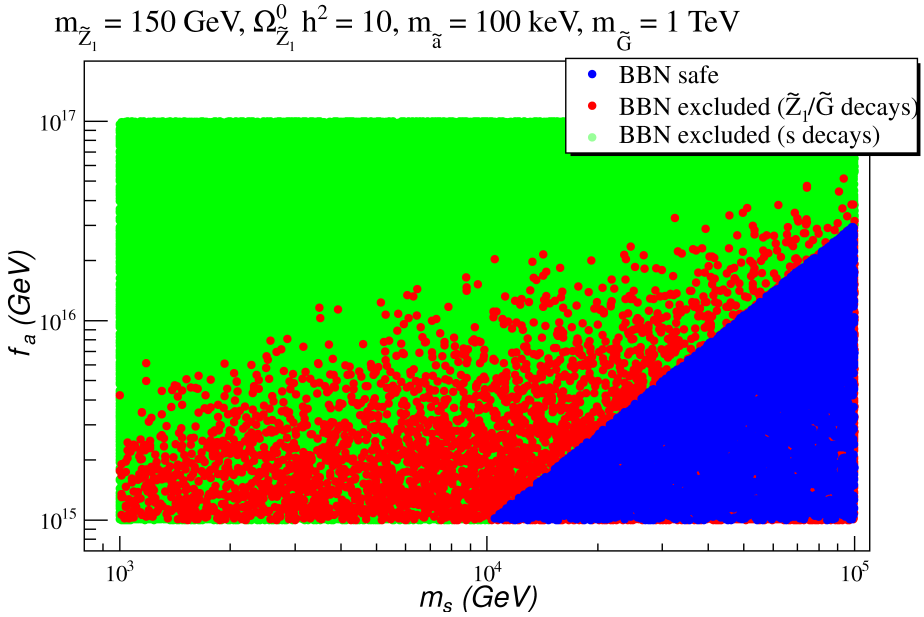

Figure 8.9: The saxion mass versus f_a for a scan over the PQMSSM parameters as discussed in the text. All points satisfy $\Omega_{DM}h^2 = 0.1123$, while the green points are excluded by BBN constraints on late entropy injection from saxion decays ($T_D <$ 5 MeV). The red points are excluded by BBN bounds on late decaying neutralinos or gravitinos and the blue points satisfy both the BBN and dark matter constraints.

Fig.8.10 shows the saxion field amplitude s_i versus f_a. As discussed in Sec.5.2, s_i parametrizes the details of the transition from the static to the oscillatory regime of

the saxion field near $T = T_s$. To compute the value of s_i, the full saxion potential for $T \gtrsim T_s$ needs to be known, which requires assuming a specific PQMSSM model as well as knowledge of the SUSY breaking mechanism. Nonetheless, natural values for s_i are f_a or M_{Pl}. Fig.8.10 shows that small values of s_i/f_a are disfavored, since they suppress the entropy dilution of the neutralino and gravitino relic densities, conflicting with the BBN bounds. However, as seen in Fig.8.10, unnaturally large s_i/f_a values are not necessary for obtaining $f_a \sim M_{GUT}$. Furthermore, smaller $\Omega_{\tilde{Z}_1}^{MSSM}h^2$ values would allow for smaller s_i/f_a.

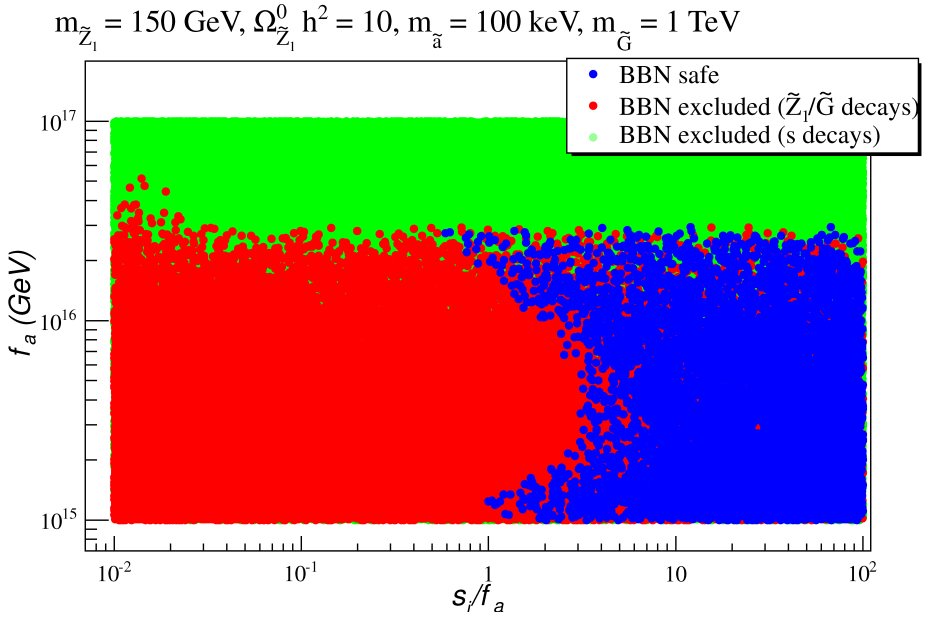

Figure 8.10: The initial saxion field amplitude (s_i) divided by f_a versus f_a for a scan over the PQMSSM parameters as discussed in the text. All points satisfy $\Omega_{DM}h^2 = 0.1123$, while the green points are excluded by BBN constraints on late entropy injection from saxion decays ($T_D < 5$ MeV). The red points are excluded by BBN bounds on late decaying neutralinos or gravitinos and the blue points satisfy both the BBN and dark matter constraints.

Finally– in Fig.8.11– we show the reheat temperature versus f_a. As shown by Eq.(5.24), large T_R increases T_e[3], resulting in an increase in the dilution of the axion, neutralino and gravitino fields. From Fig.8.11, we see that $T_R \gtrsim 10^8$ GeV is usually required to satisfy the BBN constraints on late decaying neutralinos and gravitinos. In the lower frame we show instead f_a *vs.* T_R/r, and find that all BBN-allowed points have $T_R/r < 10^6$ GeV. This rigid limit comes from the BBN bounds on late

[3]For the large saxion masses considered here, we have $T_s > T_R$ in most of the parameter space.

decaying gravitinos and is exactly the same as in the MSSM, as expected from the discussion following Eq.(6.14). Therefore, the unification of the PQ and GUT scales seems to strongly disfavor thermal leptogenesis scenarios, unless a heavier gravitino is assumed. In particular, for $m_{\widetilde{G}} = 10$ TeV, Fig.4.2 gives $\tau_{\widetilde{G}} \simeq 10^2$s and the BBN bounds are considerably weaker in this case ($\Omega_{\widetilde{G}} h^2 \lesssim 0.1$), as seen in Fig.4.1. Hence, as in the MSSM, for multi-TeV gravitinos we can have $T_R/r \lesssim 10^9$ GeV, which makes thermal leptogenesis once again viable. We also note that non-thermal leptogenesis only requires $T_R/r \gtrsim 10^6$ GeV[92, 93], while Affleck-Dine leptogenesis allows still lower T_R/r values[94].

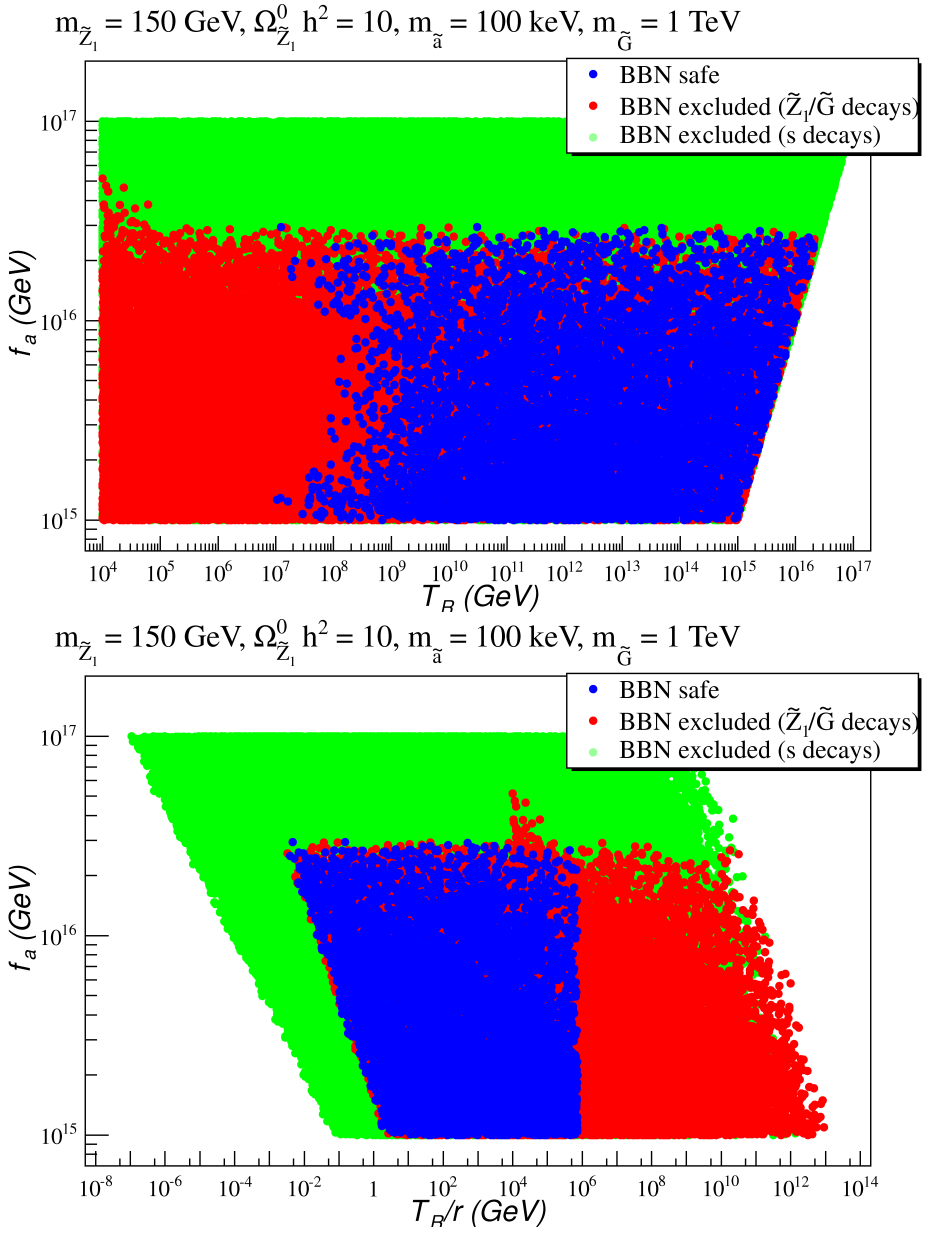

Figure 8.11: *Upper Frame:* Reheat temperature versus f_a for a scan over the PQMSSM parameters as discussed in the text. All points satisfy $\Omega_{DM}h^2 = 0.1123$, while the green points are excluded by BBN constraints on late entropy injection from saxion decays ($T_D < 5$ MeV). The red points are excluded by BBN bounds on late decaying neutralinos or gravitinos and the blue points satisfy both the BBN and dark matter constraints. *Lower Frame:* Same as above, but for the effective temperature T_R/r, relevant for thermal leptogenesis.

Neutralino LSP

So far, our results have focused on the case of the PQMSSM with an axino LSP, so that dark matter consists of an $a\tilde{a}$ mixture. Our results were largely independent of reasonable variations in $m_{\tilde{a}}$ since the axino abundance suffers a huge suppression due both to the large values of f_a and to entropy production from saxion decays. A qualitative difference results if we take $m_{\tilde{a}}$ so high that $m_{\tilde{a}} > m_{\widetilde{Z}_1}$ and the neutralino $\widetilde{Z}_1$ becomes the LSP, so dark matter would consist of an $a\widetilde{Z}_1$ mixture. In this case, gravitinos and axinos can still be produced thermally at high T_R, but now these states will cascade decay down to the stable $\widetilde{Z}_1$ state, and possibly add to the thermal neutralino abundance.

In the mixed $a\widetilde{Z}_1$ DM scenario, neutralinos are produced via axino decays at $T = T_D^{\tilde{a}}$ as well as via thermal freeze-out at $T = T_{fr}$, as discussed in Sec.7. The neutralinos from axino decay may *re-annihilate* at $T = T_D^{\tilde{a}}$, if $Y_{\tilde{a}}/r$ is sufficiently large. However, in the $f_a \sim M_{GUT}$ case considered here, neutralino re-annihilation is largely irrelevant because 1. thermal production of axinos is suppressed by $1/f_a^2$ and 2. the axino abundance at $T = T_D^{\tilde{a}}$ is also highly suppressed by the saxion entropy production ($r \gg 1$). Therefore the condition for re-annihilation, Eq.(7.13), is never achieved. Thus, for the large f_a scenario, the neutralino abundance is given by

$$\Omega_{\widetilde{Z}_1} = \Omega_{\widetilde{Z}_1}^{TP} + \frac{m_{\widetilde{Z}_1}}{m_{\tilde{a}}}\Omega_{\tilde{a}}^{TP} + \frac{m_{\widetilde{Z}_1}}{m_{\widetilde{G}}}\Omega_{\widetilde{G}}^{TP} \tag{8.16}$$

where $\Omega_{\widetilde{Z}_1}^{TP}$ is evaluated for either a MD, DD or RD universe, and $\Omega_{\tilde{a}}^{TP}$ and $\Omega_{\widetilde{G}}^{TP}$ are diluted by entropy production ratio r for $r > 1$. At the end, we must add in the

axion abundance Ω_a as calculated for a MD, DD or RD universe, with the latter case diluted as usual by entropy ratio r when $T_e < T_a$.

As already discussed in Sec.7, the heavy axino lifetime is strongly dependent on the MSSM spectrum. Thus, in order to discuss this case, it is necessary to specify a MSSM model. In Sec.7, we assumed the gravity-mediated SUSY breaking model SUGRA1, which has $m_0 = 4.5$ TeV. However, Fig.8.9 shows that PQMSSM models consistent with $f_a \sim M_{GUT}$ require very large– perhaps uncomfortably large– values of the saxion mass, with m_s typically in the tens of TeV range. In gravity-mediated SUSY breaking models, a puzzle would then arise as to why the sparticles exist in the sub-TeV range, while saxions are present at 10-50 TeV. In particular, the SUGRA1 model is inconsistent with $f_a \sim M_{GUT}$, since it has $m_s \sim m_0 \sim 4.5$ TeV. However, as mentioned before, several other possibilities exist, where m_s and $m_{\widetilde{G}}$ are naturally at the tens of TeV scale.

In Sec.7, in order to have a heavy gravitino, we assumed the Effective SUSY scenario. Another possibility consists of models with mixed moduli-anomaly mediated SUSY breaking soft terms (mirage unification, or MU)[84, 85, 86]. Since the MSSM soft terms arise from mixed moduli/anomaly mediation, their magnitude is at the TeV scale even though $m_{3/2}$ is naturally in the multi-TeV regime. Furthermore, in these scenarios we typically have $m_{\tilde{a}} \sim m_{\widetilde{G}}$ and $m_s \sim \sqrt{2} m_{\widetilde{G}}$[88]. The MU soft terms have been programmed into Isajet/Isasugra[68] and are functions of the mixed moduli-AMSB mixing parameter α, $m_{3/2}$, $\tan\beta$ and $sign(\mu)$. They also depend on the matter and Higgs field modular weights n_i, which can take values of 0, 1/2 or 1,

MM1 (Mirage Unification)					
Input Parameters (GeV)		Masses (GeV)		Other Observables	
$m_{3/2}$	40 TeV	μ	362		
α	3	$m_{\tilde{g}}$	877.4		
n_m	1/2	$m_{\tilde{u}_L}$	718.1	Δa_μ	4.2×10^{-10}
n_H	1	$m_{\widetilde{W}_1}$	360.8	$BF(b\to s\gamma)$	3.2×10^{-4}
$\tan\beta$	10	$m_{\widetilde{Z}_4}$	711.9	$BF(B_s\to\mu\mu)$	4.1×10^{-9}
		$m_{\widetilde{Z}_3}$	677.6	Z_{1B}	0.1
		$m_{\widetilde{Z}_2}$	367.6	$\Omega_{\widetilde{Z}_1}h^2$	0.026
		$m_{\widetilde{Z}_1}$	352.1		
		m_A	372		
		m_h	114.6		

Table 8.1: Masses and parameters in GeV units for the mirage unification (MM1) benchmark point, computed with Isajet 7.81 using $m_t = 173.3$ GeV.

depending on if the fields live on a D3-brane, a D7 brane or an intersection.

In Table 8.1, we show a benchmark point (MM1) for the mirage-unification model with moduli/AMSB mixing parameter $\alpha = 3$, $m_{3/2} = 40$ TeV, $\tan\beta = 10$ and $\mu > 0$ with $m_t = 173.3$ GeV. We take $m_{\widetilde{G}} = m_{3/2} = 40$ TeV, $m_{\tilde{a}} = m_{\widetilde{G}}$ and $m_s = \sqrt{2}m_{\widetilde{G}} = 56.6$ TeV. We further take modular weights n_m for matter fields equal to 1/2 and for Higgs fields $n_H = 1$. The Isajet spectra gives $m_{\tilde{g}} = 877.4$ GeV and $m_{\widetilde{Z}_1} = 352$ GeV and $\Omega^{MSSM}_{\widetilde{Z}_1}h^2 = 0.026$, where $\widetilde{Z}_1$ is mainly higgsino-like.

In Fig.8.12a, we show the axion and neutralino relic abundances versus f_a for the MM1 model, with $T_R = 10^{11}$ GeV and $s_i = 10 f_a$. We see that for $f_a \lesssim 10^{14}$ GeV, too much neutralino dark matter is produced due to axino decays and already saturates the DM constraint, even for $\Omega_a h^2 = 0$. As f_a increases, the axino abundance falls sharply since the thermal production rate is suppressed by $1/f_a^2$ and the Yield is diluted by entropy injection from saxion decays. The gravitino abundance also falls, but not as sharply, since here the diminution is only due to entropy dilution from saxion decays. The thermal neutralino abundance falls, but less sharply still, since, for the choice of parameters in Fig.8.12, the neutralino freezes-out in a MD universe, which results in a dilution smaller than $1/r$, as shown in Fig.8.4. The relic axion abundance grows with f_a, but is also diluted. Here, we dial θ_i to an appropriate value such that $\Omega_{a\tilde{Z}_1} h^2$ is fixed at the measured value of ~ 0.11. For $f_a \gtrsim 4 \times 10^{14}$ GeV, the dark matter is axion-dominated. Once we reach values of $f_a \gtrsim 10^{16}$ GeV, then the saxion decay temperature T_D drops below 5 MeV and we consider the model BBN excluded (dashed curves). When compared to Fig.8.6, we see that the neutralino LSP case easily avoids the BBN bounds on late decaying axinos, as already mentioned in Sec.7.

In Fig.8.12b, we show the value of θ_i which is needed for the same parameters. We also show the required θ_i value for $m_{\tilde{G}} = m_{\tilde{a}} = m_s/\sqrt{2} = 30$ TeV, but keeping the MSSM spectrum as in Table 8.1. The value of θ_i is again typically in the $0.04 - 0.08$ range in order to suppress overproduction of axions.

The main results from the scan over parameter space performed for the axino LSP

case, shown in Figs.8.8-8.11, still hold for the neutralino LSP scenario, since they are weakly dependent on the nature of the LSP. However, since the BBN bounds on axino decays are easily avoided in the heavy axino case, the lower bounds on T_R and s_i/f_a are now relaxed in the neutralino LSP scenario. Nonetheless, the upper bound on T_R/r, relevant for baryogenesis mechanisms, still holds (if we keep $m_{\widetilde{G}} = 1$ TeV), since it only depends on the gravitino mass, as discussed in the last Section. On the other hand, for the MM1 model, where $m_{\widetilde{G}} = 40$ TeV, the gravitino decays before BBN and $T_R/r \gtrsim 10^9$ GeV is allowed.

We also point out that the large f_a regime allows one to avoid the bound on $\Omega_{\widetilde{Z}_1}^{MSSM}$ for PQMSSM models with a neutralino LSP, shown by Eq.(7.21). As already mentioned in Sec.7, this bound is only valid for cases where the effects of the saxion field can be neglected ($T_D > T_{fr}$).

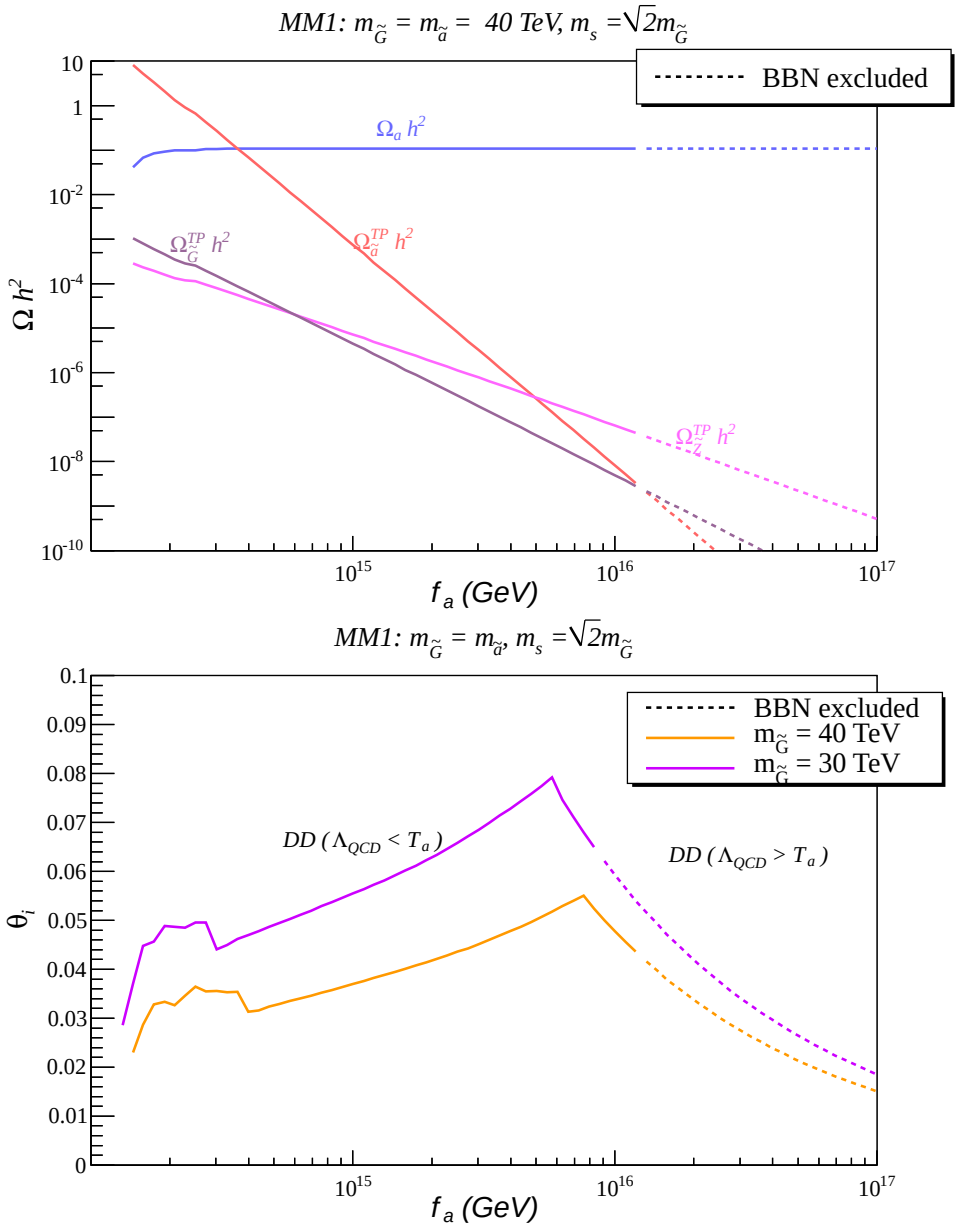

Figure 8.12: *Upper Frame:* The axion, axino, neutralino and gravitino relic densities as a function of f_a for the Mirage Unification model of SUSY breaking shown in Table 8.1, with $T_R = 10^{11}$ GeV and $s_i = 10 f_a$. The misalignment angle (θ_i) is chosen such as $\Omega_{a\widetilde{Z}_1} h^2 \simeq \Omega_a h^2 = 0.1123$. The dashed region is excluded by BBN bounds on saxion decay: $T_D < 5$ MeV. *Lower Frame:* The required value of misalignment angle θ_i for $m_{\widetilde{G}} = m_{\tilde{a}} = m_s\sqrt{2} = 30$ and 40 TeV.

8.1 Summary

We have shown the possibility of extending the usual upper bound on the Peccei-Quinn scale (f_a) to values of the order of the Grand Unification scale (M_{GUT}). We show that large f_a values usually lead to an early universe dominated by coherent oscillating saxions, which are required to decay before Big Bang nucleosynthesis. The injection of entropy during the decay of the saxion field results in a dilution of the axion relic density, which allows us to evade the usual upper bound on f_a ($\lesssim 10^{12}$ GeV). Furthermore, the dilution of the neutralino, axino and gravitino relic densities naturally evade the BBN bounds on late decaying $\widetilde{G}$'s and $\widetilde{Z}_1$'s ($\tilde{a}$'s) for an axino (neutralino) LSP. From Eqs.(8.11) and (8.13), verified by the scan over parameter space, we find that, in order to allow $f_a \sim 10^{16}$ GeV:

- $\theta_i \lesssim 0.07 - 0.1$ is necessary to satisfy the axionic dark matter relic density constraint,
- $m_s \gtrsim 50$ TeV in order to satisfy BBN constraints on late decaying saxions.

Furthermore, for the axino LSP case with a neutralino LSP with $m_{\widetilde{Z}_1} = 150$ GeV and $\Omega_{\widetilde{Z}_1} h^2 = 10$:

- $s_i/f_a \gtrsim 1$ and $T_R \gtrsim 10^8$ GeV are required to increase coherent saxion production and hence increase dilution of the neutralino relic densities and to satisfy the BBN bounds.

While the first two conditions are quite independent of the SUSY spectrum chosen (parametrized here by $\Omega^{MSSM}_{\widetilde{Z}_1} h^2$ and $m_{\widetilde{Z}_1}$), the third condition can be relaxed if

PQMSSM models with heavier neutralinos and/or smaller $\Omega_{\widetilde{Z}_1}^{MSSM}$ are considered.

We also investigated the case where $m_{\tilde{a}} \sim m_{3/2}$ and the neutralino is the LSP, so dark matter is comprised of an axion/neutralino mixture. Models such as Mirage Unification or string models based on G2 holonomy naturally give axino and saxion masses in the tens of TeV range, while maintaining at least some superpartners below the TeV scale. In these models, if $f_a \sim M_{GUT}$, then again we expect large amounts of entropy production from saxion decay, while neutralino, axino and gravitino abundances are all suppressed to tiny levels, thus helping to avoid BBN constraints.

While all our results were calculated assuming the saxion $s \to gg$ decay mode at 100%, we note that other model-dependent decay modes such as $s \to hh$ or $s \to aa$ may be present. The first of these would contribute to additional entropy production and decrease the saxion lifetime, thus helping to avoid BBN constraints. In this sense, we regard our results as conservative. On the other hand, if saxion decays into axions is significant, such decays inject relativistic axions and increase the effective value of g_* during and after BBN, introducing new constraints on ρ_s. In addition, the entropy injection from saxion production and decay is greatly diminished, which would decrease the dilution of the relic axion abundance and require smaller θ_i values.

As consequences of the $f_a \sim M_{GUT}$ scenario, we would expect the DM of the universe to be axion-dominated, with a tiny component of either axinos or neutralinos. The axion mass is expected to lie in the 10^{-10} eV range which is well below the range currently being explored by the ADMX experiment[95]. Furthermore, the $f_a \sim M_{GUT}$ case can accommodate a much wider range of $\Omega_{\widetilde{Z}_1}h^2$ values than the pure neutralino

DM scenario in MSSM models, since, for a neutralino LSP, its relic abundance is suppressed by the entropy injection, while, for an axino LSP, the neutralino contribution to the DM relic abundance is suppressed both by entropy dilution and $m_{\tilde{a}}/m_{\widetilde{Z}_1}$.

Conclusions

In this work, we presented the main consequences of PQMSSM models to the evolution of the early universe as well as to the nature of Dark Matter. As seen by the examples discussed in Secs.6-8, the cosmology of the PQMSSM is extremely rich and diverse. In Secs.6 and 7, we presented the main properties of these models, classifying them by the nature of their LSP. As shown by the results of these sections, the PQMSSM requires us to consider a drastically distinct picture of the thermal evolution of the universe in its early phases ($T_{BBN} < T < T_R$), when compared to the standard MSSM cosmology.

In the axino LSP scenario we have shown that the Dark Matter constraints on the MSSM can be easily avoided once the axion supermultiplet is included. In this case, there is a large region of the PQMSSM parameter space consistent with both BBN and DM constraints. Such freedom allowed us to consider scenarios consistent with thermal leptogenesis, which requires large re-heat temperatures. We showed that the PQMSSM can reconcile thermal leptogenesis with the Gravitino Problem if

- the gravitino is in the multi-TeV scale ($m_{\widetilde{G}} \gtrsim 30$ TeV)
- or the gravitino is the NLSP ($m_{\tilde{a}} < m_{\widetilde{G}} < m_{\widetilde{Z}_1}$).

Furthermore, saxion decays can dilute relic abundances, helping to avoid the BBN constraints on late decaying relics. In this case, a large region of the MSSM parameter space can be consistent with all cosmological constraints and still accommodate large re-heat temperatures, once the above conditions are satisfied.

This picture is drastically modified if we consider the case of a heavy axino, with a neutralino LSP, discussed in Sec.7. In this scenario, the neutralino relic abundance is always augmented by axino decays (if $T_D < T_{fr}$) or is the same as in the MSSM (if $T_D > T_{fr}$), so the Dark Matter constraint significantly restricts the allowed region of the PQMSSM parameter space. We have shown that, for most cases, we need to consider models with a higgsino or wino neutralino in order to avoid overproduction of DM. However, as shown by the Mirage Unification model discussed in Sec.8, such constraints can once again be relaxed if the effects of saxion entropy injection and dilution are included. However, in the neutralino LSP scenario, the necessary conditions for reconciling the Gravitino Problem with thermal leptogenesis are identical to the MSSM case, which requires $m_{\widetilde{G}} \gtrsim 30$ TeV. This still holds even in the case of large entropy dilution from saxion or axino decays.

Finally, we discussed PQMSSM models where the PQ scale is related to the GUT or string scales. As shown in Sec.8, these models usually imply a universe with an early saxion dominated era, followed by a large dilution of the other relics. Furthermore, in this case, DM is composed primarily of axions, with very small LSP abundances. In order to avoid the BBN constraints on saxion decays we were lead to consider models with multi-TeV saxions. However, the BBN bounds on the other late decaying relics (gravitinos, axinos and/or neutralinos) are easily avoided in this scenario, due to the large dilution of relics from saxion decays. In this scenario, the necessary conditions for implementing thermal leptogenesis are identical to the ones mentioned above, depending on the nature of the LSP.

References

[1] C. G. Callan, Jr., R. F. Dashen, and D. J. Gross, Phys. Lett. **B63**, 334 (1976).

[2] R. Jackiw and C. Rebbi, Phys. Rev. Lett. **37**, 172 (1976).

[3] T. Cheng and L. Li, *Gauge Theory of Elementary Particole Physics* (Oxford University Press, New York, 1985).

[4] R. J. Crewther, P. Di Vecchia, G. Veneziano, and E. Witten, Phys. Lett. **B88**, 123 (1979).

[5] K. Nakamura *et al.*, J. Phys. **G37**, 075021 (2010).

[6] R. D. Peccei and H. R. Quinn, Phys. Rev. Lett. **38**, 1440 (1977).

[7] S. Weinberg, Phys. Rev. Lett. **40**, 223 (1978).

[8] F. Wilczek, Phys.Rev.Lett. **40**, 279 (1978).

[9] C. Vafa and E. Witten, Phys. Rev. Lett. **53**, 535 (1984).

[10] H. Georgi and L. Randall, Nucl.Phys. **B276**, 241 (1986).

[11] J. E. Kim, Phys.Rept. **150**, 1 (1987).

[12] R. D. Peccei and H. R. Quinn, Phys. Rev. **D16**, 1791 (1977).

[13] M. A. Shifman, A. I. Vainshtein, and V. I. Zakharov, Nucl. Phys. **B166**, 493 (1980).

[14] J. E. Kim, Phys. Rev. Lett. **43**, 103 (1979).

[15] M. Dine, W. Fischler, and M. Srednicki, Phys. Lett. **B104**, 199 (1981).

[16] A. R. Zhitnitsky, Sov. J. Nucl. Phys. **31**, 260 (1980).

[17] L. Covi and J. E. Kim, New J. Phys. **11**, 105003 (2009).

[18] J. E. Kim and G. Carosi, Rev. Mod. Phys. **82**, 557 (2010).

[19] W. A. Bardeen and S.-H. Tye, Phys.Lett. **B74**, 229 (1978).

[20] D. J. Gross, R. D. Pisarski, and L. G. Yaffe, Rev. Mod. Phys. **53**, 43 (1981).

[21] L. Visinelli and P. Gondolo, Phys. Rev. **D80**, 035024 (2009).

[22] L. Duffy *et al.*, Phys. Rev. Lett. **95**, 091304 (2005).

[23] L. D. Duffy *et al.*, Phys. Rev. **D74**, 012006 (2006).

[24] S. J. Asztalos, L. J. Rosenberg, K. van Bibber, P. Sikivie, and K. Zioutas, Ann. Rev. Nucl. Part. Sci. **56**, 293 (2006).

[25] M. Schmaltz and D. Tucker-Smith, Ann. Rev. Nucl. Part. Sci. **55**, 229 (2005).

[26] N. Seiberg, Phys. Lett. **B318**, 469 (1993).

[27] H. Baer and X. Tata, *Weak scale supersymmetry: From superfields to scattering events* (Cambridge Univ. Pr., Cambridge, 2006).

[28] S. Cassel, D. M. Ghilencea, S. Kraml, A. Lessa, and G. G. Ross, arXiv: **1101.4664**, (2011).

[29] K. Rajagopal, M. S. Turner, and F. Wilczek, Nucl. Phys. **B358**, 447 (1991).

[30] P. Moxhay and K. Yamamoto, Phys. Lett. **B151**, 363 (1985).

[31] H. Baer, S. Kraml, A. Lessa, and S. Sekmen, JCAP **1011**, 040 (2010).

[32] M. Hashimoto, K. Izawa, M. Yamaguchi, and T. Yanagida, Phys.Lett. **B437**, 44 (1998).

[33] T. Higaki and R. Kitano, arXiv: **1104.0170**, (2011).

[34] M. Kawasaki, N. Kitajima, and K. Nakayama, arXiv: **1104.1262**, (2011).

[35] E. W. Kolb and M. S. Turner, *The Early universe* (Addison-Wesley Pub., New York, 1990).

[36] S. Weinberg, *Cosmology* (Oxford Univ. Pr., Oxford, 2008).

[37] S. Dodelson, *Modern cosmology* (Academic Pr., New York, 2003).

[38] A. Freitas, F. D. Steffen, N. Tajuddin, and D. Wyler, Phys.Lett. **B682**, 193 (2009).

[39] M. Pospelov and J. Pradler, Ann. Rev. Nucl. Part. Sci. **60**, 539 (2010).

[40] K. Jedamzik, Phys. Rev. **D74**, 103509 (2006).

[41] R. H. Cyburt, J. R. Ellis, B. D. Fields, and K. A. Olive, Phys. Rev. **D67**, 103521 (2003).

[42] M. Kawasaki, K. Kohri, and T. Moroi, Phys. Rev. **D71**, 083502 (2005).

[43] V. S. Rychkov and A. Strumia, Phys. Rev. **D75**, 075011 (2007).

[44] M. Bolz, A. Brandenburg, and W. Buchmuller, Nucl. Phys. **B606**, 518 (2001).

[45] J. Pradler and F. D. Steffen, Phys. Lett. **B648**, 224 (2007).

[46] K. Kohri, T. Moroi, and A. Yotsuyanagi, Phys. Rev. **D73**, 123511 (2006).

[47] W. Buchmuller, arXiv: **0710.5857**, (2007).

[48] W. Buchmuller, P. Di Bari, and M. Plumacher, Ann. Phys. **315**, 305 (2005).

[49] B. C. Allanach, K. Cranmer, C. G. Lester, and A. M. Weber, JHEP **08**, 023 (2007).

[50] H. Baer, A. D. Box, and H. Summy, JHEP **10**, 023 (2010).

[51] C. F. Berger, J. S. Gainer, J. L. Hewett, and T. G. Rizzo, JHEP **02**, 023 (2009).

[52] P. Graf and F. D. Steffen, arXiv: **1008.4528**, (2010).

[53] M. Kawasaki, K. Nakayama, and M. Senami, JCAP **0803**, 009 (2008).

[54] A. Strumia, JHEP **06**, 036 (2010).

[55] M. S. Turner, Phys. Rev. **D28**, 1243 (1983).

[56] M. S. Turner, Phys. Rev. **D33**, 889 (1986).

[57] T. Asaka and M. Yamaguchi, Phys. Rev. **D59**, 125003 (1999).

[58] R. J. Scherrer and M. S. Turner, Phys. Rev. **D31**, 681 (1985).

[59] H. Baer, S. Kraml, A. Lessa, and S. Sekmen, JCAP (2011).

[60] L. Covi, H.-B. Kim, J. E. Kim, and L. Roszkowski, JHEP **05**, 033 (2001).

[61] L. Covi, J. E. Kim, and L. Roszkowski, Phys. Rev. Lett. **82**, 4180 (1999).

[62] K. Jedamzik, M. Lemoine, and G. Moultaka, JCAP **0607**, 010 (2006).

[63] S. Hannestad, A. Mirizzi, G. G. Raffelt, and Y. Y. Y. Wong, JCAP **1008**, 001 (2010).

[64] T. Asaka and T. Yanagida, Phys. Lett. **B494**, 297 (2000).

[65] A. G. Cohen, D. B. Kaplan, and A. E. Nelson, Phys. Lett. **B388**, 588 (1996).

[66] H. Baer, S. Kraml, A. Lessa, S. Sekmen, and X. Tata, JHEP **10**, 018 (2010).

[67] F. Mahmoudi, Comput. Phys. Commun. **178**, 745 (2008).

[68] F. E. Paige, S. D. Protopopescu, H. Baer, and X. Tata, hep-ph/ **0312045**, (2003).

[69] H. Baer *et al.*, JHEP **0207**, 050 (2002).

[70] H. Baer, A. Lessa, S. Rajagopalan, and W. Sreethawong, arXiv: **1103.5413**, (2011).

[71] H. Baer, C. Balazs, and A. Belyaev, JHEP **0203**, 042 (2002).

[72] J. E. Kim, Phys. Lett. **B136**, 378 (1984).

[73] H. P. Nilles and S. Raby, Nucl.Phys. **B198**, 102 (1982).

[74] P. Svrcek and E. Witten, JHEP **0606**, 051 (2006).

[75] M. Dine and W. Fischler, Phys.Lett. **B120**, 137 (1983).

[76] G. Lazarides, C. Panagiotakopoulos, and Q. Shafi, Phys.Lett. **B192**, 323 (1987).

[77] G. Lazarides, R. K. Schaefer, D. Seckel, and Q. Shafi, Nucl.Phys. **B346**, 193 (1990).

[78] J. McDonald, Phys.Rev. **D43**, 1063 (1991).

[79] C. Pallis, Astropart.Phys. **21**, 689 (2004).

[80] J. Hasenkamp and J. Kersten, Phys.Rev. **D82**, 115029 (2010).

[81] L. Visinelli and P. Gondolo, Phys.Rev. **D81**, 063508 (2010).

[82] D. Auto, H. Baer, C. Balazs, A. Belyaev, J. Ferrandis, *et al.*, JHEP **0306**, 023 (2003).

[83] T. Blazek, R. Dermisek, and S. Raby, Phys.Rev. **D65**, 115004 (2002).

[84] K. Choi, A. Falkowski, H. P. Nilles, M. Olechowski, and S. Pokorski, JHEP **0411**, 076 (2004).

[85] K. Choi, A. Falkowski, H. P. Nilles, and M. Olechowski, Nucl.Phys. **B718**, 113 (2005).

[86] H. Baer, E.-K. Park, X. Tata, and T. T. Wang, JHEP **0706**, 033 (2007).

[87] H. Baer, E.-K. Park, X. Tata, and T. T. Wang, Phys.Lett. **B641**, 447 (2006).

[88] K. Choi and K. S. Jeong, JHEP **0701**, 103 (2007).

[89] L. Randall and R. Sundrum, Nucl.Phys. **B557**, 79 (1999).

[90] G. F. Giudice, M. A. Luty, H. Murayama, and R. Rattazzi, JHEP **9812**, 027 (1998).

[91] B. S. Acharya, K. Bobkov, G. L. Kane, J. Shao, and P. Kumar, Phys.Rev. **D78**, 065038 (2008).

[92] G. Lazarides and Q. Shafi, Phys.Lett. **B258**, 305 (1991).

[93] K. Kumekawa, T. Moroi, and T. Yanagida, Prog.Theor.Phys. **92**, 437 (1994).

[94] I. Affleck and M. Dine, Nucl.Phys. **B249**, 361 (1985).

[95] L. Duffy *et al.*, Phys.Rev.Lett. **95**, 091304 (2005).

[96] K.-Y. Choi, J. E. Kim, H. M. Lee, and O. Seto, Phys.Rev. **D77**, 123501 (2008).

Part III

Appendix

Appendix A

PQ Models

Here we present two well known examples of PQ models, the DFSZ and KSVZ models. The axion couplings and mass are strongly dependent on the energy scale we consider, since below Λ_{QCD} the QCD chiral symmetry is spontaneously broken and the axion field can mix with the other Goldstone bosons of the theory (π's and η). For simplicity, we present the axion couplings for energies well above Λ_{QCD}, which are the relevant ones for the results presented here.

A.1 DFSZ

The DFSZ model[15, 16] is the minimal extension of the PQ-Weinberg model discussed in Sec.1.1. It includes two Higgs doublets augmented with a SM singlet field (χ), which carries PQ charge. The relevant Lagrangian is:

$$\begin{aligned} \mathcal{L}_{PQ} &= \lambda_d \bar{Q}_L \phi_1 d_R + \lambda_u \bar{Q}_L \phi_2^C u_R + \lambda_d \bar{L}_L \phi_1 l_R + h.c - V(\phi_i, \chi) \\ V(\phi_i, \chi) &= \sum_{i=1,2} \left(-\mu_i^2 |\phi_i|^2 + \lambda_i |\phi_i|^4 \right) - \mu^2 |\chi|^2 + \lambda |\chi|^4 + \alpha |\phi_1|^2 |\phi_2|^2 + \beta |\phi_1^\dagger \phi_2|^2 \\ &+ (a|\phi_1|^2 + b|\phi_2|^2)|\chi|^2 + (c\phi_1^\dagger \phi_2 \chi^2 + h.c.) \end{aligned} \tag{A.1}$$

where we have omitted generation indices for simplicity. The above Lagrangian is invariant under the PQ transformation:

$$\begin{aligned} u_R &\rightarrow e^{i\alpha Q_u} u_R, \;\; d_R \rightarrow e^{i\alpha Q_d} d_R, \;\; l_R \rightarrow e^{i\alpha Q_d} l_R, \\ \phi_1 &\rightarrow e^{-i\alpha Q_d} \phi_1, \;\; \phi_2 \rightarrow e^{-i\alpha Q_u} \phi_2, \;\; \chi \rightarrow e^{-i\alpha (Q_u + Q_d)/2} \chi \, . \end{aligned} \tag{A.2}$$

The PQ symmetry is spontaneously broken by a non-zero vacuum expectation value (vev) of the χ scalar, which we rewrite as:

$$\chi \equiv \frac{1}{\sqrt{2}} e^{iw/u} e^{i\theta_\chi} (u + \eta) \tag{A.3}$$

where $u = \langle \chi \rangle$, θ_χ is a constant phase and w and η are the phase and longitudinal components of χ. However, since the ϕ_i fields carry PQ charge, the electroweak symmetry breaking also breaks the PQ scale and we rewrite ϕ_i as:

$$\phi_i \equiv \frac{1}{\sqrt{2}} e^{i\vec{\sigma}.\vec{\xi}_i/v_i} e^{i\theta_i} \begin{pmatrix} 0 \\ \\ v_i + \eta_i \end{pmatrix} \tag{A.4}$$

where $\vec{\xi}_i$ and η_i are the dynamical components and $\langle \phi_i \rangle = v_i$. After the breaking of $SU(2)_L \times U(1)_Y$, the axion field is obtained after diagonalization of the Goldstone boson current in the unitary gauge, resulting in:

$$a = \frac{1}{F}(x + \frac{1}{x})(\frac{v_1 v_2}{v^2}(v_2 \xi_1^0 - v_1 \xi_2^0) + \frac{1}{2} uw) \tag{A.5}$$

where $x = v_1/v_2$, $v = \sqrt{v_1^2 + v_2^2}$ and

$$F = (x + \frac{1}{x}) \sqrt{(\frac{v_1 v_2}{v})^2 + \frac{u^2}{4}} \ . \tag{A.6}$$

In the *invisible axion* limit ($\mu \gg \mu_i$ or $u \gg v_i$):

$$a \simeq w \ \text{ and } \ F \simeq u \tag{A.7}$$

so the axion completely decouples from the SM sector, except for terms of order v/F. Therefore the effective axion couplings are given by:

$$\mathcal{L}_{DFSZ} = \frac{i}{F} a \left(\lambda_u v_2 x \bar{u}_L u_R + \lambda_d v_1 \frac{1}{x} \bar{d}_L d_R + \lambda_l v_1 \frac{1}{x} \bar{l}_L l_R + h.c. \right) + \mathcal{O}(v^2/F^2) \ . \tag{A.8}$$

The above couplings generate anomalous $aG\tilde{G}$ and $aF\tilde{F}$ couplings through the 1-loop diagrams shown in Fig.A.1. These diagrams give:

$$\mathcal{L}_{eff}^{DFSZ} = \frac{\alpha_s}{8\pi}\frac{1}{F}N_f(x+\frac{1}{x})aG_{\mu\nu}\tilde{G}^{\mu\nu} + \frac{\alpha}{8\pi}\frac{1}{F}\frac{8}{3}N_f(x+\frac{1}{x})aF_{\mu\nu}\tilde{F}^{\mu\nu} \tag{A.9}$$

where N_f is the number of generations and $F_{\mu\nu}$ is the electromagnetic field tensor. Since the PQ scale f_a is defined so the coefficient of the $aG\tilde{G}$ is one, we take $f_a = F/N_f(x+1/x)$, giving:

$$\mathcal{L}_{eff}^{DFSZ} = \frac{\alpha_s}{8\pi}\frac{1}{f_a}aG_{\mu\nu}\tilde{G}^{\mu\nu} + \frac{\alpha}{8\pi}\frac{1}{f_a}\frac{8}{3}aF_{\mu\nu}\tilde{F}^{\mu\nu}\ . \tag{A.10}$$

Indentifying Eqs.(A.8) and (A.10) with Eq.(1.25), we have:

$$c_1^{l,q} = 0,\ \ c_2^l = c_2^d = \frac{1}{x},\ \ c_2^u = x,\ \ \text{and}\ \ c_Y = \frac{8}{3}\ \ (\text{DFSZ})\ . \tag{A.11}$$

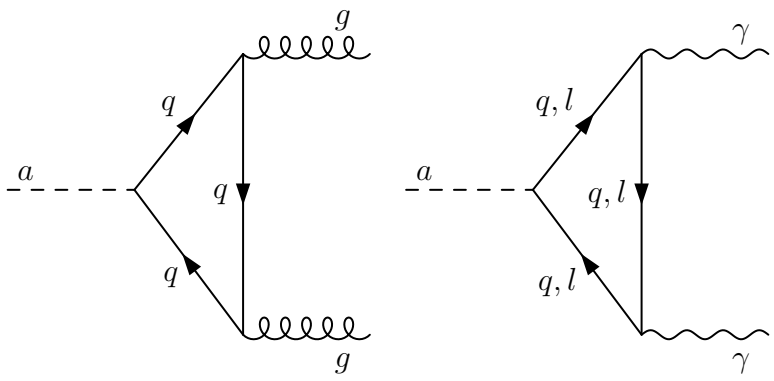

Figure A.1: 1-loop diagrams for the effective $aG\tilde{G}$ and $aF\tilde{F}$ interactions discussed in the text.

A.2 KSVZ

To implement the PQ symmetry in the SM, the KSVZ model[13, 14] introduces a new (superheavy) quark (Q) and a scalar singlet (χ). The KSVZ Lagrangian is:

$$\begin{aligned} \mathcal{L}_{KSVZ} &= \mathcal{L}_{SM} + (\lambda_Q \bar{Q}_L \chi Q_R + h.c.) - V(\chi, \phi) \\ V(\chi, \phi) &= -\mu^2 |\chi|^2 + a|\chi|^4 + b|\phi|^2 |\chi|^2 \end{aligned} \tag{A.12}$$

where the new quark is a singlet under $SU(2)_L$, but may carry hypercharge. Thus, in order to avoid a bare mass term for Q, the following discrete symmetry has to be imposed:

$$Q_L \to -Q_L, \;\; Q_R \to Q_R \;\text{ and }\; \chi \to -\chi \,. \tag{A.13}$$

Furthermore, the only fields with PQ charge are χ and Q_R, which transform as:

$$Q_R \to e^{i\alpha}, \;\; \chi \to e^{-i\alpha} \,. \tag{A.14}$$

Assuming $\mu \gg v$, the scalar field χ acquires a vev $\langle \chi \rangle = F$. Thus, we can decompose χ as:

$$\chi \equiv \frac{1}{\sqrt{2}} e^{ia/F} e^{i\theta_\chi} (F + \eta) \tag{A.15}$$

where a is the axion field. The quark Q becomes heavy ($m_Q = \lambda_Q F/\sqrt{2}$) and decouples at low energies ($\ll F$). Integrating out the Q fields we obtain the effective axion Lagrangian in the KSVZ model[1]:

$$\mathcal{L}_{eff}^{KSVZ} = \frac{\alpha_s}{8\pi} \frac{1}{f_a} a G_{\mu\nu} \tilde{G}^{\mu\nu} + \frac{\alpha_Y}{8\pi} \frac{6 e_Q^2}{f_a} a B_{\mu\nu} \tilde{B}^{\mu\nu} \tag{A.16}$$

[1] This corresponds to computing the loop diagram shown in Fig.A.1a with $q \to Q$ at energies $\ll M_Q \sim f_a$.

where e_Q is the Q hypercharge and $B_{\mu\nu}$ is the $U(1)_Y$ field tensor. In order to avoid fractional electric charges for the Q hadrons, we assume $e_Q = 0$, -1/3 or 2/3. Comparing the above equation with the effective Lagrangian in Eq.(1.25) we have:

$$c_1^{l,q} = 0, \;\; c_2^{l,q} = 0, \;\; \text{and} \;\; c_Y = 0, \; \frac{2}{3} \text{ or } \frac{8}{3} \;\; \text{(KSVZ)} \; . \tag{A.17}$$

A.3 Supersymmetric KSVZ

In order to illustrate the main consequences of supersymmetrizing PQ models, here we discuss the supersymmetric version of the KSVZ model defined in the last section. We will also present a possible implementation of supersymmetry breaking, which has the attractive feature of relating the SUSY and PQ breaking scales. The discussion presented here follows closely Ref. [72]. We start by assuming the following superpotential:

$$W = (\lambda_1 \hat{X}\hat{X}' + m^2)\hat{Z} + (\lambda_2 \hat{X}\hat{X}' + m'^2)\hat{Z}' + f\bar{\hat{Q}}'\hat{Q}\hat{X} \tag{A.18}$$

where $\hat{X}$, $\hat{X}'$, $\hat{Z}$ and $\hat{Z}'$ are singlets, while $\bar{\hat{Q}}'$ and $\hat{Q}$ are $SU(3)_C$ triplets. Under the $U(1)_{PQ}$, the above superfields transform as:

$$\hat{X} \to e^{2i\alpha}\hat{X} \;\; , \hat{X}' \to e^{-2i\alpha}\hat{X}', \;\; \hat{Q} \to e^{-i\alpha}\hat{Q}, \;\; \bar{\hat{Q}}' \to e^{-i\alpha}\bar{\hat{Q}}' \;\; \text{and} \;\; \hat{Z} \to \hat{Z}, \;\; \hat{Z}' \to \hat{Z}' \; . \tag{A.19}$$

Assuming a canonical Kahler function ($K = \sum_i \hat{\Phi}_i^\dagger \hat{\Phi}_i$), we have the following supergravity potential for the scalar fields [2][27]:

$$V_{SUGRA} = \exp[|\Phi_i|^2/M_{Pl}^2] \left(|\frac{\Phi_i^\dagger}{M_{Pl}^2} W + \frac{\partial W}{\partial \Phi_i}|^2 - 3\frac{|W|^2}{M_{Pl}^2} \right) . \tag{A.20}$$

At zero order in M_{Pl}, we recover the (global) SUSY scalar potential:

$$V_0 = |\lambda_1 X X' + m^2|^2 + |\lambda_2 X X' + m'^2|^2 + |\lambda_1 Z + \lambda_2 Z'|^2 (|X|^2 + |X'|^2) + \mathcal{O}(f) \tag{A.21}$$

where we have omitted the $X\bar{Q}Q'$ coupling for now. Minimizing the above potential we obtain

$$\langle Q \rangle = \langle \bar{Q}' \rangle = \langle \lambda_1 Z + \lambda_2 Z' \rangle = 0 \ \text{ and } \ \langle X X' \rangle = -\frac{M_S^2}{\lambda} \cos(\alpha - \beta) \tag{A.22}$$

where

$$\lambda^2 = \lambda_1^2 + \lambda_2^2, \ \ M_S^4 = m^4 + m'^4, \ \ \tan\beta = m'^2/m^2 \ \text{ and } \ \tan\alpha = \lambda_2/\lambda_1 \, . \tag{A.23}$$

The above minimization conditions are not sufficient to fix the vacuum expectation values of all fields and we need to include the $\mathcal{O}(1/M_{Pl})$ corrections in order to fully fix the above vevs. The leading order corrections give[72]:

$$\begin{aligned} \langle X \rangle &= -\langle X' \rangle = \left(\frac{M_S^2}{\lambda} \cos(\alpha - \beta) - \frac{M_S^4}{\lambda^2 M_{Pl}^2} \sin^2(\alpha - \beta) \right)^{1/2} \\ \langle Z_1 \rangle &= 0 \\ \langle Z_2 \rangle &= -\frac{1}{\sqrt{2}} M_{Pl} \end{aligned} \tag{A.24}$$

where we have defined $Z_1 \equiv \cos\alpha Z + \sin\alpha Z'$ and $Z_2 = \cos\alpha Z' - \sin\alpha Z$ for convenience. The above *vevs* clearly break $U(1)_{PQ}$ and supersymmetry, since

$$\langle F_{Z_1} \rangle \equiv \langle \frac{\partial W}{\partial Z_1} \rangle = \lambda \langle X X' \rangle = -\lambda \langle X \rangle^2 \neq 0 \, . \tag{A.25}$$

[2]Throughout this section we will use $\hat{\Phi}$ to indicate superfields, Φ to indicate its (complex) scalar component and $\tilde{\Phi}$ to indicate its fermionic component.

Note that the SUSY and $U(1)_{PQ}$ scales are both given by $\langle X\rangle \sim M_S$. Due to the SUSY breaking, the gravitino will acquire a mass given by[27]:

$$m_{3/2} = \frac{1}{M_{Pl}^2}\langle W\rangle = \frac{M_S^2}{M_{Pl}}\sin(\alpha-\beta)\frac{1}{\sqrt{2}}\ . \tag{A.26}$$

Using the above results, we proceed to investigate the spectrum of the broken phase. The fermion mass matrix in the basis (X, X', Z_1, Z_2) is given by:

$$(M_f)_{ij} = \langle\frac{\partial^2 W}{\partial\Phi_i\partial\Phi_j}\rangle = \begin{pmatrix} 0 & 0 & \lambda\langle X'\rangle & 0 \\ 0 & 0 & \lambda\langle X\rangle & 0 \\ \lambda\langle X'\rangle & \lambda\langle X\rangle & 0 & 0 \\ 0 & 0 & 0 & 0 \end{pmatrix} \tag{A.27}$$

which gives the following mass eigenstates:

$$\begin{aligned} \tilde{Z}_2 &\qquad (M_{Z_2}=0) \\ \tilde{A} &= \frac{1}{\sqrt{2}}(\tilde{X}+\tilde{X}')\ \ (M_A=0) \\ \tilde{Y} &= \frac{1}{\sqrt{2}}(Z_1+\frac{1}{\sqrt{2}}(\tilde{X}-\tilde{X}'))\ \ (M_Y=\sqrt{2}\lambda x) \\ \tilde{\bar{Y}} &= \frac{1}{\sqrt{2}}(Z_1-\frac{1}{\sqrt{2}}(\tilde{X}-\tilde{X}'))\ \ (M_{\bar{Y}}=-\sqrt{2}\lambda x) \end{aligned} \tag{A.28}$$

where $x \equiv \langle X\rangle$. The $\tilde{Y}$ and $\tilde{\bar{Y}}$ form a Dirac spinor of mass $M_Y \sim M_S$, while $\tilde{Z}_2$ is the Goldstino generated from SUSY breaking (since $\langle F_{Z_2}\rangle \neq 0$) and $\tilde{A}$ is the $U(1)_{PQ}$ Goldstino. Furthermore, the fermion components of the $\hat{Q}$ and $\hat{Q}'$ superfields combine into a Dirac fermion with mass $M_Q = fx$.

To compute the scalar masses we define:

$$\begin{aligned} A &= \frac{1}{\sqrt{2}}(X+X'),\ \ X_2=\frac{1}{\sqrt{2}}(X-X') \\ B_1 &= M_S^2\cos(\beta-\alpha)Z_1\ \text{ and }\ B_2 = M_S^2\sin(\beta-\alpha)Z_2 \end{aligned} \tag{A.29}$$

so the scalar potential can now be written as:

$$\begin{aligned} V_{SUGRA} &= \lambda^2|Z_1|^2(|A|^2+|X_2|^2) \\ &+ |\frac{\lambda_1}{2}(A^2-X_2^2)+m^2|^2+|\frac{\lambda_2}{2}(A^2-X_2^2)+m'^2|^2 \\ &+ \frac{1}{M_{Pl}^2}\left(\frac{\lambda}{2}(A^2-X_2^2)Z_1+B_1+B_2\right)\left(\frac{3\lambda}{2}(A^{\dagger 2}-X_2^{\dagger 2})Z_1^\dagger+B_1^\dagger+B_2^\dagger\right)+h.c. \\ &+ \mathcal{O}(f) \end{aligned} \tag{A.30}$$

where we have once again neglected the heavy squark terms, since they do not mix with the other scalars. Shifting the fields by their *vevs*, we obtain the following leading order mass terms:

$$\begin{aligned} V_{SUGRA} &= 2\lambda^2x^2(|X_2|^2+|Z_1|^2) \\ &+ \left(-x^2\lambda^2+\lambda_1m^2+\lambda_2m'^2+2\frac{\langle B_2\rangle^2}{M_{Pl}^4}\right)\frac{(A+A^\dagger)^2}{4} \\ &+ \left(x^2\lambda^2-\lambda_1m^2-\lambda_2m'^2+2\frac{\langle B_2\rangle^2}{M_{Pl}^4}\right)\frac{(A-A^\dagger)^2}{4} \\ &+ \left(\frac{\langle B_2\rangle^2}{M_{Pl}^4}+\frac{M_S^4\sin^2(\alpha-\beta)}{M_{Pl}^2}(2+\frac{\langle Z_2\rangle^2}{M_{Pl}^2})\right)|Z_2|^2+\dots . \end{aligned} \tag{A.31}$$

Using

$$\begin{aligned} x^2 &= \frac{M_S^2}{\lambda}\cos(\alpha-\beta)-\frac{M_S^4}{\lambda^2M_{Pl}^2}\sin^2(\alpha-\beta) \\ \langle Z_2\rangle &= -\frac{1}{\sqrt{2}}M_{Pl} \\ \langle B_2\rangle &= -M_S^2\sin(\beta-\alpha)\langle Z_2\rangle \\ m_{3/2} &= \frac{M_S^2}{M_{Pl}}\frac{\sin(\alpha-\beta)}{\sqrt{2}} \end{aligned} \tag{A.32}$$

we obtain

$$m_{A_R}^2=4m_{3/2}^2,\ \ m_{A_I}^2=0,\ \ m_{Z2}^2=6m_{3/2}^2\ \text{ and }\ m_{X_2}^2=m_{Z_1}^2=2\lambda^2x^2 \tag{A.33}$$

where $A = (A_R + iA_I)/\sqrt{2}$. Despite having a *soft* mass, the Z_2 scalar has no tree level couplings with any of the other fields and can be neglected. On the other hand, the Q, Q', X_2 and Z_1 scalars have mass of order the SUSY breaking scale. Assuming $m_{3/2} \sim 1$ TeV, we have $M_S \sim 10^{11}$ GeV. Therefore, the low energy effective theory will simply consist of the A field.

From the above results we see that the low energy theory (at energies $\ll \langle X \rangle$) consists of the A_R, A_I, $\tilde{A}$ and $\widetilde{G}$ fields, which correspond to the saxion (s), axion (a), axino ($\tilde{a}$) and gravitino ($\widetilde{G}$) states, respectively. Therefore, for the supersymmetric KSVZ model presented here, we have:

$$m_s = 2m_{3/2}, \quad m_a = 0, \quad m_{\tilde{a}} = 0 \quad \text{and} \quad m_{\widetilde{G}} = m_{3/2} \tag{A.34}$$

However, the axino mass receives large 1-loop contributions from the diagram shown in Fig.A.2[30, 29] and acquires a mass of the order of the gravitino mass suppressed by a loop factor:

$$m_{\tilde{a}} = \frac{1}{62}\lambda_Q^2 m_{3/2} \, . \tag{A.35}$$

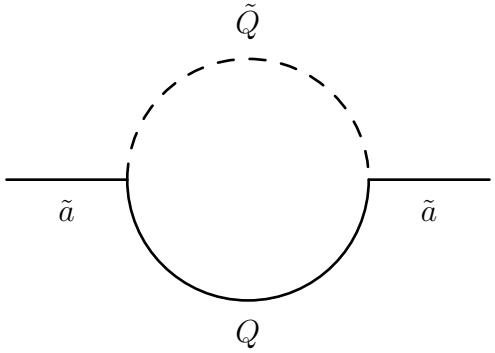

Figure A.2: 1-loop diagram contributing to the axino mass in the supersymmetric KSVZ model.

Appendix B

Axion and Neutralino Relic Densities

Here we derive explicit expressions for the neutralino and axion relic densities for the case of an early matter-dominated universe. From the discussion in Sec.5.3, we see that the Hubble parameter in a radiation (RD), matter (MD) or decaying-particle-dominated (DD) universe can be written as:

$$H(T) = \sqrt{\frac{4\pi^3}{45} g_*(T)} \frac{T_{eff}^2}{M_{Pl}} \tag{B.1}$$

where

$$T_{eff} = T \times \begin{cases} 1 & \text{, for RD} \\ \left(\frac{T_e}{T}\right)^{1/4} & \text{, for MD} \\ \left(\frac{g_*(T)}{g_*(T_D)}\right)^{1/4} \frac{T}{T_D} & \text{, for DD} \end{cases}$$

with T_e, T_D as defined in Sec.5.3. To compute the axion relic density, we use Eq.(5.17):

$$\rho_a^{CO} = \frac{1}{2} \chi f(\theta_i) m_a(T_a) m_a^0 \theta_i^2 f_a^2 \left(\frac{R_{osc}}{R}\right)^3 \tag{B.2}$$

with the oscillation temperature, T_a, given by the oscillation condition (Eq.(5.11)):

$$3H(T_a) = m_a(T_a) \ . \tag{B.3}$$

In a MD or RD universe, entropy is conversed so that

$$\left(\frac{R_{osc}}{R}\right)^3 = \frac{g_*(T) T^3}{g_*(T_a) T_a^3} \ , \tag{B.4}$$

while for the decaying particle regime, entropy is injected by the decaying particle, resulting in:

$$\left(\frac{R_{osc}}{R}\right)^{3/2} = \frac{g_*(T) T^4}{g_*(T_a) T_a^4} \ . \tag{B.5}$$

Using the above results we obtain

$$\Omega_a = \begin{cases} \Omega_a^{RD}/r \text{ , if } T_e < T_a \\ \Omega_a^{MD} \text{ , if } T_S < T_a < T_e \\ \Omega_a^{DD} \text{ , if } T_D < T_a < T_S \\ \Omega_a^{RD} \text{ , if } T_a < T_D \end{cases} \tag{B.6}$$

where r is the entropy dilution factor given by $r = S(T \ll T_D)/S(T \gg T_e) \simeq T_e/T_D$ and[1]

$$\begin{aligned} \Omega_a^{RD}h^2 &= \begin{cases} 9.23 \times 10^{-3}\theta_i^2 f(\theta_i)\frac{1}{g_*(T_a)^{1/4}}\left(\frac{f_a}{10^{12}}\right)^{3/2} & \text{, if } T_a < \Lambda_{QCD} \\ 1.32\ \theta_i^2 f(\theta_i)\frac{1}{g_*(T_a)^{5/12}}\left(\frac{f_a}{10^{12}}\right)^{7/6} & \text{, if } T_a > \Lambda_{QCD} \end{cases} \\ \Omega_a^{MD}h^2 &= \begin{cases} 7.5 \times 10^{-5}\ \theta_i^2 f(\theta_i) T_D \left(\frac{f_a}{10^{12}}\right)^2 & \text{, if } T_a < \Lambda_{QCD} \\ 1.4\ \theta_i^2 f(\theta_i)\frac{1}{g_*(T_a)^{4/11}}\left(\frac{f_a}{10^{12}}\right)^{14/11}\frac{T_D}{T_e^{4/11}} & \text{, if } T_a > \Lambda_{QCD} \end{cases} \end{aligned} \tag{B.7}$$

$$\Omega_a^{DD}h^2 = \begin{cases} 7.5 \times 10^{-5}\ \theta_i^2 f(\theta_i) T_D \left(\frac{f_a}{10^{12}}\right)^2 & \text{, if } T_a < \Lambda_{QCD} \\ 1.72\ \theta_i^2 f(\theta_i)\frac{g_*(T_D)^{1/4}}{\sqrt{g_*(T_a)}} T_D^2 \left(\frac{f_a}{10^{12}}\right)^{3/2} & \text{, if } T_a > \Lambda_{QCD} \end{cases} . \tag{B.8}$$

The oscillation temperatures are given by:

$$\begin{aligned} T_a^{RD} &= \begin{cases} 1.23 \times 10^2 \frac{1}{g_*(T_a)^{1/4}}\left(\frac{10^{12}}{f_a}\right)^{1/2} & \text{, if } T_a < \Lambda_{QCD} \\ 8.71 \times 10^{-1}\frac{1}{g_*(T_a)^{1/12}}\left(\frac{10^{12}}{f_a}\right)^{1/6} & \text{, if } T_a > \Lambda_{QCD} \end{cases} \\ T_a^{MD} &= \begin{cases} 6.1 \times 10^2 \left(\frac{1}{\sqrt{g_*(T_a)}T_e}\frac{10^{12}}{f_a}\right)^{2/3} & \text{, if } T_a < \Lambda_{QCD} \\ 8.6 \times 10^{-1}\left(\frac{1}{\sqrt{g_*(T_a)}T_e}\frac{10^{12}}{f_a}\right)^{2/11} & \text{, if } T_a > \Lambda_{QCD} \end{cases} \\ T_a^{DD} &= \begin{cases} 0.11 \times 10^2 \left(\frac{\sqrt{g_*(T_D)}}{g_*(T_a)}\frac{10^{12}}{f_a}T_D^2\right)^{1/4} & \text{, if } T_a < \Lambda_{QCD} \\ 9.0 \times 10^{-1}\left(\frac{\sqrt{g_*(T_D)}}{g_*(T_a)}\frac{10^{12}}{f_a}T_D^2\right)^{1/8} & \text{, if } T_a > \Lambda_{QCD} \end{cases} . \end{aligned} \tag{B.9}$$

[1] All dimensional quantities in this Section are in GeV units.

To compute the neutralino relic density, we use Eq.(4.8)

$$\frac{\rho_{\widetilde{Z}_1}}{s} = m_{\widetilde{Z}_1} Y_{\widetilde{Z}_1}(T_{fr}) \left(\frac{R_{fr}^3}{R_0^3}\right) \tag{B.10}$$

where the neutralino yield at freeze-out can be approximated by the equilibrium yield

$$\bar{Y}_{\widetilde{Z}_1}(T_{fr}) = \frac{2}{s(T_{fr})} \left(\frac{m_{\widetilde{Z}_1} T_{fr}}{2\pi}\right)^{3/2} e^{-m_{\widetilde{Z}_1}/T_{fr}} , \tag{B.11}$$

and T_{fr} is determined from the freeze-out condition, Eq.(4.7),

$$\bar{Y}_{\widetilde{Z}_1}(T_{fr}) = \kappa \frac{H(T_{fr})}{\langle\sigma v\rangle s(T_{fr})} \tag{B.12}$$

where $\kappa = 1(3/2)$ for a radiation (matter) dominated universe[96]. Using the $H(T)$ and R^3 expressions for a MD, RD and DD universe discussed above, we obtain:

$$\Omega_{\widetilde{Z}_1} = \begin{cases} \Omega_{\widetilde{Z}_1}^{RD}/r \text{ , if } T_e < T_{fr} \\ \Omega_{\widetilde{Z}_1}^{MD} \text{ , if } T_S < T_{fr} < T_e \\ \Omega_{\widetilde{Z}_1}^{DD} \text{ , if } T_D < T_{fr} < T_S \\ \Omega_{\widetilde{Z}_1}^{RD} \text{ , if } T_{fr} < T_D \end{cases} \tag{B.13}$$

with

$$\begin{aligned} \Omega_{\widetilde{Z}_1}^{RD} h^2 &= 8.5 \times 10^{-11} m_{\widetilde{Z}_1} \frac{1}{\sqrt{g_*(T_{fr})}} \frac{1}{T_{fr}} \frac{1}{\langle\sigma v\rangle} \\ \Omega_{\widetilde{Z}_1}^{MD} h^2 &= \frac{3}{2} \times 8.5 \times 10^{-11} m_{\widetilde{Z}_1} \frac{1}{\sqrt{g_*(T_{fr})}} \frac{T_D}{\sqrt{T_e} T_{fr}^{3/2}} \frac{1}{\langle\sigma v\rangle} \\ \Omega_{\widetilde{Z}_1}^{DD} h^2 &= \frac{3}{2} \times 8.5 \times 10^{-11} m_{\widetilde{Z}_1} \frac{\sqrt{g_*(T_D)}}{g_*(T_{fr})} \frac{T_D^3}{T_{fr}^4} \frac{1}{\langle\sigma v\rangle} \end{aligned} \tag{B.14}$$

where $\langle\sigma v\rangle$ must be evaluated at T_{fr} and the freeze-out temperatures in each regime

are given by

$$\begin{aligned} T_{fr}^{RD} &= m_{\widetilde{Z}_1}/\ln[\frac{3\sqrt{5}}{2^{3/2}\pi^3}\langle\sigma v\rangle M_{Pl} m_{\widetilde{Z}_1}^{3/2}\frac{1}{\sqrt{g_*(T_{fr})T_{fr}}}] \\ T_{fr}^{MD} &= m_{\widetilde{Z}_1}/\ln[\frac{3\sqrt{5}}{2^{3/2}\pi^3}\langle\sigma v\rangle M_{Pl} m_{\widetilde{Z}_1}^{3/2}\frac{1}{\sqrt{g_*(T_{fr})T_e}}] \\ T_{fr}^{DD} &= m_{\widetilde{Z}_1}/\ln[\frac{3\sqrt{5}}{2^{3/2}\pi^3}\langle\sigma v\rangle M_{Pl} m_{\widetilde{Z}_1}^{3/2}\frac{\sqrt{g_*(T_D)}}{g_*(T_{fr})}\frac{T_D^2}{T_{fr}^{5/2}}] \ . \end{aligned} \tag{B.15}$$

Finally, the temperature T_S which marks the transition from the MD to the DD regime can be estimated by matching the expressions for the relic density for $T_{a,fr} < T_S$ and $T_{a,fr} > T_S$. Using the above results we obtain:

$$T_S = \left(\frac{g_*(T_D)}{g_*(T^{MD})}T_D^4 T_e\right)^{1/5} \tag{B.16}$$

where $T^{MD} = T_a^{MD}$ for axions and $T^{MD} = T_{fr}^{MD}$ for neutralinos.